SYNTHESIS, FUNCTIONALIZATION AND CATALYTIC APPLICATION OF SILICA, MESOPOROUS SILICA NANOPARTICLES AND THEIR 3-D SCAFFOLDS

THESIS

Submitted To The

UNIVERSITY OF PUNE

For The Degree Of

DOCTOR OF PHILOSOPHY
In
CHEMISTRY

By

ANAL KUMAR GANAI

Research Guide

Dr. B. L. V. PRASAD

Research Co-Guide

Dr. SAYAM SEN GUPTA

DIVISION OF PHYSICAL AND MATERIAL CHEMISTRY
NATIONAL CHEMICAL LABORATORY, PUNE – 411008

March 2013

राष्ट्रीय रासायनिक प्रयोगशाला
(वैज्ञानिक तथा औद्योगिक अनुसंधान परिषद)
डॉ. होमी भाभा मार्ग पुणे - 411 008. भारत
NATIONAL CHEMICAL LABORATORY
(Council of Scientific & Industrial Research)
Dr. Homi Bhabha Road, Pune - 411 008. India.

CERTIFICATE

This is to certify that the work incorporated in the thesis entitled: "**Synthesis, Functionalization and Catalytic Application of Silica, Mesoporous Silica Nanoparticles and Their 3-D Scaffolds**" submitted by Mr. Anal Kumar Ganai, for the degree of Doctor of Philosophy in Chemistry to the University of Pune, has been carried out by him under my supervision at Physical and Material Chemistry Division, National Chemical Laboratory, Pune-411008, India. All the materials from other sources have been duly acknowledged in this thesis.

B. L. V. Prasad
(Research Guide)

Communication Channels
☎ +91-20-2590 2000
+91-20-2590 (DID)
FAX
+91-20-2590 2601(DIR)
+91-20-2590 2660 (COA)
WEBSITE
www.ncl-india.org

राष्ट्रीय रासायनिक प्रयोगशाला
(वैज्ञानिक तथा औद्योगिक अनुसंधान परिषद)
डॉ. होमी भाभा मार्ग पुणे - 411 008. भारत
NATIONAL CHEMICAL LABORATORY
(Council of Scientific & Industrial Research)
Dr. Homi Bhabha Road, Pune - 411 008. India.

CERTIFICATE

This is to certify that the work incorporated in the thesis entitled: "**Synthesis, Functionalization and Catalytic Application of Silica, Mesoporous Silica Nanoparticles and Their 3-D Scaffolds**", submitted by Mr. Anal Kumar Ganai, for the degree of Doctor of Philosophy in Chemistry to the University of Pune, has been carried out by him under my joint supervision at Chemical Engineering and Process Development Division, National Chemical Laboratory, Pune-411008, India. All the materials from other sources have been duly acknowledged in this thesis.

Sayam Sen Gupta

Sayam Sen Gupta
(Research Co-Guide)

Communication Channels
☎ +91-20-2590 2000
+91-20-2590 (DID)
FAX
+91-20-2590 2601(DIR)
+91-20-2590 2660 (COA)
WEBSITE
www.ncl-india.org

Declaration

I, hereby declare that all the experiments embodies in this thesis entitled **"Synthesis, Functionalization and Catalytic Application of Silica, Mesoporous Silica Nanoparticles and Their 3-D Scaffolds"** submitted for the degree of Doctor of Philosophy in Chemistry, to the University of Pune has been carried out by me at Physical and Material Chemistry Division and Chemical Engineering and Process Development Division, National Chemical Laboratory, Pune, India, under the guidance of Dr. B. L. V. Prasad and co-guidance of Dr. Sayam Sen Gupta. The work is original and has not been submitted in part or full by me, for any degree or diploma to this or to any other University.

Anal Kumar Ganai

Dedicated

To my beloved Parents

"uttishthata jagrata prapya varan nibodhata"

Acknowledgements

In the journey of last five years many people have contributed significantly and helped me to reach this level. This thesis will be incomplete without acknowledging them. First of all, I would like to thank my thesis supervisor and co-guide, ***Dr. B. L. V. Prasad*** *and* ***Dr. Sayam Sen Gupta****, Scientists, National Chemical Laboratory, Pune respectively. Their dedication to do noble science, logical way of thinking has gained my immense respect. Numerous discussions with them helped me understand science in a better way. During the course of this thesis, I gained constant support and constructive criticism. I will be highly benefitted by their scientific and non-scientific lessons. Their high degree of collaborative work helped me to understand different lab ethics and work in different lab environments. I salute them for their ethics and desire to perform high quality research. I will be highly thankful to the Almighty if I gained some of their qualities in me to do science for my entire life. Last but not least, the freedom to do science I got from them for the last five years really helped me to prepare this thesis works. I believe that the essential habits they cultivated in me such as attending seminars, group meetings, yearly resolutions and planning will give me the confidence to start an independent scientific career.*

I would also like to thank my collaborator ***Dr. Guruswamy Kumaraswamy****, Scientist, National chemical Laboratory, Pune for his valuable comments and suggestions. I learned worthy scientific lessons after discussing many times with him. I like to take opportunity to thank Dr. Srinivas Hotha, Scientiest, IISER-Pune to support me with some of my experiments during initial days of my Ph.D. He was ever ready to clear doubts, however trivial they were. Special thanks go to Dr. C. S. Gopinath for his help and scientific discussions regarding XPS. It was my pleasure to work with people of such high quality with better scientific knowledge.*

I would like to thank the Council of Scientific and Industrial Research (CSIR) for the award of research fellowship. I thank DST, New Delhi for giving me financial support for attending international conference. I am thankful to Dr. S. Pal, Director and Ex-Head of the Physical and Material Chemistry Department, Dr. S. Sivaram, Ex-Director, Dr. V. V.Ranade, Deputy Director, Head of the Department, Chemical Engineering and Processing Division and Dr. B. D. Kulkarni, Ex-Deputy Director, National Chemical Laboratory to carry out my research work and extending all possible infrastructural facilities for completion of my research work. I take this opportunity to thank Dr. Anil Kumar, Chairman, Physical and Material Chemistry Division for always being supportive. I thank all scientists of the physical and material chemistry division for being very supportive. I also acknowledge Mr. R. Gholap, Mr. Ketan, Mr. Naren, Mr.

Anuj, Mr. Pandiraj and Mr. Pankaj from Centre for Materials Characterization for their help in characterizations with NMR, SEM and TEM.

It was my pleasure to work with Dr. Kamendra Sharma and Dr. Pratap S Chandran during my Ph.D. I learned many experimental techniques and scientific skills which helped me to construct my work. Numerous discussions with them provided me to learn many aspects of life. I thank all my colleagues and lab-mates (past and present) for their helpful hand and cheerful attitude that had made my working atmosphere very easy and enjoyable. I thank all of my senior lab-mates in Dr. Prasad's Group; Dr. Vijay, Dr. Pratap Chandran, Dr. Sanjay Singh, Dr. Deepti, Dr. Manasi, Dr. Virginia, Dr. Priyanka, Dr. Satabdi for being very supportive during my work. I enjoyed a lot to work with other labmates, Vilas, Ravi, Balanagulu, Pushpanjali, Jhumur, Prabhu, Pravin, Arun, Poulomidi for their presence in lab and make healthy fun and support during work. It was my pleasure to work with all of my labmates in Sayam Sir's Lab, Dr. Malvi, Dr. Mrityunjoy, Debasis, Dr. Basab, Chaka, Sushma, Munmun, Soumen, Neha, Vinita, Kundan, Santanu and Hasan for their support during my stay in the lab. My special heartful thanks and best wishes goes to Sushma and Pravin for helping me during my research work. I would also like to thank some of my senior lab-mates Dr. Manasi Kasture, Dr. Bharmana Malvi, Dr. Bibhas Ranjan Sarkar, Dr. Satabdi Porel Mukherjee for being affectionate about me. Here I would like to mention one name who was my labmate and my dear brother, Late Agnimitra Banerjee. I learned lots about life from him and spending time together was really enjoyable. There is lots of empty space for you in my heart. Agni, I miss you dear, stay well wherever you are. I would like to acknowledge the friendship of Debasisda (DD), Sujitda, Pati, Anupam, Subhodeep (dosu), Prithvi, Arijit, Saikat, Roopadi, and many more in NCL, who made my stay enjoyable. It was my great pleasure to know and communicate with such many persons of high dignity. I hope the lessons will help me to construct my personal, professional and political life in a better way. I would also like to acknowledge the financial support of Prof. Enoki and his group in Tokyo Institute of Technology during my visit in Tokyo.

This thesis will be incomplete without the blessings of my loving parents. They have always been there for me. Without their support and encouragement I could not come across a long distance. They showed me a dream from my childhood days and I hope to fulfil little bit of that. I wish I will get such parents in each of my rebirths, if there is any. I am grateful to my grandmother for giving me enormous blessings. Finally, I will like to thank Google and Microsoft Word for helping me to search literature and correcting my English during paper and thesis writing.

Anal

Abstract

Surface functionalization has emerged as one of the most important research areas in the field of advanced functional materials. Surfaces determine how objects interact with their environment and surface chemistry is a research domain of great interest, particularly in the study and design of nanostructures. Various techniques based on physical and chemical methods are available to functionalize the surface. The chemistry developed for surface functionalization mainly uses silanes on oxides, thiols on gold and electrostatic interactions for charged surfaces. Chemical covalent attachment of molecules on the surface offers great advantages over physical adsorption based strategies. Nanomaterials/particles to which functional molecules have been covalently attached through appropriate chemistries have wide spread applications in catalysis, separation, decontamination, drug delivery and sensor designing. In this thesis work, catalytic application of the functionalized nanoparticles has been discussed. Nanoparticles show higher catalytic activity because of their high surface area and colloidal nature. Because dispersions of these particles in appropriate solvents can be quite stable, they display the advantages of both homogeneous and heterogeneous catalytic systems. But the main problem in nanoparticle based catalysis lies in separating them from the reaction mixture without any aggregation and loss of catalytic activity. Thus there is a need to make macroscopic structure with the help of nanoparticles which will address the separation issue also. This will also help to develop continuous flow reactors for industrial application.

In the last decade, scientists have focused on the assembly schemes that allow building macroscopic structures from nanoscopic building blocks. In catalysis, hierarchical macroscopic structure is important because the macropore can favour mass transfer of the reactants where as the active site of the catalyst can be located in the mesopore or micropore. To make hierarchical materials different techniques has been pursued by the scientists. Mainly, surfactants and amphiphilic copolymers can be used as templates to synthesize ordered mesoporous and macropourous materials. Macropores have been fabricated in the system using latex spheres, nanoparticles, emulsions as templates.

In the content of this thesis work, silica and mesoporous silica nanoparticles were specially chosen since they are ideal candidates for functionalization due to their large surface area (~1000 m^2/g), large and tunable pore sizes (2-50 nm), hydrothermal stability and thicker walls that can be easily functionalized using simple silanol chemistry. Different functional organic groups such as amines, thiols, vinyls, carboxylic acids, sulphonic acids were installed on the surface of different siliceous materials. The functional groups installed by such modifications can be used to anchor various synthetic catalysts, bio-molecules and polymers to generate novel functional materials.

One more aim of the present work was to develop a complex hierarchical functional material which can display good catalytic activity. To achieve that aim, different level of complexity has been incorporated into the system starting from fabrication of very simple functionalized material. Various functionalized nanomaterials were synthesized, characterized and their catalytic activity was studied. We also demonstrated that these functional nanomaterials could be assembled and stitched together through covalent bonds and would yield functional 3-dimensional, porous materials.

Table of Contents

List of Figures

List of Schemes

List of Tables

List of abbreviations

AzPTES	3-azidopropyltriethoxysilane
BET	Braunauer-Emmett-Teller
BJH	Barrett-Joyner-Halenda
$C_{12}E_9$	Poly(ethylene glycol) diglycidyl ether
CP-MAS	Cross-Polarization Magic Angle Spinning
CLSM	Confocal Laser Scanning Microscopy
CuAAC	Cu (I) catalyzed azide-alkyne cycloaddition
CTAB	Cetyltrimethyl ammonium bromide
HRTEM	High Resolution Transmission Electron Microscopy
ICP	Inductively Coupled Plasma
LC-MS	Liquid Chromatography-Mass Spectrometer
MCM	Mobil's Composition Material
NMR	Nuclear Magnetic Resonance
SBA	Santa Barbara Amorphous
SEM	Scanning Electron Microscopy
TEOS	Tetraethyl orthosilicate
TEM	Transmission Electron Microscopy
TGA	Thermo Gravimetric Analysis
UV-Vis	Ultraviolet-Visible
XRD	X-Ray Diffraction

Chapter 1

Introduction and literature survey

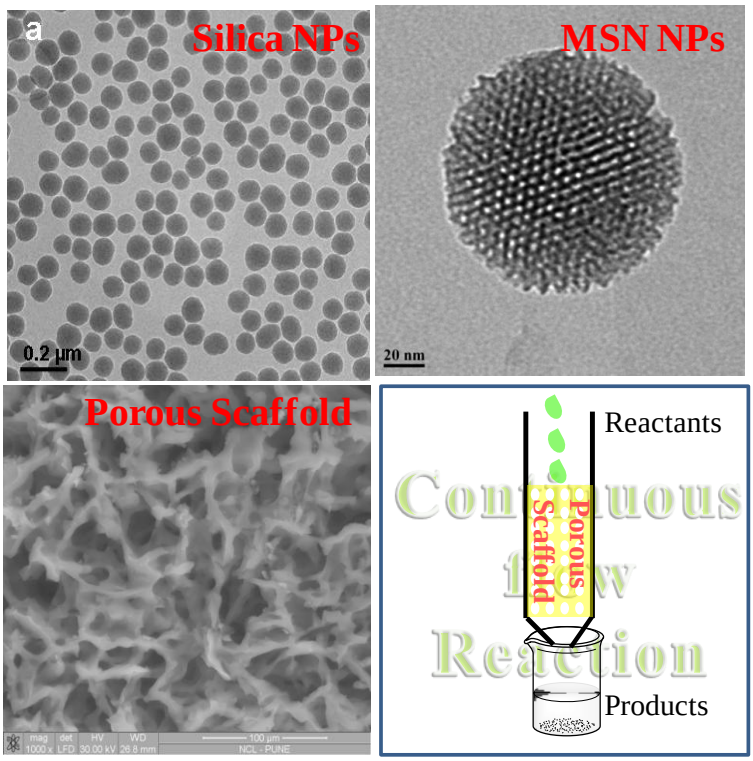

This chapter provides an introduction to the thesis. Salient features of reported synthetic procedures of silica and mesoporous silica and their functionalization procedures are presented. In addition, important aspect of self assembly of functionalized nanoparticles to generate porous network are also discussed. Using this discussion as a back drop, the chapter wise organization of the thesis is presented.

1.1 Introduction:

The enigma of "Life" has been captivating researchers from many different fields. From a chemist's simple perspective, "Life" is a result of many chemical reactions. Researchers actually draw inspiration and try to mimic living systems in their laboratory. A quick look at any "living system" reveals that it is a beautiful arrangement of molecular entities of different length scales in a hierarchical way that draws an optimal performance from every entity involved. The amount of hierarchy necessary for mimicking living systems has been attracting the attention of many people of scientific community. The work carried out as a part of this thesis is one such example where hierarchical materials with increasing amount of complexity were designed and prepared making sure that each material included plays an important and crucial role in its function. These materials were then thoroughly characterized and evaluated for their catalytic activity. The reasons for designing materials with 'catalytic activity' are again inspired by nature.

In this context, living cells represent a perfect chemical factory where nutrients are converted into complex chemical building blocks needed for the cell metabolism.[1,2] In our cells, enzymes happily react with a substrate and then pass the product on to another enzyme to perform the next bit of chemistry. Such examples of multienzymatic systems are observed in numerous biosynthetic pathways such as in polyketide biosysnthesis.[3,4] These metabolic pathways serve as an inspiration for chemists to develop similar synthetic systems so that multistep organic synthesis of a desired compound can be performed in one pot without isolation of the intermediates. However, mimicking the living cell is still a distant goal for synthetic chemists. In this context, a considerable effort has been made to design complex hierarchical system that can carry out sequential reactions.[5]

As we embarked on our journey to create multifunctional hierarchical catalytic system, we identified certain features of the cell that are key for the development of such a complex hierarchical systems.

1. Most of the reaction in a cell is carried out by enzymes which are catalytic in nature.
2. These enzymes keep floating in the milieu of the cell material which is a semi-heterogeneous system.
3. These enzymes are well separated from each other in the system.

4. The product of one enzymatic reaction becomes the substrate of another one.
5. All these are part of a system that stays together.

We identified silica/mesoporous silica as the material that can be modified to incorporate most of the above features. This thesis thus describes our efforts to prepare a multifunctional silica based catalytic system that incorporates most of the above features. We set the stage of this thesis in this chapter by introducing advantages of semi heterogeneous systems, synthesis of organic-inorganic hybrid materials, various techniques available for surface functionalization and different available methodologies for the formation of functionalized porous materials. In that process we also discuss the concept of self-assembly, the methods used for assembly of colloidal nanoparticles, and the various templates/matrices used for colloidal assembly. Finally, this chapter outlines the salient features of the other chapters of this thesis.

1.2 Semi heterogeneous catalysis:

The development of stable, efficient, and selective catalysts is an ongoing research challenge in applied science and involves a multi-disciplinary approach, notably organometallic chemistry and materials science.[6] Catalysis plays an important role in chemical industry. A major part of chemical industry involve products made using catalysts in the field of energy, food, fuels, polymers, textiles, pharma, agrochemicals, detergents, paints, cosmetics, and food additives etc.[7] Catalysis is principally divided into two branches: homogeneous catalysis, when the catalyst is in the same phase as the reaction mixture (typically in liquid phase), and heterogeneous catalysis, where the catalyst stays in a different phase (typically solid/liquid, solid/gas or solid/liquid/gas). Table 1.1 summarizes a comparison between the main features of homogeneous and heterogeneous catalysis.

Feature	Homogeneous Catalysis	Heterogeneous Catalysis
Form	Metal complex	Solid, often metal and metal oxide
Activity	High	Variable
Selectivity	High	Variable
Reaction condition	Mild	Drastic
Problem of diffusion	None	Possible
Recycling	Difficult	Easy
Separation from products	Difficult	Easy
Average time of life	Variable	Long
Sensitivity of poisons	Low	High

Table 1.1: Schematic comparison between homogeneous and heterogeneous catalysis.

In chemical industries, precious metals such as Ir, Pt and Au are routinely being used to carry out important chemical reactions. But their application in industrial processes has been limited due to difficulties of catalyst separation.[8] Thus from the industrial perspective, it is important to develop efficient methodologies for immobilization of metal complexes onto a support. In recent years, a significant amount of research has been performed to design dispersible matrices for catalyst immobilization such as soluble polymers, per fluorinated compound etc.[9-11] This permits reactions to be performed under near homogeneous conditions and also allows catalyst separation after the reaction by methods like centrifugation or precipitation by the addition of another solvent. Such a methodology is very attractive since it combines the best of homogeneous and heterogeneous catalysis.[12] Several dispersible matrices have been explored to date. Nanoparticles have emerged very attractive dispersible matrices for supporting homogeneous organic reactions.[12] They are considered semi-heterogeneous since they readily disperse in many solvents and the high surface area of these particles allows higher catalyst loading capacity than many conventional support matrices leading to an improved catalytic activity. Some of these particles are even amenable to magnetic separation, thus, making catalyst separation very easy. Silica nanoparticles are widely exploited as a solid support due to many advantages over other nanoparticles such as (i) easy functionalization of silica surface using well established silane chemistry, (ii) formation of colloidal dispersions in various solvents, (iii) easy separation by centrifugation, (iv) tunability

of the surface polarity (v) high thermal and oxidative stability and overall (vi) high surface/volume ratio. Thus in this thesis work silica nanopartilcles have been chosen for the construction of materials with different features as explained previously.

1.3 Silica and mesoporous silica nanoparticles as support:

Silicon (27.2 wt %) is the most abundant element in the earth's crust after oxygen (45.5%).[13] Many living organisms produce siliceous structures. For example, plants produce phytoliths, sponges produce spicules and diatoms produce cell walls made-up of silica (Figure 1.1).[14] The patterned silica cell wall of diatoms is synthesized intracellularly by condensation of silicic acid present in water over polyamines or phosphoproteins as templates.[15] Silica is manufactured in several forms including fused quartz, crystal, fumed silica (or pyrogenic silica), colloidal silica, silica gel, aerogel, silica nanoparticles and mesoporous silica particles like SBA-15, MCM-41 etc. Colloidal silica is a suspension of fine amorphous, nonporous, and typically spherical silica nanoparticles in liquid phase. In this thesis we have mainly concentrated on silica and mesoporous silica nanoparticles because of their ability to form stable dispersion in solution. In the following, we will discuss about the strategies for the preparation of silica and mesoporous silica nanoparticles.

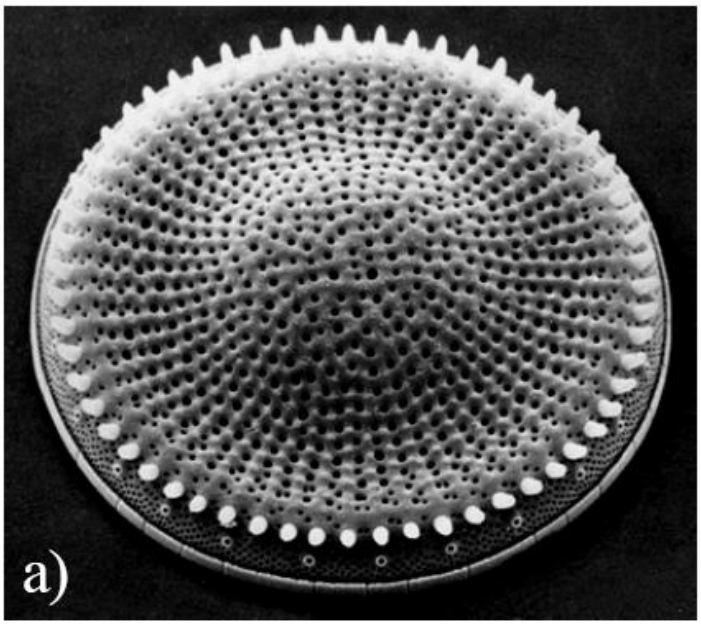

Figure 1.1: SEM image of hierarchical porous structure of cell walls of Diatoms (SEM photo by the late F.E. Round, courtesy of D.G. Mann, Royal Botanic Garden Edinburgh)

1.3.1 Silica nanoparticles:

Two strategies are mainly used for the synthesis of silica nanoparticles: the sol–gel synthesis and reverse microemulsion synthesis.[16] The sol–gel synthesis of monodisperse solid silica particles ranging in size from 50 nm to 2 mm was first reported in 1968 by Stöber and co-workers[17] based on earlier work by G. Kolbe.[18] This method basically involves the controlled hydrolysis and condensation of silica precursors, such as tetraethyl orthosilicate (TEOS), in ethanol using ammonia as a catalyst. In general, the hydrolysis reaction gives the slightly hydrolyzed TEOS monomer (Scheme 1.1, Equation 1). This hydrolyzed intermediate undergoes condensation to eventually form silica as shown in Scheme 1.1 (Scheme 1.1, Equation 2). The resultant particles are stabilized by electrostatic repulsion due to charge imparted by the adsorbed ionic species on silica surface (Scheme 1.2). The size of the particles can be tuned by adjusting the reaction conditions. For example, by varying the TEOS concentration from 0.05 M to 0.67 M and keeping the other reactant conditions constant silica particles from 20 to 880 nm in size can be obtained.[19] Further, by varying the amount of ammonia, different size particles can be obtained as shown in Table 1.2.

$$Si(OR)_4 + H_2O \longrightarrow (RO)_3SiOH + ROH \qquad \text{Equation 1}$$

$$(RO)_3SiOH + H_2O \longrightarrow SiO_2 + 3ROH \qquad \text{Equation 2}$$

Scheme 1.1: Synthesis of Stöber spherical silica particles.

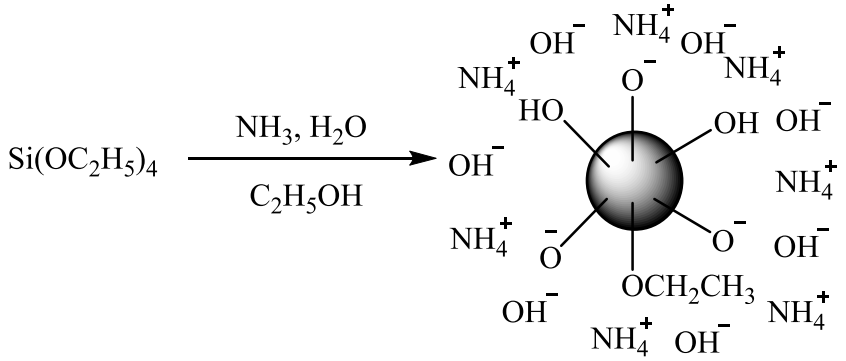

Scheme 1.2: Stabilization of the silica particles.

TEOS (mL)	H_2O (mL)	NH_3 (mL)	Absolute ethanol (mL)	TEOS added after 3 h (mL)	Size of SiO_2 nanopariticles (nm)
1.5	1	1.7	50	1	37.5±1.5
1.5	1	1.8	50	1	51.7±4.7
1.5	1	2	50	1	61.3±4.2
1.5	1	3	50	1	146±6.1
1.5	1	20	50	1	398±10.2

Table 1.2: The size variation silica nanoparticles with different ammonia concentration. (Adapted from Ph.D Thesis of S. Pratap Chandran)

Another common method for the synthesis of monodisperse silica nanoparticles uses reverse phase, or water-in-oil, microemulsions.[20,21] Reverse phase microemulsions are highly tailorable systems that consist of nanometer sized water droplets stabilized by a surfactant in a predominantly organic phase. The micelles in the microemulsion essentially act as ‘‘nanoreactors’’ that assist in controlling the kinetics of particle nucleation and growth. The size and number of micelles within the microemulsion can be tuned by varying the water to surfactant ratio. This method provides greater control over particle size and size-distribution.

1.3.2 Mesoporous silica nanoparticles:

Mesoporous silica particles (pore size 2-50 nm) are attractive as heterogeneous catalysts or catalyst support due to properties such as well-defined crystalline structure, high internal surface area, uniform pore sizes, good thermal stability and highly acidic sites in the protonated form.[22-24] The first synthetic procedure of mesoporous silica was patented around 1970.[25] But because of lack of proper analytical tools, the remarkable features of this product were not recognized.[26] Later the breakthrough came with the discovery of M41S family of mesoporous materials by Mobil Corporation laboratories and was named as Mobil Crystalline Materials, or MCM-41 in the year 1992.[27,28] These particles are typically synthesized using a surfactant templated sol–gel method. Mobil scientists have employed amphiphilic long chain alkyl quaternary ammonium halide surfactant molecules

[$C_nH_{2n+1}(CH_3)_2NX$, X = Cl, Br and n = 8-16] as the structure-directing agent for in situ polymerization of orthosilicic acid (Figure 1.2).[28] The synthesis can be performed either in acidic or basic conditions, and various silica sources such as fumed silica, sodium silicate, or tetra-alkyl oxide of silane can be used. The morphology of the particles could also be varied.[29] MCM-41 type materials possess one dimensional channel with diameters that can be tuned from 2–10 nm.[30] Later works concentrated on the control of the morphology of the particles by manipulation of the pH during synthesis or by the addition of cosolvents.[31, 32]

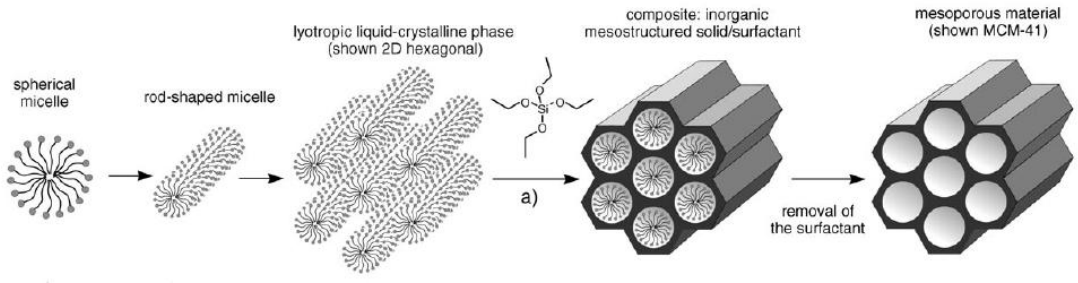

Figure 1.2: Surfactant templated method for the formation of ordered mesoporous silica materials (adapted from reference 23)

A simple and fast alternate route to MCM-41 that leads to uniform nanosized spherical particles (MSNs) was developed by Victor Lin and coworkers.[33,34] Here, the synthesis of MSNs is performed at a low surfactant concentration to make the assembly of the ordered mesophases strongly dependent upon the interaction between the cationic surfactant and the growing anionic oligomers of orthosilicic acid, which in turn limits the assembly of mesophases to small sizes. In the synthetic procedure, the surfactant cetyltrimethyl ammonium bromide (CTAB) is initially dissolved in basic aqueous solution and the mixture is vigorously stirred at elevated temperature. Tetraethylorthosilicate (TEOS) is added, and the solution is kept stirring at an elevated temperature for 2 hrs. After the reaction is complete, the as-synthesized product is filtered and washed with abundant water and methanol. After drying under vacuum, the organic surfactant is removed by either acid wash or calcination. The inorganic silica framework that is left may have a hexagonal, disordered, or cubic pore structure, depending upon the specific synthetic conditions. The diameters of these particles range from 60 to 200 nm. They have been utilized in a variety of applications, including catalysis,[35] drug delivery,[36,37] and imaging.[38]

1.4 Functionalization of silica and mesoporous silica particles:

The applications of pure inorganic siliceous materials are limited because only silanol groups are present on their surface. However, their range of applications can be increased several folds by tailoring the properties of these materials by incorporation of organic functional groups. The enormous functional variation of organic chemistry combined with the advantages of a thermally stable and robust inorganic solid matrix allows the creation of a wide range of novel materials for various applications.[39-42]

1.4.1 Surface functionalization of silica nanoparticles:

The chemical properties of the silica surface are mainly determined by the various silanol and siloxane groups that are present on the external as well as the internal structure. The modification or transformation of surfaces can be achieved by various covalent and physical methods. Physical methods include physisorption of positively charged organic molecules onto the negatively silica nanoparticle surface by electrostatic interaction, weak van der Waal's interaction and dipolar interaction. Covalent attachment of organic moieties to the particle surface is preferred, not only to avoid desorption from the particle surface but also to control the number and orientation of the immobilized organic counterpart. For covalent attachment, the particle surface first needs to be modified with suitable functional groups (e.g., thiol, amine, and carboxyl groups).[43-45] This is typically done by applying a stable additional silica coating (post-coating) that contains the functional group(s) of interest. Silanes with three alkoxy groups are the usual starting point for surface modification (Scheme 1.3). However, other hydrolysable group like acyloxy, halogen or amine were also used as silane coupling agent. For the Stöber nanoparticles, surface modification is usually done after nanoparticle synthesis to avoid potential secondary nucleation. Surface modification of microemulsion nanoparticles can be achieved in the same manner or via direct hydrolysis and co-condensation of TEOS and other organosilanes in the microemulsion solution.[46]

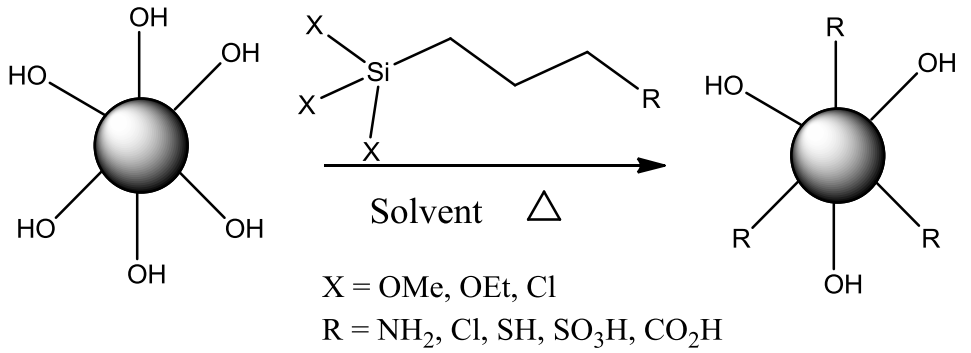

Scheme 1.3: Surface modification of silica nanoparticles.

In addition to the creation of the reactive sites for conjugation with other organic molecules, the functional groups also change the colloidal stability of the particles in solution. For example, postcoating with amine-containing organosilane compounds neutralizes the negative surface charge of nanoparticles at neutral pH and hence reduces the overall charge of the nanoparticles. As a result, colloidal stability decreases and severe particle aggregation takes place in aqueous medium. To solve this problem, inert negatively charged organosilane compounds containing phosphonate or other groups are introduced as a critical dispersing agent during post-coating. Consequently, the nanoparticles possess a net negative charge and are well dispersed in aqueous solution.[47] Other stabilization reagents such as organosilane compounds that contain polyethylene glycol (PEG, a neutral polymer), can also be added to the nanoparticle surface. The PEGylated surface is highly hydrophilic and enhances the aqueous dispersibility of the silica nanoparticles.[48]

After the nanoparticles are modified with different functional groups, they can act as a scaffold for further grafting of organic moieties by means of standard organic chemistry (Scheme 1.4). For example, carboxyl-modified nanoparticles have pendent carboxylic acids, making them suitable for covalent coupling of amine-containing molecules or bio macromolecules via water-soluble carbodiimide reagents.[49] Disulfide-modified compounds can be immobilized onto thiol-functionalized nanoparticles by disulfide-coupling chemistry.[50] Amine-modified nanoparticles can be coupled to a wide variety of organic molecules via succinimidyl esters and iso(thio)cyanates.[51] Recently, numerous examples, where azide functionalized particles are coupled with alkyne terminated organic molecule using Cu(I) catalysed "Click Reaction" have been reported.[52,53]

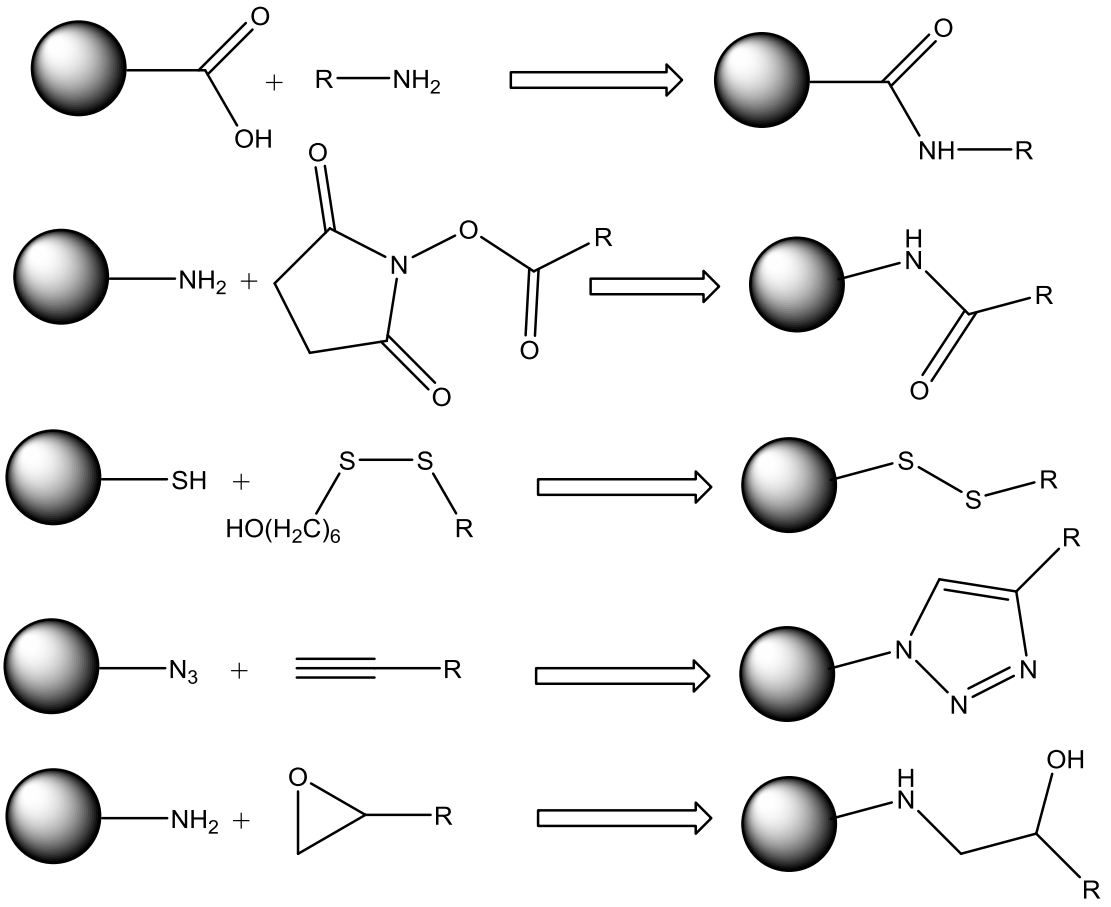

Scheme 1.4: Representative schemes for the attachment of organic molecules onto the surface of silica NPs

1.4.1.1 Mechanism of surface functionalization:

Organosilanes, that are mostly used to prepare functional silica nanoparticles, have one organic substituent and three hydrolysable substituents. In the vast majority of surface treatment applications, the alkoxy groups of the trialkoxysilanes are hydrolyzed to form silanol-containing species. Reaction of these silanes involves four steps (Scheme 1.5). Initially, hydrolysis of the three labile groups occurs followed by condensation of oligomers. The oligomers then hydrogen bond with OH groups of the substrates. Finally, during drying or curing, a covalent linkage is formed with the substrate with concomitant loss of water. Although described sequentially, these reactions can occur simultaneously after the initial hydrolysis step. At the interface, usually only one bond is formed between each silicon of the organosilane and the substrate surface. The two remaining silanol groups are present either in condensed or free form. The R group remains available for covalent reaction or physical interaction

with other phases. Silanes can modify surfaces under anhydrous conditions consistent with monolayer and vapour phase deposition requirements. Extended times (8-16 hrs) at elevated temperatures (70 ^{o}C -120 ^{o}C) are typical.

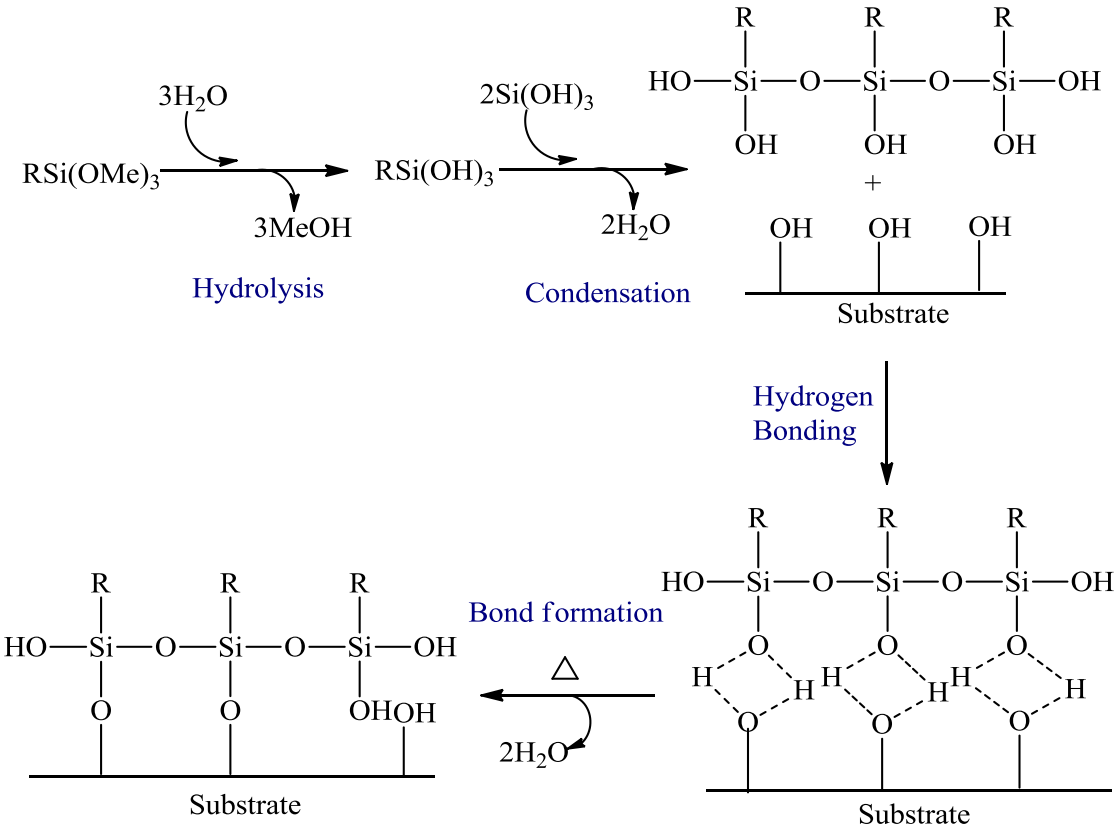

Scheme 1.5: Schematic representation of surface functionalization

1.4.2 Surface functionalization of mesoporous silica nanoparticles (MSNs):

Surface functionalized mesoporous materials have found wide spread applications in catalysis, separation, decontamination, drug delivery and sensor design.[23,54] In literature, mesoporous silica materials functionalized by various organic functional groups including amines,[55,56] thiols,[57] carboxylic acid,[58] sulfonic acid,[59] vinyl[60] and nitrogen based heterocycles[61] have been reported. These organic functional groups present on the surface of mesoporous material have been used to anchor various synthetic catalysts, bio-molecules and polymers to generate novel functional materials. Mesoporous silica nanoparticles (MSNs) can be covalently linked with such organic functional groups using two different synthetic strategies.[23] These are known as post-synthesis modification (also known as grafting) and direct synthesis or co-condensation, as discussed below.

1.4.2.1 Co-Condensation method:

This is one of the most popular methods to synthesize organically functionalized mesoporous silica material. This method is also known as "one pot" co-condensation method. This functionalization method is a direct synthesis method, in which along with TEOS the organoalkoxysilane is introduced into the basic aqueous CTAB solution during the condensation, therefore named the co-condensation functionalization method (Figure 1.3). With this synthetic approach, it is possible to control the morphology of the particles by the addition of functional co-condensing reagents. Victor Lin and coworkers have reported a co-condensation method for incorporating various organic functional groups into the pores of MSN.[36,62] The desired triethoxysilane is condensed into the walls of the MSNs during synthesis of the nanoparticle to lead to uniform incorporation of the organic functionality throughout the particles. The degree of functionalization and the particle size can be modified by adjusting the reagent concentration, size, and the hydrophobicity or hydrophilicity of the co-condensing reagents. The organic functionality can also have a pronounced effect on the pore structure of the nanoparticle. The co-condensing reagents are organo-substituted trialkoxysilanes (organoalkoxysilanes), and their influence on particle morphology depends upon the abilities of their organic groups to stabilize or destabilize the micelles during the formation of the MSN.

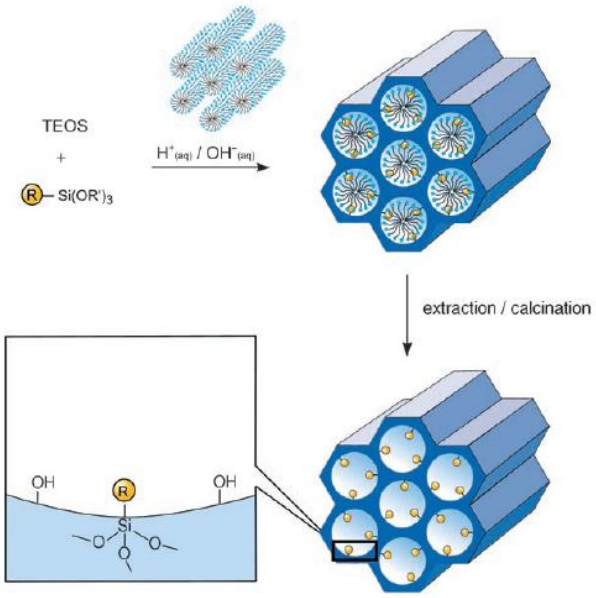

Figure 1.3: Co-condensation method (direct synthesis) for the organic modification of mesoporous silica nanoparticles (adapted from reference 23)

1.4.2.2 Postsynthetic functionalization method ("Grafting"):

Alternatively, as-synthesized MSNs can be functionalized via post-synthesis modification, for example, by reacting MSN nanoparticles with a variety of trialkoxysilanes to effect condensation with the silanol group on the silica surface (Figure 1.4). One advantage of the grafting method is the preservation of the particle morphology and pore structure. Silanols located on the exterior surface and at the openings of the mesopores are kinetically more accessible than silanols located on the interior pore walls. Thus, most organic functional groups that are added to mesoporous materials through this post synthetic grafting method have been shown to be located on the exterior surface or congregated at the mesopore opening. However, this method is particularly advantageous for selectively functionalizing the exterior surface of silica.

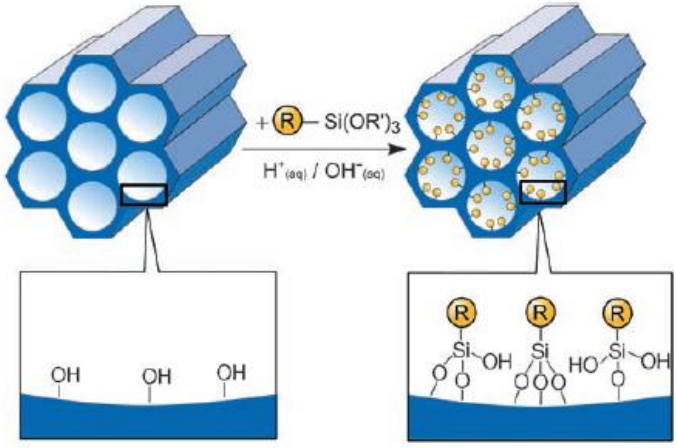

Figure 1.4: Grafting method for the organic modification of mesoporous silica nanoparticles (adapted from reference 23)

1.4.2.3 Selective functionalization of mesoporous silica nanoparticles:

The chemistry of the formation of mesoporous silica nanoparticles allows selective functionalization of the two different surfaces namely outer and inner surface.[63] Selective functionalization of the inner and outer surfaces of MSNs with different trialkoxysilanes offers different functionalities at different sites.[64] Conjugation of MSNs with two different alkoxysilanes can be performed through a two-step surface modification as shown in Scheme 1.6. This method consists of gradual functionalization conducted in several steps. These steps include: a) grafting of selected organic groups on the external surface of the silica containing the template

species necessary to conserve the mesopore; b) removing of the template agent by acidic ethanol extraction; and c) grafting of new and different organic groups inside the pores. The resulting organo-inorganic materials preserve the characteristic structural organization (hexagonally packed arrays) of mesoporous silica, while introducing chemical anisotropy. These unique materials can be used as highly selective molecular adsorbents and catalysts.

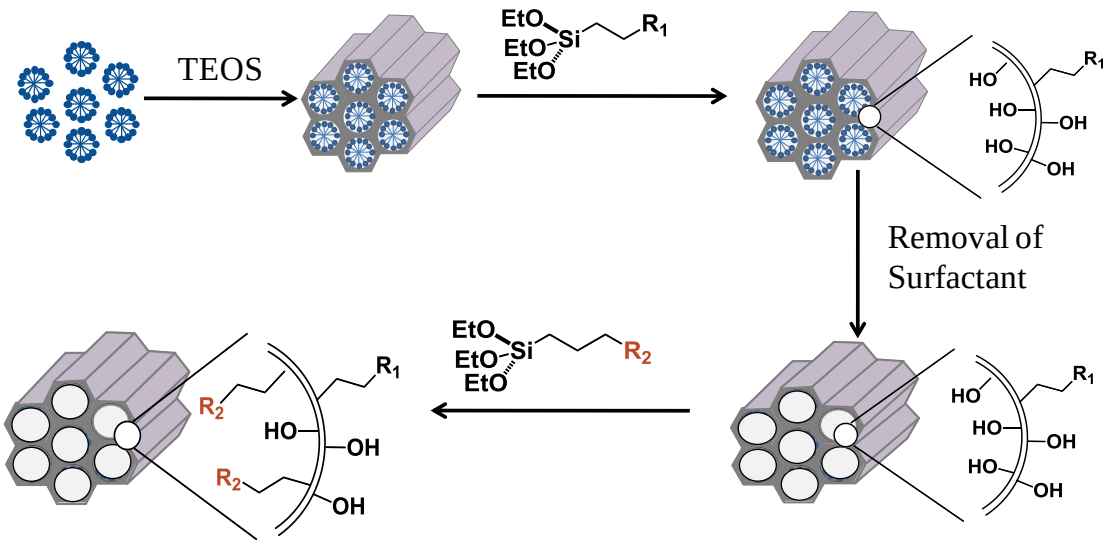

Scheme 1.6: Schematic illustration for the synthesis and selective functionalization of MSNs.

1.5 Assembly of nanoparticles:

Self-assembly of building blocks such as colloids, molecules, polymers, etc. results in formation of structures over larger length scale as compared to the "monomeric" building blocks. In current years, ensembles of inorganic nanoparticles have motivated many researchers because of the possibilities to exploit collective properties of individual nanoparticle and their utilization in functional devices.[65] Assemblies of nanoparticles can be used to improve the mechanical properties of composite materials, and can also allow multiple tasks to be performed simultaneously or in sequence. Self assembled nanoparticulate structures can form through either equilibrium or non-equilibrium routes.[66,67] Common examples of equilibrium self assembly include inorganic crystals, organic crystals and several surfactant/block copolymer microphase separated structures. On the other hand non-

equilibrium systems consist of replication of DNA which is far from equilibrium. Whitesides et. al. proposed that self-assembly of molecules can happen through covalent interactions or through non-covalent forces such as van der Waals, electrostatic, hydrogen bonding and hydrophobic interactions.[67] For the assembly of larger particles (meso or macroscopic objects), several other interactions such as capillarity and external fields such as electric, magnetic and gravitational fields play an important role.

The organizations of nanoparticles to generate self-assembled structures has found various applications[68] in diverse areas such are in photonic,[69] sensing,[70] electronics[71] and drug delivery[72] among others. In addition to having self assembled nanostructures, high porosity is also essential in applications such as, catalysis, sensing, drug delivery, sorption, separation, and tissue engineering.[73,74] Porosity at multiple length scales such as, micropores (< 2 nm), mesopores (2-50 nm) or macropores (>50 nm) are required for many applications.[75] In this thesis, we describe the formation of porous structure by self assembly and therefore restrict ourselves to literature appropriate to these systems.

1.5.1 Strategies to form porous structure:

The desire to construct a material with well defined pores has always been one of the most active areas in materials science engineering, because of its fundamental scientific interest, as well as many modern-day technological applications.[76] Porous materials can have porosity of a single length scale or multiple length scales. It is considered as a hierarchical material if it comprises pores of different orders of length scales viz. micropores, mesopores and macropores. In this context, brief overviews of the different strategies to generate hierarchical porous structure are presented below.

1.5.1.1 Template directed self assembly of colloids:

One of the common methods to prepare hierarchical porous materials is the use of templates. Self-assembled molecular aggregates or supramolecular assemblies are generally employed as the structure-directing agents. Template-assisted self assembly involves use of 1D, 2D or 3D substrates which is having sites for colloidal particle localization. Templated assembly thus gives rise to complex structures

decided by the shape of the template.[77] The formation of structured materials using templates can be summarized as follows: (a) colloidal particles/precursor solution are mixed with the template, (b) the particles occupies the empty spaces/voids or the surface of these templates and organize to form an inverse structure and, (c) the templates are finally removed after fixation, for example, by chemical crosslinking of the colloidal structure. Generally, templates can be classified as soft and hard templates.

Soft templates can typically be removed by controlled heat treatment or by mild dissolution conditions and are usually organic molecules. These include surfactant micelles, amphiphilic copolymers or biological molecules like DNA, virus, proteins among others.[76,78] These templates usually give rise to mesopores in the material after self organization. On the other hand, some large-sized substances, such as colloidal crystals,[79] inorganic salt and ice crystals,[80] mesoporous silica materials like MCM- 41, MCM-48, SBA-15, and porous polycarbonate[81] can be considered as hard templates and are added in the synthesis to direct the creation of macroporous structures. Harsh acid or alkali leaching processes are usually required to remove these hard templates and to generate highly ordered inverse macroporous structures.

The different methods that have been reported for organizing colloids using templates include spray drying,[82] dynamic templating using breath figures[83,84], polymerization induced phase separation,[85,86] and layer by layer assembly[87,88] among others. The different types of templates used for assembling nanoparticles include emulsion droplets,[89,90] vesicles, bubbles, colloidal crystals,[91-94] polymer foams,[95,96] membranes,[97] polymer gels,[98,99] biopolymers, biological templates,[100,101] and liquid crystals among others.

Colloidal crystals, for example, have been used as the template to form inverse replica materials as shown in Figure 1.5. At first, colloidal crystals (dark sphere in Figure 1.5) are mixed with precursor solution or nanoparticles. Removal of crystals leads to formation of three-dimensionally ordered macroporous (3DOM) materials or hollow sphere array of nanoparticles. Many natural inexpensive and environmentally benign biological templates such as bacterial threads,[102] echinoid skeletal plates[103] egg-shell membranes,[104] insect wings,[105] pollen grains,[106] plant leaves,[100] and wood celluloses[107] can be used to form inverse inorganic structures having different morphologies.

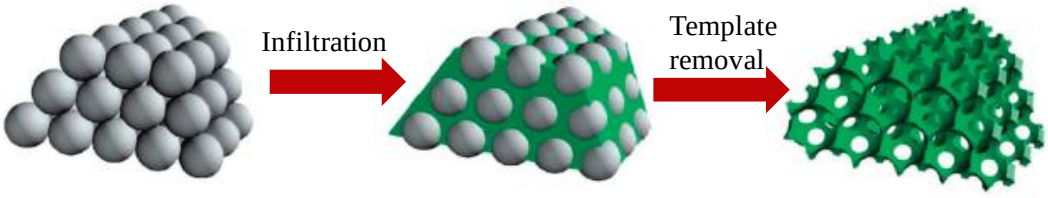

Figure 1.5: Schematic of the colloidal crystal templating process: The template with the structure of an opal (i.e., a close-packed array of uniform spheres) is infiltrated with precursor material. Processing and template removal produce the inverted structure.

Recently, ice-segregation-induced self-assembly (ISISA) processes for the preparation of materials with highly sophisticated porous structures has also been reported.[80] This method has been be used to generate porous structures made of polymer–inorganic nanocomposites and silica honeycomb structure.

Block copolymers are also used as templates as they spontaneously self assemble by segregation of chemically different blocks into a range of morphologies such as, spherical micelles, vesicles, cylindrical, lamellae, gyroid, etc.[108] The spacing between micro-domains in block copolymers entirely depends on molecular weight and chain length of the homopolymers.[109] Thus it is possible to tune spatial organization of colloids by either using different morphologies or copolymer compositions.[110]

Use of surfactant micelles and liquid crystals as a templating agent are one of the most important routes for organization of colloids.[67,111] Liquid crystals (LCs) are matter in a state that has properties in between conventional liquid and solid crystal. The formation of mesoporous silica nanoparticles, which is already discussed in the previous section, is also an example of templating surfactant micelles. In this thesis work, we have assembled nanoparticles using surfactant as a template.

1.5.1.1.1 Surfactant:

Surfactants are compounds that lower the surface tension of a liquid. They are amphiphilic in nature, containing both hydrophobic tail and hydrophilic head groups.[112] Surfactant molecules can be classified depending on the charge of the head group. There are three classes of surfactant molecules: cationic, anionic, and non-ionic surfactants. A cationic surfactant will have a hydrophobic tail group and

positively charged head group. Anionic surfactants include sulfates, sulfonates, carboxylates and phosphates, which are attached to a hydrophobic tail group. Another important category of surfactants include non-ionic surfactant. Here polar head group is uncharged and mostly contains of hydrophilic groups like polyoxyethers or polyhydroxyls. The most popular among the polyoxyether surfactants are fatty alcohol ethoxylates also referred to as C_nE_m, where C represents the hydrophobic carbon chain and E is the polyoxyethylene hydrophilic part (n is generally above 5 while m typically varies between 2-20). The most important characteristic of C_nE_m surfactants that distinguishes them from ionic surfactant is that they are unaffected by the presence of electrolytes or change in pH.

1.5.1.1.2 Assemblies of surfactant:

Surfactant forms micelles above the Kraft temperature.[112] The minimum concentration to form micelles is known as critical micelle concentration (CMC). After reaching the cmc, any added surfactant is incorporated into micelles. At high concentrations, surfactants are also known to form liquid crystalline phases. This liquid crystalline behaviour arises due to collective orientation of ordered surfactant aggregates in a specific direction. These surfactant aggregates that form liquid crystalline structures are having much larger length scale than the size of surfactant molecules.

The shape of a micelle depends on the chemical structure of the surfactant molecule. The packing parameter (g), as proposed by Israelachvili et. al. can be used to explain why certain liquid crystals form in solution. [112] The packing parameter is defined as $g = v_o/(a_e l_o)$, where v_o is the volume of the hydrophobic tail, a_e is the equilibrium area of the head group on the micelle surface, and l_o is the chain length of the tail. Table 1.3 comprises how the packing parameter is related to the typical shape of the micelle. Low values of g indicate that the interface between the micelle and solution is highly curved, whereas higher values mean the interface is less curved. As the g value increases, spherical, rod-like, and disc-like micelles are found in solution (Figure 1.6). The value $g > 1$ indicates reverse miceller structure which means water in oil aggregated structures.

$g = v_o/(a_e l_o)$	0-0.33	0.33-0.5	0.5-1	>1
Micelle shape	Spherical micelles	Cylindrical micelles	Flat bilayers or Lamellar micelles	Inverted spherical or cylindrical micelles
Phase changes upon increasing surfactant concentration	Cubic(I) to 2D hex. to cubic (V_1) to lamellar	2D hex. to cubic (V_1) to lamellar	Lamellar or cubic (V_1) to lamellar	Lamellar

Tables 1.3: Values of g and the resultant surfactant aggregate morphologies

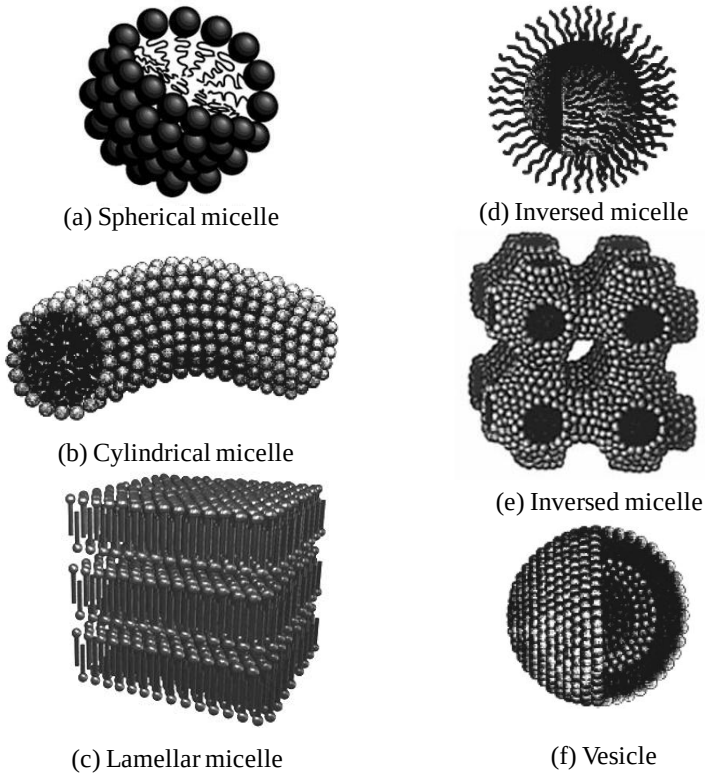

Figure 1.6: Different structures formed by surfactants w.r.t. temperature and concentration change.

The value of packing parameter (g) is also a function of surfactant concentration. Micelles often transform from spherical aggregates to other geometries for example, long rod- or thread-like micelles, or into bilayers with increase in surfactant concentration. The relation of the molecular packing parameter with the micellar aggregate architecture and resultant mesophase structure is shown in Figure 1.7. Upon further increase in surfactant concentration, surfactant aggregates form ordered lattices. For example, cylindrical micelles can pack to form ordered hexagonal structure. These ordered assemblies such as lamellar and hexagonal

assemblies exhibit liquid crystalline properties. The length scale in these liquid crystals is given by the average micellar spacing and spans from 1nm to 100 nm. Thus, such states are also known as mesophases.

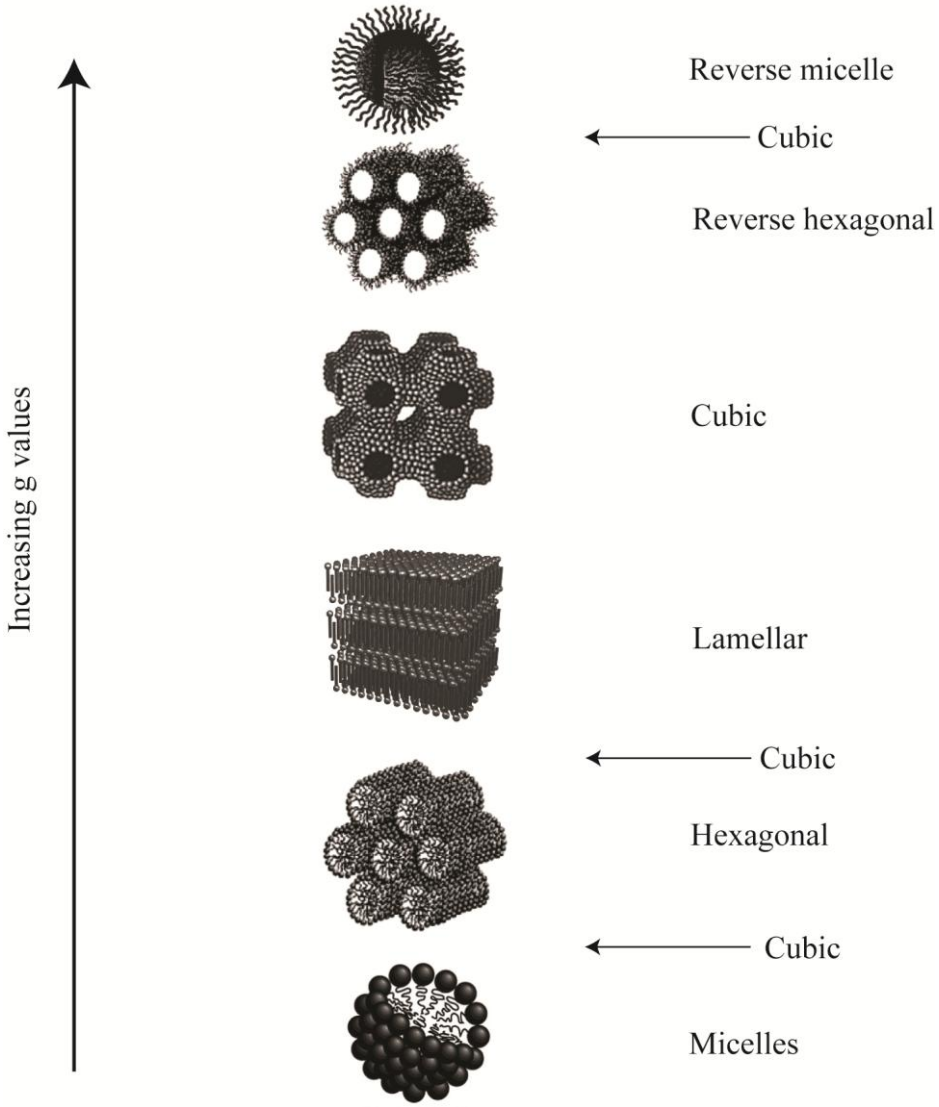

Figure 1.7: Different types of mesophases formed by changing the value of g by varying temperature or concentration of surfactant.

1.5.1.1.3 Surfactant assemblies as template to create porous structure:

Surfactant mesophases can also be used as templates to confine reactants within nanometer-sized domains. The liquid crystalline mesophase partitions space into hydrophilic and hydrophobic regions. Because of this the hydrophilic and hydrophobic reactants segregate into corresponding regions. Attard et al. reported the use of non-ionic surfactant mesophase to template the formation of silica by the condensation of tetramethyl orthosilicate (TMOS).[113] A mixture of $C_{12}E_8/H_2O$/TMOS

was used to form a hexagonal mesophase (H_1), and the TMOS was hydrolyzed and condensed within this under acidic conditions to form silica. This composite was calcined to remove the surfactant resulting in an ordered hexagonal silica structure having pores size in the order of nm. Similarly ordered silica structures were formed by using lamellar phase of another surfactant, $C_{16}E_8$. After that, a significant advancement has happened to form various kinds of porous silica structure using liquid crystals of surfactant assemblies.[114-116] Recently, Guruswamy et. al. demonstrated the formation of macroporous silica materials using templating of non-ionic surfactant $C_{12}E_9$.[117] The silica nanoparticles are assembled using dynamic templating of surfactant hexagonal domains to generate a network of nano particulate strands. Dispersed particles (>10 nm), independent of particle chemistry, assemble into networks, when the surfactant matrix cools into the hexagonal phase. After removal of surfactant, a macroporous material can be accessed.[118]

1.5.1.2 Multiple templating approach to generate hierarchical porous materials:

Hierarchically porous materials can be generated by using multiple structure directing templates to form micro or mesopores in combination with larger pores.[119,120] A common approach to the synthesis of hierarchically porous materials employs macroscopic templates around which mesoporous inorganics are condensed. For example, early attempts to prepare meso/macroporous materials involved synthesis of mesoporous silica around sacrificial polymer lattices. Ordered macroporous structures have been obtained by synthesizing micro or mesoporous structures around polymer colloidal crystals, or using the breath figure technique. More complex morphologies, like non-spherical macropores have been formed by using salt crystals as templates, or by combination with top-down techniques such as micromolding. Emulsions and foams have also been employed as templates for the synthesis of hierarchically porous materials. There are also reports on controlled phase separation of porogens to generate macroporosity.

Hierarchically porous materials can also be generated by starting with preformed micro- or mesoporous particles and assembling these so as to generate macroporosity. For example, meso/macroporous materials were formed by cross linking surface functionalized mesoporous silica particles around triblock copolymer assemblies.[121] Controlled freezing of silica microsphere dispersions has also been

employed to produce hierarchically porous materials. Recently, a route that embedded polymer "protected" functionalized mesoporous silica particles in a porous silica matrix was also reported.[122]

1.6 Physico-chemical characterization:

The functionalized inorganic–organic hybrid silica and mesoporous silica nanoparticles can be characterized by various techniques, which provide important information about size, shape, morphology and surface properties of the hybrid particles. In this section, a brief discussion of various characterization techniques related to self assembly and particle characterization of silica and mesoporous silica nanoparticles has been documented.

Scanning electron microscopy (SEM) and transmission electron microscopy (TEM) are important techniques for characterization of size and morphology of silica and mesoporous silica particles. From high resolution transmission electron microscopy (HRTEM) the size of the mesopore could be easily determined.

Powder X-ray diffraction is the most commonly used tool to identify and measure the uniqueness of structure, phase purity, degree of crystallinity and unit cell parameters of mesoporous silica materials. The mesoporous silica materials exhibit characteristic high intensity peaks in the low angle region between $2\theta = 0.5\text{-}10^{o}$.

Fourier transform infrared (FTIR) spectroscopy is widely used for characterizing silica materials. In the case of porous silicates, the FTIR spectra in the 400–1300 cm^{-1} region provides information about the structural details. For example, peaks at 466, 800, 1070 and 1220 cm^{-1} are typical of Si-O-Si bands that are associated with formation of silica framework. After functionalization characteristic peaks of the organic molecules grafted onto the surface are generated.

Thermo gravimetric analysis or TGA is a technique in which the weight loss of a sample is studied with increasing temperature. It is widely used for studying the weight percentage of templates in mesoporous material synthesis and to estimate the organic /inorganic contents in modified mesoporous materials.

Gas adsorption-desorption studies are one of the widely used technique for determining the surface area, pore size, pore volume and pore size distribution of porous solid materials. By this technique, the amount of gas adsorbed by a solid is measured, which in turn is directly related to the porous properties and pore structure

of the material. Surface area is estimated from the Brauner-Emmett-Teller (BET) equation, based on monolayer adsorption of gases.

^{29}Si and ^{13}C Cross Polarization Magic Angle Spinning (CPMAS) NMR experiments are utilized to confirm the structure of the organic group present on the surface. ^{29}Si solid-state NMR allows us to distinguish silicon atoms involved in siloxane bridges (Q_4), single silanol (Q_3) and geminal silanol groups (Q_2) on the surface of silica. ^{13}C solid-state NMR determines the number of carbon groups present on the surface.

X-ray Photoelectron spectroscopy (XPS) can be used to study the chemical composition and its probable oxidation state present on the silica surface.

1.7 Outline of the thesis:

This thesis is divided into six chapters with proper references at the end of each chapter.

Chapter 1: A comprehensive review of literature on silica and mesoporous silica nanoparticles: method of synthesis, hybrid inorganic-organic mesoporous materials, methods and mechanism of surface modification with organic functional groups is provided. A brief introduction of different self assembling techniques to make hierarchical porous material is also summarized in this chapter.

Chapter 2: As a first step towards our desire to create multifunctional materials, creation of anchoring groups for catalyst immobilization on silica surface is attempted in this chapter. Specifically, a molecular hook has been created using "Click Chemistry" on the surface of silica nanoparticles. An example of immobilization of metal ion has been demonstrated using Au ion. These materials have been characterized by various techniques such as TEM, Thermo gravimetric analysis, IR, ^{13}C and ^{29}Si solid state NMR spectroscopy and XPS etc. The resulting composite material has been used as a catalyst to carry out Hashmi's phenol synthesis – a reaction in which Au(III) activates a terminal alkyne to isomerize o-alkynylfurans to phenols. Efforts were made to understand the fate of the catalyst using XPS analysis.

Chapter 3: This chapter discusses the immobilization of two catalysts on solid support to study tandem reactions. To prove this concept, a metal nanoparticle, Au in our case, has been put inside mesoporous silica nanoparticles to result in core-shell architecture. The other catalyst, an enzyme named glucosidase has been grafted on

silica surface. The catalytic activity of glucosidase grafted Au@mSiO_2 on 4-nitrophenyl-β-glucopyranoside, where glucosidase will catalyse the 1st step to generate 4-nitrophenol, which acts as a substrate for the next reduction step which is catalysed by the Au nanoparticles present inside the mesoporous silica shell was studied using UV Spectroscopy in detail.

Chapter 4: This chapter describes about the selective functionalization of mesoporous silica nanoparticles. The hydrophobicity and hydrophilicity of the inner and outer surface of the mesoporous silica nanoparticles have been tuned. Hydrophilic PEG group was grafted outside the surface of mesoporous silica nanoparticles, whereas the inner surface was functionalized with methyl groups. These materials have been characterized by various analytical techniques.

Chapter 5: The functionalized mesoporous nanoparticles were assembled into free-standing hierarchical materials using dynamic templating of surfactant hexagonal domains, a facile general technique to organize nanoparticles into a network of particulate strands and obtain self-standing structures. The controllable tuning over nanoparticle mesoporosity and scaffold macroporosity has been demonstrated. The spatial variation of macropore along the 3D scaffold has been shown. These materials have been characterized by various analytical techniques such as powder XRD, SEM, TEM, FT-IR, optical microscopy and nitrogen adsorption-desorption experiments. In the latter part of this chapter, the preparation of a catalyst embedded scaffold has been described and its catalytic activity was studied for five cycles.

Chapter 6: This chapter presents an overall summary of the work done and describes the major findings of the studies. Future directions based on the work reported in the thesis are also discussed.

1.8 References:

1. Chi, Y.; Scroggins, S. T.; Frèchet, J. M. J., One-Pot Multi-Component Asymmetric Cascade Reactions Catalyzed by Soluble Star Polymers with Highly Branched Non-Interpenetrating Catalytic Cores. *Journal of the American Chemical Society*, **2008**, 130, (20), 6322-6323.

2. Vriezema, D. M.; Garcia, P. M. L.; Sancho Oltra, N.; Hatzakis, N. S.; Kuiper, S. M.; Nolte, R. J. M.; Rowan, A. E.; van Hest, J. C. M., Positional Assembly of Enzymes in Polymersome Nanoreactors for Cascade Reactions. *Angewandte Chemie International Edition*, **2007**, 46, (39), 7378-7382.

3. Staunton, J.; Wilkinson, B., Biosynthesis of Erythromycin and Rapamycin. *Chemical Reviews*, **1997**, 97, (7), 2611-2630.

4. Khosla, C., Harnessing the Biosynthetic Potential of Modular Polyketide Synthases. *Chemical Reviews*, **1997**, 97, (7), 2577-2590.

5. Wasilke, J.-C.; Obrey, S. J.; Baker, R. T.; Bazan, G. C., Concurrent Tandem Catalysis. *Chemical Reviews*, **2005**, 105, (3), 1001-1020.

6. Hagen, J., *Industrial Catalysis: A practical Approach*. 2nd Edition; Wiley-VCH: **2006**.

7. Dal Santo, V.; Liguori, F.; Pirovano, C.; Guidotti, M., Design and Use of Nanostructured Single-Site Heterogeneous Catalysts for the Selective Transformation of Fine Chemicals. *Molecules*, **2010**, 15, (6), 3829-3856.

8. Mueller, C.; Vogt, D., Immobilization and compartmentalization of homogeneous catalysts. *Handb. Green Chem.: Green Catal.* **2009**, 1, 127-152.

9. Madhavan, N.; Jones, C. W.; Weck, M., Rational approach to polymer-supported catalysts: Synergy between catalytic reaction mechanism and polymer design. *Accounts of Chemical Research*, **2008**, 41, (9), 1153-1165.

10. Pagliaro, M.; Ciriminna, R., New fluorinated functional materials. *Journal of Materials Chemistry*, **2005**, 15, (47), 4981-4991.

11. Dickerson, T. J.; Reed, N. N.; Janda, K. D., Soluble polymers as scaffolds for recoverable catalysts and reagents. *Chemical Reviews*, **2002**, 102, (10), 3325-3344.

12. Astruc, D.; Lu, F.; Aranzaes, J. R., Nanoparticles as recyclable catalysts: The frontier between homogeneous and heterogeneous catalysis. *Angewandte Chemie - International Edition*, **2005**, 44, (48), 7852-7872.

13. Greenwood, N. N.; Earnshaw, A., *Chemistry of the elements*. 2nd Edition; 1995.

14. Mock, T.; Samanta, M. P.; Iverson, V.; Berthiaume, C.; Robison, M.; Holtermann, K.; Durkin, C.; BonDurant, S. S.; Richmond, K.; Rodesch, M.; Kallas, T.; Huttlin, E. L.; Cerrina, F.; Sussman, M. R.; Armbrust, E. V., Whole-genome expression profiling of the marine diatom Thalassiosira pseudonana identifies genes involved in silicon bioprocesses. *Proceedings of the National Academy of Sciences*, **2008**, 105, (5), 1579-1584.

15. Pohnert, G., Biomineralization in Diatoms Mediated through Peptide- and Polyamine-Assisted Condensation of Silica. *Angewandte Chemie International Edition*, **2002**, 41, (17), 3167-3169.

16. Wang, L.; Zhao, W.; Tan, W., Bioconjugated silica nanoparticles: Development and applications. *Nano Research*, **2008**, 1, (2), 99-115.

17. Stöber, W.; Fink, A.; Bohn, E., Controlled growth of monodisperse silica spheres in the micron size range. *Journal of Colloid and Interface Science*, **1968**, 26, (1), 62-69.

18. Kolbe, G., *PhD thesis*, Jena, Germany. **1956**.

19. Wang, X.-D.; Shen, Z.-X.; Sang, T.; Cheng, X.-B.; Li, M.-F.; Chen, L.-Y.; Wang, Z.-S., Preparation of spherical silica particles by Stöber process with high concentration of tetra-ethyl-orthosilicate. *Journal of Colloid and Interface Science*, **2010**, 341, (1), 23-29.

20. Rieter, W. J.; Kim, J. S.; Taylor, K. M. L.; An, H.; Lin, W.; Tarrant, T.; Lin, W., Hybrid Silica Nanoparticles for Multimodal Imaging. *Angewandte Chemie International Edition*, **2007**, 46, (20), 3680-3682.

21. Arriagada, F. J.; Osseo-Asare, K., Synthesis of Nanosize Silica in a Nonionic Water-in-Oil Microemulsion: Effects of the Water/Surfactant Molar Ratio and Ammonia Concentration. *Journal of Colloid and Interface Science*, **1999**, 211, (2), 210-220.

22. Wan, Y.; Zhao, On the Controllable Soft-Templating Approach to Mesoporous Silicates. *Chemical Reviews*, **2007**, 107, (7), 2821-2860.

23. Hoffmann, F.; Cornelius, M.; Morell, J.; Fröba, M., Silica-Based Mesoporous Organic–Inorganic Hybrid Materials. *Angewandte Chemie International Edition*, **2006**, 45, (20), 3216-3251.

24. Stein, A.; Melde, B. J.; Schroden, R. C., Hybrid Inorganic–Organic Mesoporous Silicates-Nanoscopic Reactors Coming of Age. *Advanced Materials*, **2000**, 12, (19), 1403-1419.

25. Chiola, V.; Ritsko, J. E.; Vanderpool, C. D., Process for producing low-bulk density silica. *Application No. US 3556725D A filed on 26-Feb-1969; Publication No. US 3556725 A* 1971.

26. Di Renzo, F.; Cambon, H.; Dutartre, R., A 28-year-old synthesis of micelle-templated mesoporous silica. *Microporous Materials*, **1997**, 10, (4-6), 283-286.

27. Kresge, C. T.; Leonowicz, M. E.; Roth, W. J.; Vartuli, J. C.; Beck, J. S., Ordered mesoporous molecular sieves synthesized by a liquid-crystal template mechanism. *Nature*, **1992**, 359, 710-712.

28. Beck, J. S.; Vartuli, J. C.; Roth, W. J.; Leonowicz, M. E.; Kresge, C. T.; Schmitt, K. D.; Chu, C. T. W.; Olson, D. H.; Sheppard, E. W., A new family of mesoporous molecular sieves prepared with liquid crystal templates. *Journal of the American Chemical Society*, **1992**, 114, (27), 10834-10843.

29. Sadasivan, S.; Khushalani, D.; Mann, S., Synthesis and shape modification of organo-functionalised silica nanoparticles with ordered mesostructured interiors. *Journal of Materials Chemistry*, **2003**, 13, (5), 1023-1029.

30. Bagwe, R. P.; Yang, C.; Hilliard, L. R.; Tan, W., Optimization of Dye-Doped Silica Nanoparticles Prepared Using a Reverse Microemulsion Method. *Langmuir*, **2004**, 20, (19), 8336-8342.

31. Grűn, M.; Unger, K. K.; Matsumoto, A.; Tsutsumi, K., Novel pathways for the preparation of mesoporous MCM-41 materials: control of porosity and morphology. *Microporous and Mesoporous Materials*, **1999**, 27, (2-3), 207-216.

32. Cai, Q.; Luo, Z.-S.; Pang, W.-Q.; Fan, Y.-W.; Chen, X.-H.; Cui, F.-Z., Dilute Solution Routes to Various Controllable Morphologies of MCM-41 Silica with a Basic Medium. *Chemistry of Materials*, **2001**, 13, (2), 258-263.

33. Huh, S.; Wiench, J. W.; Yoo, J.-C.; Pruski, M.; Lin, V. S. Y., Organic Functionalization and Morphology Control of Mesoporous Silicas via a Co-Condensation Synthesis Method. *Chemistry of Materials*, **2003**, 15, (22), 4247-4256.

34. Trewyn, B. G.; Slowing, I. I.; Giri, S.; Chen, H.-T.; Lin, V. S. Y., Synthesis and Functionalization of a Mesoporous Silica Nanoparticle Based on the Sol-Gel Process

and Applications in Controlled Release. *Accounts of Chemical Research*, **2007**, 40, (9), 846-853.

35. Chen, H.-T.; Huh, S.; Wiench, J. W.; Pruski, M.; Lin, V. S. Y., Dialkylaminopyridine-Functionalized Mesoporous Silica Nanosphere as an Efficient and Highly Stable Heterogeneous Nucleophilic Catalyst. *Journal of the American Chemical Society*, **2005**, 127, (38), 13305-13311.

36. Slowing, I.; Trewyn, B. G.; Lin, V. S. Y., Effect of Surface Functionalization of MCM-41-Type Mesoporous Silica Nanoparticles on the Endocytosis by Human Cancer Cells. *Journal of the American Chemical Society*, **2006**, 128, (46), 14792-14793.

37. Slowing, I. I.; Trewyn, B. G.; Lin, V. S. Y., Mesoporous Silica Nanoparticles for Intracellular Delivery of Membrane-Impermeable Proteins. *Journal of the American Chemical Society*, **2007**, 129, (28), 8845-8849.

38. Taylor, K. M. L.; Kim, J. S.; Rieter, W. J.; An, H.; Lin, W.; Lin, W., Mesoporous Silica Nanospheres as Highly Efficient MRI Contrast Agents. *Journal of the American Chemical Society*, **2008**, 130, (7), 2154-2155.

39. Kesanli, B.; Lin, W., Mesoporous silica anchored Ru catalysts for highly enantioselective hydrogenation of [small beta]-ketoesters. *Chemical Communications*, **2004**, 0, (20), 2284-2285.

40. Terry, T. J.; Stack, T. D. P., Covalent Heterogenization of a Discrete Mn(II) Bis-Phen Complex by a Metal-Template/Metal-Exchange Method: An Epoxidation Catalyst with Enhanced Reactivity. *Journal of the American Chemical Society*, **2008**, 130, (14), 4945-4953.

41. Schiel, J. E.; Mallik, R.; Soman, S.; Joseph, K. S.; Hage, D. S., Applications of silica supports in affinity chromatography. *Journal of Separation Science*, **2006**, 29, (6), 719-737.

42. Nozawa, K.; Osono, C.; Sugawara, M., Biotinylated MCM-41 channels as a sensing element in planar bilayer lipid membranes. *Sensors and Actuators B: Chemical*, **2007**, 126, (2), 632-640.

43. Soto-Cantu, E.; Cueto, R.; Koch, J.; Russo, P. S., Synthesis and Rapid Characterization of Amine-Functionalized Silica. *Langmuir*, **2012**, 28, (13), 5562-5569.

44. Moller, K.; Kobler, J.; Bein, T., Colloidal suspensions of mercapto-functionalized nanosized mesoporous silica. *Journal of Materials Chemistry*, **2007**, 17, (7), 624-631.

45. An, Y.; Chen, M.; Xue, Q.; Liu, W., Preparation and self-assembly of carboxylic acid-functionalized silica. *Journal of Colloid and Interface Science*, **2007**, 311, (2), 507-513.

46. Chen, S.; Sui, J.; Chen, L.; Pojman, J. A., Polyurethane–nanosilica hybrid nanocomposites synthesized by frontal polymerization. *Journal of Polymer Science Part A: Polymer Chemistry*, **2005**, 43, (8), 1670-1680.

47. Santra, S.; Yang, H.; Dutta, D.; Stanley, J. T.; Holloway, P. H.; Tan, W.; Moudgil, B. M.; Mericle, R. A., TAT conjugated, FITC doped silica nanoparticles for bioimaging applications. *Chemical Communications*, **2004**, 0, (24), 2810-2811.

48. Zheng, M.; Davidson, F.; Huang, X., Ethylene Glycol Monolayer Protected Nanoparticles for Eliminating Nonspecific Binding with Biological Molecule. *Journal of the American Chemical Society*, **2003**, 125, (26), 7790-7791.

49. Qhobosheane, M.; Santra, S.; Zhang, P.; Tan, W., Biochemically functionalized silica nanoparticles. *Analyst*, **2001**, 126, (8), 1274-1278.

50. Hilliard, L. R.; Zhao, X.; Tan, W., Immobilization of oligonucleotides onto silica nanoparticles for DNA hybridization studies. *Analytica Chimica Acta*, **2002**, 470, (1), 51-56.

51. Xiao, S.-J.; Brunner, S.; Wieland, M., Reactions of Surface Amines with Heterobifunctional Cross-Linkers Bearing Both Succinimidyl Ester and Maleimide for Grafting Biomolecules. *The Journal of Physical Chemistry B*, **2004**, 108, (42), 16508-16517.

52. Nandivada, H.; Jiang, X.; Lahann, J., Click Chemistry: Versatility and Control in the Hands of Materials Scientists. *Advanced Materials*, **2007**, 19, (17), 2197-2208.

53. Nebhani, L.; Barner-Kowollik, C., Orthogonal Transformations on Solid Substrates: Efficient Avenues to Surface Modification. *Advanced Materials*, **2009**, 21, (34), 3442-3468.

54. Vallet-Regí, M.; Balas, F.; Arcos, D., Mesoporous Materials for Drug Delivery. *Angewandte Chemie International Edition*, **2007**, 46, (40), 7548-7558.

55. Wang, X.; Lin, K. S. K.; Chan, J. C. C.; Cheng, S., Preparation of ordered large pore SBA-15 silica functionalized with aminopropyl groups through one-pot synthesis. *Chemical Communications*, **2004**, 0, (23), 2762-2763.

56. Wang, X.; Lin, K. S. K.; Chan, J. C. C.; Cheng, S., Direct Synthesis and Catalytic Applications of Ordered Large Pore Aminopropyl Functionalized SBA-15 Mesoporous Materials. *The Journal of Physical Chemistry B*, **2005**, 109, (5), 1763-1769.

57. Wei, Q.; Nie, Z.; Hao, Y.; Chen, Z.; Zou, J.; Wang, W., Direct synthesis of thiol-ligands-functionalized SBA-15: Effect of 3-mercaptopropyltrimethoxysilane concentration on pore structure. *Materials Letters*, **2005**, 59, (28), 3611-3615.

58. Yang, C.-m.; Zibrowius, B.; Schuth, F., A novel synthetic route for negatively charged ordered mesoporous silica SBA-15. *Chemical Communications*, **2003**, 0, (14), 1772-1773.

59. Marschall, R.; Rathousky, J.; Wark, M., Ordered Functionalized Silica Materials with High Proton Conductivity. *Chemistry of Materials*, **2007**, 19, (26), 6401-6407.

60. Wei, Q.; Chen, H.-Q.; Nie, Z.-R.; Hao, Y.-L.; Wang, Y.-L.; Li, Q.-Y.; Zou, J.-X., Preparation and characterization of vinyl-functionalized mesoporous SBA-15 silica by a direct synthesis method. *Materials Letters*, **2007**, 61, (7), 1469-1473.

61. Li, J.; Qi, T.; Wang, L.; Liu, C.; Zhang, Y., Synthesis and characterization of imidazole-functionalized SBA-15 as an adsorbent of hexavalent chromium. *Materials Letters*, **2007**, 61, (14-15), 3197-3200.

62. Huh, S.; Wiench, J. W.; Trewyn, B. G.; Song, S.; Pruski, M.; Lin, V. S. Y., Tuning of particle morphology and pore properties in mesoporous silicas with multiple organic functional groups. *Chemical Communications*, **2003**, 0, (18), 2364-2365.

63. Kecht, J.; Schlossbauer, A.; Bein, T., Selective Functionalization of the Outer and Inner Surfaces in Mesoporous Silica Nanoparticles. *Chemistry of Materials*, **2008**, 20, (23), 7207-7214.

64. de Juan, F.; Ruiz-Hitzky, E., Selective Functionalization of Mesoporous Silica. *Advanced Materials*, **2000**, 12, (6), 430-432.

65. Nie, Z.; Petukhova, A.; Kumacheva, E., Properties and emerging applications of self-assembled structures made from inorganic nanoparticles. *Nature Nanotechnology*, **2010**, 5, 15-25.

66. Grzybowski, B. A.; Wilmer, C. E.; Kim, J.; Browne, K. P.; Bishop, K. J. M., Self-assembly: from crystals to cells. *Soft Matter*, **2009**, 5, (6), 1110-1128.

67. Whitesides, G. M.; Grzybowski, B., Self-Assembly at All Scales. *Science*, **2002**, 295, (5564), 2418-2421.

68. Velev, O. D.; Gupta, S., Materials Fabricated by Micro- and Nanoparticle Assembly – The Challenging Path from Science to Engineering. *Advanced Materials*, **2009**, 21, (19), 1897-1905.

69. Jain, P. K.; Eustis, S.; El-Sayed, M. A., Plasmon Coupling in Nanorod Assemblies: Optical Absorption, Discrete Dipole Approximation Simulation, and Exciton-Coupling Model. *The Journal of Physical Chemistry B*, **2006**, 110, (37), 18243-18253.

70. Sudeep, P. K.; Joseph, S. T. S.; Thomas, K. G., Selective Detection of Cysteine and Glutathione Using Gold Nanorods. *Journal of the American Chemical Society*, **2005**, 127, (18), 6516-6517.

71. Tseng, R. J.; Tsai, C.; Ma, L.; Ouyang, J.; Ozkan, C. S.; Yang1, Y., Digital memory device based on tobacco mosaic virus conjugated with nanoparticles. *Nature Nanotechnology*, **2006**, 1, 72-77.

72. Dujardin, E.; Hsin, L.-B.; Wang, C. R. C.; Mann, S., DNA-driven self-assembly of gold nanorods. *Chemical Communications*, **2001**, 0, (14), 1264-1265.

73. Stein, A., Advances in Microporous and Mesoporous Solids-Highlights of Recent Progress. *Advanced Materials*, **2003**, 15, (10), 763-775.

74. Davis, M. E., Ordered porous materials for emerging applications. *Nature*, **2002**, 417, 813-821.

75. Soler-Illia, G. J. d. A. A.; Sanchez, C. m.; Lebeau, B. n. d.; Patarin, J. l., Chemical Strategies To Design Textured Materials: from Microporous and Mesoporous Oxides to Nanonetworks and Hierarchical Structures. *Chemical Reviews*, **2002**, 102, (11), 4093-4138.

76. Yuan, Z.-Y.; Su, B.-L., Insights into hierarchically meso-macroporous structured materials. *Journal of Materials Chemistry*, **2006**, 16, (7), 663-677.

77. Grzelczak, M.; Vermant, J.; Furst, E. M.; Liz-MarzÃ¡n, L. M., Directed Self-Assembly of Nanoparticles. *ACS Nano*, **2010**, 4, (7), 3591-3605.

78. Tsukamoto, R.; Muraoka, M.; Seki, M.; Tabata, H.; Yamashita, I., Synthesis of CoPt and $FePt_3$ Nanowires Using the Central Channel of Tobacco Mosaic Virus as a Biotemplate. *Chemistry of Materials*, **2007**, 19, (10), 2389-2391.

79. Yang, P.; Deng, T.; Zhao, D.; Feng, P.; Pine, D.; Chmelka, B. F.; Whitesides, G. M.; Stucky, G. D., Hierarchically Ordered Oxides. *Science*, **1998**, 282, (5397), 2244-2246.

80. Gutièrrez, M. a. C.; Ferrer, M. a. L.; del Monte, F., Ice-Templated Materials: Sophisticated Structures Exhibiting Enhanced Functionalities Obtained after Unidirectional Freezing and Ice-Segregation-Induced Self-Assembly. *Chemistry of Materials*, **2008**, 20, (3), 634-648.

81. Kar, M.; Pauline, M.; Sharma, K.; Kumaraswamy, G.; Sen Gupta, S., Synthesis of Poly-l-glutamic Acid Grafted Silica Nanoparticles and Their Assembly into Macroporous Structures. *Langmuir*, **2011**, 27, (19), 12124-12133.

82. Iskandar, F.; Mikrajuddin; Okuyama, K., In Situ Production of Spherical Silica Particles Containing Self-Organized Mesopores. *Nano Letters*, **2001**, 1, (5), 231-234.

83. Bunz, U. H. F., Breath Figures as a Dynamic Templating Method for Polymers and Nanomaterials. *Advanced Materials*, **2006**, 18, (8), 973-989.

84. Sakatani, Y.; Boissière, C. d.; Grosso, D.; Nicole, L.; Soler-Illia, G. J. A. A.; Sanchez, C. m., Coupling Nanobuilding Block and Breath Figures Approaches for the Designed Construction of Hierarchically Templated Porous Materials and Membranes. *Chemistry of Materials*, **2007**, 20, (3), 1049-1056.

85. Amatani, T.; Nakanishi, K.; Hirao, K.; Kodaira, T., Monolithic Periodic Mesoporous Silica with Well-Defined Macropores. *Chemistry of Materials*, **2005**, 17, (8), 2114-2119.

86. Nakanishi, K.; Kobayashi, Y.; Amatani, T.; Hirao, K.; Kodaira, T., Spontaneous Formation of Hierarchical Macro-Mesoporous Ethane-Silica Monolith. *Chemistry of Materials*, **2004**, 16, (19), 3652-3658.

87. Boker, A.; He, J.; Emrick, T.; Russell, T. P., Self-assembly of nanoparticles at interfaces. *Soft Matter*, **2007**, 3, (10), 1231-1248.

88. Lin, Y.; Skaff, H.; Emrick, T.; Dinsmore, A. D.; Russell, T. P., Nanoparticle Assembly and Transport at Liquid-Liquid Interfaces. *Science*, **2003**, 299, (5604), 226-229.

89. Imhof, A.; Pine, D. J., Ordered macroporous materials by emulsion templating. *Nature*, **1997**, 389, 948-951.

90. Zhang, H.; Hardy, G. C.; Khimyak, Y. Z.; Rosseinsky, M. J.; Cooper, A. I., Synthesis of Hierarchically Porous Silica and Metal Oxide Beads Using Emulsion-Templated Polymer Scaffolds. *Chemistry of Materials*, **2004**, 16, (22), 4245-4256.

91. Velev, O. D.; Kaler, E. W., Structured Porous Materials via Colloidal Crystal Templating: From Inorganic Oxides to Metals. *Advanced Materials*, **2000**, 12, (7), 531-534.

92. Davis, S. A.; Breulmann, M.; Rhodes, K. H.; Zhang, B.; Mann, S., Template-Directed Assembly Using Nanoparticle Building Blocks: A Nanotectonic Approach to Organized Materials. *Chemistry of Materials*, **2001**, 13, (10), 3218-3226.

93. Rhodes, K. H.; Davis, S. A.; Caruso, F.; Zhang, B.; Mann, S., Hierarchical Assembly of Zeolite Nanoparticles into Ordered Macroporous Monoliths Using Core-Shell Building Blocks. *Chemistry of Materials*, **2000**, 12, (10), 2832-2834.

94. Stein, A.; Li, F.; Denny, N. R., Morphological Control in Colloidal Crystal Templating of Inverse Opals, Hierarchical Structures, and Shaped Particles. *Chemistry of Materials*, **2007**, 20, (3), 649-666.

95. Zhang, Y.; Zha, S.; Liu, M., Dual-Scale Porous Electrodes for Solid Oxide Fuel Cells from Polymer Foams. *Advanced Materials*, **2005**, 17, (4), 487-491.

96. Huerta, L.; Guillem, C.; Latorre, J.; Beltran, A.; Beltran, D.; Amoros, P., Large monolithic silica-based macrocellular foams with trimodal pore system. *Chemical Communications*, **2003**, 0, (12), 1448-1449.

97. Caruso, R. A.; Antonietti, M., Sol-Gel Nanocoating: An Approach to the Preparation of Structured Materials. *Chemistry of Materials*, **2001**, 13, (10), 3272-3282.

98. Breulmann, M.; Davis, S. A.; Mann, S.; Hentze, H. P.; Antonietti, M., Polymer–Gel Templating of Porous Inorganic Macro-Structures Using Nanoparticle Building Blocks. *Advanced Materials*, **2000**, 12, (7), 502-507.

99. Caruso, R. A.; Giersig, M.; Willig, F.; Antonietti, M., Porous "Coral-like" • TiO_2 Structures Produced by Templating Polymer Gels. *Langmuir*, **1998**, 14, (22), 6333-6336.

100. Valtchev, V.; Smaihi, M.; Faust, A.-C.; Vidal, L., Biomineral-Silica-Induced Zeolitization of Equisetum Arvense. *Angewandte Chemie International Edition*, **2003**, 42, (24), 2782-2785.

101. Dong, A.; Wang, Y.; Tang, Y.; Ren, N.; Zhang, Y.; Yue, Y.; Gao, Z., Zeolitic Tissue Through Wood Cell Templating. *Advanced Materials*, **2002**, 14, (12), 926-929.

102. Davis, S. A.; Patel, H. M.; Mayes, E. L.; Mendelson, N. H.; Franco, G.; Mann, S., Brittle Bacteria: A Biomimetic Approach to the Formation of Fibrous Composite Materials. *Chemistry of Materials*, **1998**, 10, (9), 2516-2524.

103. Dujardin, E.; Peet, C.; Stubbs, G.; Culver, J. N.; Mann, S., Organization of Metallic Nanoparticles Using Tobacco Mosaic Virus Templates. *Nano Letters*, **2003**, 3, (3), 413-417.

104. Danumah, C.; Vaudreuil, S.; Bonneviot, L.; Bousmina, M.; Giasson, S.; Kaliaguine, S., Synthesis of macrostructured MCM-48 molecular sieves. *Microporous and Mesoporous Materials*, **2001**, 44-45, (0), 241-247.

105. Cook, G.; Timms, P. L.; Göltner-Spickermann, C., Exact Replication of Biological Structures by Chemical Vapor Deposition of Silica. *Angewandte Chemie International Edition*, **2003**, 42, (5), 557-559.

106. Hall, S. R.; Bolger, H.; Mann, S., Morphosynthesis of complex inorganic forms using pollen grain templates. *Chemical Communications*, **2003**, 0, (22), 2784-2785.

107. Wang, L.-Q.; Shin, Y.; Samuels, W. D.; Exarhos, G. J.; Moudrakovski, I. L.; Terskikh, V. V.; Ripmeester, J. A., Magnetic Resonance Studies of Hierarchically Ordered Replicas of Wood Cellular Structures Prepared by Surfactant-Mediated Mineralization. *The Journal of Physical Chemistry B*, **2003**, 107, (50), 13793-13802.

108. Matsen, M. W.; Schick, M., Self-assembly of block copolymers. *Current Opinion in Colloid & Interface Science*, **1996**, 1, (3), 329-336.

109. Cheng, J. Y.; Ross, C. A.; Smith, H. I.; Thomas, E. L., Templated Self-Assembly of Block Copolymers: Top-Down Helps Bottom-Up. *Advanced Materials*, **2006**, 18, (19), 2505-2521.

110. Wang, H.; Lin, W.; Fritz, K. P.; Scholes, G. D.; Winnik, M. A.; Manners, I., Cylindrical Block Co-Micelles with Spatially Selective Functionalization by Nanoparticles. *Journal of the American Chemical Society*, **2007**, 129, (43), 12924-12925.

111. Eglin, D.; Mosser, G.; Giraud-Guille, M.-M.; Livage, J.; Coradin, T., Type I collagen, a versatile liquid crystal biological template for silica structuration from nano- to microscopic scales. *Soft Matter*, **2005**, 1, (2), 129-131.

112. Israelachvili, J. N., *Intermolecular and Surface Forces.* 3rd Edition; 1992.

113. Attard, G. S.; Glyde, J. C.; Goltner, C. G., Liquid-crystalline phases as templates for the synthesis of mesoporous silica. *Nature*, **1995**, 378, 366-368.

114. Göltner, C. G.; Henke, S.; Weissenberger, M. C.; Antonietti, M., Mesoporous Silica from Lyotropic Liquid Crystal Polymer Templates. *Angewandte Chemie International Edition*, **1998**, 37, (5), 613-616.

115. Thomas, A.; Schlaad, H.; Smarsly, B.; Antonietti, M., Replication of Lyotropic Block Copolymer Mesophases into Porous Silica by Nanocasting: Learning about Finer Details of Polymer Self-Assembly. *Langmuir*, **2003**, 19, (10), 4455-4459.

116. Antonietti, M., Surfactants for novel templating applications. *Current Opinion in Colloid & Interface Science*, **2001**, 6, (3), 244-248.

117. Sharma, K. P.; Kumaraswamy, G.; Ly, I.; Mondain-Monval, O., Self-Assembly of Silica Particles in a Nonionic Surfactant Hexagonal Mesophase. *The Journal of Physical Chemistry B*, **2009**, 113, (11), 3423-3430.

118. Sharma, K. P.; Ganai, A. K.; Gupta, S. S.; Kumaraswamy, G., Self-Standing Three-Dimensional Networks of Nanoparticles With Controllable Morphology by Dynamic Templating of Surfactant Hexagonal Domains. *Chemistry of Materials*, **2011**, 23, (6), 1448-1455.

119. Kuang, D.; Brezesinski, T.; Smarsly, B., Hierarchical Porous Silica Materials with a Trimodal Pore System Using Surfactant Templates. *Journal of the American Chemical Society*, **2004**, 126, (34), 10534-10535.

120. Li, Z.; Wei, X.; Ming, T.; Wang, J.; Ngai, T., Dual templating synthesis of hierarchical porous silica materials with three orders of length scale. *Chemical Communications*, **2010**, 46, (46), 8767-8769.

121. Sun, J.-H.; Shan, Z.; Maschmeyer, T.; Coppens, M.-O., Synthesis of Bimodal Nanostructured Silicas with Independently Controlled Small and Large Mesopore Sizes. *Langmuir*, **2003**, 19, (20), 8395-8402.

122. Li, F.; Stein, A., Functional Composite Membranes Based on Mesoporous Silica Spheres in a Hierarchically Porous Matrix. *Chemistry of Materials*, **2010**, 22, (12), 3790-3797.

Chapter 2

'Clicking' molecular hooks on silica nanoparticles to immobilize metal complexes: the case of gold catalyst immobilization

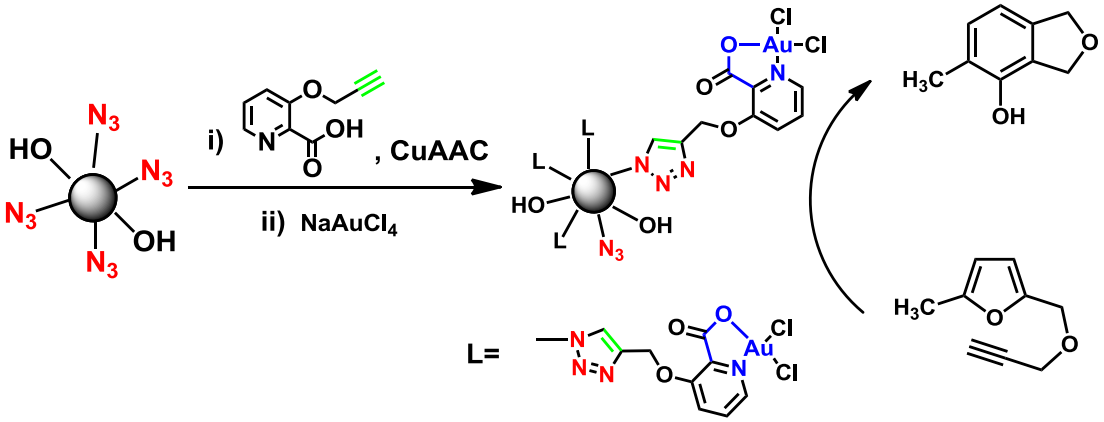

In this chapter, we demonstrate that silica chemistry in combination with the [3+2] Huisgen's cycloaddition could be used to generate a functional group on the surface of silica nanoparticles which can effectively bind to catalytically active metal ions. To show that we have chosen Au(III) ions as an example. The synthesis and characterization of silica nanoparticles in which Au(III) has been immobilized through a 1,2,3-triazole linkage using an alkynalated picolinic acid exploiting ''click chemistry'' has been discussed. The Au(III) immobilized silica nanoparticles have been thoroughly characterized using FT-IR, ^{13}C CP MAS NMR and XPS. The utility of these particles as an easily separable catalyst for the Hashmi phenol synthesis is also described.

Part of the work discussed in this chapter has been published in
Anal Kr. Ganai, Rima Bhardwaj, Srinivas Hotha, Sayam Sen Gupta and B. L. V. Prasad, New J. Chem., **2010**, 34, 2662-2670.

2.1 Introduction:

Preparation of a multifunctional catalytic system is the grand theme of this thesis. As a first step in that direction in this chapter we describe the preparation of a 'semi-heterogeneous catalyst' by immobilizing a catalytically active metal ionic species on silica nanoparticle surface.

Apart from this, immobilization of molecular catalysts onto solid support is of growing commercial and academic interest, because they can combine the advantages of heterogeneous and homogeneous catalysts.[1] It is easy to separate immobilized metal complexes from the reaction mixtures and recycle them. It is also much easier to tailor and fine tune heterogeneous catalysts in such a way that they remain active and selective as their homogeneous counterparts. Thus it is important to develop a methodology for immobilization of those industrially important precious metal complexes.[2] In the recent years, a significant amount of time has been spent to design dispersible matrices for catalyst immobilization.[3-5] Several such dispersible matrices have been explored. Nanoparticles have emerged as alternative dispersible matrix for supporting homogeneous organic reactions.[6] They are considered semi-heterogeneous since they readily disperse in many solvents and the high surface area of these particles allows higher catalyst loading capacity than many conventional support matrices leading to an improved catalytic activity. In the previous chapter we have already discussed that among several nanoparticles that can be used as a support, the use of silica nanoparticles as a matrix for immobilization has been widespread. This can be attributed to the advances made in the last decade or so regarding the development of methodologies that allows easy surface functionalization of silica nanoparticles using well established silane chemistry. Several organic groups can now be covalently attached to silica nanoparticle surface using silanol chemistry discussed in the previous chapter. These organic functionalities can then be used to immobilize metal ions.[7-9] Further, silica particles can also be synthesized with a magnetic core, thus, avoiding catalysts separation by filtration alone. Thus silica nanoparticles have been chosen for immobilization of precious metal complexes.

Bulk gold reveals great stability and chemical inertness, but it has been proved to be an excellent catalyst in the molecular and nanosized form. After the path breaking research done by Haruta et. al. and Hutchings et. al. simultaneously and independently on supported gold nanoparticles catalysts for the selective low-

temperature oxidation of CO,[10] and the hydrochlorination of ethyne to vinyl chlorides,[11] scientists have published many reports on the catalytic application of Au nanoparticles.[12,6] There are numerous examples available in the literature where Au nanoparticles have been immobilized on various kinds of mesoporous solid support[13] including zeolite,[14] aluminosilicates,[15] SBA-15[16] and MCM-41.[17] Although heterogeneous catalysis is still predominant, since the last decade or so gold mediated homogeneous reactions emerged as one of the best choices for effecting a variety of chemical transformations with wide range of functional group tolerance such as epoxides, ketones, aldehydes, and acids.[18-20] Hashmi et al. extended the possibilities of gold-catalyzed reactions to newer avenues, including the conversion of alkyne terminated furan to phenol that combines the C-C and C-O bonds formation.[21] Since then, it has been found that soluble gold compounds can catalyze many selective organic reactions.[22] Although molecular Au species have been shown to display excellent reactivity, efforts to make heterogeneous/semi-heterogeneous catalysts based on Au complexes have been rather sparse (Figure 2.1).[23]

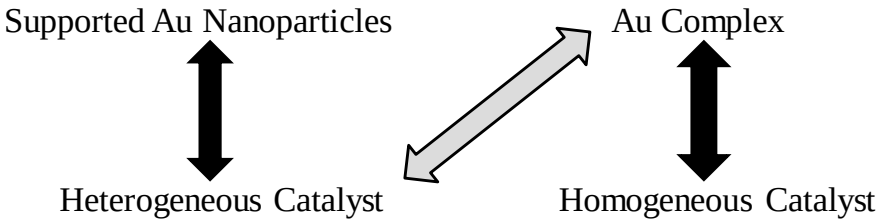

Figure 2.1: Current status by gold catalysis. Explored combination (black) and a less explored combination (gray).

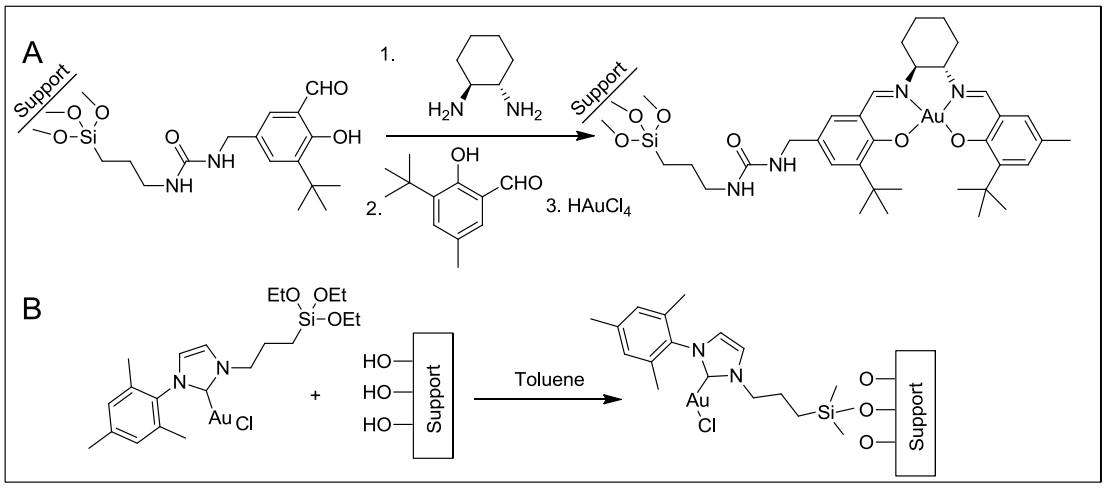

Scheme 2.1: (A) Au(III) Schiff base complexes synthesized by Corma and co workers. (Adapted from ref. 25) (B) N-heterocyclic carbine gold complexes synthesized by Corma et al. Adapted from Ref. 24.

Corma and co-workers have immobilized several Au(III) and Au(I) complexes that contain Au(III) Schiff bases onto MCM-41 (Scheme 2.1) and have used them as catalysts for Suzuki, Sonogoshira and Heck C-C bond formation reactions as well as hydroamination reaction.[24-28]

Among several reactions that have been developed with homogeneous Au catalysts, activation of carbon-carbon π-bonds with Au(III) complexes as electrophiles have been a more recent phenomenon.[18] Gold has come to be regarded as an exceedingly mild, relatively carbophilic Lewis acid, leading to the development of a broad array of reactions that proceed by the activation of unsaturated carbon-carbon bonds. Such C-C bond formation reactions are unique for Au which are otherwise very difficult to obtain with other transition metals. The excellent selectivity coupled with interesting possibilities for the synthesis of many novel molecular scaffolds invigorated interest among various scientific disciplines resulting in elegant strategies for easy synthesis of chemical architectures which are otherwise not possible. The dynamic and exorbitant price of gold puts the chemistry of gold in an uncomfortable position though these reactions occur with catalytic quantities of gold. Thus, immobilization of gold could enable the use of gold catalysts with increased efficiency due to the increased local concentration of the Au. However, there are very few reports of heterogenized Au(III) complexes that activate carbon-carbon π-bonds as electrophiles. Nanoparticles of gold supported on nanocrystalline CeO_2 have been used to catalyze Hashmi's phenol synthesis - a reaction in which Au(III) activates a terminal alkyne to isomerizes ω-alkynylfurans to phenols.[29] (Scheme 2.2) Further, initial leaching of Au was observed in the first run of the reaction.

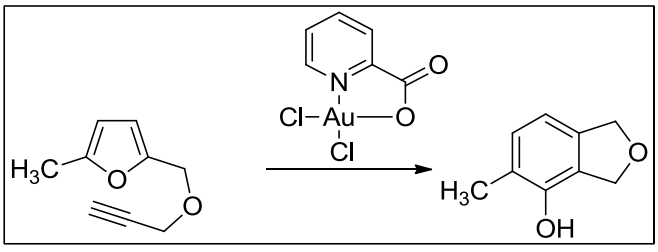

Scheme 2.2: Reaction scheme of Au(III) catalysed phenol synthesis.

We would like to mention that while immobilization of nanoparticles and molecular species on solid supports have been accomplished earlier, creating a

ligating group that can act like hook to attach to the metal ion of interest have not been reported. We envisaged that, Au(III) ion could be immobilized on the surface of silica nanoparticles using Huisgen's 1, 3 dipolar cycloaddition reaction (Cu(I) catalyzed azide-alkyne cycloaddition reaction, CuAAC). The CaAAC is one of the popular "click" reactions, resulting in 1,2,3-triazoles linkage. (Scheme 2.3) It has been discussed in the previous chapter that among various surface functionalization techniques, CuAAC has become the most powerful ''click chemistry'' tool for conjugation between appropriately functionalized binding partners on surfaces via a 1,2,3-triazole linkage.[30,31]

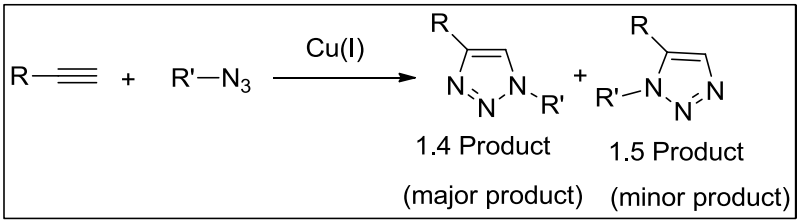

Scheme 2.3: Cu(I) catalysed "click" reaction

In this chapter, the synthesis and characterization of azide grafted silica nanoparticles has been discussed. Au(III) has been immobilized on the surface of silica through a 1,2,3-triazole linkage using an alkynalated picolinic acid exploiting azide-alkyne "click chemistry". As a model study for the activation of carbon-carbon π-bonds as electrophiles, the catalytic activity of the Au(III) immobilized on silica nanoparticle was investigated for the Hashmi's phenol synthesis.[29] The immobilized picolinic acid moiety on the silica surface has a dual role. It anchors the Au(III) and also increases the rate of the isomerisation reaction as has been reported by Hashmi before.[32] The fate of Au(III) at the end of each run is also discussed.

2.2 Experimental section:

2.2.1 Materials:

Ludox AS40 (50% by weight), 3-hydroxy picolinic acid, o-hydroxy bezoic acid, Sodium tetrachloro aurate (III) dihydtare ($NaAuCl_4$), propargyl bromide, chloropropyltriethoxysilane (99%), t-butylammonium chloride, disodium bathophenanthroline sulphonate, copper iodide were obtained from Sigma Aldrich and used as received. Triethylamine was obtained from Spectrochem India. Sodium Azide was obtained from Loba Chemie, India. All other chemicals and solvents were obtained from Merck, India and used as received. 3-azidopropyltriethoxysilane

(AzPTES), sodium dithiocarbamate and azide grafted silica nanoparticles (N_3-Silica) were prepared as per the details provided below. Millipore water was used for the preparation and reactions of silica nanoparticles.

2.2.2 Synthesis:

2.2.2.1 Synthesis of 3-azidopropyltriethoxysilane, AzPTES:

3-Chloropropyltriethoxysilane (abbreviated as Cl-PTES; 2 g, 8.3 mmol) was added to a solution of sodium azide (1.08 g, 16.6 mmol) and tetrabutylammonium bromide (0.644 g, 2 mmol) in dry acetonitrile (50 mL), under nitrogen atmosphere. The reaction mixture was stirred under reflux for 18 h. After completion of the reaction, the solvent was removed under reduced pressure. The crude mixture was diluted in n-pentane and the suspension was filtered over Celite. Solvent was removed from the resulting filtrate and the crude oil obtained was distilled under reduced pressure of 0.025 mbar at 62 ^{0}C to give AzPTES (3-azidopropyltriethoxysilane) as a colourless liquid. Yield: 1.52 g, 74%. ^{1}H NMR (500 MHz, $CDCl_3$): d 0.66 (t, 2H, J ¼ 8.25 Hz), 1.21 (t, 3H, J ¼ 6.88 Hz), 1.66–1.73 (m, 2H), 3.25 (t, 2H, J ¼ 7.16 Hz), 3.80 (q, 2H, J ¼ 6.88 Hz). ^{13}C NMR (50 MHz, $CDCl_3$) d 7.59, 18.23, 22.64, 53.8, 58.41. FT-IR (NaCl, cm^{-1}): 2098 (-N=N$^+$=N$^-$, *s)* For the ^{1}H and ^{13}C NMR spectra see Appendix-2.

2.2.2.2 Synthesis of alkyne terminated ligands (L1 and L2):

2.2.2.2a Synthesis of prop-2-ynyl 3-(prop-2-ynyloxy)picolinate (1b):

To an ice cooled suspension of 3-hydroxy picolinic acid **1a** (2.5g, 0.018mol) in 30 mL anhydrous N,N- dimethylformamide was added K_2CO_3 (11.7g, 0.085 mol) at 0 °C. After 30 min, propargyl bromide (4.0mL, 5.3g, 0.045 mol) was added drop wise and stirred for 5h at room temperature. At the end of the reaction (monitored by TLC), 40 mL water was added and extracted with diethyl ether (3x50mL), combined organic layers were washed with brine solution (2x20mL), dried over anhydrous sodium sulphate and concentrated in vacuo to obtain crude residue that was purified by silica gel column chromatography using ethyl acetate-petroleum ether (1:3) to get the title compound **1b** (3.4g, 89%) as a gum. (Scheme 2.4)

^{1}H NMR (200.13 MHz, $CDCl_3$): δ 2.54(t, 1H, J = 2.5Hz), 2.60(t, 1H, J = 2.4Hz), 4.84(d, 2H, J = 2.4Hz), 4.98(d, 2H, J = 2.5Hz), 7.46(dd, 1H, J = 4.4, 8.6Hz), 7.57(dd, 1H, J = 1.3, 8.6Hz), 8.36(dd, 1H, J = 1.1, 4.4Hz); ^{13}C NMR (50.32 MHz, $CDCl_3$): δ

52.8, 56.7, 75.3, 77.1, 77.1, 77.2, 122.4, 127.1, 138.5, 142.0, 153.7, 163.5; For the ^{1}H and ^{13}C NMR spectra see Appendix-2. Mol. Wt. Calcd for $C_{12}H_9NO_3Na$:238.204; Found, 238.162

2.2.2.2b Synthesis of prop-2-ynyl 3-(prop-2-ynyloxy)picolinic acid (L1):

LiOH (223mg, 9.3 mmol) in water (5 mL) was added to solution of compound **1b** (1.0 g, 4.65 mmol) in 15 mL of CH_3OH:THF (1:2) at 0 °C. The reaction mixture was stirred at room temperature until the complete consumption of starting material (TLC) and then solution was neutralized using amberlite IR120 (H^+), filtered and the resin was washed with water and MeOH. The combined methanolic solution was concentrated under reduced pressure and the crude product (0.9 g) was recrystallized from aqueous ethanol to give the compound **L1** (0.6 g, 73%) as a solid. (Scheme 2.4) m.p 63 ^{o}C ; ^{1}H NMR (200.13 MHz, $CDCl_3$): δ 2.75(t, 1H, J = 2.4Hz), 4.06(d, 2H, J = 2.4Hz), 6.67(dd, 1H, J = 4.5, 8.6Hz), 6.80(dd, 1H, J = 1.2, 8.6Hz), 7.34(dd, 1H, J = 1.2, 4.5Hz); ^{13}C NMR (50.32 MHz, $CDCl_3$): δ 56.5, 78.9, 79.6, 122.3, 126.7, 141.7, 142.1, 151.6, 167.0; For the ^{1}H and ^{13}C NMR spectra see Appendix-2. Mol. Wt. Calcd for $C_9H_7NO_3$:177.157; Found, 178.214 (M^++1)

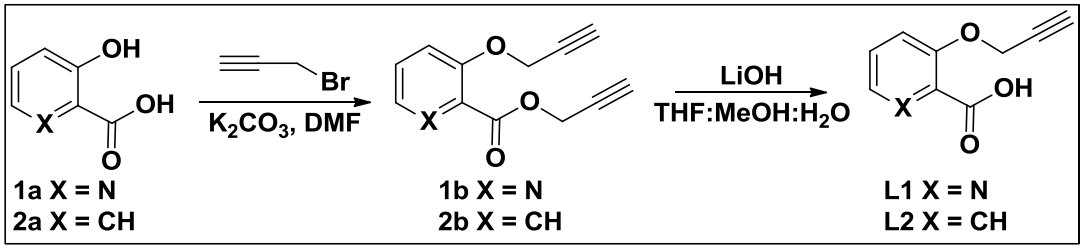

Scheme 2.4: Synthesis of ligand **L1** and ligand **L2**

2.2.2.2c Synthesis of prop-2-ynyl 2-(prop-2-ynyloxy)benzoate (2b):

It has been synthesized according to the above procedure. (Scheme 2.4) m.p. 167 ^{o}C; ^{1}H NMR (200.13 MHz, $CDCl_3$): δ 2.52(t, 1H, J = 2.5Hz), 2.55(t, 1H, J = 2.4Hz), 4.80(d, 2H, J = 2.4Hz), 4.89(d, 2H, J = 2.5Hz), 7.04(t, 1H, J = 7.5Hz), 7.13(d, 1H, J = 8.5Hz), 7.49(t, 1H, J = 7.7Hz), 7.86(dd, 1H, J = 1.6, 7.7Hz); ^{13}C NMR (50.32 MHz, $CDCl_3$): δ 52.3, 56.8, 74.9, 76.1, 77.8, 78.1, 114.4, 119.9, 121.3, 132.0, 133.8, 157.3, 164.8; For the ^{1}H and ^{13}C NMR spectra see Appendix-2. LRMS Calcd for $C_{13}H_{10}O_3Na$:237.217; Found, 237.062

2.2.2.2d Synthesis of prop-2-ynyl 2-(prop-2-ynyloxy)benzoic acid (L2):

It has been prepared by following the above procedure (for ***L1***) from compound **2b** (Scheme 2.4).

m.p 65 ^{o}C; ^{1}H NMR (200.13 MHz, $CDCl_3$): δ 2.58(t, 1H, J = 2.4Hz), 4.74(d, 2H, J = 2.4Hz), 7.20-7.35(m, 2H), 8.27(dd, 1H, J = 1.7, 4.3Hz), 8.38(d, 1H, J = 2.6Hz); ^{13}C NMR (50.32 MHz, $CDCl_3$): δ 55.9, 76.7, 77.5, 121.5-123.7, 138.2, 142.7, 153.6; For the ^{1}H and ^{13}C NMR spectra see Appendix-2. Mol. Wt. Calcd for $C_{10}H_8O_3$:176.169; Found, 177.108

2.2.2.3 Synthesis of azide-grafted silica nanoparticles (N_3-Silica):

Ludox silica sol (2.4 g) was diluted with 30 mL of a DI water ethanol (1:1) mixture and placed in a Teflon beaker. AzPTES (494 mg, 2 mmol) was added to the homogeneous dispersion. The reaction mixture was stirred for 23 h at room temperature, after which the reaction mixture was centrifuged at 12000 rpm for 30 min. The clear supernatant liquid was decanted from the solid deposit. The solid mass obtained was sonicated with ethanol for 20 min and then centrifuged three times. It was then dried at 50 ^{o}C under high vacuum for 6 h. The particles were characterized by NMR, FT-IR, TEM and elemental analysis. Yield: 0.512 g

2.2.2.4 Synthesis of ligand (L1 or L2) functionalized Silica nanoparticles using CuAAC:

For CuAAC, the azide functionalized silica nanoparticles were incubated with 5 equivalents of the alkyne substituted ligand (**L1** or **L2**) in DMF: H_2O solvent mixture (8:2) containing CuI (2.0 equivalent), disodium bathophenanthrolene sulphonate (2.0 equivalent), sodium ascorbate (4 equivalent) and triethylamine (5.0 equivalents). In a typical reaction, azide grafted silica nanoparticles (150 mg, 0.1071 mmol of azide) was incubated with **L1** (94.78 mg, 0.5355 mmol, 5 eq) in 12ml DMF/3ml H_2O mixture containing sodium ascorbate (84.82 mg, 0.4284 mmol, 4 eq) and copper iodide (40.698 mg, 0.2142 mmol, 2 eq) and disodium sulphonated bathophenanthroline (115.56 mg, 0.2142 mmol, 2 eq) and triethylamine (54 mg, 0.5355 mmol, 5 eq). The reaction mixture was subjected to three freeze-pump-thaw cycles for rigorous exclusion of dioxygen. The CuAAC was allowed to proceed for 24 h with stirring. After completion of the reaction, the mixture was taken into a centrifuge tube and centrifuged for 20 min at 12000 rpm. The supernatant liquid was decanted off and the solid residue was washed with DMF (2 times), ethanol (2 times),

0.1 M sodium ascorbate (2 times), 0.1 M N,N-diethyldithiocarbamate sodium in ethanol (4 times) and ethanol (2 times). It was finally washed with 0.1 M HCl (2 times) and then stored as a suspension in ethanol. This sample will henceforth be called as Silica-**L1**. For preparation of samples for NMR and IR, a part of the functionalized silica nanoparticles solution was washed in ethanol and dried under vacuum at 60 °C. Yield: 123 mg

Similar protocol was adopted for CuAAC of the ligand **L2** with Silica-Azide to afford the conjugate Silica-**L2**. Yield: 112 mg

2.2.2.5 Synthesis of Silica-Au-L1:

Functionalized silica nanoparticle Silica-**L1** was dispersed in methanol and then $NaAuCl_4$ was added and heated at 60 ^oC. In a typical reaction, 50 mg of Silica-**L1** (0.03882 mmol) was dispersed in 2.5ml methanol followed by the addition of 16.85 mg $NaAuCl_4$ (0.0465 mmol, 1.2 eq). The reaction mixture was heated to 60 ^oC for 10 hrs. After completion of the reaction, the mixture was taken into a centrifuge tube and centrifuged for 10 min at 12000 rpm. The supernatant liquid was decanted off and the solid residue was washed with methanol (5 times) to afford Silica-**Au-L1**. It was finally stored as a suspension in ethanol. For preparation of samples for IR, a part of the Silica-**Au-L1** solution was washed in ethanol and dried under vacuum at 60 ^oC. Yield: 41 mg

2.2.2.6 General procedure of Hashmi reaction for the synthesis of 4-methyl-1, 3-dihydroisobenzofuran-5-ol using Silica-Au-L1:

Catalyst silica-Au-**L1** (2 mol% Au, 28.2 mg, 0.01027 mmol) in acetonitrile (1mL) was added to solution of 2-methyl-5-(prop-2-ynyloxy) methyl furan (75 mg, 0.5136 mmol) in acetonitrile (0.5 mL) at 0 °C. The reaction mixture was stirred at room temperature and periodically monitored by LC- MS until the complete consumption of starting material. After the completion of starting material catalyst was separated by centrifuging at 6000 rpm and then washed with acetonitrile, sonicated and dried for 30min. Recovered catalyst was reused for one more cycle of same reaction.

A number of catalysis reactions have been done using silica-Au-**L1** with the help of Dr. Srinivas Hotha, National Chemical Laboratory, using same protocol discussed above. The reactions will be discussed in detail later in this chapter (Scheme 2.6). The NMR of the final products is listed below.

*2-methyl-5-(prop-2-ynyloxy) methyl furan (**3**)*

To an ice cooled solution of (5-methylfuran-2-yl)methanol **3** (400mg, 3.6mmol) in 5 mL anhydrous N,N-dimethyl formamide at 0 °C NaH (60% in mineral oil) (168 mg, 4.2mmol) was added. After 30 min, at 0 °C propargyl bromide (500mg, 4.2 mol) was added drop wise and stirred for 2h at room temperature. At the end of reaction (monitored by TLC), 6 mL water was added and extracted with diethyl ether (3x10mL), combined organic layers were washed with brine (2x5mL), dried over anhydrous sodium sulphate and concentrated in vacuo, crude residue was purified by silica gel column chromatography to get 2-methyl-5-(prop-2-ynyloxy)methyl furan **4** (478mg,yield 89%).

^{1}H NMR (200.13 MHz, $CDCl_3$): δ 2.28(d, 3H, J = 0.8Hz), 2.45(t, 1H, J = 2.4Hz), 4.14(d, 2H, J = 2.4Hz), 4.49(s, 2H), 5.91(m, 1H), 6.24(d, 1H, J = 3.0Hz); ^{13}C NMR (50.32 MHz, $CDCl_3$): δ 13.6, 58.4, 63.1, 74.7, 79.4, 106.2, 111.1, 148.8, 152.9; Mol. Wt. Calcd for $C_9H_{10}O_2$:150.068; Found, 149.176

*4-methyl-1, 3-dihydroisobenzofuran-5-ol (**4**)*

$AuCl_3$ (4mg, 0.013mmol) in acetonitrile (0.5mL) was added to a solution of 2-methyl-5-(prop-2-ynyloxy)methyl furan **4** (100mg, 0.67mmol) in acetonitrile (1mL) at 0 °C. The reaction mixture was stirred at room temperature until the complete consumption of starting material and then quenched with Et_3N and concentrated in *vacuo*. The crude residue was purified by silica gel column chromatography using ethyl acetate-petroleum ether (1:20) to get the title product **5** (90mg, 90%).

Mp 71°C; ^{1}H NMR (200.13 MHz, $CDCl_3$): δ 2.25(s, 3H), 5.13(bs, 2H), 5.14(bs, 2H), 5.77(s, 1H), 6.70(d, 1H, J = 7.5Hz), 7.04(d, 1H, J = 7.5Hz); ^{13}C NMR (50.32 MHz, $CDCl_3$): δ 15.2, 71.7, 74.0, 112.7, 122.2, 124.9, 130.5, 138.6, 148.4; For the ^{1}H and ^{13}C NMR spectra see Appendix-2. Mol. Wt. Calcd for $C_9H_{10}O_3$:150.174; Found, 150.938

5-methyl-2-tosylisoindolin-4-ol (6)

Reaction was carried out for 5 h with substrate 5. The reaction conditions were kept similar to those followed in the reaction of 3 to give 4 as delineated above. m.p. 178 ^{0}C; ^{1}HNMR (200.13MHz, $CDCl_3$): δ 2.19 (s, 3 H), 2.40 (s, 3 H), 4.60 (m, 4H), 5.00 (brs, 1H), 6.64 (d, 1 H, J = 7.6 Hz), 6.99 (d, 1 H, J = 7.5 Hz), 7.30 (d, 2 H, J = 8.0 Hz), 7.75 (d, 2 H, J = 8.4 Hz); ^{13}C NMR (100.61 MHz, $CDCl_3$): δ 15.1, 21.5, 51.6,

54.0, 114.4, 120.1, 122.5, 127.6 (2C), 129.8 (2C), 130.7, 135.5, 135.8, 143.7, 149.0; For the ^{1}H and ^{13}C NMR spectra see Appendix-2; M_w Calcd for $C_{16}H_{17}NO_3S$: 303.092; Found, 304.291 ($M^+ + 1$).

When the reaction was carried out with substrate 7 two products 8 and 9 were obtained. The reaction conditions were again kept the same as those delineated above.

Dihydroisobenzofuran-4-ol (8)

m.p. 130–135 ^{0}C; ^{1}H NMR (400.13 MHz, $CDCl_3$): δ 5.13, 5.15 (2s, 4 H), 5.67 (brs, 1 H), 6.66 (d, 1 H, J = 8.1 Hz), 6.81 (d, 1 H, J = 7.6 Hz), 7.15 (t, 1 H, J = 7.8 Hz); ^{13}C NMR (100.61 MHz, $CDCl_3$): δ 71.4, 73.7, 112.8, 113.4, 124.9, 128.8, 141.2, 149.9. For the ^{1}H and ^{13}C NMR spectra see Appendix-2; Mw Calcd for $C_8H_8O_2$: 136.052; Found, 137.114 ($M^+ + 1$).

1,3-Dihydroisobenzofuran-5-ol (9)

m.p. 120 ^{0}C; ^{1}H NMR (200.13 MHz, CDCl3): δ 5.06 (s, 4 H), 5.50 (brs, 1 H), 6.66–6.78 (m, 2 H), 7.08 (d, 1 H, J = 8.0 Hz); ^{13}C NMR (50.32 MHz, $CDCl_3$): δ 73.3, 73.4, 107.9, 114.6, 121.8, 130.7, 140.7, 155.5. For the ^{1}H and ^{13}C NMR spectra see Appendix-2; M_w Calcd for $C_8H_8O_2$: 136.052; Found, 137.020 ($M^+ + 1$).

When the reaction was carried out with substrate 10 two products 11 and 12 were obtained. The reaction conditions were again kept the same as those delineated above.

2-Tosylisoindolin-4-ol (11)

m.p. 145–150 ^{0}C; ^{1}H NMR (200.13 MHz, $CDCl_3$): δ 2.40 (s, 3 H), 4.53 (s, 4 H), 5.27 (s, 1 H), 6.68 (td, 2 H, J=2.4, 8.2 Hz), 7.00 (d, 1 H, J=8.2Hz), 7.31 (m, 2 H), 7.75 (m, 2 H); ^{13}C NMR (100.61 MHz, $CDCl_3$): d 21.5, 53.2, 53.7, 109.5, 115.2, 123.6, 127.6(2C), 127.9, 129.9(2C), 133.6, 137.7, 143.8, 155.6. For the ^{1}H and ^{13}C NMR spectra see Appendix-2; M_w Calcd for $C_{15}H_{15}NO_3S$: 289.077; Found, 290.203 ($M^+ + 1$).

2-Tosylisoindolin-5-ol (12)

m.p. 170 ^{0}C; ^{1}H NMR (200.13 MHz, $CDCl_3$): δ 2.40 (s, 3 H), 4.67 (s, 4 H), 5.52 (brs, 1 H), 6.64 (d, 1 H, J=8.1 Hz), 6.72 (d, 1 H, J=7.6 Hz), 7.10 (t, 1 H, J = 7.9 Hz), 7.31 (m, 2 H), 7.77 (m, 2 H); ^{13}C NMR (50.32 MHz, $CDCl_3$): δ 21.6, 51.6, 54.1, 114.1, 114.7, 122.8, 127.6 (2C), 129.4, 129.9 (2C), 133.6, 138.3, 143.8, 150.9. For the ^{1}H and ^{13}C NMR spectra see Appendix-2; M_w Calcd for $C_{15}H_{15}NO_3S$: 289.077; Found, 290.276 ($M^+ + 1$).

2.3 Results and Discussion:

Our strategy to prepare the desired "molecular hook" for immobilizing gold (III) complex onto silica is displayed in Scheme 2.5. The first step in this endeavor was the synthesis of azide grafted silica particles. The azide grafted silica nanoparticles (N_3-silica) were synthesized by the condensation of azidopropyltriethoxysilane (AzPTES) onto commercially available silica colloidal particles (Ludox AS40; 22±3 nm particle size) as presented in Scheme 2.5. The organosilica precursor AzPTES was obtained by the displacement of the chloro group in 3-chloropropyltriethoxysilane with an azido group using sodium azide. The azide grafted silica nanoparticles were characterized by TEM (Figure 2.2), TGA[33] (Figure 2.4 b), FT-IR (Figure 2.5 b), multinuclear (^{29}Si, ^{13}C) solid state NMR (Figure 2.6 a and 2.7 a).

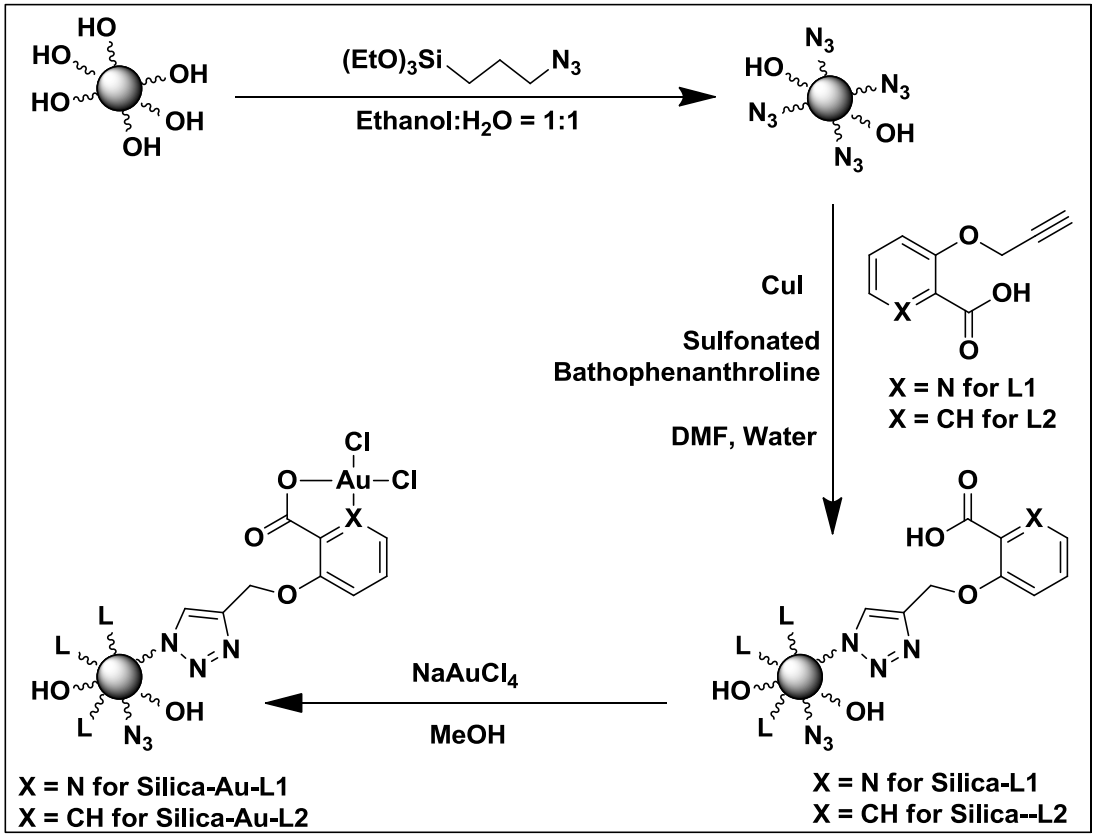

Scheme 2.5: Synthesis of Silica-Au-**L1** conjugate

The second step in our strategy was to modify the silica surface to bear the moieties **L1** or **L2** that would serve as hooks/anchors to immobilize Au(III). The ligand **L1** was chosen such that a robust five membered ring would form once the

Au(III) ligates. For doing control experiment ligand **L2** was anchored on the surface of silica nanoparticles. Due to the absence of nitrogen in **L2**, it can be expected that five membered ring will not form with Silica-Au-**L2** and hence Au(III) anchoring may not be facile. Ligands **L1** and **L2** were immobilized on silica surface applying "Click Reaction". The CuAAC reaction was carried out using CuI/sulfonated bathophenanthroline in DMF and H_2O mixture at a ratio of 80:20 for 24 hrs. After the reaction, an extensive washing protocol was followed to remove the Cu(I), ascorbate and any unreacted starting materials. One of the key steps in the washing was the usage of dithiocarbamate to remove the Cu(I), as reported earlier.[34] The ligand grafted silica nanoparticles Silica-**L1** and Silica-**L2** were characterized by TGA (Figure 2.4 c), FT-IR (Figure 2.5 c), multinuclear (^{29}Si, ^{13}C) solid state NMR (Figure 2.6 b and 2.7 b). The extent of the reaction was estimated using FT-IR spectroscopy, by monitoring the decrease in the integrated intensity of the $\upsilon_{as}(N_3)$ at 2100 cm^{-1}. XPS analysis was done to know the chemical composition of the surface (Figure 2.8).

In the final step, after thorough optimization, Au(III) was incorporated onto silica-**L1** nanoparticle by incubating them with $NaAuCl_4$ in methanol solution at 55 °C to afford Silica-Au-**L1** (Scheme 2.5). Control reactions were performed with Silica-**L2** keeping same reaction condition. As expected Au(III) did not bind with Silica-**L2** because of absence of picolinic acid moiety. All these materials were characterized FT-IR (Figure 2.5 e) spectroscopy. ICP analysis was done to know the amount of Au present in the Silica-Au-**L1** and Silica-Au-**L2** (Table 2.2). Chemical composition of the surface was determined using XPS analysis (Figure 2.9).

The catalytic activity of Silica-Au-**L1** was studied on Hashmi's phenol synthesis using different substrates. Control experiments were performed using Silica-Au-**L2**. The reactions were monitored by LC-MS analysis. (Figure 2.11 and Figure 2.12) The detailed characterizations of different materials are discussed below.

2.4 Characterizations:

2.4.1 Transmission electron microscopy:

The TEM of azide grafted silica nanoparticles is shown in Figure 2.2. The size of commercially available silica colloidal solution is around 22 nm. The size of the azide grafted silica nanoparticles was determined to be about 22±3 nm from TEM

studies. This indicates that after azide grafting the size and morphology of silica particles remains same.

2.4.2 N_2 Adsorption isotherm:

The N_2 adsorption and desorption isotherm of Ludox Silica particles are presented in Figure 2.3. This isotherm signifies that the particles are not porous and solid in nature. This also agrees well with the TEM presented in Figure 2.2.

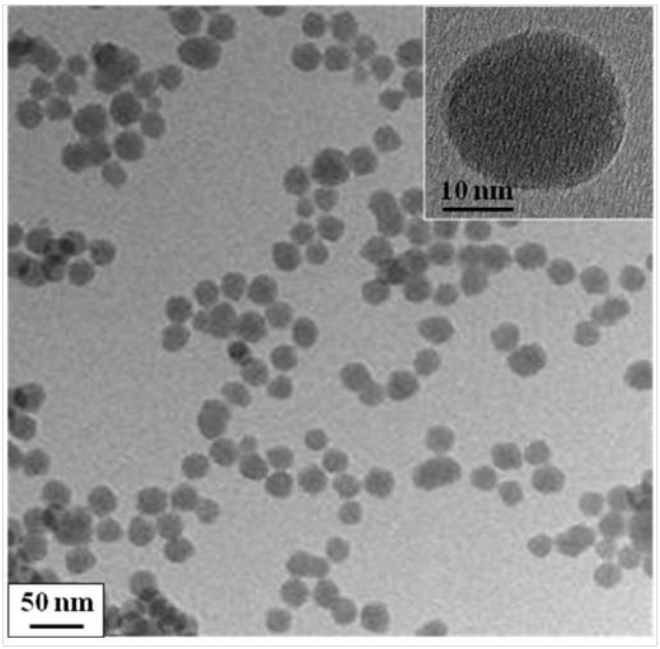

Figure 2.2: TEM of Silica-azide

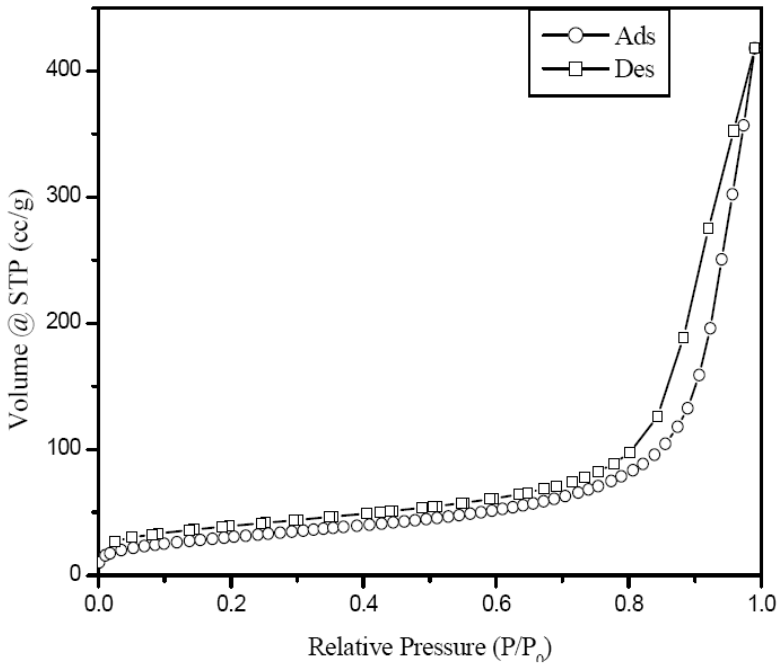

Figure 2.3: Nitrogen adsorption-desorption isotherms of Silica Nanoparticles

2.4.3 Elemental and Thermo gravimetric analysis:

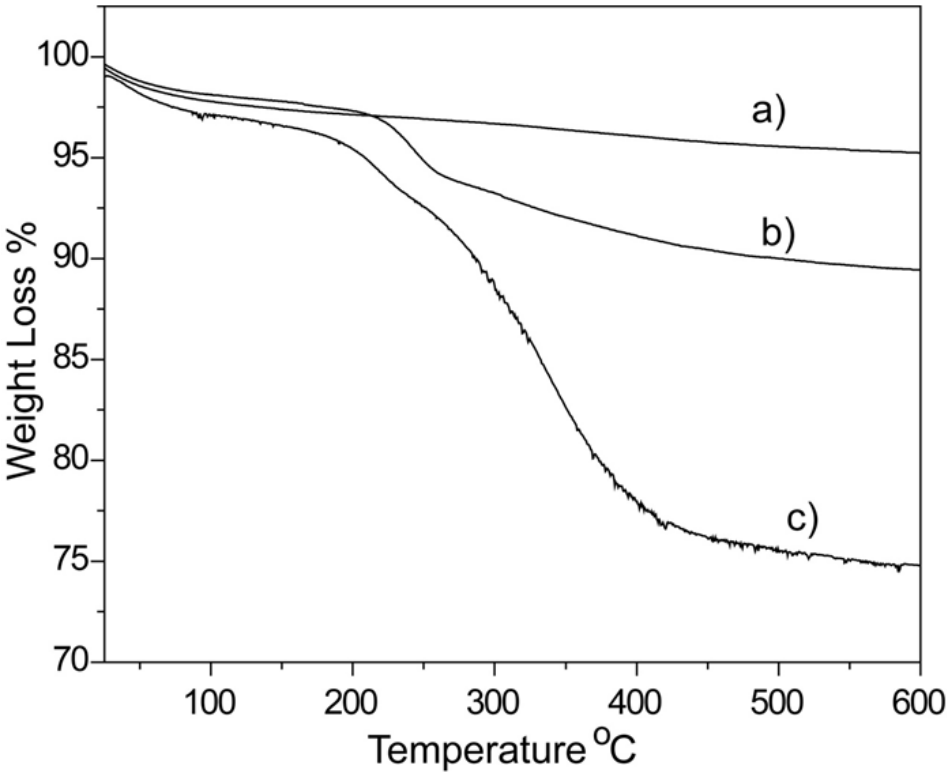

Figure 2.4: Thermo gravimetric analysis (TGA) of (a) bare Ludox, (b) N_3-silica, (c) Silica-**L1**

The thermo gravimetric analysis of the different functionalized silica materials are presented in Figure 2.4. Elemental and thermogravimatric analyses confirmed a grafting ratio of 0.7 mmol of azidopropyl group per gram of silica particle (Figure 2.4 a and 2.4 b). The nitrogen content was found out to be 3.4% while the TGA data displayed a loss of 7.2 % weight. Taking into consideration that the average particle size is 22 nm and a surface area of 110 m^2/g, (surface area was calculated from N_2 adsorption, Figure 2.3) the grafting density was determined to be 3.7 azidopropyl groups/nm^2. It has been calculated that 3-5 silanol sites/nm^2 are available for condensation of organosilane molecules on the silica surface for monolayer coverage.[35,36] Therefore, the grafting density of 3.7 azidopropyl groups/nm^2 signifies monolayer coverage of the azidopropyl groups on the silica surface. The TG-DTA analysis of Silica-**L1** (Figure 2.4 c) indicated a mass loss of 20 % between 200 ºC and

600 ºC which corresponds to a loading of 0.65 mmol of **L1**/gm of silica. The graft density was estimated to be about 3.6 group/nm^2 (6 µmol/m^2).

	Weight Loss (%)	**Ligand Grafting Density (mmol/gm)**
Ludox	2	-
N_3-Silica	7.2	0.684
Silica-L1	19.62	0.65
Silica-Au-L1	-	0.65
Silica-L2	-	0.59
Silica-Au-L2	-	-

Table 2.1: The calculated ligand grafting density and gold loading on different functionalized silica particles

2.4.4 FT-IR spectroscopy

The FT-IR spectra of the various functionalized silica nanoparticles are presented in the Figure 2.5. In the FT-IR spectrum, the peak at ~2100 cm^{-1} (which is absent in the starting Ludox particle) is the characteristic stretching vibration of organic azide (Figure 2.5 a and 2.5 b). Other significant peaks were observed at 1210, 1070, 800 and 466 cm^{-1} respectively. These peaks are typical of Si-O-Si bands that are associated with the formation of the silica networks. Therefore, the FT-IR spectra indicate that the azido group was efficiently incorporated on the surface of the silica nanoparticles.

The FT-IR spectra of Silica-**L1** and Silica-**L2** show a decrease in the azide peak intensity. The extent of "click" reaction was estimated using IR spectroscopy by monitoring the decrease in the integrated intensity of the $\upsilon_{as}(N_3)$ at 2100 cm^{-1} (Figure 2.5). Control reactions performed in the absence of CuI showed no conversion of the azide. The attachment of **L1** was further confirmed by the appearance of the υ(C=O) at 1610 cm^{-1} arising from the carboxylic moiety present in **L1**. The amount of grafted ligand in silica-**L1** was determined to be 0.53 mmol/g of silica by semi-quantitative IR.[37] This corresponds to a conversion of 75% of the available azides to the

corresponding triazoles. The grafting density of Silica-**L1** obtained by FT-IR was slightly lower than that estimated by TG-DTA. This could be due to the fact that the increase in the molar mass of the nanoparticle due to the addition of **L1** was not considered during the estimation of the extent of reaction. For control experiments, ligand **L2** was grafted onto the silica nanoparticles using similar methodology described above. It should be noted that **L2** has only one carboxylate ligand and hence is not expected to bind Au(III). The grafting density of ligand in Silica-**L2** was determined to be 0.59 mmol/g of silica which corresponds to the conversion of 85% of the available azides to the corresponding triazoles.

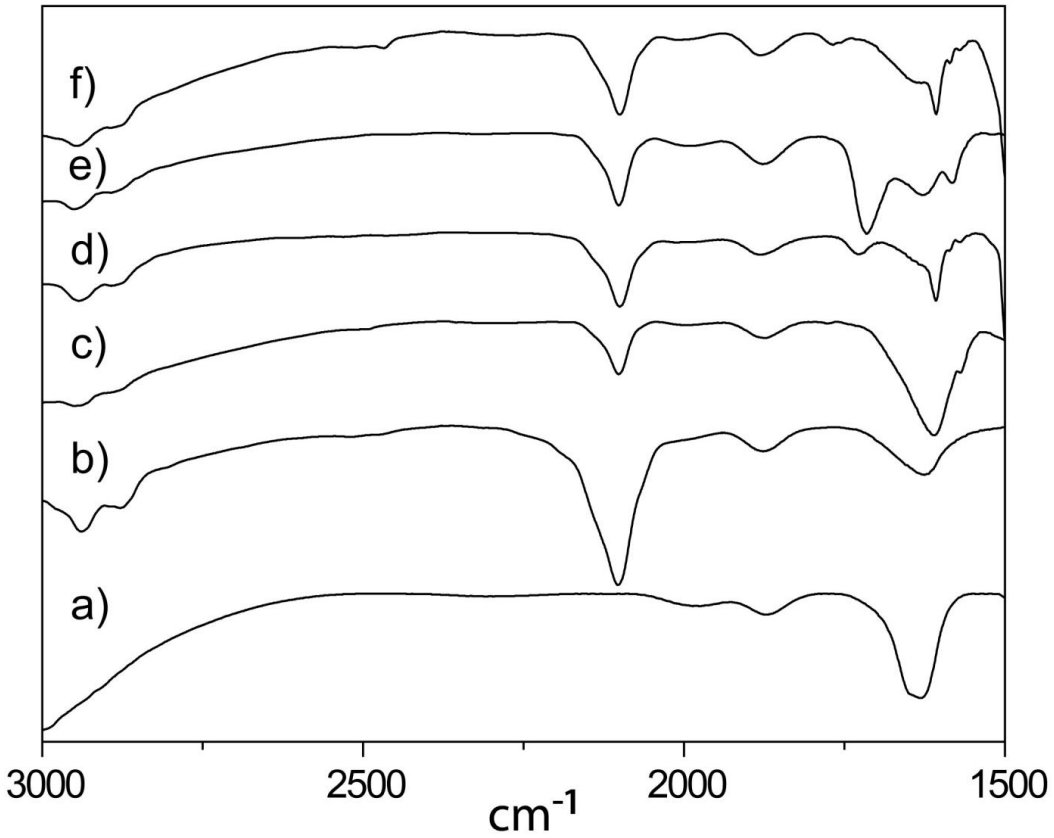

Figure 2.5: Infrared spectra of (a) bare Ludox, (b) N_3-silica, (c) Silica-**L1** (d) Silica-**L2** (e) Silica-Au-**L1**, and (f) Silica-Au-**L2**

The IR spectra of Silica-Au-**L1** showed that the γ(CO) shifted significantly from 1610 cm^{-1} to 1720 cm^{-1}, suggesting the binding of Au(III) to the O-atom of carboxylic acid of **L1**. Such shifts have been reported before for related Au(III) complexes with carboxylic containing ligands.[38,39] Similar attempts were made to incorporate Au(III) onto Silica-**L2**. However, the FT-IR of the resultant compound

formed (Silica-Au-**L2**) displayed no shift in the γ(CO) stretch as observed in Silica-Au-**L1**. This was expected since the ligand **L2** does not have the bidentate picolinic acid moiety present as in **L1** that was necessary to bind the Au(III).

2.4.5 Solid state CP-MAS NMR spectroscopy

2.4.5.1 ^{13}C CP-MAS NMR spectroscopy

Figure 2.6 represents the solid state ^{13}C CP-MAS NMR spectra of the functionalized silica materials. The solid state ^{13}C CP-MAS NMR spectrum of the azide grafted silica particles shows three peaks corresponding to C1 (10.81 ppm), C2 (23.66 ppm), C3 (54.95 ppm) that can be assigned to the three C-atoms of the azido-propyl chain. This spectra conclusively proves the incorporation of azide group on the silica surface.

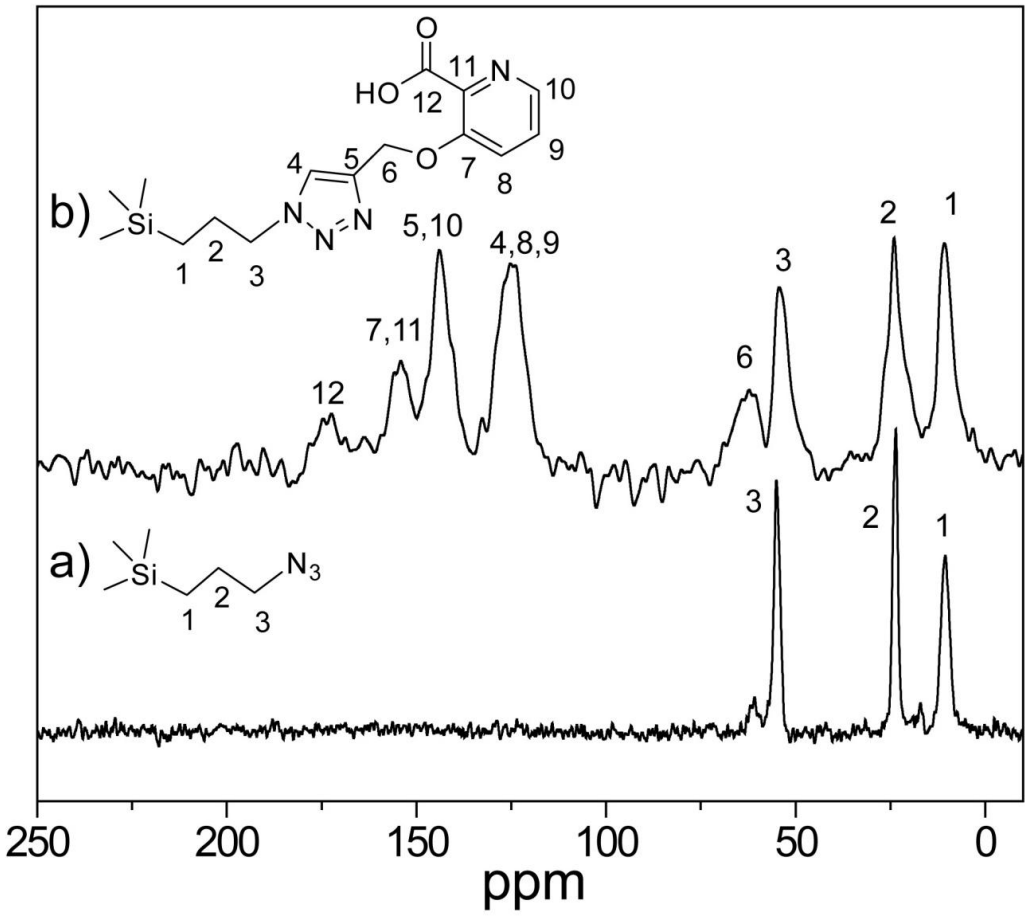

Figure 2.6: ^{13}C CP-MAS NMR of (a) N_3-silica and (b) Silica-**L1**

The solid state 13C CP-MAS NMR spectra of silica-**L1** displayed extra peaks in addition to the C1, C2 and C3 observed in N_3-silica (Figure 2.6 b). The extra resonances at 128 ppm and 144 ppm correspond to the C4 and C5 atoms of the

triazole indicating a covalent linkage of **L1** via the triazole ring. The C7 peak observed at 183 ppm is due to the presence of the C=O group of the carboxylic acid.

2.4.5.2 ^{29}Si CP-MAS NMR spectroscopy

The ^{29}Si CP MAS NMR spectra of the different functionalized silica materials are presented in Figure 2.7. The ^{29}Si CP MAS NMR spectra of N_3-Silica exhibit prominent peaks at around -111, -101, -67 and -58 ppm (Figure 2.7 a). The peaks at -111 and -101 ppm are assigned to the different types of the Si-sites namely Q3 [$(SiO)_3Si(OH)$] and Q4 [$(SiO)_4Si$]. Two other distinct peaks observed at -58 and -67 ppm are ascribed to the functionalized sites of the Si-framework namely T2 [$R(SiO)_2Si(OH)$] and T3 [$R(SiO)_3Si$] respectively, where R is the azidopropyl group. Thus, all these data conclusively proves that the azidopropyl group was grafted successfully onto the silica nanoparticle.

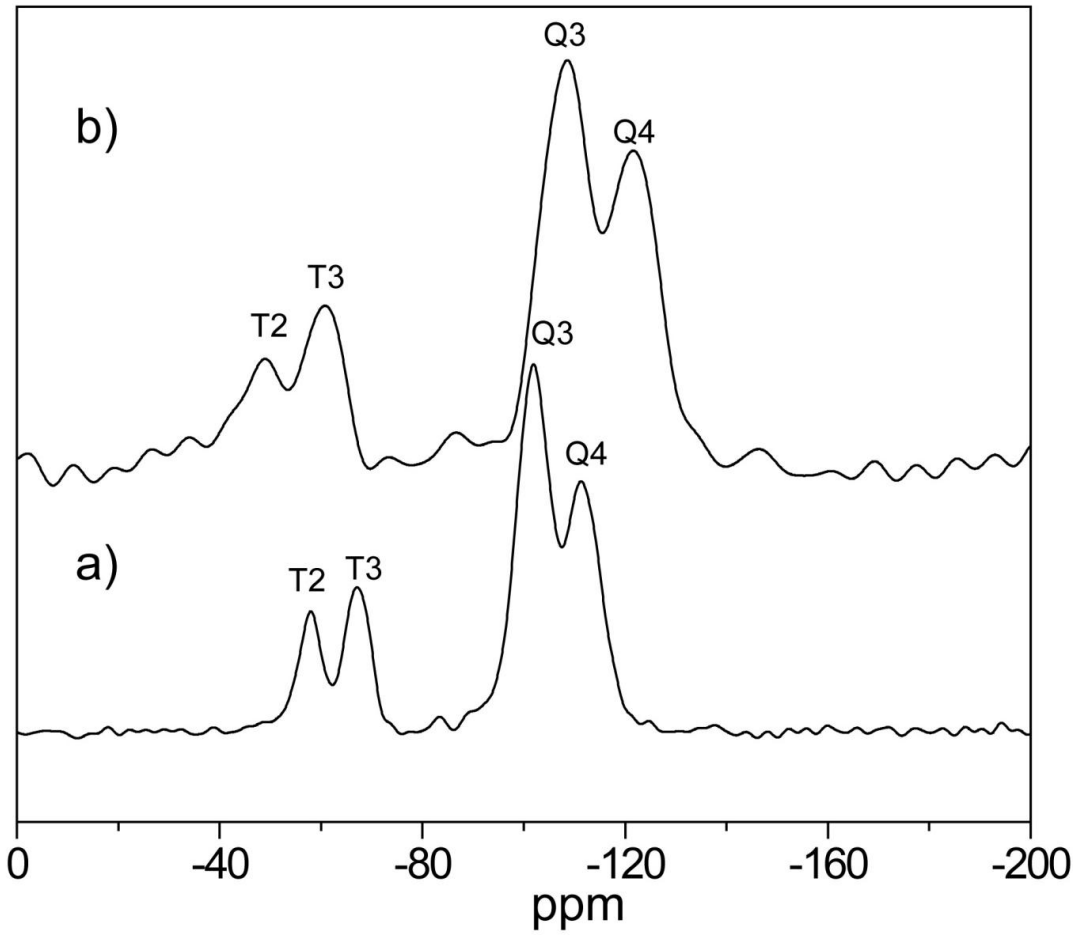

Figure 2.7: ^{29}Si CP-MAS NMR of (a) N_3-silica and (b) Silica-**L1**

The ^{29}Si CP MAS spectrum of silica-**L1** showed little or no change from the starting azide grafted silica particles indicating that the Si-sites do not undergo any chemical change during the reaction and its work-up (Figure 2.7 b). This is expected since the T1 and T2 Si-sites are that from the azido-propyl modified silica and should not undergo any change during the course of the click reaction.

2.4.6 ICP analysis:

ICP analysis was carried out to determine the amount of Cu and Au present in the materials (Table 2.1). After click reaction the presence of Cu in Silica-**L1** and Silica-**L2** was tested using ICP analysis. No appreciable amount of Cu was found which indicates that the extensive washing protocol used was sufficient to remove all the Cu from these hybrid materials.

	[Au] (mmol/gm)
Ludox	-
N_3-Silica	0.005
Silica-L1	-
Silica-Au-L1	0.339
Silica-L2	-
Silica-Au-L2	0.09

Table 2.2: The calculated Au concentration in different functionalized silica particles.

From the ICP analysis, Au concentration was determined to be 0.34 mmol/g of Silica-**L1**. This corresponds to the fact that Au(III) was bound to 55% of the available sites of the picolinic acid moiety of silica-**L1**. The Au concentration determined by ICP was found out to be only 0.09 mmol/g of Silica-Au-**L2**. This was expected since the ligand **L2** does not have the bidentate picolinic acid moiety present as in **L1**. The small amount of Au(III) seen from ICP was probably due to some non-specific binding to the surface silanol groups.

2.4.7 X-ray photoelectron spectroscopy:

The chemical composition of silica-**L1** was also verified with X-ray photoelectron spectroscopy. All the pristine spectra have been background corrected using the Shirley algorithm[40] and the curves deconvoluted using standard curve fitting

programs. The signals from Si 1s core level could be resolved into three components mainly occurring at 102.0, 103.4, 105.1 eV (Figure 2.8 A). These are assigned to Si-O-H, Si-O-Si, Si-O-C respectively. Three chemically distinct components are observed at 284.3, 285.7 and 287.9 eV in the case of the C1s core level spectrum (Figure 2.8 B). The peak at ~284 eV was ascribed to the adventious carbon. The peak at higher binding energy at ~286 eV could be ascribed to the carbon bound to N. On the other hand the peak at ~288eV could be ascribed to the –C=O carbon. The O1s signals can be deconvoluted to three components at 531.1, 532.6, 533.8 eV which proves the presence of different components of O1s (Figure 2.8 D). The high BE component at 533.8 eV is accredited to the loading of **L1** onto Silica azide. Two chemically distinct components are observed at 399.1, 400.2 and 402.0 eV in the case of the N1s core level spectrum (Figure 2.8 C). The higher binding energy was assigned to the pyridine N present in the **L1** molecule attached to silica.

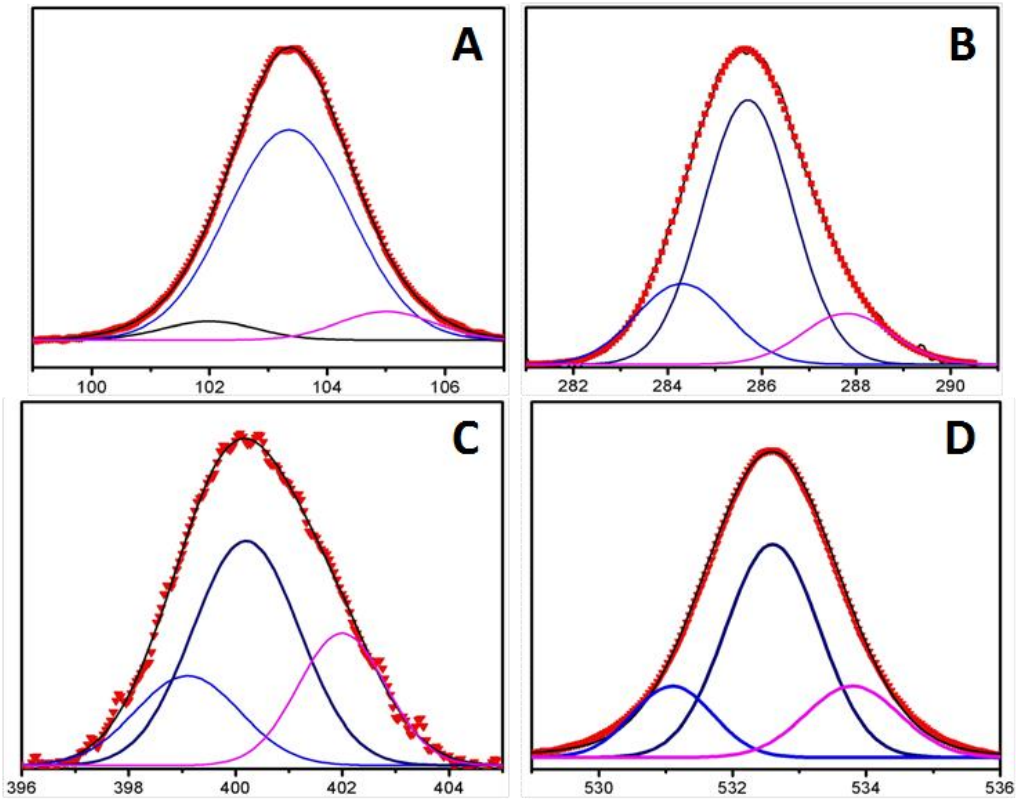

Figure 2.8: XPS of Silica-**L1** (A) Si 2p (B) C 1s (C) N 1s (D) O 1s core levels Silica-**L1**

The chemical composition of silica-Au-**L1** was also probed using X-Ray photoelectron spectroscopy (Figure 2.9). The spectra have been background corrected

using the Shirley algorithm prior to curve resolution. The signals from the Si 2p, C1s, O1s and N1s were more or less similar to the earlier peaks observed for the starting silica-L1. (Figure 2.9 A, B, C, D) Further, the Au 4f core level signals could be resolved into two chemically distinct species corresponding to Au(I) and Au (III) (Figure 2.9 E). The pair at 84.6 and 88.2 eV can be assigned as the spin orbit coupling of Au $4f_{7/2}$ and Au $4f_{5/2}$ respectively of Au(I).

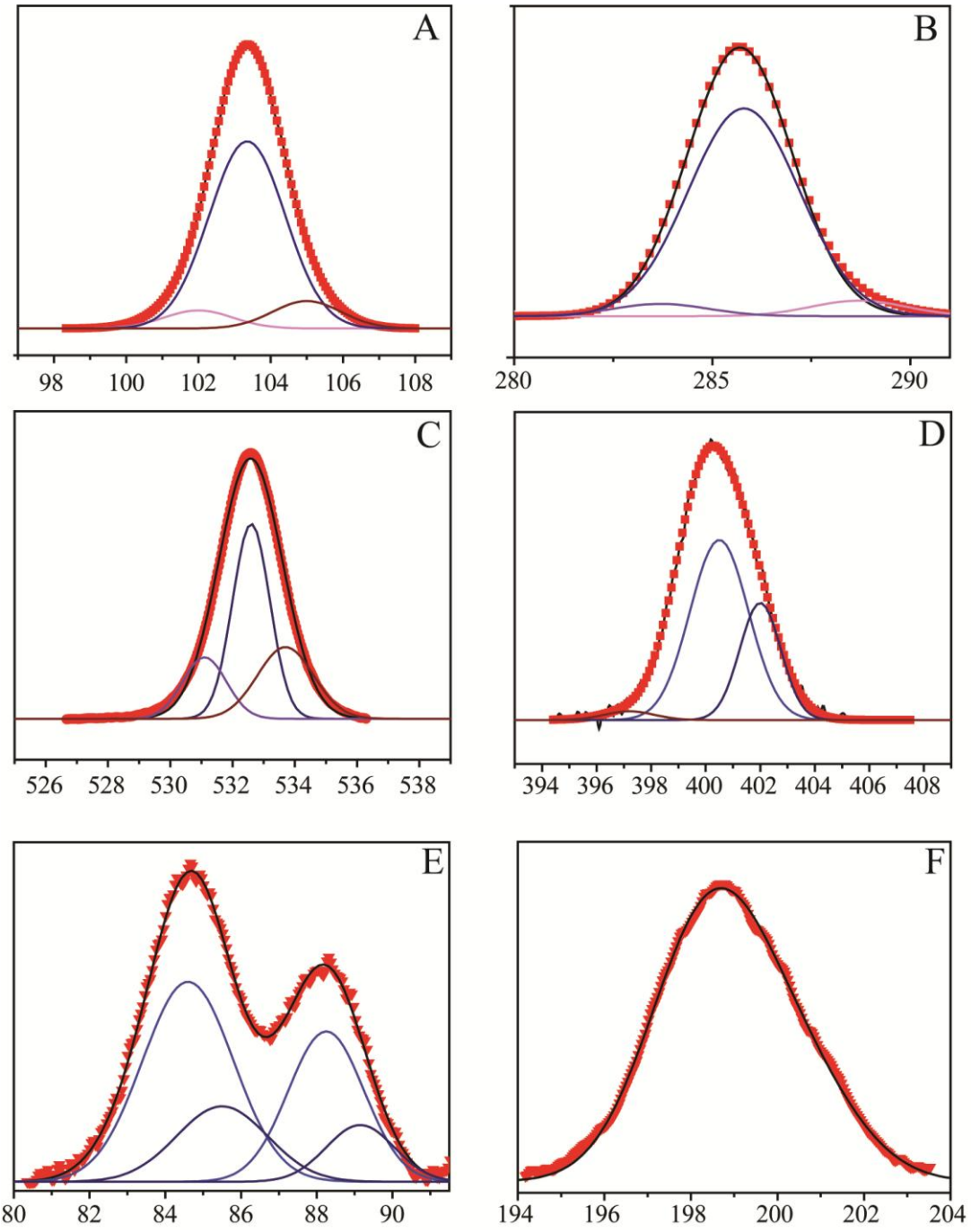

Figure 2.9: XPS of Silica-Au-**L1** (A) Si 2p (B) C 1s (C) N 1s (D) O 1s (E) Au 4f (F) Cl 2p core levels of Silica-Au-**L1.**

The presence of signals at 85.5 eV and 89.1 eV is related to the presence of Au (III). It can be clearly seen that the Au (III) component is less when compared to Au (I) which is unusual. To probe this further, we prepared the complex bis(pyridine-2-carboxylato)-gold(III) perchlorate and recorded its XPS.[39] Interestingly, here also we could see peaks corresponding to Au (III) and Au (I) which is similar to the XPS of Silica-Au-**L1** (Figure 2.10). The ambiguous detection of Au(I) can be attributed to the electron donating capability of **L1** to Au(III) and strong X-ray radiation while recording XPS.[41] However, we would like to mention that this did not influence in anyway the catalytic nature of the complex as can be seen further. The presence of chloride was confirmed from the peak at 198.8 eV (Figure 2.9 F).

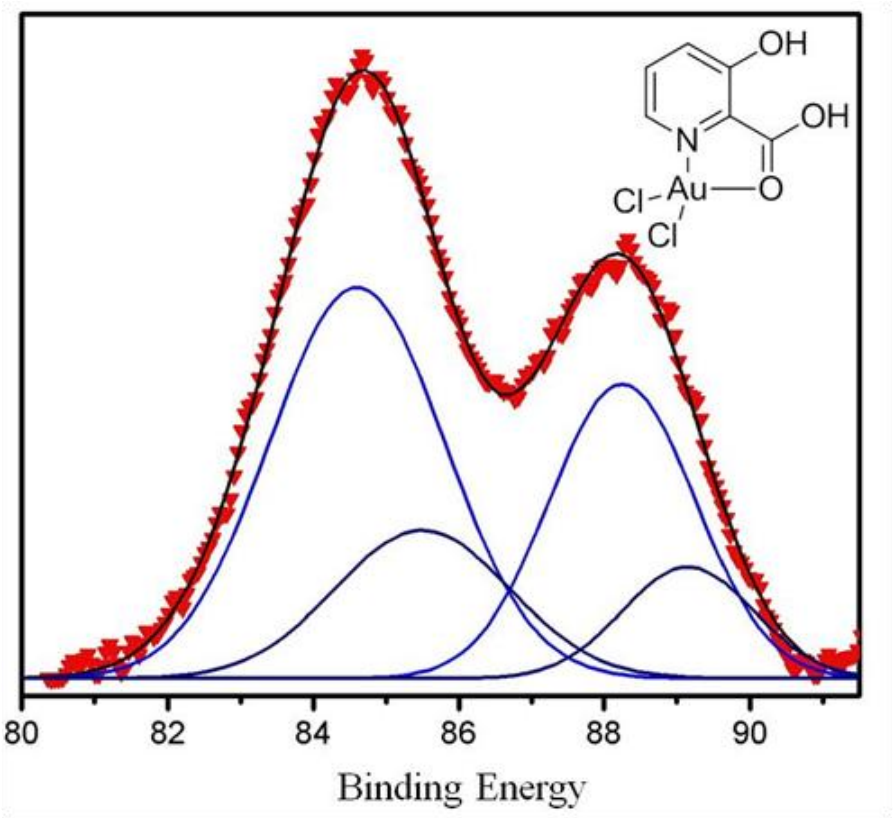

Figure 2.10: XPS of Au 4f of the complex bis(pyridine-2-carboxylato)-gold(III) perchlorate.

2.5 Hashmi phenol synthesis by Au immobilized silica nanoparticles

The catalysts silica-Au-**L1** and silica-Au-**L2** were then evaluated for their ability to activate alkyne moiety of furanyl propargyl ether to trigger intramolecular Diels-Alder reaction to give isobenzofuran (Scheme 2.6). Accordingly, 5-methylfuranyl propargyl ether (3) was treated with silica-Au-**L1** (2 mol% Au) in acetonitrile leading to the formation of the isobenzofuran (4). The reaction was found

to be very exothermic and hence it was carried out at 0 °C. The reaction was complete in about 100 min as was observed from complete disappearance of the starting material, compound 3, by LC-MS analysis (Figure 2.11). Isolation of the product showed the yield of the reaction to be 90%. The same reaction, carried out using $AuCl_3$ as the catalyst, took more than 3 h to undergo completion clearly exemplifying the advantages of silica-Au-**L1** over $AuCl_3$. This is expected since the picolinic acid ligand that binds the Au(III) in silica-Au-**L1** is known to accelerate the rate of the reaction as has been shown by Hashmi et. al.[32] In the control experiment, formation of isobenzofuran was not observed using silica-Au-**L2**. The catalyst silica-Au-**L2** does not contain appreciable amounts of Au(III) since **L2**, a monodentate ligand having only carboxylic acid moiety, is unable to bind Au(III) effectively. This also clearly shows that the presence of Au(III) in silica-Au-**L1** is key to the progress of this reaction.

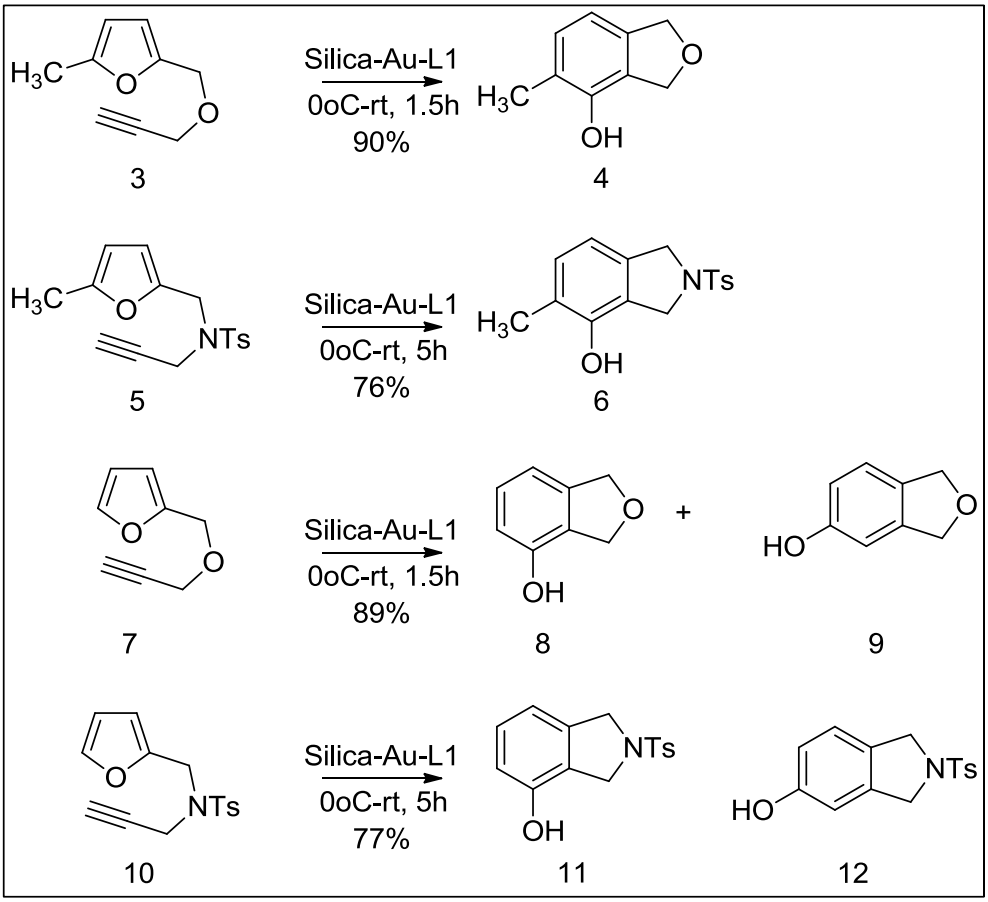

Scheme 2.6: Experimental details of the Hashmi reaction performed using silica-Au-**L1** conjugate on various substrates.

Cycle 1: Hashmi Reaction (Time Course Study)

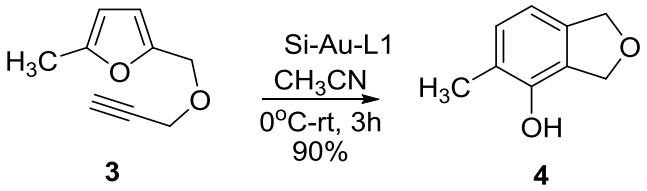

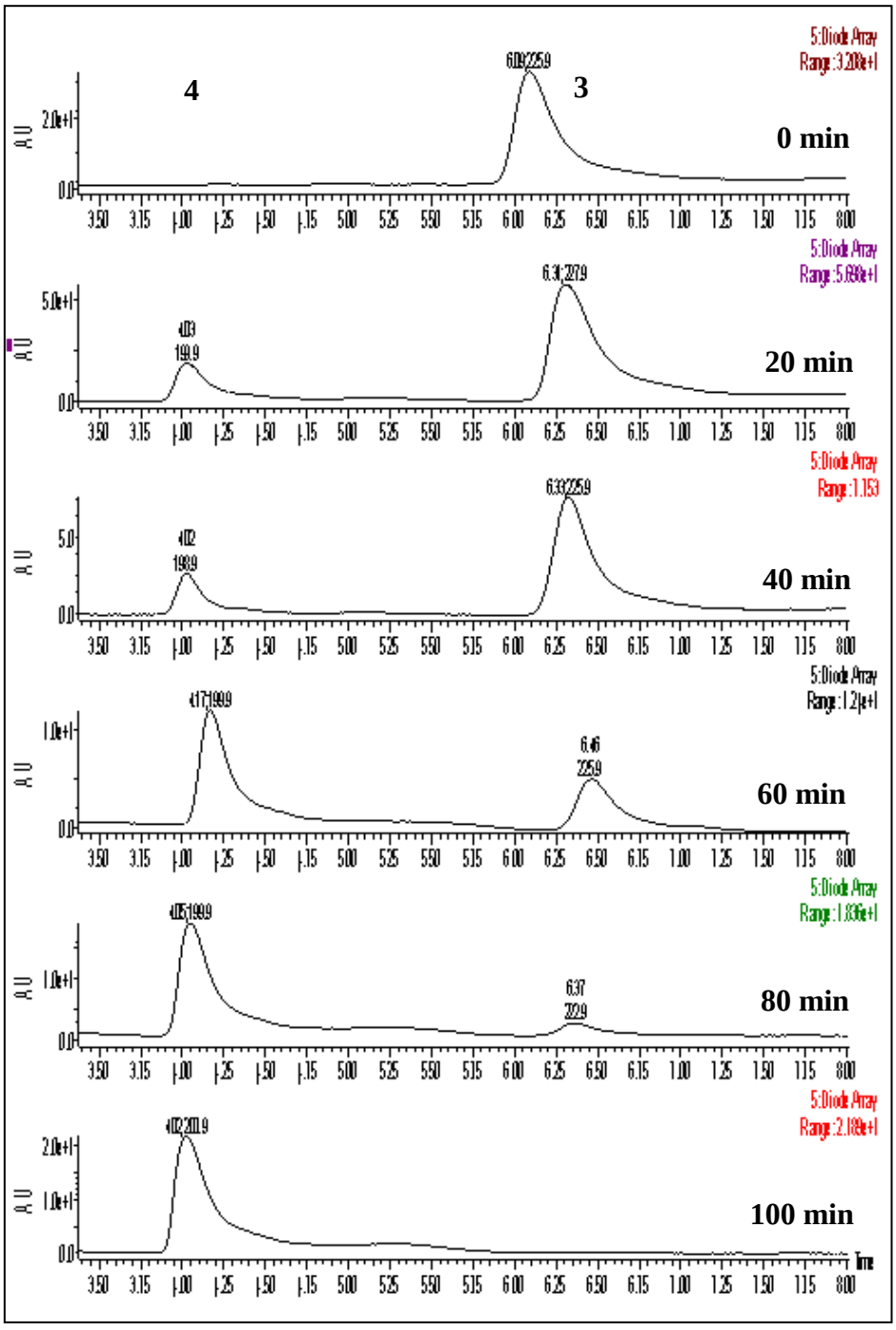

Figure 2.11: Time dependent LC-MS spectra for 1st cycle

Cycle 2: Hashmi Reaction (Time Course Study)

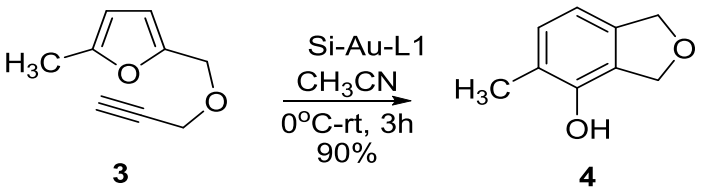

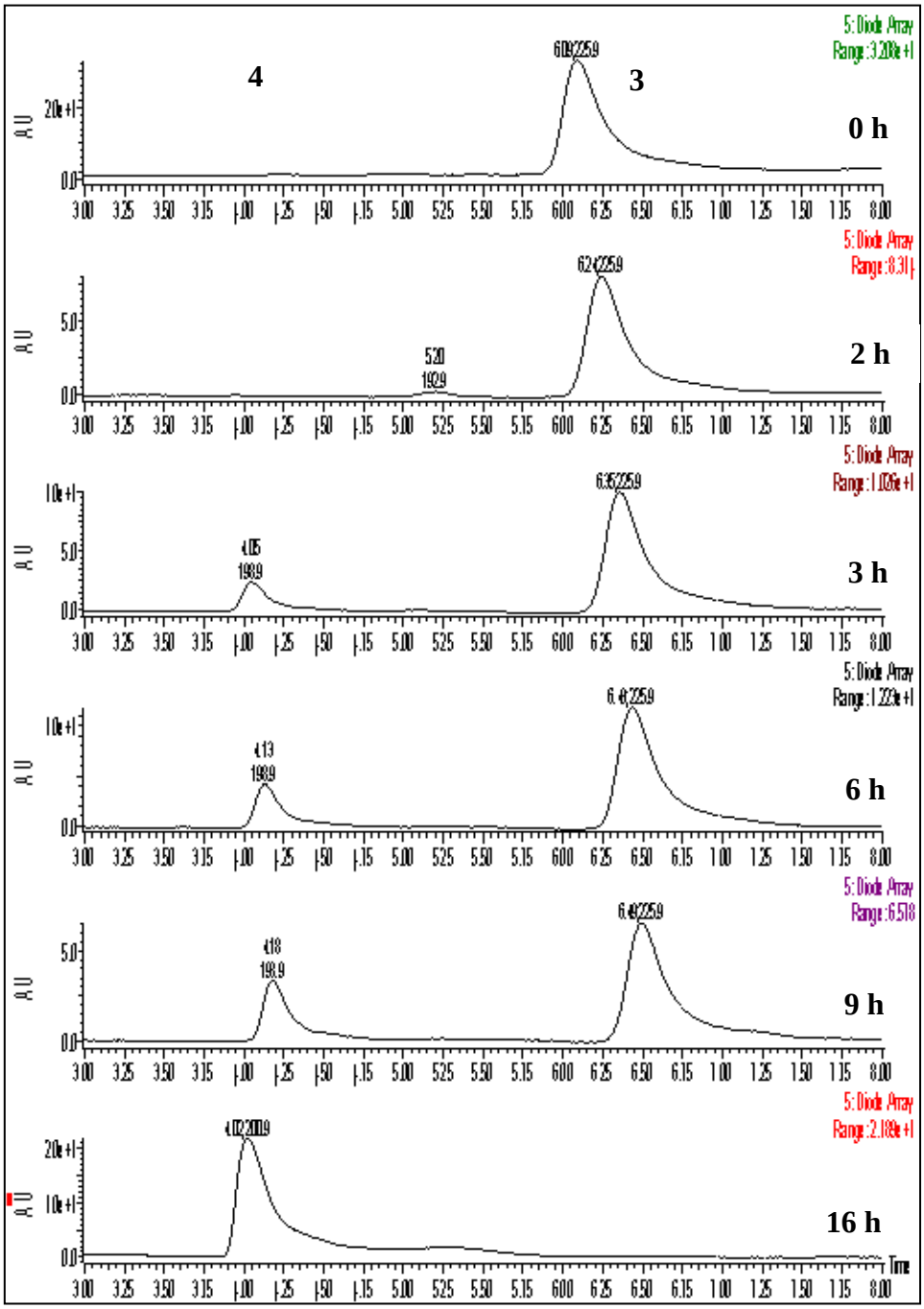

Figure 2.12: Time dependent LC-MS spectra for 2nd cycle

At the end of the reaction, the silica-Au-**L1** could be isolated from the reaction mixture by centrifugation. Isolated silica-Au-**L1** particles were washed three times with acetonitrile, sonicated and then resuspended in acetonitrile to perform the Hashmi's reaction on compound 3 again (Figure 2.12). This isolated catalyst was again found to be active for the synthesis of isobenzofuran 4 albeit taking longer periods of time for completion (16 hrs). Subsequently, this catalyst was found to be inactive for the synthesis of isobenzofurans. Therefore it was obvious that the catalyst was losing activity during the progress of the reaction. One possibility for this deactivation might be the leaching of Au during the progress of the reaction. The amount of Au present in silica-Au-**L1** was estimated after each catalytic cycle by ICP. It was determined that the amount of gold even after three cycles of reaction was within 15% of the initial loading. This negates the possibility of Au leaching as the reaction progresses.

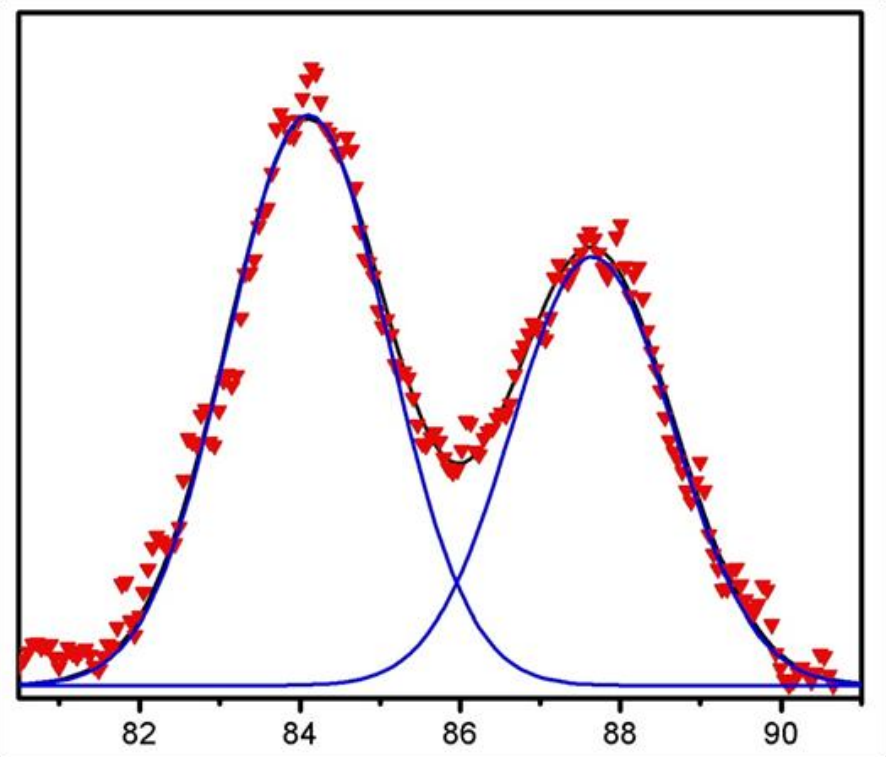

Figure 2.13: XPS of Au 4f of the spent catalyst after 2nd run

Then, to find the reasons for the loss of catalytic activity after the second cycle, the XPS of the spent catalyst has been analyzed (Figure 2.13). Unfortunately it displayed the spin orbit pair at 84.1 and 87.7 eV that can be assigned to Au(0). The presence of Au(0) indicates that during the progress of the reaction, the Au(III) complex was getting reduced to Au(0) thereby slowly rendering the catalyst inactive.

As mentioned earlier, the reaction is very exothermic, and the heat generated during the reaction may have reduced Au(III) to Au(0) which corroborate the recent findings by Shi and co-workers.[42]

2.6 Conclusion:

In conclusion, a successful strategy to immobilize Au(III) onto silica nanoparticles through CuAAC "click chemistry" protocol has been demonstrated. The catalyst has been thoroughly and extensively characterized using a variety of analytical and spectroscopic techniques. The catalyst was found to activate the carbon-carbon π- bond of alkynyl group in Hashmi's phenol synthesis. The same catalyst is being evaluated for other Au(III) catalyzed cascade reactions initiated by heteroatom nucleophiles with π-electrophiles. The developed methodology is a generic one and can be extended to immobilizing other metal complexes and/or other surfaces including magnetic core-shell systems. Moreover, this study allowed to gain enough expertise in silica functionalization that was necessary for our further investigations.

2.7 References:

1. Hagen, J., *Industrial Catalysis: A practical Approach*. 2nd Edition; Wiley-VCH: 2006.

2. Mueller, C.; Vogt, D., Immobilization and compartmentalization of homogeneous catalysts. *Handb. Green Chem.: Green Catal.*, **2009,** 1, 127-152.

3. Dickerson, T. J.; Reed, N. N.; Janda, K. D., Soluble polymers as scaffolds for recoverable catalysts and reagents. *Chemical Reviews*, **2002,** 102, (10), 3325-3344.

4. Madhavan, N.; Jones, C. W.; Weck, M., Rational approach to polymer-supported catalysts: Synergy between catalytic reaction mechanism and polymer design. *Accounts of Chemical Research*, **2008,** 41, (9), 1153-1165.

5. Pagliaro, M.; Ciriminna, R., New fluorinated functional materials. *Journal of Materials Chemistry*, **2005,** 15, (47), 4981-4991.

6. Astruc, D.; Lu, F.; Aranzaes, J. R., Nanoparticles as recyclable catalysts: The frontier between homogeneous and heterogeneous catalysis. *Angewandte Chemie International Edition*, **2005,** 44, (48), 7852-7872.

7. Schatz, A.; Hager, M.; Reiser, O., Cu(II)-Azabis(oxazoline)-complexes immobilized on superparamagnetic magnetite@silica-nanoparticles: A highly selective and recyclable catalyst for the kinetic resolution of 1,2-Diols. *Advanced Functional Materials*, **2009,** 19, (13), 2109-2115.

8. Stevens, P. D.; Li, G.; Fan, J.; Yen, M.; Gao, Y., Recycling of homogeneous Pd catalysts using superparamagnetic nanoparticles as novel soluble supports for Suzuki, Heck, and Sonogashira cross-coupling reactions. *Chemical Communications*, **2005**, (35), 4435-4437.

9. Tandukar, S.; Sen, A., N-heterocyclic carbene-palladium complex immobilized on silica nanoparticles. Recyclable catalyst for high yield Suzuki and Heck coupling reactions under mild conditions. *Journal of Molecular Catalysis A: Chemical*, **2007,** 268, (1-2), 112-119.

10. Haruta, M.; Yamada, N.; Kobayashi, T.; Iijima, S., Gold catalysts prepared by coprecipitation for low-temperature oxidation of hydrogen and of carbon monoxide. *Journal of Catalysis*, **1989,** 115, (2), 301-309.

11. Hutchings, G. J., Vapor phase hydrochlorination of acetylene: Correlation of catalytic activity of supported metal chloride catalysts. *Journal of Catalysis*, **1985,** 96, (1), 292-295.

12. Hashmi, A. S. K.; Hutchings, G. J., Gold Catalysis. *Angewandte Chemie International Edition*, **2006,** 45, (47), 7896-7936.

13. Corma, A.; Garcia, H., Supported gold nanoparticles as catalysts for organic reactions. *Chemical Society Reviews* **2008,** 37, (9), 2096-2126.

14. Horvath, D.; Polisset-Thfoin, M.; Fraissard, J.; Guczi, L., Novel preparation method and characterization of Au-Fe/HY zeolite containing highly stable gold nanoparticles inside zeolite supercages. *Solid State Ionics*, **2001,** 141-142, (0), 153-156.

15. Lin, H.-P.; Chi, Y.-S.; Lin, J.-N.; Mou, C.-Y.; Wan, B.-Z., Direct Synthesis of MCM-41 Mesoporous Aluminosilicates Containing Au Nanoparticles in Aqueous Solution. *Chemistry Letters*, **2001,** 30, (11), 1116-1117.

16. Zhu, J.; Kanya, Z.; Puntes, V. F.; Kiricsi, I.; Miao, C. X.; Ager, J. W.; Alivisatos, A. P.; Somorjai, G. A., Encapsulation of Metal (Au, Ag, Pt) Nanoparticles into the Mesoporous SBA-15 Structure. *Langmuir*, **2003,** 19, (10), 4396-4401.

17. Mukherjee, P.; Ranjan Patra, C.; Kumar, R.; Sastry, M., Entrapment and catalytic activity of gold nanoparticles in amine-functionalized MCM-41 matrices synthesized by spontaneous reduction of aqueous chloroaurate ions. *PhysChemComm*, **2001,** 4, (5), 24-25.

18. Gorin, D. J.; Sherry, B. D.; Toste, F. D., Ligand Effects in Homogeneous Au Catalysis. *Chem. Rev. (Washington, DC, U. S.)*, **2008,** 108, (8), 3351-3378.

19. Hashmi, A. S. K., Gold-catalyzed organic reactions. *Chemical Reviews*, **2007,** 107, (7), 3180-3211.

20. Hashmi, A. S. K.; Rudolph, M., Gold catalysis in total synthesis. *Chemical Society Reviews*, **2008,** 37, (9), 1766-1775.

21. Hashmi, A. S. K.; Schwarz, L.; Choi, J.-H.; Frost, T. M., A New Gold-Catalyzed C−C Bond Formation. *Angewandte Chemie International Edition*, **2000,** 39, (13), 2285-2288.

22. Stephen, A.; Hashmi, K., Homogeneous catalysis by gold. *Gold Bulletin*, **2004,** 37, (1-2), 51-65.

23. de Almeida, M. P.; Carabineiro, S. A. C., The Best of Two Worlds from the Gold Catalysis Universe: Making Homogeneous Heterogeneous. *ChemCatChem*, **2012,** 4, (1), 18-29.

24. Corma, A.; Gutiérrez-Puebla, E.; Iglesias, M.; Monge, A.; Pérez-Ferreras, S.; Sánchez, F., New Heterogenized Gold(I)-Heterocyclic Carbene Complexes as Reusable Catalysts in Hydrogenation and Cross-Coupling Reactions. *Advanced Synthesis & Catalysis*, **2006,** 348, (14), 1899-1907.

25. Comas-Vives, A.; Gonzalez-Arellano, C.; Corma, A.; Iglesias, M.; Sánchez, F.; Ujaque, G., Single-Site Homogeneous and Heterogeneized Gold(III) Hydrogenation Catalysts: Mechanistic Implications. *Journal of the American Chemical Society*, **2006,** 128, (14), 4756-4765.

26. Corma, A.; Gonzalez-Arellano, C.; Iglesias, M.; Navarro, M. T.; Sanchez, F., Synthesis of bifunctional Au-Sn organic-inorganic catalysts for acid-free hydroamination reactions. *Chemical Communications*, **2008**, (46), 6218-6220.

27. Corma, A.; Gonzalez-Arellano, C.; Iglesias, M.; Perez-Ferreras, S.; Sanchez, F., Heterogenized gold(I), gold(III), and palladium(II) complexes for C-C bond reactions. *Synlett*, **2007**, (11), 1771-1774.

28. Gonzalez-Arellano, C.; Corma, A.; Iglesias, M.; Sanchez, F., Soluble gold and palladium complexes heterogenized on MCM-41 are effective and versatile catalysts. *European Journal of Inorganic Chemistry*, **2008**, (7), 1107-1115.

29. Carrettin, S.; Blanco, M. C.; Corma, A.; Hashmi, A. S. K., Heterogeneous gold-catalysed synthesis of phenols. *Advanced Synthesis & Catalysis*, **2006,** 348, (10-11), 1283-1288.

30. Rostovtsev, V. V.; Green, L. G.; Fokin, V. V.; Sharpless, K. B., A stepwise huisgen cycloaddition process: Copper(I)-catalyzed regioselective "ligation" of azides and terminal alkynes. *Angewandte Chemie International Edition*, **2002,** 41, (14), 2596-2599.

31. Nebhcni, L.; Barner-Kowollik, C., Orthogonal transformations on solid substrates: Efficient avenues to surface modification. *Advanced Materials*, **2009,** 21, (34), 3442-3468.

32. Hashmi, A. S. K.; Weyrauch, J. P.; Rudolph, M.; Kurpejovic, E., Gold catalysis: The benefits of N and N,O ligands. *Angewandte Chemie International Edition*, **2004,** 43, (47), 6545-6547.

33. Bartholome, C.; Beyou, E.; Bourgeat-Lami, E.; Chaumont, P.; Zydowicz, N., Nitroxide-Mediated Polymerizations from Silica Nanoparticle Surfaces: "Graft from" • Polymerization of Styrene Using a Triethoxysilyl-Terminated Alkoxyamine Initiator. *Macromolecules*, **2003,** 36, (21), 7946-7952.

34. Terry, T. J.; Stack, T. D. P., Covalent Heterogenization of a Discrete Mn(II) Bis-Phen Complex by a Metal-Template/Metal-Exchange Method: An Epoxidation Catalyst with Enhanced Reactivity. *Journal of the American Chemical Society*, **2008,** 130, (14), 4945-4953.

35. Cousinie, S.; Gressier, M.; Alphonse, P.; Menu, M. J., Silica-based nanohybrids containing dipyridine, urethan, or urea derivatives. *Chemistry of Materials*, **2007,** 19, (26), 6492-6503.

36. Cousinie, S.; Gressier, M.; Reber, C.; Dexpert-Ghys, J.; Menu, M. J., Europium(III) complexes containing organosilyldipyridine ligands grafted on silica nanoparticles. *Langmuir*, **2008,** 24, (12), 6208-6214.

37. Malvi, B.; Sarkar, B. R.; Pati, D.; Mathew, R.; Ajithkumar, T. G.; Sen Gupta, S., "Clickable" SBA-15 mesoporous materials: Synthesis, characterization and their reaction with alkynes. *Journal of Materials Chemistry*, **2009,** 19, (10), 1409-1416.

38. Dar, A.; Moss, K.; Cottrill, S. M.; Parish, R. V.; McAuliffe, C. A.; Pritchard, R. G.; Beagley, B.; Sandbank, J., Complexes of gold(III) with mononegative bidentate N,O-ligands. *Journal of the Chemical Society, Dalton Transactions*, **1992**, (12), 1907-1913.

39. Vicente, J.; Chicote, M. T.; Bermudez, M. D., 2-[(Dimethylamino)methyl]phenylgold(III) complexes. *Journal of Organometallic Chemistry*, **1984,** 268, (2), 191-5.

40. Shirley, D. A., High-Resolution X-Ray Photoemission Spectrum of the Valence Bands of Gold. *Physical Review B*, **1972,** 5, (12), 4709.

41. Singh, S.; Prasad, B. L. V., Nearly complete oxidation of Au(0) in hydrophobized nanoparticles to Au(3+) ions by N-bromosuccinimide. *Journal of Physical Chemistry C*, **2007,** 111, (39), 14348-14352.

42. Chen, Y. F.; Yan, W. M.; Akhmedov, N. G.; Shi, X. D., 1,2,3-Triazole as a Special "X-Factor" in Promoting Hashmi Phenol Synthesis. *Organic Letter*, **2010,** 12, (2), 344-347.

Chapter 3

Development of a multifunctional catalyst for a "relay" reaction: A proof of a concept

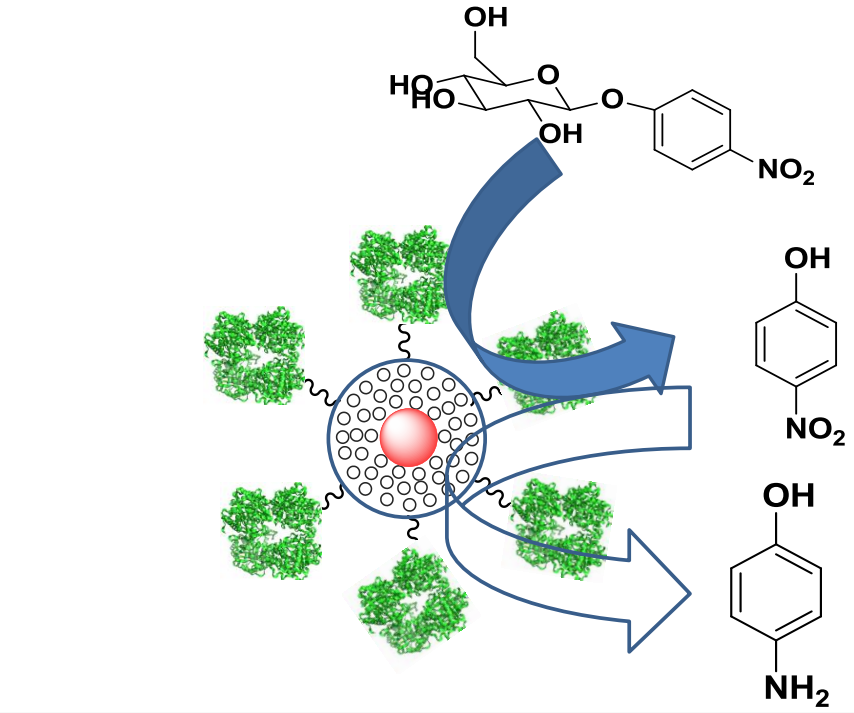

In the chapter the proof of concept of the preparation of a multifunctional catalyst that carry out a "relay" reaction has been demonstrated. The catalyst consists of a surface bound enzyme on a metal core silica shell nanoparticle architecture carries the 1st reaction and the metal nanoparticles bring out the 2nd reaction on the product released from the 1st reaction. In particular, the catalytic activity of glucosidase grafted Au@mSiO$_2$ on 4-nitrophenyl-β-glucopyranoside were studied, where, glucosidase will catalyse the 1st step to generate 4-nitrophenol, which acts as a substrate for the next reduction step which is catalysed by Au nanoparticles present inside the mesoporous silica shell.

Part of the work discussed in this chapter has been published in
Anal Kr. Ganai, Pravin Shinde, Basab B. Dhar, Sayam Sen Gupta, B.L.V. Prasad, *RSC Adv.*, **2013**, 3, 2186-2191

3.1 Introduction:

One of the reasons to choose silica as a matrix was the possibility of covalent grafting of molecular systems on its surface and also its amorphous nature that allows it to be a compatible material to cover any metal/metal oxide surface to reveal a core-shell architecture. A single homogeneous catalyst has been immobilized on the surface of silica nanoparticles and its catalytic activity has been discussed in the last chapter. For multistep organic synthesis, it would be nicer if a single catalyst can carry out two consecutive reactions.[2] The pain of separating heterogeneous catalyst after each reaction would decrease if such a multifunctional catalyst could be developed.[3] Also, the advantage of such system lies in the fact that multiple catalysts operating in tandem would eliminate the time and yield losses associated with the isolation and purification of intermediates in multistep sequences. Hence a lot of effort has been directed towards development of such concurrent tandem catalytic systems. In this chapter mainly we have focused on developing a composite catalyst which can carry out two consecutive reactions.

To create such a composite catalyst for two concurrent reactions, immobilizations of several catalysts are required.[1] Immobilization of catalyst is important for industrialization of homogenous catalyst.[2] But it is not easy to anchor different catalysts on the solid support precisely. The closeness of the active sites of the catalysts also can hamper the reaction sequence. To overcome these issues, porous matrices has been extensively used which acts as a nano reactor. A catalyst can be grafted inside the pore of a porous support, where the pore can be used for transporting reactant molecules. Among other solid supports, mesoporous silica materials with controllable porosity[4] and well-ordered arrays of uniform nanometer-sized channel pores[5] have been extensively used as hard templates for the immobilization of homogeneous catalysts. Two separate catalysts, one is inside the pore and other is on the surface of the particles, could be immobilized in such a system.

Many industrially relevant reactions are known to be catalysed by metal nanoparticles or enzymes.[6-8] However, the high cost and their limited supply of the catalytic component is a major hurdle for utilization in various industrial processes.[9] Even in the realm of nanoparticles, different architectures like core-shell particles loaded inside porous matrices,[10-13] polymer nano conjugates,[14-16] and carbon

supported catalysts[17] have all been proposed and tested. There were already many literature reports where mesoporous silica coated metal nanoparticles[18] were used as a nano-reactor[19] for various catalytic reactions e.g. catalytic reductions of p-nitrophenol[20,21] or photo-catalytic activities in the degradation of phenols and Cr (VI). Although most of the efforts have been directed towards development of organometallic complex based tandem catalytic systems, the combination of enzyme and transition metal catalysis seems to have received much less attention.

In this premise, the design and synthesis of enzyme grafted mesoporous silica, which in turn is coated on a metal nanoparticle surface is an appealing concept because a multistep reaction sequence requiring either a cooperative or independent catalytic performance of the metal and enzyme can be carried out. In literature, there are many examples of bifunctional mesoporous material catalysts in which two different organic functional groups such as, bronsted acid with bronsted base, amines with sulphonic acid, are incorporated to do successive two reactions.[22-24] But to the best of our knowledge, immobilization of enzymes on the surface of mesoporous silica coated on nanoparticles in such a way that two concurrent reactions can be carried out has not been reported. As one could expect, development of such intricate systems is laden with several major challenges. First, the metal catalyst and the enzyme should be incorporated in a matrix in such a way that the metal catalyst does not interact with the plethora of functional groups present in the enzyme there by denaturating it leading to activity loss.[25] Secondly, we should be able to recover both the enzyme and the metal nanoparticles ensuring that the metal and enzyme are not leached into the reaction mixture. The metal should also have appropriate surface passivation such that their aggregation during the reaction is prevented.[26] Finally both the enzyme and the nanoparticles should be easily accessible to the substrates. One way to overcome all these challenges would be to incorporate both the metal catalyst and enzyme in a heterogeneous support[12,27,28] in a manner that they do not interact with each other, yet are accessible to small organic molecules.

We hereby present the design and synthesis of mesoporous silica nanoparticles (MSN) coated on gold nanoparticles in a core-shell architecture with an enzyme grafted on the outside silica surface. This design allows a two step reaction to be carried out by these two catalysts either independently or cooperatively without interference between themselves. This hybrid material has several features that make

them attractive. (i) The synthesis of Au nanoparticles encapsulated in MSN is performed by a simple one-pot procedure on which enzymes can be grafted easily on the external surface. (ii)This hybrid material allows two concurrent reactions to be carried out in tandem such that the product released by the first reaction becomes substrate to the second reaction. This can be compared to "relay" race where the performance of the 2nd participant depends on the first. (iii) At the end of the reaction the hybrid MSN can be separated by simple centrifugation and subsequently reused. As a proof of concept, a cascade reaction was carried out where the first step involved the hydrolysis of 4-nitrophenyl-β-glucopyranoside by the enzyme glucosidase that was anchored on the external surface of MSN. In the subsequent step, the 4-nitrophenol released from the first reaction diffuses inside the pores of MSN where it is reduced to the corresponding amine by gold nanoparticle in presence of $NaBH_4$.[4,14] The detailed kinetics of both the reaction steps is also discussed.

3.2 Experimental section:

3.2.1 Materials:

Tetraethyl orthosilicate (TEOS), cetyltrimetmylammonium bromide (CTAB), β-glucosidase, 4-nitrophenyl-β-glucopyranoside, $NaBH_4$, $HAuCl_4$ and (3-glycidyloxypropyl) trimethoxysilane were purchased from Sigma Aldrich and were used as received. All the other solvents were purchased from Merck, India and used as received.

3.2.2 Synthesis:

3.2.2.1 Preparation of Au nanoparticles:

Au Nanoparticles was prepared by borohydride reduction method.[29] 500 mL of 10^{-4} M $HAuCl_4$ was prepared. To this solution 50 mg $NaBH_4$ was added slowly. The reaction mixture was left overnight for complete reduction.

3.2.2.2 Preparation of Au@mSiO$_2$ particles:

In a round bottom flask, 20 mL of the above prepared Au sol was taken. Cetyltrimethylammonium bromide (CTAB, 0.007 mg, 10^{-3}mol) was dissolved in that solution and stirred for half hour. NaOH (aq) (2.00 M, 100 uL) was then added to CTAB solution, followed by drop wise addition of tetraethyl orthosilicate (20 μL, 0.091 mmol). The reaction mixture was stirred for 2 hrs and then centrifuged twice

with ethanol. To remove the CTAB completely, the particles were refluxed overnight in ethanol. Then the solution was centrifuged again and these particles were stored as dispersion in ethanol for further usage.

3.2.2.3 Grafting of epoxide groups onto Au@mSiO$_2$:

The grafting of epoxide functional group was performed according to a procedure reported before.[27] In a typical reaction, 15 mg of Au@mSiO$_2$ nanoparticles were dispersed in 50 mL dry toluene. To this dispersion, (3-glycidyloxypropyl)trimethoxysilane (10 μL, 0.04 mmol) was added and the resultant reaction mixture was heated at 85 ^{o}C for 12 hrs. After completion of the reaction, the resultant epoxide grafted core shell nanoparticles were centrifuged and washed several times with ethanol to remove the unreacted (3-glycidyloxypropyl)trimethoxysilane.

3.2.2.4 Immobilization of enzyme:

Covalent enzyme anchoring was carried out following reported methods.[27,30,31] First epoxide grafted Au@mSiO$_2$ nanoparticles (3 mg) were dispersed in PBS buffer (pH = 7.4, 0.1 mM) by sonication. Then these were incubated with beta-glucosidase (2 mg, 1.48 X 10^{-8} mol) over a night at 4 ^{o}C. The resulting hybrid nanoparticles, Au@mSiO$_2$@glucosidase, were separated by centrifugation, washed several times with PBS buffer to remove unreacted and absorbed enzyme. The particles was dispersed in 4 mL of PBS Buffer and used as a stock. Enzyme conjugated nanoparticles were stored at 4 ^{o}C. The amount of enzyme immobilized on Au@mSiO$_2$@glucosidase nanoparticles was determined using UV-Vis spectroscopy by monitoring the absorbance at 280 nm. Unfunctionalized Au@mSiO$_2$ nanoparticles were used as a blank for all measurements.

3.3 Results and Discussion:

Our strategy to synthesize enzyme grafted hybrid material involves three steps (Scheme 3.1). The first step in this endeavour was the synthesis of Au core mesoporous silica shell (Au@mSiO$_2$) nanoparticles. In the second step, epoxide was grafted on the outside surface of these particles using general silane chemistries. Finally, β-glucosidase was immobilized by the ring opening of epoxide by the NH_2 groups of lysine present in β-glucosidase to prepare the hybrid catalyst, Au@mSiO$_2$@glucosidase.

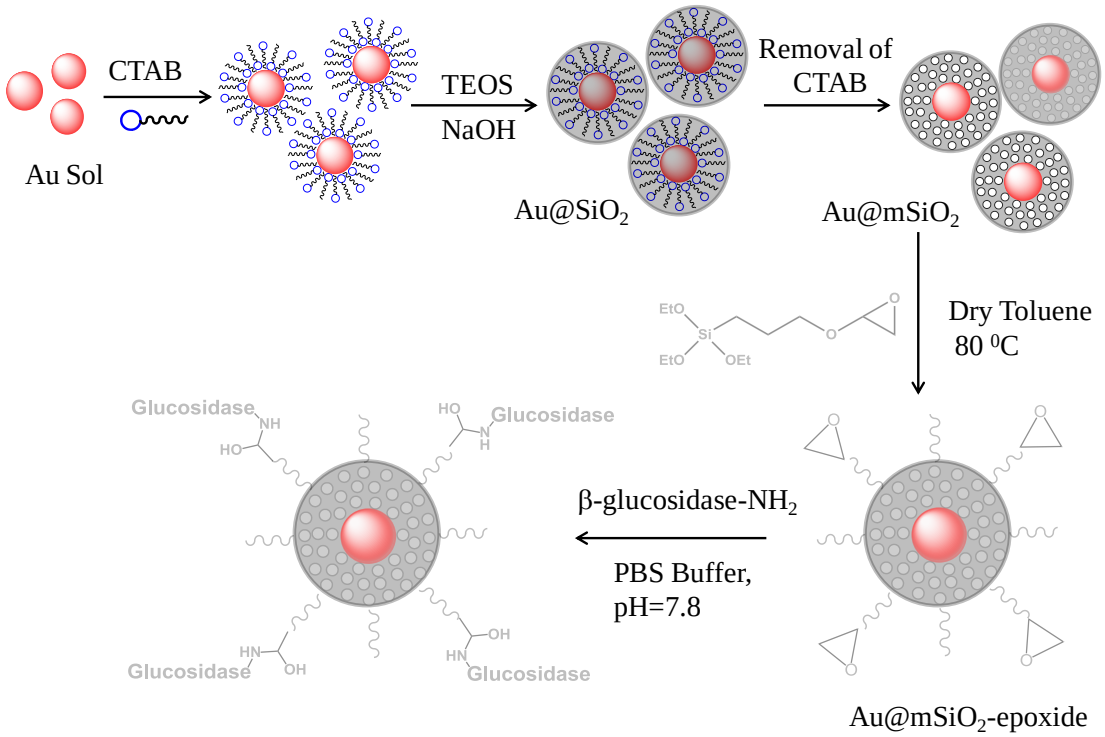

Scheme 3.1: Schematic illustration of the synthetic procedure for gold nanocrystal /mesoporous silica core–shell NPs.

The core shell nanoparticles ($Au@mSiO_2$) were synthesized using sol-gel procedure with preformed Au nanoparticles. The Au nanoparticles were prepared by borohydride reduction of metal precursor ($HAuCl_4$). For preparing silica shell on Au nanoparticles, we used typical Stober Method. The nanoparticles were treated with ionic surfactant cetyltrimethylammonium bromide (CTAB). CTAB serves not only as a stabilizing surfactant for Au nanocrystals in the aqueous phase but also as the organic template for the formation of mesopores in the sol–gel reaction.[32] The resulting core-shell nanoparticles were separated by centrifugation, redispersed in ethanol, and then characterized by transmission electron microscopy. After silica coating, it has been observed that the particles were well dispersed in water. Finally, the CTAB templates from the as-synthesized material was removed by heating them at reflux in ethanol to collect $Au@mSiO_2$ particles.

The grafting of epoxide functional group was done using well established silane chemistry. $Au@mSiO_2$ nanoparticles were treated with (3-glycidyloxypropyl)trimethoxysilane in dry toluene for 16 hrs at 80 ^oC. After washing with ethanol for three times the material was characterized with infra-red spectroscopy and TGA analysis in presence of air.

The epoxy grafted $Au@mSiO_2$ nanoparticles were reacted with β-glucosidase in PBS buffer (pH=7.8, 0.1 mM) so that the amino groups of lysine in β-glucosidase induces ring-opening of the epoxy group on the surface of $Au@mSiO_2$ leading to covalent immobilization of the enzyme on the surface of the nanoparticle ($Au@mSiO_2$@glucosidase). After completion of the reaction, the material was washed with buffer system several times until the supernatant showed no UV absorption characteristic of the enzyme. Control experiments were performed to check that no enzymes were electrostatically attached onto $Au@mSiO_2$ nanoparticles surface. First, the β-glucosidase grafted $Au@mSiO_2$ was washed with NaCl (0.1M) to destabilize electrostatic attraction between nanoparticles surface and non-covalently bound enzymes so that they can be easily washed out. Since no enzymes were observed in the supernatant during these washings, we conclude that our synthetic procedure leads to the covalent attachment of enzyme to the nanoparticle surface and that any of the non-covalently bound enzymes get washed away during the purification. Secondly, incubation of β-glucosidase to bare $Au@mSiO_2$ (particles that did not have the epoxy group grafted on them) did not show any attachment of the enzyme on the nanoparticle surface.

3.4 Characterizations:

3.4.1 XRD Analysis:

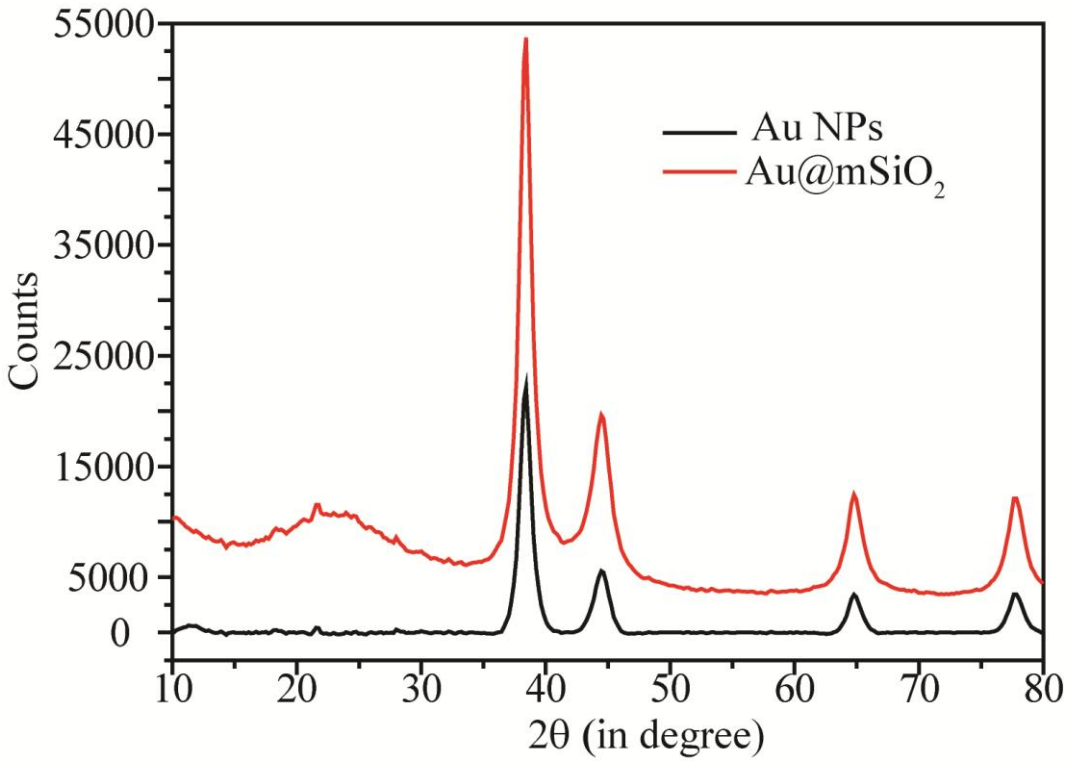

Figure 3.1: Wide angle Powder XRD patterns of Au nanoparticles and mesoporous silica coated Au nanoparticles.

The XRD of Au nanoparticles and mesoporous silica coated gold nanoparticles were shown in Figure 3.1. The formation of metallic gold nanoparticles after borohydride reduction was confirmed by the X-ray powder diffraction (XRD) pattern. Au nanoparticles show four Au diffraction peaks at 2θ = 38.15 °, 44.43 °, 64.62 ° and 76.58 °. These can be assigned to (111), (200), (220), and (311) reflections of the cubic (fcc) gold lattice (JCPDS cards: No. 04-0784).[5] The wide-angle XRD pattern of mesoporous silica coated Au nanoparticles show all the above peaks of Au nanoparticles along with a very broad signal at 2θ = 22.31°, which suggest the presence of amorphous silica in the core shell particles. The average particle size of the metal core calculated by the Scherrer equation using the half width of the intense (111) reflection was ~8 nm, which is comparable with the value obtained from TEM images.

3.4.2 TEM analysis:

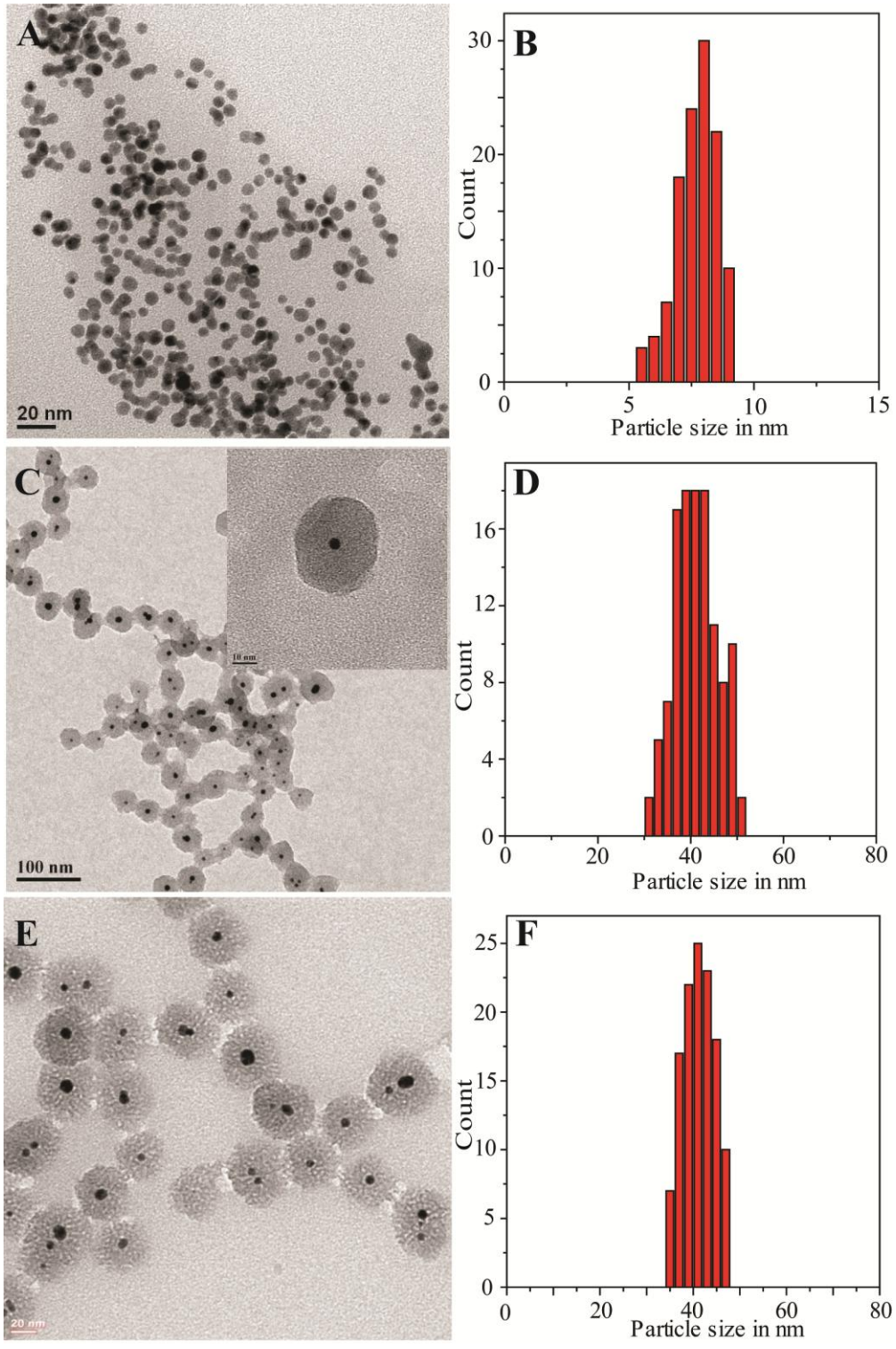

Figure 3.2: (A), (C), (E) TEM images of as prepared Au nanoparticles, Au@SiO_2 and Au@mSiO_2. (B), (D), (F) particle size distribution of as prepared Au nanoparticles, Au@SiO_2 and Au@mSiO_2 respectively.

TEM analysis was performed to determine the size and morphology of prepared Au nanoparticles, silica coated Au nanoparticles and Au@mSiO_2 nanoparticles presented in Figure 3.2. It is reported that size of Au nanoparticles prepared by sodium borohydride will be around 8-10 nm. We observe that size of the Au nanoparticles was around ~8 nm from TEM of image analysis and these are spherical in shape. After silica coating, the size of the particles was determined to be ~ 42 nm. This indicates that ~34 nm silica shell has been deposited on the surface of Au nanoparticles. When CTAB was removed from Au@SiO_2 nanoparticles, the pores became visible in TEM picture. The size of the particles remains same after template removal also.

3.4.3 XPS Analysis:

To investigate the chemical composition of the Au@mSiO_2, X-ray photoelectron spectrum (XPS), has been performed (Figure 3.3). We did not observe any peak of Au at 84.57 eV and 88.21 eV for Au $4f_{7/2}$ and Au $4f_{5/2}$. Since, the typical detection depth of the XPS is 10 nm, the absence of peak from metallic gold conclusively suggest that all the Au particles are covered with silica.[10]

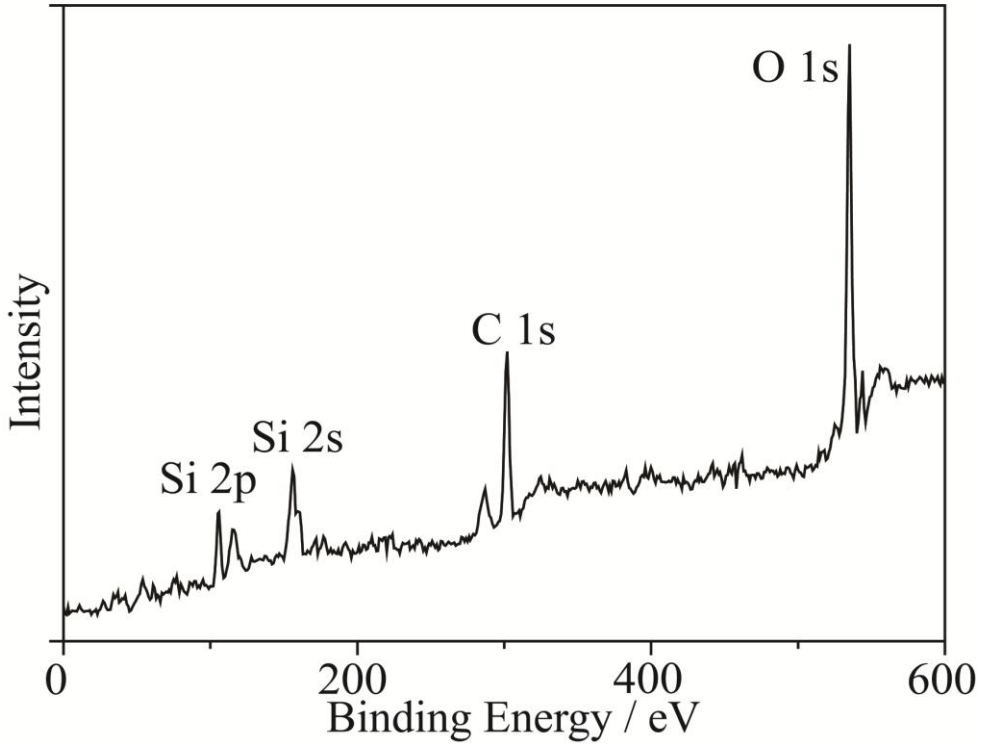

Figure 3.3: XPS spectrum of Au@mSiO_2

3.4.4 UV-Visible Spectroscopy:

The UV-Vis spectra of the various materials are presented in the Figure 3.4. The bare Au nanoparticles displayed UV-Vis absorbance band at 520 nm, that is characteristic of the plasmon resonance bands of spherical gold nanoparticles. After the silica encapsulation, the peak shifted from 520 to 533 nm, which can be attributed to the coating of silica shell which changes the effective dielectric.[33]

The UV-Vis spectra after epoxide grafting shows absorbance at 535 nm. After enzyme immobilization, the Au@mSiO$_2$@glucosidase nanoparticles displayed UV-Vis absorbance band at 520 nm and 270 nm (Figure 3.4), that is characteristic of the plasmon resonance bands of spherical gold nanoparticles and glucosidase enzyme, respectively. This data conclusively proves that enzyme was covalently grated on the surface of silica.

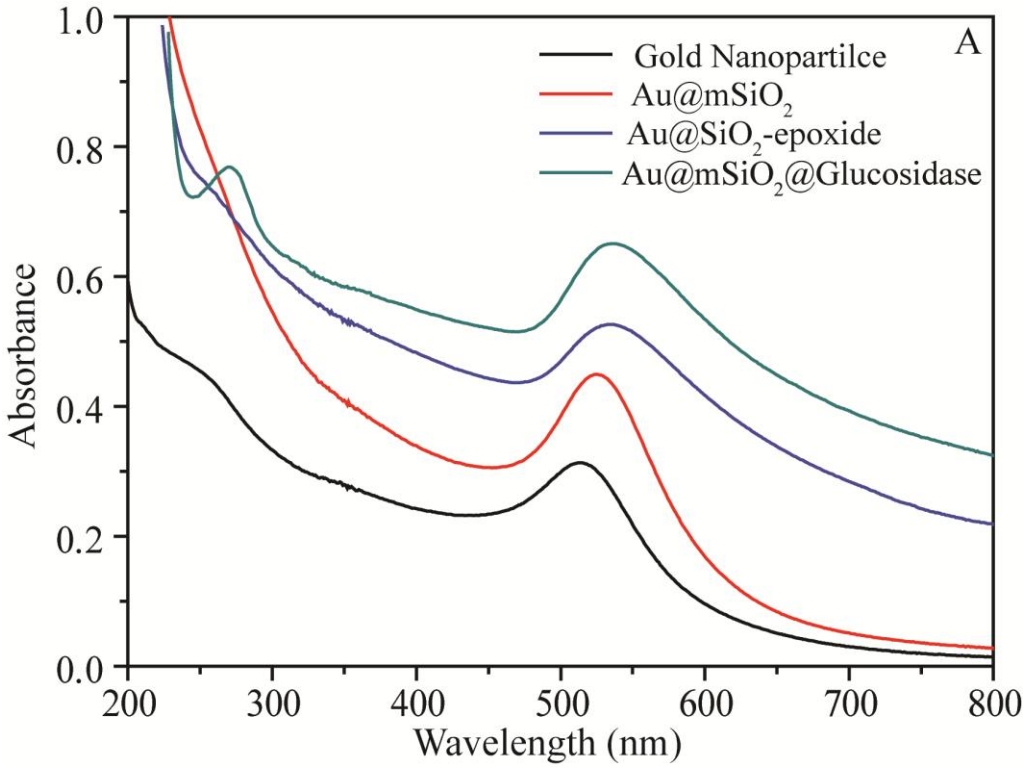

Figure 3.4: UV-Vis spectra of Au NPs, Au@SiO$_2$, Au@mSiO$_2$ and Au@mSiO$_2$-Glucosidase

3.4.5 TGA and elemental analysis:

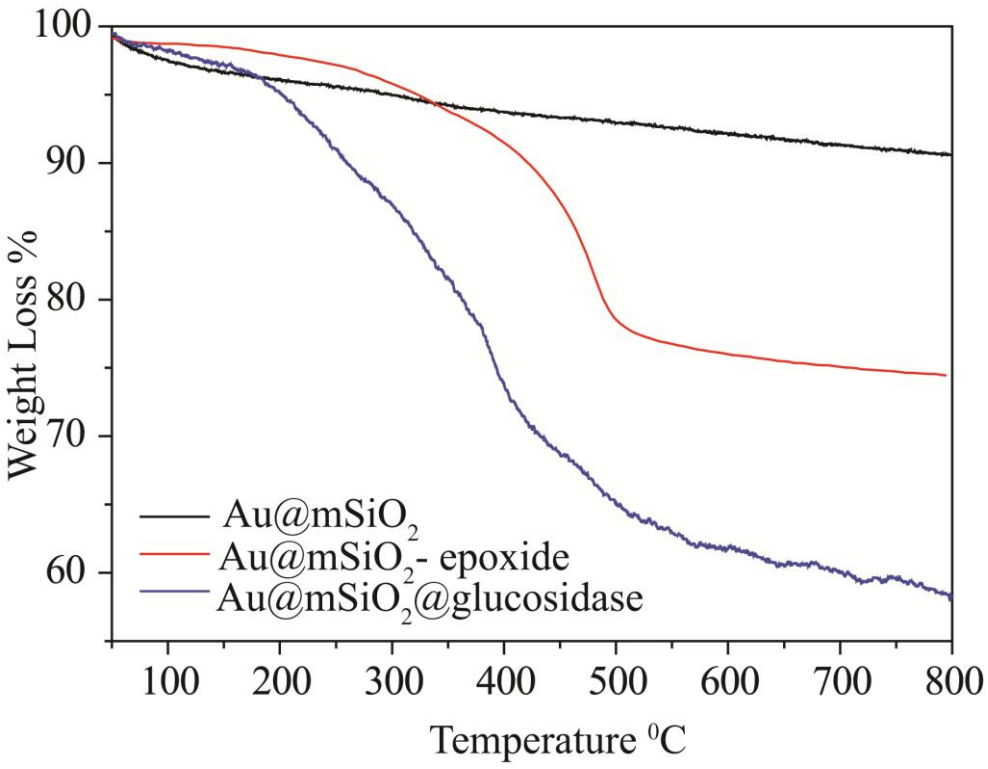

Figure 3.5: TGA of different functionalized materials of core shell nanoparticles

To determine the amount of epoxides and enzymes present on the surface of core shell particles, TGA analysis was performed and presented in Figure 3.5. Nearly 20% weight loss has been observed after grafting Au@$mSiO_2$ nanoparticles with (3-glycidyloxypropyl)trimethoxysilane which is due to the combustion of organic moiety present on the surface of Au@$mSiO_2$. The epoxide grafting density as determined from TGA analysis was ~1.8 moles/g of sample. These data proves the successful incorporation of epoxide groups in the materials. After enzyme immobilization, Au@$mSiO_2$-glucosidase shows around 40% weight loss, which is due to the presence of epoxide group and enzymes in the material. After subtracting the amount for epoxide group we have calculated the amount of enzyme present in the final material, which came out as $1.25x10^{-6}$ mmol per gram.

Atomic absorption spectroscopy (AAS) was applied to study the content of gold per gram of Au@$mSiO_2$. The weight % of gold was determined to be 33.5%.

3.4.6 Nitrogen adsorption-desorption studies:

Nitrogen adsorption and desorption isotherms of mesoporous Au@SiO_2 materials are presented in the Figure 3.6A. The isotherm exhibit the characteristic type IV isotherm with steep increase in adsorption at P/P_0 = 0.3-0.5 due to capillary condensation of the nitrogen in the mesopores. N_2 adsorption/desorption isotherms show a BET surface area of 381 m^2/g and the corresponding BJH pore size distribution (Figure 3.6B) demonstrate that Au@mSiO_2 has well-developed mesopores with an average size of 1.6 nm. This nitrogen-sorption analysis divulged that the cavity of mesoporous was accessible by N_2 molecules, which may allow other guest molecules to diffuse into the hollow cavities. These values are consistent with mesoporous core shell materials reported before.

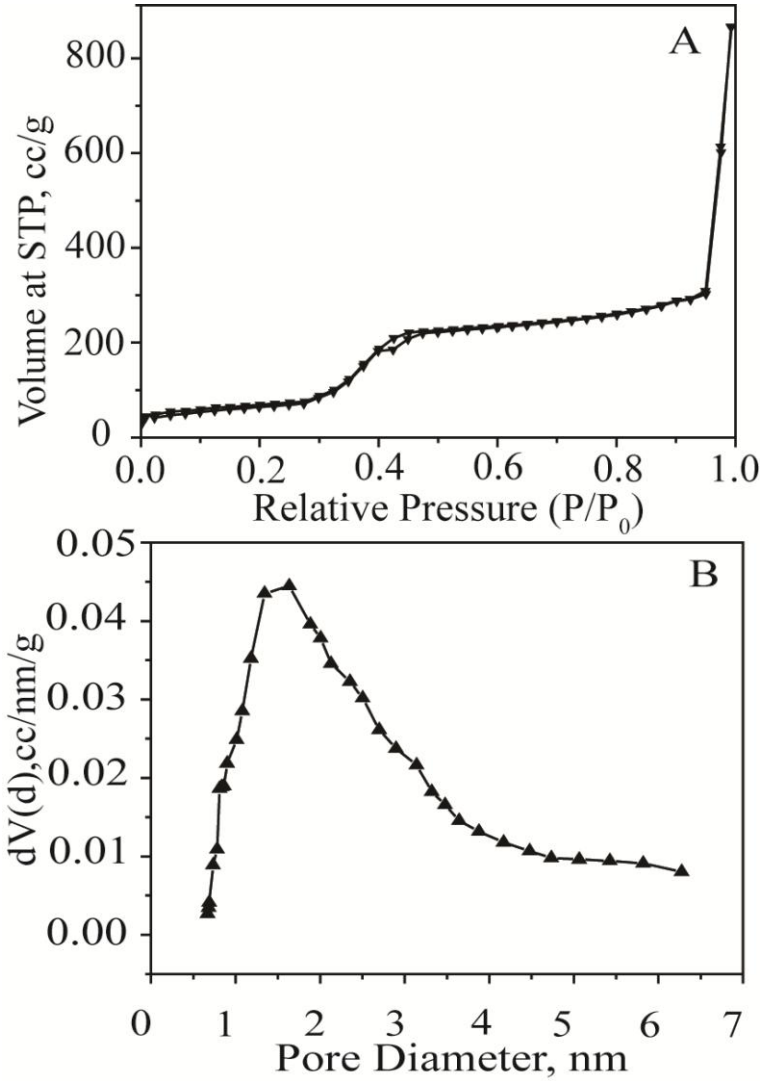

Figure 3.6: (A) Nitrogen adsorption-desorption isotherms and (B) pore size distribution of mesoporous Au@SiO_2

3.4.7 IR Spectroscopy:

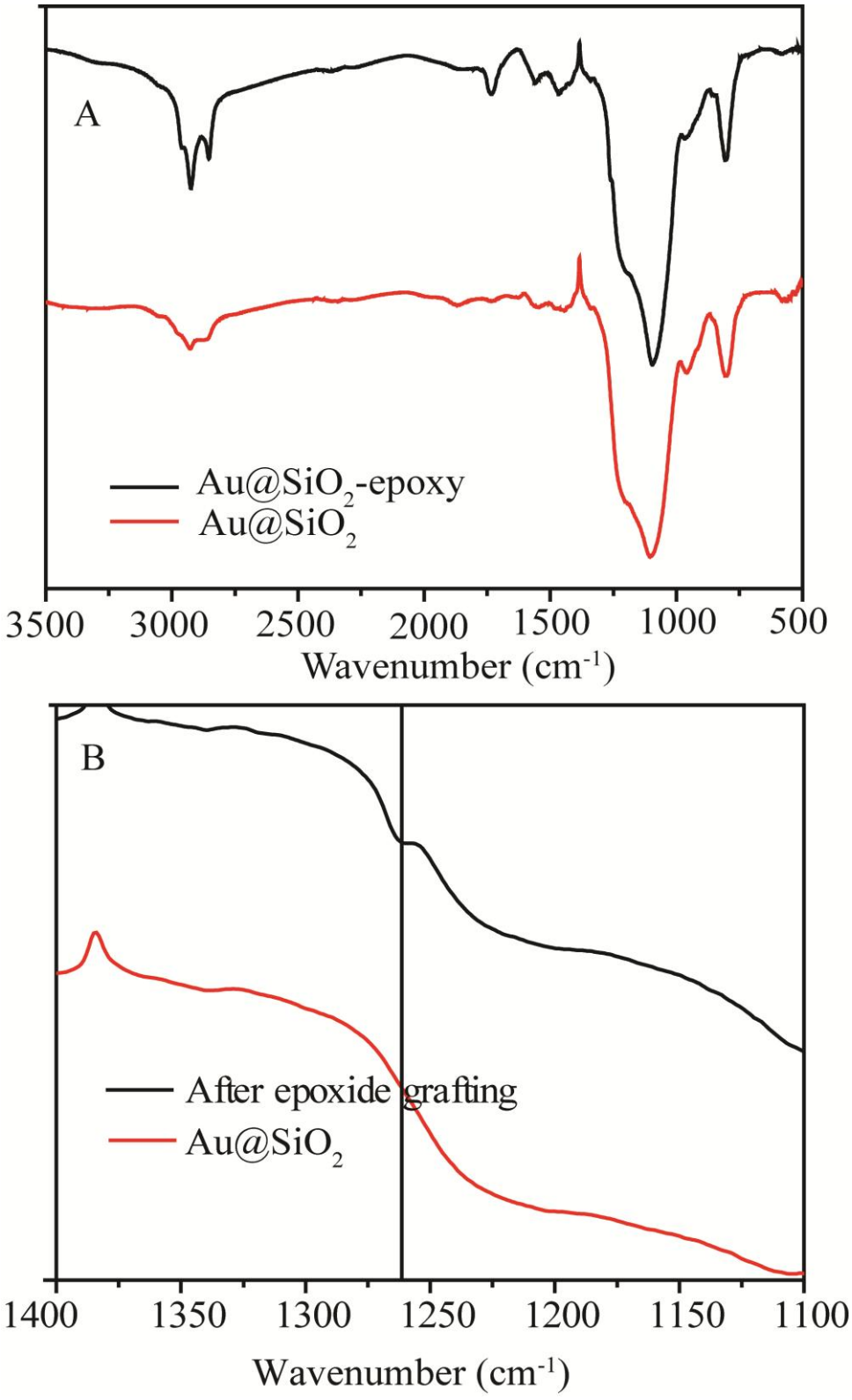

Figure 3.7: (A) IR Spectra of Au@mSiO2 and Au@mSiO$_2$-epoxy nanoparticles (B) In the zoomed IR spectra a peak appearing at 1260 cm^{-1} after the epoxy grafting indicates successful incorporation of epoxide in Au@mSiO$_2$.

IR spectroscopy has been done to show the epoxide grafting on the surface of silica shell. The samples also showed transmittance peaks at 1080, 805 and 465 cm^{-1} respectively. (Figure 3.7A) These peaks are typical of Si-O-Si bands that are associated with the formation of the silica networks. It is observed that the peak intensity at 3000 cm^{-1} corresponding to the stretching frequency of $–CH_2$ had increased after epoxide grafting, indicating presence of glycidyl group. In the zoomed IR spectra (Figure 3.7B) the peak at 1260 cm^{-1}, which is characteristic for epoxide group, was absent in Au@mSiO_2. This also indicates successful incorporation of epoxide in Au@mSiO_2.

3.5 Catalytic performance of mesoporous silica coated Au nanoparticle:

The activities of the immobilized bifunctional catalyst Au@mSiO_2@glucosidase was tested in a tandem sequence involving the hydrolysis of 4-nitrophenyl-β-glucopyranoside to 4-nitrophenol and subsequent reduction of 4-nitrophenol to 4-aminophenol (Scheme 3.2). First, 4-nitrophenyl-β-glucopyranoside was added to Au@mSiO2@glucosidase to initiate its hydrolysis to the corresponding 4-nitrophenol by the immobilized β-glucosidase on the silica surface efficiently. The kinetics of this hydrolysis reaction was studied by UV-Vis spectroscopy (Figure 3.8 A). The gradual increase in the peak height at 400 nm with time indicated the formation of 4-nitrophenol. The absorbance vs. time data for this particular reaction was fitted according to the first order equation $A_t = A_o e^{-kt}$, where A_o and A_t stands for absorbance at time, t = 0 and t minute respectively. From this plot the first order rate constant k was determined to be 4.16×10^{-2} min^{-1} ($R^2 = 0.9996$).

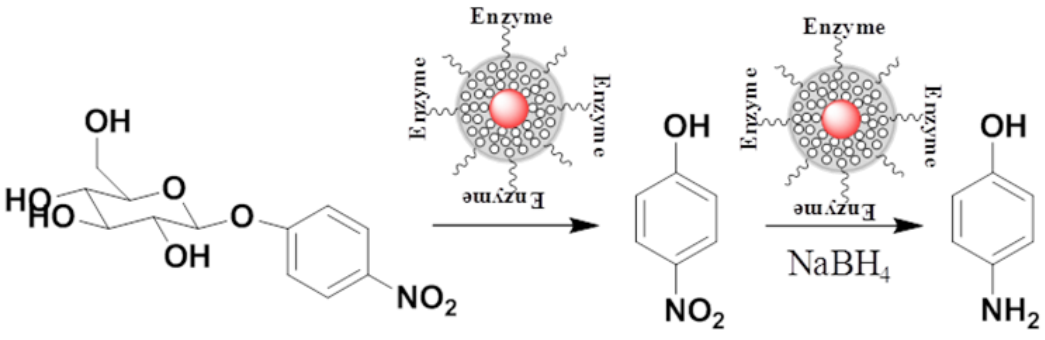

Scheme 3.2: The schematic illustration of tandem reaction using enzyme loaded Au@mSiO_2

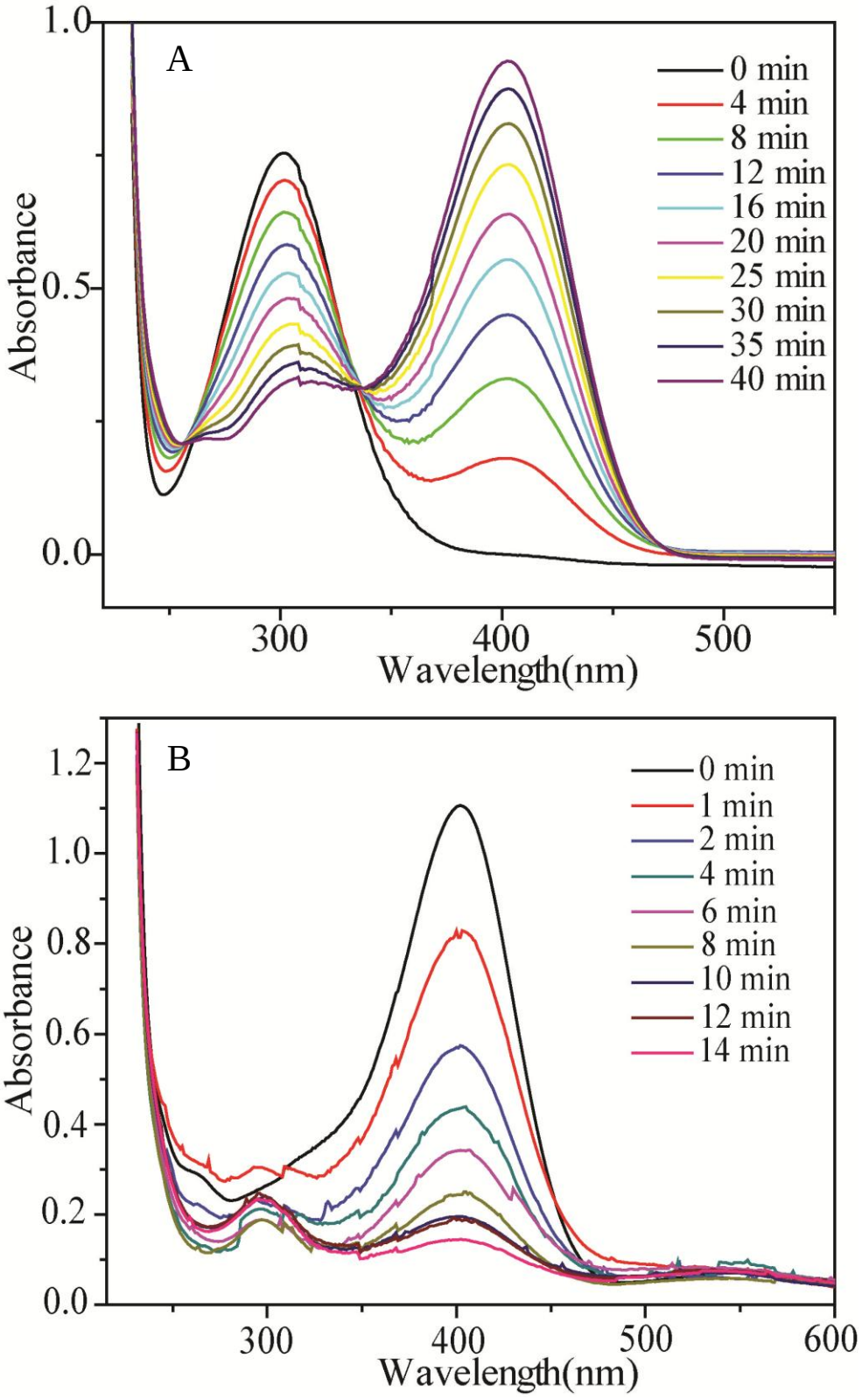

Figure 3.8: (A) Time-dependent UV-vis absorption spectral changes of the 1st reaction mixture catalyzed by Au@mSiO$_2$@glucosidase. (B) Time-dependent UV-vis absorption spectral changes of the 2nd reaction mixture catalyzed by enzyme Au@mSiO$_2$@glucosidase.

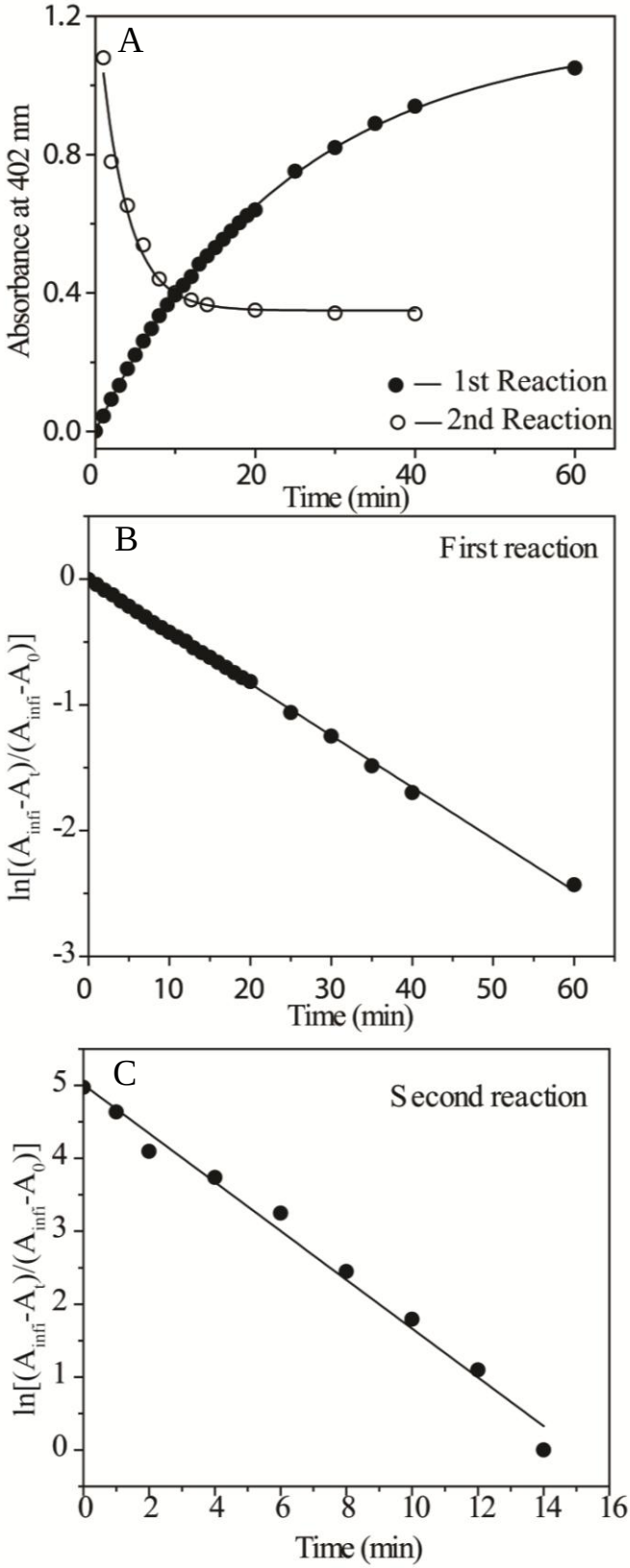

Figure 3.9: (A) Combined plot of 1st and 2nd reaction for exponential change of OD. (B) and (C) Plot of $\ln[(A_{infi}-A_t)/(A_{infi}-A_0)]$ versus time using β-glucosidase immobilized Au@mSiO_2.

After completion the hydrolysis reaction, excess $NaBH_4$ was added to the reaction mixture so that the gold core present inside the nanoparticle could reduce the 4-nitrophenol generated by the previous reaction into the corresponding 4-aminophenol. The presence of pores in the silica coated Au nanoparticle allows both the 4-nitrophenol and $NaBH_4$ to diffuse through the pores into the surface of the Au nanoparticle where the subsequent reduction reaction takes place. Control reaction performed with porous silica nanoparticles without any Au nanoparticles embedded inside show no reaction until a period of 24 hrs indicating that the presence of the gold nanoparticle as a catalyst is essential for this reaction. The kinetics of 4-nitrophenol reduction in presence of Au@mSiO_2@glucosidase was studied by UV-Vis spectroscopy (Figure 3.8 B). After the addition of $NaBH_4$, it was found that the peak height at 400 nm gradually decreased with time. The decrease in peak intensity at 400 nm with time can be used to calculate the rate constant of this reduction reaction. The ratio of C_t to C_0, where C_t is the concentration of 4-nitrophenol at time, t, and C_0 is the initial 4-nitrophenol concentration, was determined from that of the respective absorbance (A_t/A_0) at 410 nm. This reaction follows first order kinetics with rate constant of 3.0 $x10^{-1}$ min^{-1} which was obtained from $\ln[(A_t - A_{infi})/(A_{infi}-A_0)]$ vs. time plot as well as absorbance vs. time plot considering the rate equation $At = A_o e^{-kt}$ (Figure 3.9 B and C). Thus, we were able to perform two reactions in tandem in a one-pot sequence using our Au@mSiO_2@glucosidase nanoparticle.

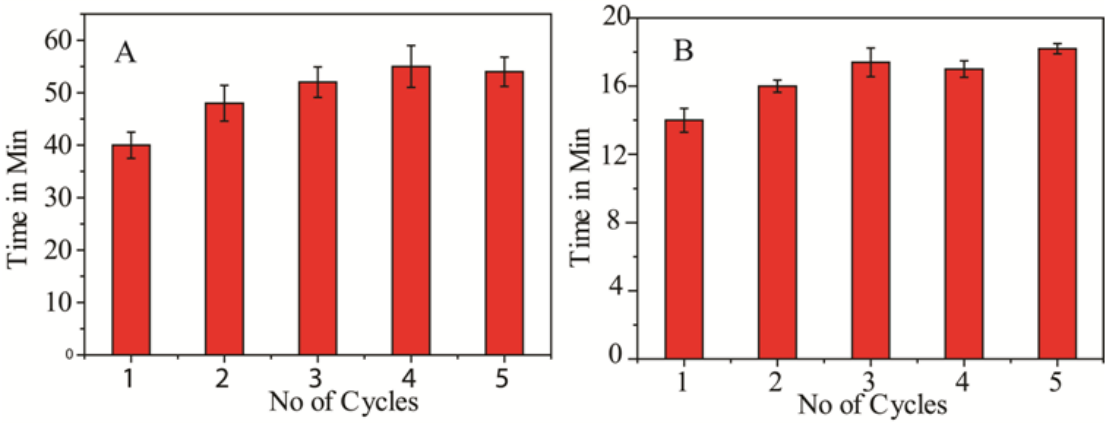

Figure 3.10: (A) Recyclability for 5 cycles for the 1st reaction. (B) Recyclability for 5 cycles for the 2nd reaction.

We were also able to recover the Au@mSiO_2@glucosidase nanoparticle by simple centrifugation after completion of the reactions. We then attempted to check if Au@mSiO_2@glucosidase nanoparticle could be recycled for more catalytic cycles.

Although Au@mSiO_2@glucosidase nanoparticle were able the carry both the hydrolysis reaction and the subsequent reduction reaction independently for 5 catalytic cycles, the activity for cascade reaction rapidly decreased in successive cycles.(Figure 3.10) We attribute this to the possibility of $NaBH_4$ denaturing the enzyme because of very high pH generated due to the hydrolysis of $NaBH_4$.

3.6 Conclusion:

In conclusion, the construction of a bifunctional "relay" catalyst that could carry out a sequential two step reaction has been successfully demonstrated. Au nanoparticle has been successfully encapsulated inside the mesoporous silica shell followed by enzyme immobilization. In addition, the catalytic activity of these materials was tested using a model reaction, where the product released by the first reaction becomes substrate to the second reaction. This study also indicates that the mesopores in the silica shell could allow the transport of small species into the cavity and is necessary to design multifunctional catalyst. Moreover, this strategy may be easily extended to encapsulate other metal NPs inside the mesoporous silica shell and functionalized the silica surface with desirable chemical moiety using well established silane chemistry.

3.7 References:

1. Wasilke, J.-C.; Obrey, S. J.; Baker, R. T.; Bazan, G. C., Concurrent Tandem Catalysis. *Chemical Reviews*, **2005**, 105, (3), 1001-1020.

2. Hagen, J., *Industrial Catalysis: A practical Approach*. 2nd Edition ed.; Wiley-VCH: 2006.

3. Astruc, D.; Lu, F.; Aranzaes, J. R., Nanoparticles as recyclable catalysts: The frontier between homogeneous and heterogeneous catalysis. *Angewandte Chemie - International Edition*, **2005**, 44, (48), 7852-7872.

4. Lee, J.; Park, J. C.; Bang, J. U.; Song, H., Precise Tuning of Porosity and Surface Functionality in Au@SiO_2 Nanoreactors for High Catalytic Efficiency. *Chemistry of Materials*, **2008**, 20, (18), 5839-5844.

5. Du, X.; He, J., Amino-functionalized silica nanoparticles with center-radially hierarchical mesopores as ideal catalyst carriers. *Nanoscale*, **2012**, 4, (3), 852-859.

6. Ishida, T.; Haruta, M., Gold Catalysts: Towards Sustainable Chemistry. *Angewandte Chemie International Edition*, **2007**, 46, (38), 7154-7156.

7. Stratakis, M.; Garcia, H., Catalysis by Supported Gold Nanoparticles: Beyond Aerobic Oxidative Processes. *Chemical Reviews*, **112**, (8), 4469-4506.

8. Christensen, C. H.; Norskov, J. K., Green Gold Catalysis. *Science*, **2010**, 327, (5963), 278-279.

9. Hagen, J., *Industrial Catalysis: A practical Approach*, *Wiley-VCH*, **2006**.

10. Tan, L.; Chen, D.; Liu, H.; Tang, F., A Silica Nanorattle with a Mesoporous Shell: An Ideal Nanoreactor for the Preparation of Tunable Gold Cores. *Advanced Materials*, **2010**, 22, (43), 4885-4889.

11. Han, J.; Fang, P.; Jiang, W.; Li, L.; Guo, R., Ag-Nanoparticle-Loaded Mesoporous Silica: Spontaneous Formation of Ag Nanoparticles and Mesoporous Silica SBA-15 by a One-Pot Strategy and Their Catalytic Applications. *Langmuir*, **2012**, 28, (10), 4768-4775.

12. Wang, S.; Zhang, M.; Zhang, W., Yolk-Shell Catalyst of Single Au Nanoparticle Encapsulated within Hollow Mesoporous Silica Microspheres. *ACS Catalysis*, **2011**, 1, (3), 207-211.

13. Lopez-Sanchez, J. A.; Dimitratos, N.; Hammond, C.; Brett, G. L.; Kesavan, L.; White, S.; Miedziak, P.; Tiruvalam, R.; Jenkins, R. L.; Carley, A. F.; Knight, D.; Kiely, C. J.; Hutchings, G. J., Facile removal of stabilizer-ligands from supported gold nanoparticles. *Nat Chem*, **2011**, 3, (7), 551-556.

14. Carregal-Romero, S.; Buurma, N. J.; Pérez-Juste, J.; Liz-Marzán, L. M.; Hervés, P., Catalysis by Au@pNIPAM Nanocomposites: Effect of the Cross-Linking Density. *Chemistry of Materials*, **2010**, 22, (10), 3051-3059.

15. Li, G. L.; Tai, C. A.; Neoh, K. G.; Kang, E. T.; Yang, X., Hybrid nanorattles of metal core and stimuli-responsive polymer shell for confined catalytic reactions. *Polymer Chemistry*, **2011**, 2, (6), 1368-1374.

16. Wu, S.; Dzubiella, J.; Kaiser, J.; Drechsler, M.; Guo, X.; Ballauff, M.; Lu, Y., Thermosensitive Au-PNIPA Yolk–Shell Nanoparticles with Tunable Selectivity for Catalysis. *Angewandte Chemie International Edition*, **2012**, 51, (9), 2229-2233.

17. Karimi, B.; Behzadnia, H.; Bostina, M.; Vali, H., A Nano-Fibrillated Mesoporous Carbon as an Effective Support for Palladium Nanoparticles in the Aerobic Oxidation

of Alcohols "on Pure Water". *Chemistry – A European Journal*, **2012**, 18, (28), 8634-8640.

18. Liu, S.; Han, M.-Y., Silica-Coated Metal Nanoparticles. *Chemistry – An Asian Journal*, **2010**, 5, (1), 36-45.

19. Fang, X.; Liu, Z.; Hsieh, M.-F.; Chen, M.; Liu, P.; Chen, C.; Zheng, N., Hollow Mesoporous Aluminosilica Spheres with Perpendicular Pore Channels as Catalytic Nanoreactors. *ACS Nano*, **2012**, 6, (5), 4434-4444.

20. Ge, J.; Zhang, Q.; Zhang, T.; Yin, Y., Core-Satellite Nanocomposite Catalysts Protected by a Porous Silica Shell: Controllable Reactivity, High Stability, and Magnetic Recyclability. *Angewandte Chemie*, **2008**, 120, (46), 9056-9060.

21. Zhang, Q.; Zhang, T.; Ge, J.; Yin, Y., Permeable Silica Shell through Surface-Protected Etching. *Nano Letters*, **2008**, 8, (9), 2867-2871.

22. Zeidan, R. K.; Hwang, S.-J.; Davis, M. E., Multifunctional Heterogeneous Catalysts: SBA-15-Containing Primary Amines and Sulfonic Acids. *Angewandte Chemie*, **2006**, 118, (38), 6480-6483.

23. Huang, Y.; Xu, S.; Lin, V. S. Y., Bifunctionalized Mesoporous Materials with Site-Separated Brønsted Acids and Bases: Catalyst for a Two-Step Reaction Sequence. *Angewandte Chemie International Edition*, **2011**, 50, (3), 661-664.

24. Margelefsky, E. L.; Zeidan, R. K.; Davis, M. E., Cooperative catalysis by silica-supported organic functional groups. *Chemical Society Reviews*, **2008**, 37, (6), 1118-1126.

25. Polizzi, K. M.; Bommarius, A. S.; Broering, J. M.; Chaparro-Riggers, J. F., Stability of biocatalysts. *Current Opinion in Chemical Biology*, **2007**, 11, (2), 220-225.

26. Lam, E.; Hrapovic, S.; Majid, E.; Chong, J. H.; Luong, J. H. T., Catalysis using gold nanoparticles decorated on nanocrystalline cellulose. *Nanoscale*, **2012**, 4, (3), 997-1002.

27. Brun, N.; Babeau Garcia, A.; Deleuze, H.; Achard, M. F.; Sanchez, C.; Durand, F.; Oestreicher, V.; Backov, R., Enzyme-Based Hybrid Macroporous Foams as Highly Efficient Biocatalysts Obtained through Integrative Chemistry. *Chemistry of Materials*, **2010**, 22, (16), 4555-4562.

28. Brady, D.; Jordaan, J., Advances in enzyme immobilisation. *Biotechnology Letters*, **2009**, 31, (11), 1639-1650.

29. Gole, A.; Dash, C.; Ramakrishnan, V.; Sainkar, S. R.; Mandale, A. B.; Rao, M.; Sastry, M., Pepsin-Gold Colloid Conjugates: Preparation, Characterization, and Enzymatic Activity. *Langmuir*, **2001**, 17, (5), 1674-1679.

30. Georgelin, T.; Maurice, V.; Malezieux, B.; Siaugue, J.-M.; Cabuil, V., Design of multifunctionalized γ-Fe_2O_3@SiO_2 core–shell nanoparticles for enzymes immobilization. *Journal of Nanoparticle Research*, **2010**, 12, (2), 675-680.

31. Singh, R.; Zhang, Y.-W.; Nguyen, N.-P.-T.; Jeya, M.; Lee, J.-K., Covalent immobilization of β-1,4-glucosidase from Agaricus arvensis onto functionalized silicon oxide nanoparticles. *Applied Microbiology and Biotechnology*, **2011**, 89, (2), 337-344.

32. Kim, J.; Kim, H. S.; Lee, N.; Kim, T.; Kim, H.; Yu, T.; Song, I. C.; Moon, W. K.; Hyeon, T., Multifunctional Uniform Nanoparticles Composed of a Magnetite Nanocrystal Core and a Mesoporous Silica Shell for Magnetic Resonance and Fluorescence Imaging and for Drug Delivery. *Angewandte Chemie*, **2008**, 120, (44), 8566-8569.

33. Wong, Y. J.; Zhu, L.; Teo, W. S.; Tan, Y. W.; Yang, Y.; Wang, C.; Chen, H., Revisiting the Stober Method: Inhomogeneity in Silica Shells. *Journal of the American Chemical Society*, **2011**, 133, (30), 11422-11425.

Chapter 4

Selective functionalization to impart hydrophobicity and hydrophilicity in desired locations of mesoporous silica nanoparticles

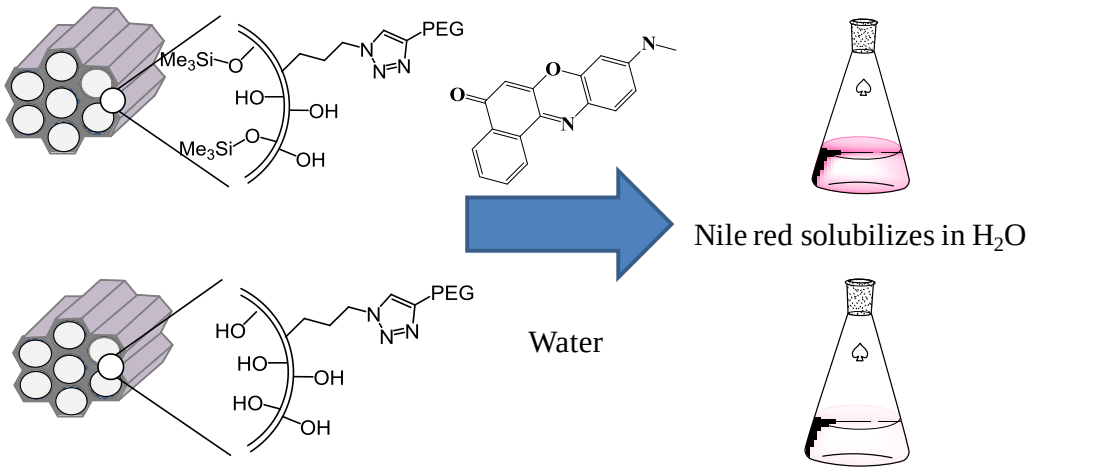

In this chapter, we describe the synthesis and characterization of mesoporous silica material with hydrophilic and hydrophobic groups grafted in the outer and inner surface respectively. Here, hydrophilic PEG groups have been installed on the outer surface using "Click Chemistry" while the hydrophobic (trimethylsilyl group) have been incorporated inside the pores using silane chemistry. All the materials have been thoroughly characterized using various techniques such as TEM, IR, N_2 Adsorbtion, XRD, TGA analysis. The presence of hydrophilic and hydrophobic group on outer and inner surface of mesoporous silica was confirmed by localizing the hydrophobic dye nile red inside the pores.

4.1 Introduction:

In the last two chapters, we have discussed the grafting of different functional groups on the surface of silica materials and studied their catalytic activity. By that process we showed that mesoporosity in the material as an additional utility parameter that provides high surface area and helps in transporting chemical reagents. In this chapter we take an effort to impart additional molecular functionality to the mesoporous silica nanoparticle in a pre-determined way, which can provide control over many key properties, including hydrothermal stability, surface polarity, and the density of attached organic moieties, that are crucial for applications in separation, sorption, catalysis, templating, and host-guest chemistry.[1-3] Such controlled functionalization of silica surfaces also falls in line with the overall theme of our work where we want to mimic a 'living cell'. In a living cell there are several regions with clear localizations of hydrophilic/hydrophobic pockets that bring out highly selective actions for cellular functions. Apart from this, in recent years such multifunctional materials are gaining interest because of their application in drug delivery systems.[4-6] Thus, the selective functionalization of specific locations namely inside and outside surface of mesoporous materials becomes a point of interest to gain greater control over the surface properties.[7]

In literature, there have been a few successful strategies reported for differential chemical functionalization on the internal and external surfaces of mesoporous materials. Cheng and Landry showed spatial chemical selectivity on mesoporous silica, exploiting the slower diffusion in the nanoscale pores that the exterior is modified preferentially to the interior.[8] Recently, Bein group at University of Munich reported selective functionalization of mesoporous silica nanoparticles by using sequential co-condensation of functionalized groups in the process of nanoparticle growth.[9] De Juan and Ruiz-Hitzky demonstrated an alternative approach for selective functionalization of the external and internal surfaces of the mesoporous silicate material MCM-41.[10] They grafted one desired organic group on the exterior surface where the pore spaces being filled by a surfactant template. Following that procedure, it was possible to specifically change the nature of the internal surface versus the whole surface of the silica. The basis of this method consists of gradual functionalization conducted in several steps discussed earlier in the introduction chapter. This methodology provides greater control over the other in terms of

chemical functionalization because of more amenability to molecular engineering. Herein, we followed this methodology for the preparation of multifunctional material to tune the polarity of the inner and exterior surface of mesoporous silica nanoparticles.

The application of these kinds of multi functionalized materials is wide spread. One of the main usages of mesoporous silica nanoparticles that have attracted considerable attention is drug delivery systems.[4-6] The main issue for its usages as a drug delivery vehicle is its dispersibility in water medium.[11] The external surface functionalization of mesoporous silica plays an important role in its colloidal stability of the nanoparticles and their interactions with the environment, for example with living cells and other biological substrates.[12,13] In order to increase the water solubility and the biocompatibility, the porous nanoparticles could be coated by soft organic macromolecules such as dendrimers[14] or phospholipids.[15-17] Pegylation of nanoparticle surface is also widely accepted methodology for increasing water dispersibility of nanoparticles. On the other hand, the functionalization of the internal pore system with organic moieties is needed in order to fine-tune the host-guest interactions and chemistry, such as the drug uptake and stabilization.[13] Since drugs are usually loaded in the pores for delivery, the inner surface modification is of paramount important for efficient loading of drugs, in particular hydrophobic drugs and their controlled release.[18] For the surface modification, the grafting reaction of hydroxyl groups on the surface with organic functional groups, which interacts better with a specified target, has been widely used.[19,20]

In this context, developing of a mesoporous material having hydrophilic external surface and hydrophobic internal surface is necessary. The chemistry of formation of mesoporous silica nanoparticles could help us to functionalize the interior and exterior surface with two different organic functionalities. In this chapter, we have functionalized azide and trimethylsilyl group on the external and internal surface of mesoporous silica nanoparticle respectively. Later on, PEG molecule was introduced on the external surface of mesoporous silica nanoparticles using copper(I) catalyzed alkyne-azide cycloaddition (CuAAC) reactions known as “Click reaction”, which has been already discussed in Chapter 2.[21] All these functionalized materials were characterized thoroughly using powder XRD, TEM analysis, Infrared spectroscopy, N_2 adsorption desorption isotherm, and elemental analysis. Subsequently, the materials utility in getting a hydrophobic dye, Nile Red, dispersed

in water is demonstrated. We would like to note that if needed we can switch the functionalities and make the internal surface a hydrophilic and the external a hydrophobic one.

4.2 Experimental section:

4.2.1 Materials:

Tetraethyl orthosilicate (TEOS), CTAB, hexamethyldisilazane, disodium banthophenanthroline sulfonate, copper iodide, Nile Red were used as received from Sigma Aldrich. All other chemicals were used as obtained from Sigma Aldrich. All the other solvents were purchased from Merck India. 3-Azidopropyltriethoxysilane (AzPTES), sodium dithiocarbamate were prepared as reported before.

4.2.2 Synthesis:

4.2.2.1 Synthesis of mesoporous silica nanoparticles (MSN):

Mesoporous Silica Nanoparticles (MSN) were prepared by following the reported procedure with slight modifications. Cetyltrimethylammonium bromide (CTAB, 1.00 g, 2.74×10^{-3} mol) was dissolved in 480 mL of millipore water. NaOH (aq) (2.00 M, 3.50 mL) was then added to CTAB solution, followed by adjusting the solution temperature to 80°C. Tetraethyl orthosilicate (5.0 mL, 21.9 mmol) were then added drop wise and the mixture was stirred vigorously at 80 °C for 2 hrs. The resulting white precipitate was isolated by filtration, washed with abundant methanol, and dried under vacuum at 100 °C for 12 h. Yield: 1.8 g

4.2.2.2 Synthesis of MSN particles (MSN-N_3) with organoazide grafted in the outer surface:

The grafting of organoazide was performed according to procedure discussed before. In a typical reaction, 1.8 g of MSN particle (MSN) was added to 150 mL dry toluene and the reaction mixture was sonicated until it formed a clear dispersion. To this dispersion was added azidopropyltriethoxy silane (AzPTES) (0.500 mL; 2 mmol) and the resultant reaction mixture was heated at 85 ^{o}C for 16 hrs. After completion of the reaction, the resultant azide grafted MSN particles (MSN-N_3) were washed several times with ethanol to remove the unreacted AzPTES. Finally, the CTAB template was removed from these azide grafted MSN particles by treating MSN-N_3 particles the with 3 ml conc. HCl in 120 mL EtOH under reflux for 6 hours. The reaction mixture was centrifuged at 8000 rpm for 20 mins and again kept it under reflux with only ethanol for 20 hrs for complete removal of surfactant. The resultant solution was

centrifuged and washed an additional three times with ethanol to afford azide grafted MSN particles. These particles were stored as dispersion in ethanol for further usage.

4.2.2.3 Synthesis of MSN particles (CH_3-MSN-N_3) with organoazide and methyl grafted in the outer and inner surface respectively:

MSN particles (CH_3-MSN-N_3) with organoazide grafted in the outer surface and methyl group grafted in inner surface was synthesized by grafting methyl group onto MSN-N_3 mesoporous nanoparticles. In short, MSN-N_3 nanoparticle (500 mg) was dispersed in 50 mL dry dichloromethane. In this reaction mixture hexamethyldisilazane (0.150 mL, 0.9 mmol) was added and stirred at room temperature for 8 hrs. After the completion of reaction, the reaction mixture was centrifuged and the resultant solid powder was washed with an additional three times with ethanol to afford CH_3-MSN-N_3. The sample was stored in EtOH for further usage. Yield: 460 mg.

4.2.2.4 Pegylation on CH_3-MSN-N_3 to generate hydrophilic environment on the outer surface of mesoporous silica using CuAAC:

For CuAAC, the azide functionalized silica nanoparticles CH_3-MSN-N_3 were incubated with 1 equivalents of the PEG-alkyne in DMF: H_2O solvent mixture (8:2) containing CuI (2.0 equivalent), disodium bathophenanthrolene sulphonate (2.0 equivalent), sodium ascorbate (4 equivalent). In a typical reaction, azide grafted silica nanoparticles (150 mg, 0.135 mmol of azide) was incubated with PEG-alkyne (270 mg, 0.135 mmol, 1 eq) in 12mL DMF/3mL H_2O mixture containing sodium ascorbate (54 mg, 0.27 mmol, 2 eq) and copper iodide (25 mg, 0.135 mmol, 1 eq) and disodium sulphonated bathophenanthroline (80 mg, 0.135 mmol, 1 eq). The reaction mixture was subjected to three freeze-pump-thaw cycles for rigorous exclusion of dioxygen. The CuAAC was allowed to proceed for 24 hrs with stirring. After completion of the reaction, the mixture was taken into a centrifuge tube and centrifuged for 20 min at 12000 rpm. The supernatant liquid was decanted off and the solid residue was washed with DMF (2 times), ethanol (2 times), 0.1 M sodium ascorbate (2 times), 0.1 M N,N-diethyldithiocarbamate sodium in ethanol (4 times) and ethanol (2 times). It was finally stored as a suspension in ethanol. This sample will henceforth be called as CH_3-MSN-PEG. Yield: 145 mg

Similar protocol was adopted for CuAAC of the PEG-alkyne with only Silica-Azide (MSN-N_3) to afford the MSN-PEG. Yield: 112 mg

4.3 Results and Discussion:

Our strategy to create hydrophilic outer surface and hydrophobic inner surface of mesoporous silica nanoparticles is displayed in Scheme 4.1. The first step in this endeavour was the synthesis of azide grafted mesoporous silica particles (MSN-N_3). These were synthesized by the condensation of azidopropyltriethoxysilane (AzPTES) onto silica nanoparticles that still retain the cetyltrimethylammonium bromide (CTAB) template inside as presented in Scheme 4.1. The organosilica precursor AzPTES was obtained by the displacement of the chloro group in 3-chloropropyltriethoxysilane with an azido group using sodium azide. Detailed discussion has been given in Chapter 2. As the pores are still filled with CTAB, the azide groups are preferentially incorporated only on the external surface of MSNs. The resulting material is then refluxed with HCl and ethanol mixture in order to extract the CTAB template as reported by Lin. The resulting solid, porous azide grafted mesoporous silica nanoparticles (MSN-N_3) is externally covered by azidopropyl groups. Subsequently this material is then internally functionalized using hexamethyldisilazane in dry DCM to generate MSN particles (CH_3-MSN-N_3) with organoazide and methyl group grafted in the outer and inner surface respectively. The presence of methyl group inside the pore, confers hydrophobic nature to the pores.

The last step of our strategy was to impart hydrophilicity at the external silica surface using pegylation. As, the azide groups are already incorporated on the external surface of mesoporous silica, CuAAC can be employed to anchor any alkynylated hydrophilic molecule, PEG in our case. PEG-alkyne of molecular wt ~ 2000 was chosen in such a way that it is not possible for it to go inside the pore. PEG-alkyne was "clicked" on the external surface of CH_3-MSN-N_3 using "Click Reation". The CuAAC reaction was carried out using CuI/sulfonated bathophenanthroline in DMF and H_2O mixture at a ratio of 80:20 for 24 hrs. After the reaction, an extensive washing protocol was followed to remove the Cu(I), ascorbate and any unreacted starting materials. One of the key steps in the washing was the usage of dithiocarbamate to remove the Cu(I), as discussed earlier in Chapter 2. For performing control experiments, MSN-PEG was prepared by "Click Reaction" between MSN-N_3 and PEG-alkyne. In this control samples, the inside pore was not hydrophobized as earlier. It has been observed that water dispersibility increases after installing PEG on the surface of material.

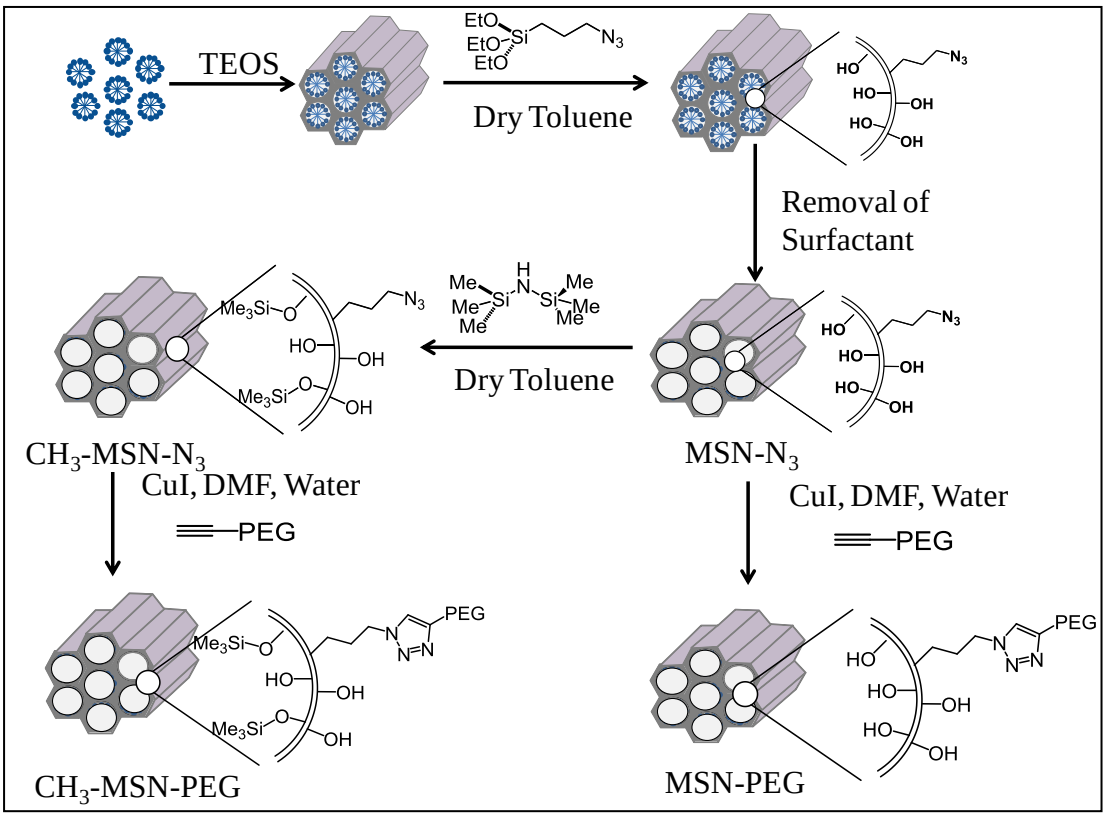

Scheme 4.1: Schematic representation of the selective grafting reactions on the external surface of mesoporous silica nanoparticles by PEG groups and by trimethylsilyl groups on the internal surface (nanopores).

4.4 Characterizations:

All these material was characterized by XRD analysis (Figure 4.1), TEM analysis (Figure 4.2), FT-IR (Figure 4.3), TGA (Figure 4.4), and N_2 adsorption isotherm (Figure 4.5). The extent of the click reaction was estimated using FT-IR spectroscopy, by monitoring the decrease in the integrated intensity of the $\upsilon_{as}(N_3)$ at 2100 cm^{-1}.

4.4.1 Powder X-ray diffraction:

The powder XRD patterns of all MSN materials (MSN-N_3, CH_3-MSN-N_3, CH_3-MSN-PEG) are shown in Figure 4.1. All materials showed the characteristic high intensity (100) diffraction peak at 2θ ~2.2º. The other significant peaks corresponding to (110) and (200) diffractions were also observed indicating the retention of well-ordered one-dimensional hexagonal mesoporous channels of MSN materials under the functionalization environment. However, the higher order (110) and (200) diffractions

became less resolved as the number of functionalizing steps increased (Figure 4.1). This shows that the long-range order decreases slightly upon incorporation of different functionalizing groups.

The powder XRD patterns of click products obtained by clicking PEG-alkyne with CH_3-MSN-N_3 and presented are Figure 4.1. The powder XRD patterns showed an intense (100) diffraction peak near 2θ ~2.2˚, indicating well-ordered hexagonal arrays and showing that the mesoporosity of the material does not change after undergoing CuAAC reaction.

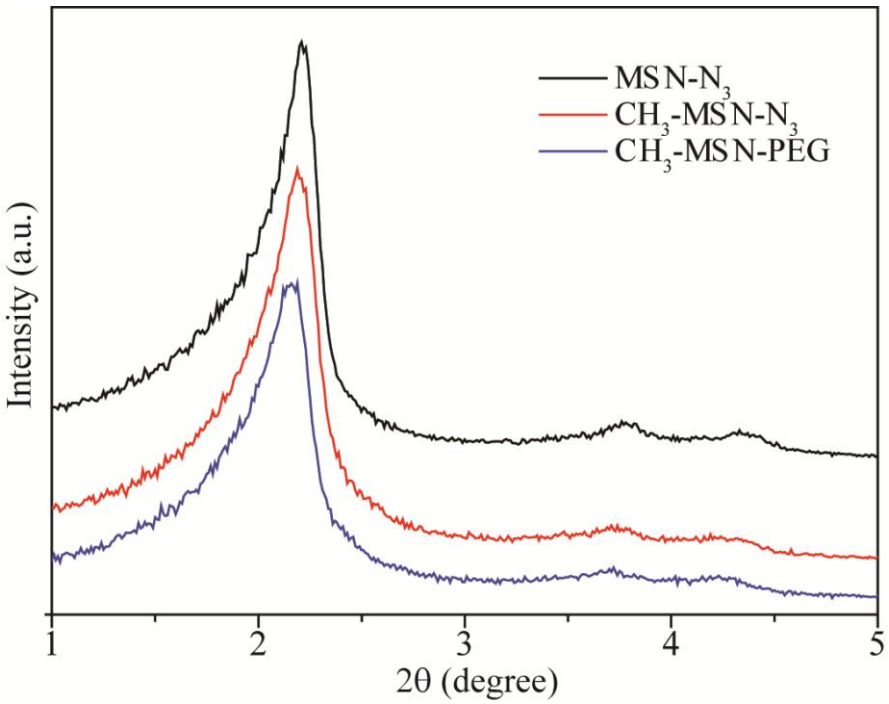

Figure 4.1: Powder XRD patterns of different MSN samples (a) MSN-N_3; (b) CH_3-MSN-N_3 (c) CH_3-MSN-PEG.

4.4.2 TEM analysis:

TEM images and particle size distribution displays formation of well-ordered two-dimensional hexagonal mesoporous particles with an elongated sphere-like morphology having particle size of 75±30 nm (Fig. 4.2). The TEM pictures indicate that the mesoporosity and morphology of the particles was retained in the different functionalization steps. Hence, incorporation of the azidopropyl group and click reaction did not interfere with the structural properties of MSN. It is clearly seen from the mean of the particle size distribution that the size of the particle remains unaltered upon different functionalization.

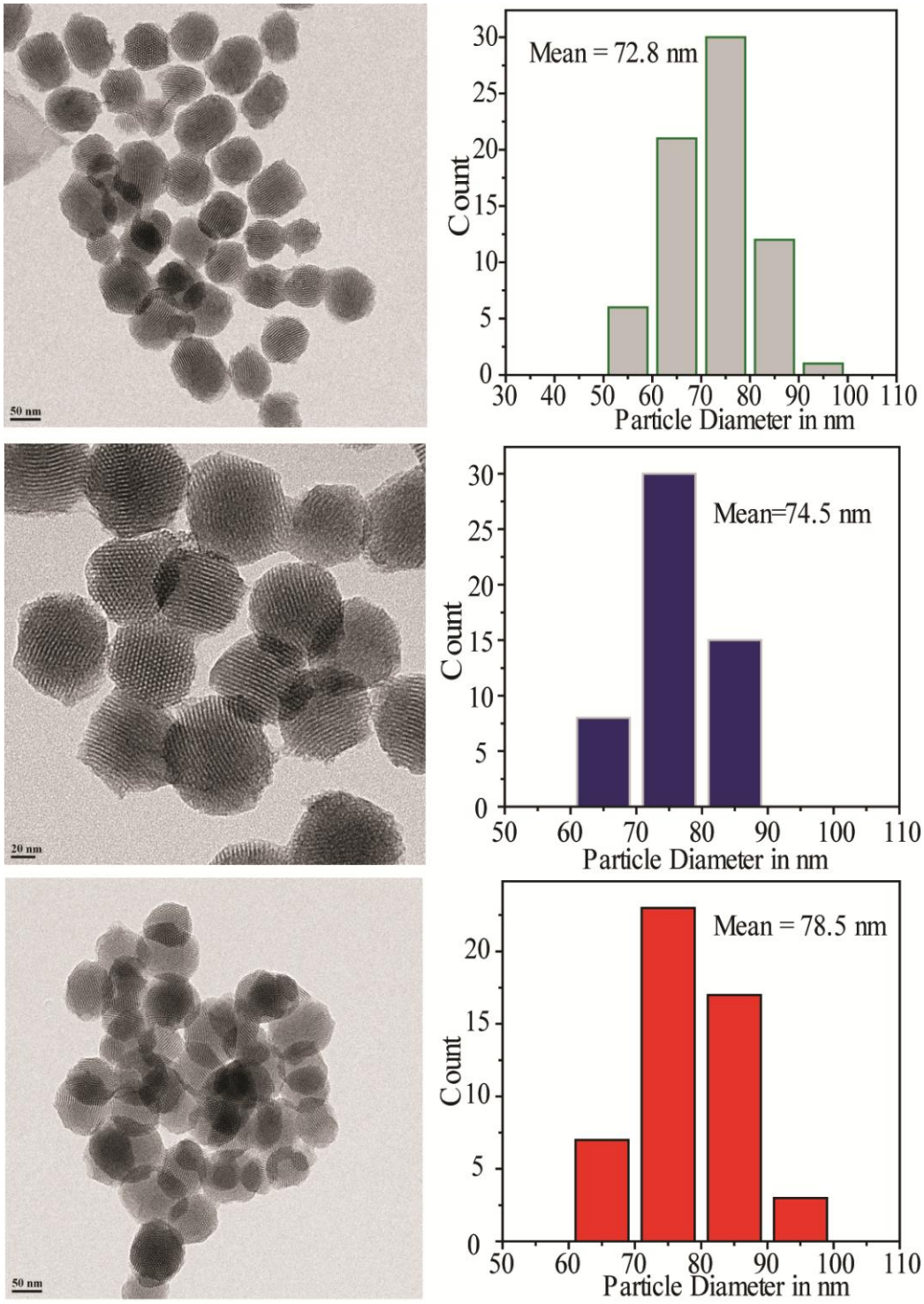

Figure 4.2: TEM images and particle size distribution of different azide functionalized MSN materials: (a) MSN-N_3; (b) CH_3-MSN-N_3 (c) CH_3-MSN-PEG.

4.4.3 FT-IR spectroscopy:

The FT-IR spectra of various materials are presented in the Figure 4.3. The spectra of the azido-functionalized mesoporous materials (MSN-N_3) display an absorbance at ~2100 cm^{-1}, which is the characteristic stretching vibration of an organic azide (N_3). The presence of this peak in the materials shows that the azidopropyl group were successfully incorporated into the MSN samples. The samples also showed absorbance peaks at 1230, 1080 and 805 cm^{-1} respectively. These peaks are typical of Si-O-Si bands that are associated with the formation of the silica networks. Weak peaks associated with Si-OH groups in the 940-960 cm^{-1} range were also observed for the functionalized mesoporous materials. The strong peak around 1658 cm^{-1} might be attributed to the bending vibration of H_2O. Thus, the FT-IR spectra indicate that the azido groups were efficiently incorporated in the matrix of the mesoporous materials. The extent of the click reaction was estimated using FT-IR spectroscopy, by monitoring the decrease in the integrated intensity of the $\nu_{as}(N_3)$ at 2100 cm^{-1} which corresponds to the conversion of 65% of the available azides to the corresponding triazoles.

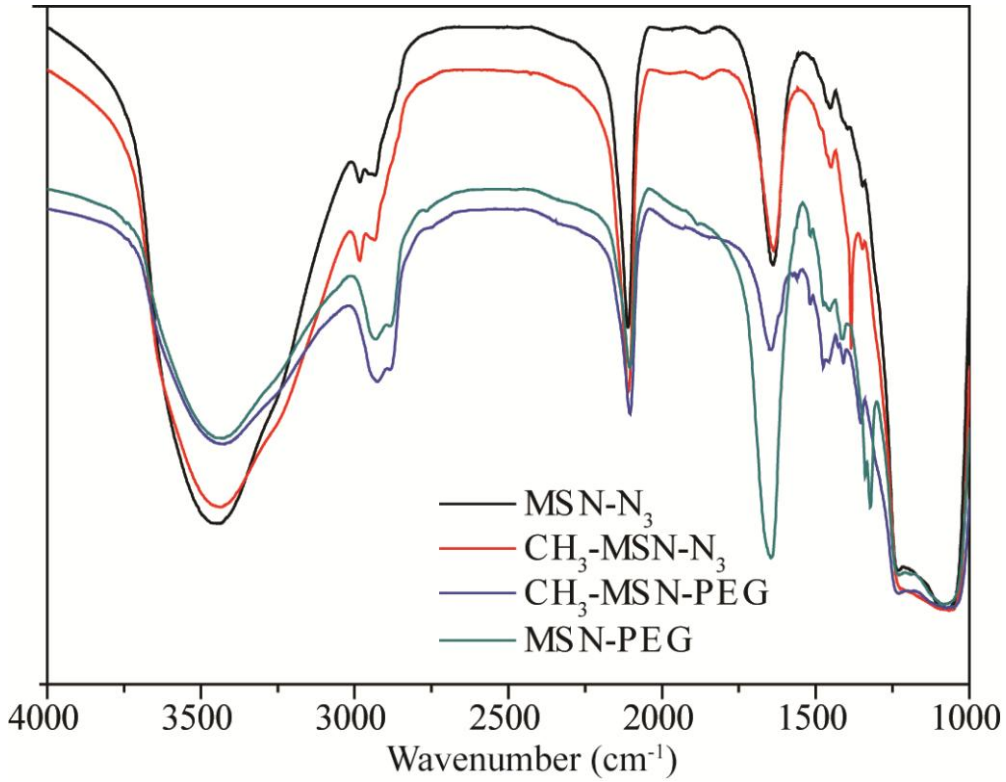

Figure 4.3: FT-IR spectra of (a) MSN-N_3; (b) CH_3-MSN-N_3; (c) CH_3-MSN-PEG (d) MSN-PEG.

4.4.4 Thermo gravimetric analysis:

The thermo gravimetric analysis of the different functionalized mesoporous silica materials are presented in Figure 4.4. The amount of azido-propyl groups present in the N_3-MSN were determined by the weight loss obtained in the thermo gravimetric analysis (TGA). The samples were heated in air at 5 °C/ minute to 800 °C so that the azidopropyl groups were completely decomposed and removed from the samples. Fig. 4.3 shows the TGA thermographs of the N_3-MSN sample, where the weight loss between 150 – 750 °C can be used to estimate that 0.9 mmol of azide groups are present per gm of MSN-N_3. Also from the elemental analysis the amount of azide groups present on the surface of N_3-MSN was determined to be 1.08 mmol/g. The TGA analysis of CH_3-MSN-N_3 indicates a weight loss of 3% between 150 – 750 °C with respect to N_3-MSN. This value corresponds to a loading of 0.4 mmol of trimethylsilyl group per gram of CH_3-MSN-N_3. Again, the TGA of CH_3-MSN-PEG shows a huge weight loss between 150 – 750 °C. This is ascribed to the higher amount of organic content in the material. This data also explains that PEG has been incorporated in the sample by 'Click Reaction'. The elemental analysis also shows increase of carbon content in the material. All these data conclusively indicate that PEG was installed in the sample followed by grafting of trimethylsilyl group.

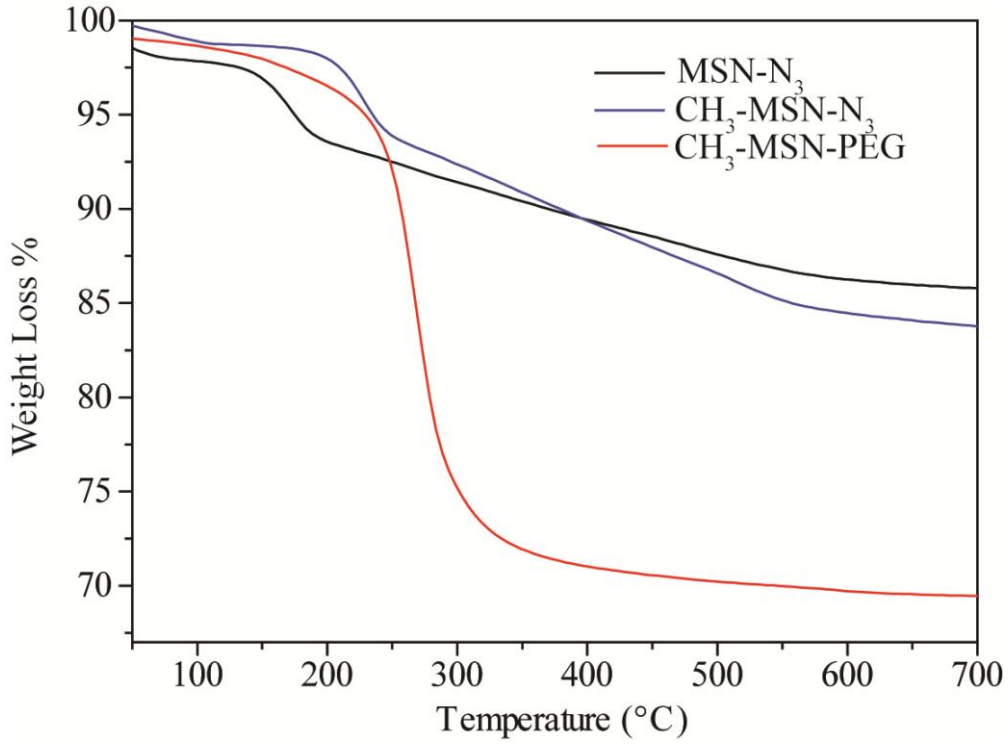

Figure 4.4: TGA analysis of (a) MSN-N_3; (b) CH_3-MSN-N_3 (c) CH_3-MSN-PEG.

4.4.5 Nitrogen adsorption-desorption studies:

The nitrogen adsorption-desorption isotherms of various functionalized mesoporous material are presented in Figure 4.5. Nitrogen adsorption-desorption isotherm of N_3-MSN exhibit the characteristic type IV isotherm with slight increase in adsorption at P/P_0 0.2-0.4 due to the capillary condensation of the nitrogen in the mesopores. The BJH pore-size distribution (PSD) analysis shows very narrow PSD values in the range 2.5 nm. The pore diameter, BET surface area and pore volume are listed in Table 4.1. These values are consistent with other organo-functionalized MSNs reported before.[22,23] The pore size distribution also shows that the pore size has been decreased upon various organic functionalization. The N_2 adsorption-desorption isotherm of CH_3-MSN-N_3 CH_3-MSN-PEG displayed similar profile to its parent N_3-MSN, which indicates that the material did not undergo any physical change during the course of hydrophobization; the click reaction and its subsequent workup.

Sample Name	**M_{BET} (m^2/g)**	**Pore Diameter (nm)**	**Pore Volume (cm^3/g)**
MSN-N_3	965	2.64	0.87
CH_3-MSN-N_3	898	2.53	0.86
CH_3-MSN-PEG	810	2.45	0.80

Table 4.1: Physical properties of functionalized mesoporous materials

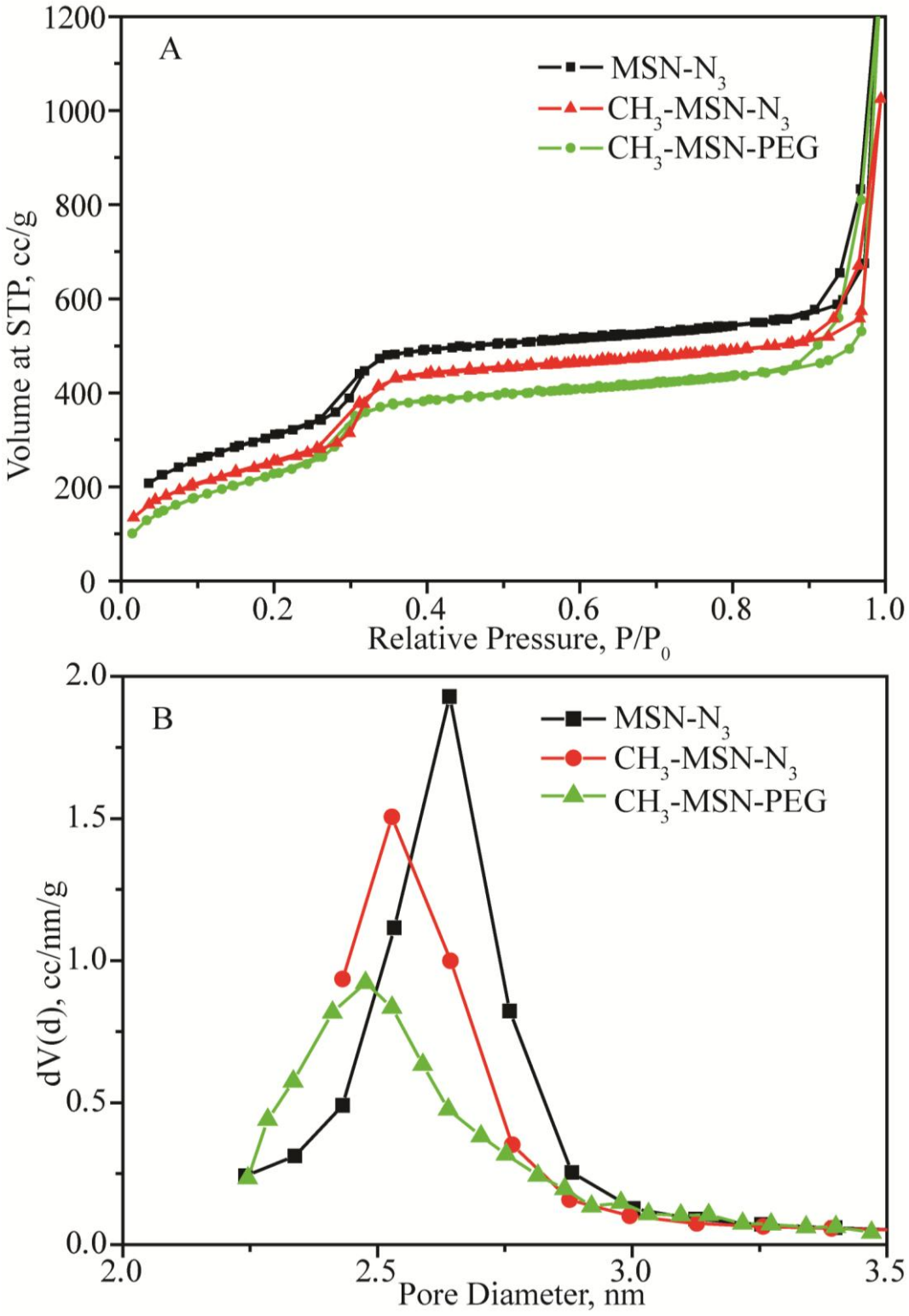

Figure 4.5: Nitrogen adsorption-desorption isotherms (A) and pore size distribution (B) of (a) MSN-N_3; (b) CH_3-MSN-N_3 (c) CH_3-MSN-PEG

4.5 Hydrophoboic dye encapsulation:

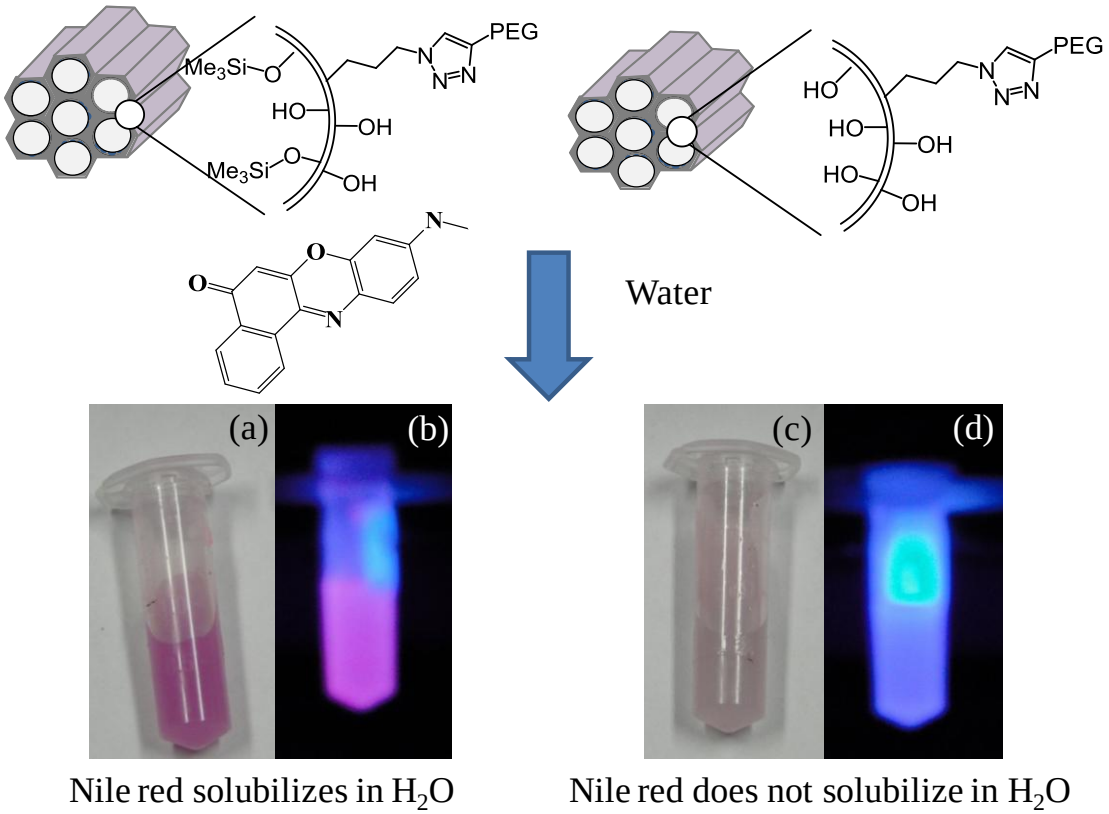

Scheme 4.2. Schematic illustration of hydrophobic dye encapsulation, Nile Red in our case. (a) and (b) are the pictures of the Nile red containing water solution taken under normal light and UV light in presence of CH_3-MSN-PEG. (c) and (d) are the pictures of the Nile red containing water solution taken under normal light and UV light in presence of MSN-PEG.

After preparing the material our aim was to show application in the field of hydrophobic dye encapsulation. We chose a hydrophobic dye Nile red which is sparingly soluble in water. We made a clear dispersion of CH_3-MSN-PEG in water having concentration of 20 mg/mL. The dispersed solution was mixed with Nile red. The solution turned red after some time. This is due to the fact that Nile red, being hydrophobic dye, gets encapsulated in the mesopores of CH_3-MSN-PEG samples and this gives an impression that it is solubilised in water. For doing control experiment PEG alkyne was anchored on the surface of azide mesoporous silica nanoparticles (MSN-N_3) without the trimethyl silyl functionalization inside. Due to the absence of

these hydrophobic groups inside the mesopores the hydrophobicity was not generated in the material. This material (MSN-PEG) was also subjected to the hydrophobic dye encapsulation experiment keeping same reaction condition. As expected this solution did not turn red. From the above discussion, it can be concluded that the dye has been encapsulated inside the mesopore of CH_3-MSN-PEG.

4.6 Conclusion:

In conclusion, a successful strategy for the preparation of hydrophilic exterior and hydrophobic interior surface in mesoporous silica nanoparticles through traditional silane chemistry and CuAAC "click chemistry" protocol has been demonstrated. The surface functionalized mesoporous silica nanoparticles have been thoroughly and extensively characterized using a variety of analytical and spectroscopic techniques. These materials also subjected to hydrophobic dye encapsulation. This material can be a potential candidate for the separation of hydrophilic and hydrophobic dye from a mixture or for drug delivery applications. This strategy can be used to synthesize other mesoporous silica nanoparticle having two different organic functionalities.

4.7 References:

1. Stein, A.; Melde, B. J.; Schroden, R. C., Hybrid Inorganic-Organic Mesoporous Silicates-Nanoscopic Reactors Coming of Age. *Advanced Materials*, **2000,** 12, (19), 1403-1419.

2. Wang, Y.; Caruso, F., Mesoporous Silica Spheres as Supports for Enzyme Immobilization and Encapsulation. *Chemistry of Materials*, **2005,** 17, (5), 953-961.

3. Wan, Y.; Shi, Y.; Zhao, D., Supramolecular Aggregates as Templates: Ordered Mesoporous Polymers and Carbons. *Chemistry of Materials*, **2007,** 20, (3), 932-945.

4. Vivero-Escoto, J. L.; Slowing, I. I.; Trewyn, B. G.; Lin, V. S. Y., Mesoporous Silica Nanoparticles for Intracellular Controlled Drug Delivery. *Small*, **2010,** 6, (18), 1952-1967.

5. Slowing, I. I.; Trewyn, B. G.; Giri, S.; Lin, V. S. Y., Mesoporous Silica Nanoparticles for Drug Delivery and Biosensing Applications. *Advanced Functional Materials*, **2007,** 17, (8), 1225-1236.

6. Mortera, R.; Vivero-Escoto, J.; Slowing, I. I.; Garrone, E.; Onida, B.; Lin, V. S. Y., Cell-induced intracellular controlled release of membrane impermeable cysteine from

a mesoporous silica nanoparticle-based drug delivery system. *Chemical Communications*, **2009,** 0, (22), 3219-3221.

7. Giri, S.; Trewyn, B. G.; Lin, V. S. Y., Mesoporous silica nanomaterial-based biotechnological and biomedical delivery systems. *Nanomedicine*, **2007,** 2, (1), 99-111.

8. Cheng, K.; Landry, C. C., Diffusion-Based Deprotection in Mesoporous Materials: A Strategy for Differential Functionalization of Porous Silica Particles. *Journal of the American Chemical Society*, **2007,** 129, (31), 9674-9685.

9. Kecht, J.; Schlossbauer, A.; Bein, T., Selective Functionalization of the Outer and Inner Surfaces in Mesoporous Silica Nanoparticles. *Chemistry of Materials* **2008,** 20, (23), 7207-7214.

10. de Juan, F.; Ruiz-Hitzky, E., Selective Functionalization of Mesoporous Silica. *Advanced Materials*, **2000,** 12, (6), 430-432.

11. Cauda, V.; Argyo, C.; Bein, T., Impact of different PEGylation patterns on the long-term bio-stability of colloidal mesoporous silica nanoparticles. *Journal of Materials Chemistry*, **2010,** 20, (39), 8693-8699.

12. Manzano, M.; Aina, V.; Areán, C. O.; Balas, F.; Cauda, V.; Colilla, M.; Delgado, M. R.; Vallet-Regí, M., Studies on MCM-41 mesoporous silica for drug delivery: Effect of particle morphology and amine functionalization. *Chemical Engineering Journal*, **2008,** 137, (1), 30-37.

13. Rosenholm, J. M.; Lindén, M., Towards establishing structure activity relationships for mesoporous silica in drug delivery applications. *Journal of Controlled Release*, **2008,** 128, (2), 157-164.

14. Radu, D. R.; Lai, C.-Y.; Jeftinija, K.; Rowe, E. W.; Jeftinija, S.; Lin, V. S. Y., A Polyamidoamine Dendrimer-Capped Mesoporous Silica Nanosphere-Based Gene Transfection Reagent. *Journal of the American Chemical Society*, **2004,** 126, (41), 13216-13217.

15. Wang, L.-S.; Wu, L.-C.; Lu, S.-Y.; Chang, L.-L.; Teng, I. T.; Yang, C.-M.; Ho, J.-a. A., Biofunctionalized Phospholipid-Capped Mesoporous Silica Nanoshuttles for Targeted Drug Delivery: Improved Water Suspensibility and Decreased Nonspecific Protein Binding. *ACS Nano*, **2010,** 4, (8), 4371-4379.

16. Cauda, V.; Engelke, H.; Sauer, A.; Arcizet, D.; Brauchle, C.; Radler, J.; Bein, T., Colchicine-Loaded Lipid Bilayer-Coated 50 nm Mesoporous Nanoparticles

Efficiently Induce Microtubule Depolymerization upon Cell Uptake. *Nano Letters*, **2010,** 10, (7), 2484-2492.

17. Liu, J.; Stace-Naughton, A.; Jiang, X.; Brinker, C. J., Porous Nanoparticle Supported Lipid Bilayers as Delivery Vehicles. *Journal of the American Chemical Society*, **2009,** 131, (4), 1354-1355.

18. Kim, M. S.; Jeon, J. B.; Chang, J. Y., Selectively functionalized mesoporous silica particles with the PEGylated outer surface and the doxorubicin-grafted inner surface: Improvement of loading content and solubility. *Microporous and Mesoporous Materials*, **2013,** 172, (0), 118-124.

19. Vallet-Regí, M.; Balas, F.; Arcos, D., Mesoporous Materials for Drug Delivery. *Angewandte Chemie International Edition*, **2007,** 46, (40), 7548-7558.

20. Doadrio, J. C.; Sousa, E. M. B.; Izquierdo-Barba, I.; Doadrio, A. L.; Perez-Pariente, J.; Vallet-Regi, M., Functionalization of mesoporous materials with long alkyl chains as a strategy for controlling drug delivery pattern. *Journal of Materials Chemistry*, **2006,** 16, (5), 462-466.

21. Nebhani, L.; Barner-Kowollik, C., Orthogonal Transformations on Solid Substrates: Efficient Avenues to Surface Modification. *Advanced Materials*, **2009,** 21, (34), 3442-3468.

22. Moitra, N.; Trens, P.; Raehm, L.; Durand, J.-O.; Cattoen, X.; Chi Man, M. W., Facile route to functionalized mesoporous silica nanoparticles by click chemistry. *Journal of Materials Chemistry*, **2011,** 21, (35), 13476-13482.

23. Huh, S.; Wiench, J. W.; Yoo, J.-C.; Pruski, M.; Lin, V. S. Y., Organic Functionalization and Morphology Control of Mesoporous Silicas via a Co-Condensation Synthesis Method. *Chemistry of Materials*, **2003,** 15, (22), 4247-4256.

Chapter 5

Assembling mesoporous silica nanoparticles to generate functional hybrid silica scaffolds with controllable hierarchical porosity by dynamic templating

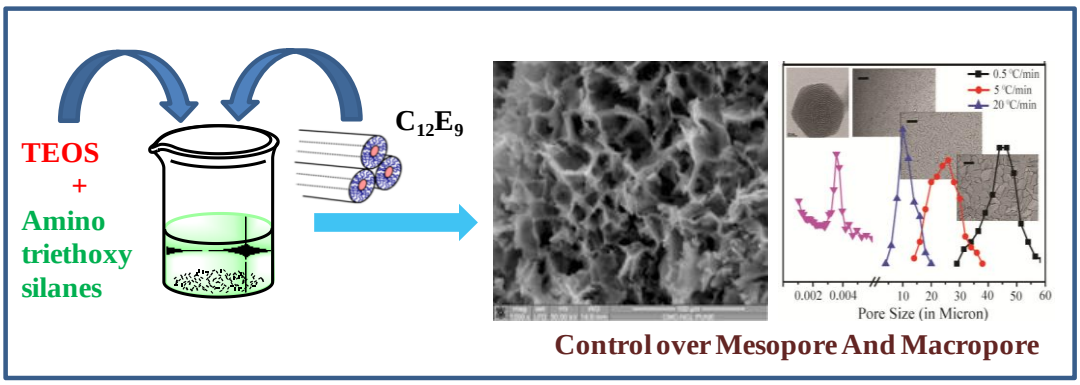

In this chapter mesoporous silica nanopartices have been assembled using non ionic surfactant to form hierarchical monolithic scaffold. The independent control over nanoparticle mesoporosity and scaffold macroporosity has been shown. The methodology allowed controllable spatial variation in macroporosity in the scaffold. The monolith was also functionalizable with different organic molecules. The catalytic activity of the scaffold was also studied in detail after embedding a catalyst inside the mesopore.

Part of the work discussed in this chapter has been published in

Anal Kr. Ganai, Sushma Kumari, Kamendra P. Sharma, Chakadola Panda, Guruswamy Kumaraswamy, Sayam Sen Gupta, *Chem. Commun.*, **2012**, 48, 5292-5294.

Kamendra P. Sharma, Anal Kr. Ganai, Sayam Sen Gupta, and Guruswamy Kumaraswamy, *Chem. Mater.*, **2011**, 23 (6), 1448–1455 (Cover Page Article).

5.1 Introduction:

One of the goals of nano-chemistry is to extend the traditional length scales of synthetic chemistry and exploit the collective properties of organized assemblies. Structurally organized inorganic nano-scale materials have attracted much attention since they offer a desirable combination of an extensive internal reactive surface along with narrow nanopores with facile molecular transport through broad "highways" leading to and from these pores.[1] Hence they have found widespread interest in emerging applications such as catalysis, storage and controlled release systems among others.[2]

Inorganic materials, in spite of having diversity in composition, generally lack the structural variety of supramolecular and other organic structures.[3] However, the discovery of the synthesis for mesoporous silica materials using organic templates was a breakthrough in the design of strategies for the preparation of well-organized inorganic and hybrid materials.[4,5] A variety of organic templates have been used to imprint inorganic structures resulting in materials whose shape is controlled at both the microscopic and the nanoscopic level. Lately, attempts have also been made to reproduce biological structures that, besides functionality, offer organization across a large range of length scales such as in diatoms. Synthesis of complex structured materials with different levels of space organization (e.g., hierarchical materials) is increasingly being pursued by several research groups. However, there has been limited success in developing routes that afford structures having morphological complexity with sophisticated levels of structure organization at different length scale. The most common methodology to develop such structures is the combined use of different templates that allow for the achievement of bimodal and even trimodal pore structured materials. The final template removal (e.g., by thermal or dissolution treatments) yields a hierarchically organized material with a structure that is a replica of that of the original template. Synthesis of such hierarchically porous materials (the porosity comes after template removal) that afford control of pore characteristics at each length scale, and allow chemical functionalization, have significant potential for applications in areas as diverse as catalysis, tissue engineering and chromatographic separations.[6-8] Although many advanced porous materials have been reported, it is still a challenging task to produce hierarchically porous structures, avoiding the closure of pores, controlling independently the sizes of the mesopores and the

macropores, achieving porosity with three-dimensional interconnectivity of pores, and managing the shrinkage of the whole structure while retaining the macroscopic shape.[9]

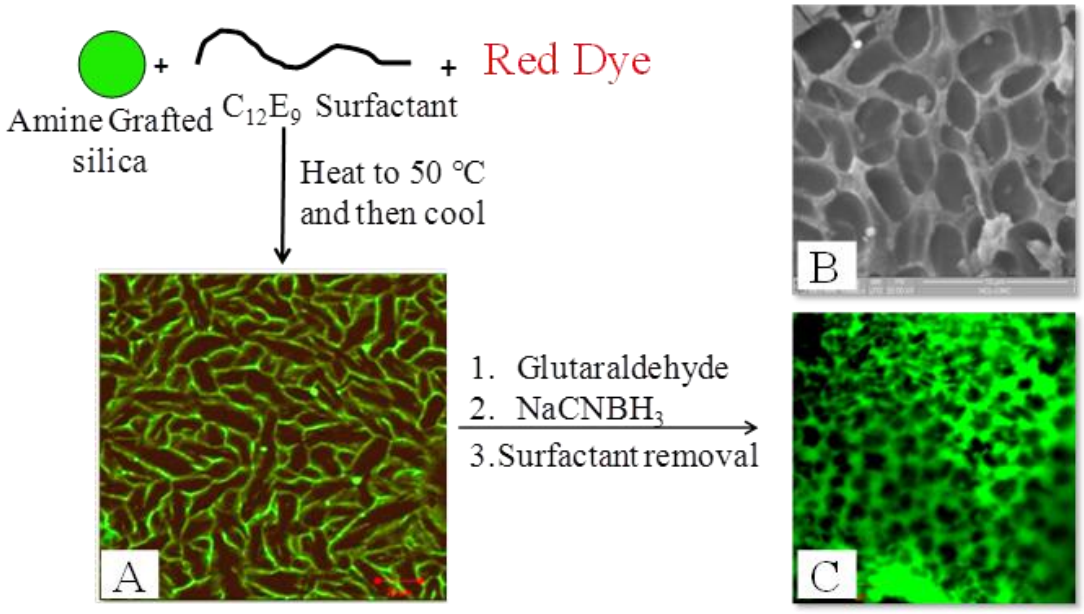

Figure 5.1: Schematic illustration of assembling nanoparticles using non-ionic surfactant $C_{12}E_9$. (A) Confocal micrograph of fluorescently tagged silica particles in surfactant dispersion. (B) SEM of Scaffold (C) Confocal image of the scaffold. (Taken from the Ph.D thesis of Kamendra P Sharma with permission)

Recently, our group in collaboration with Dr. Guruswamy Kumaraswamy's group in National Chemical Laboratory, Pune have developed a methodology to prepare macroporous materials by assembling nanoparticles using dynamic templating of non-ionic surfactant ($C_{12}E_9$, poly(ethylene glycol) diglycidyl ether) hexagonal (H_1) mesophases.[10] Dynamic templating of surfactant hexagonal domains is a facile technique to organize inorganic, organic, and biological nanoparticles into a network of particulate strands (Figure 5.1). The $C_{12}E_9$-water system organizes into a hexagonal phase (H_1) having surfactant concentrations between about 35 and 70 % by weight, at room temperature.[11,12] This system undergoes a phase transition from H_1 to an isotropic micellar phase at a temperature $T_{HI} \approx 40$ °C. To demonstrate this fluorescently tagged amine grafted silica nanoparticles were mixed with non-ionic surfactant water mixture at a fixed ratio of 1:1 by weight and heated above T_{HI}. Subsequently these samples were allowed to cool down at room temperature. During

this phase transition, the silica particles were expelled from the H_1 phase and confined to the isotropic regions. As the H_1 domains grow, the particles were concentrated in the isotropic phase until they impinge to form the networks. This was observed using confocal microscopy where fluorescently labelled particles assembled on the domain boundaries of the hexagonal phase of the surfactant (Fig 5.1 A). To stabilize the particulate network against dispersion after H_1 template removal, amine grafted silica particles were crosslinked with glutaraldehyde upon network formation. Subsequent to cross-linking, the surfactant could be readily removed by washing with water, to yield a free-standing particulate macroporous solid (Fig 5.1 B). The confocal microscopy image of the particulate suspension and SEM and confocal micrographs of the self standing scaffold has been shown in Figure 5.1.

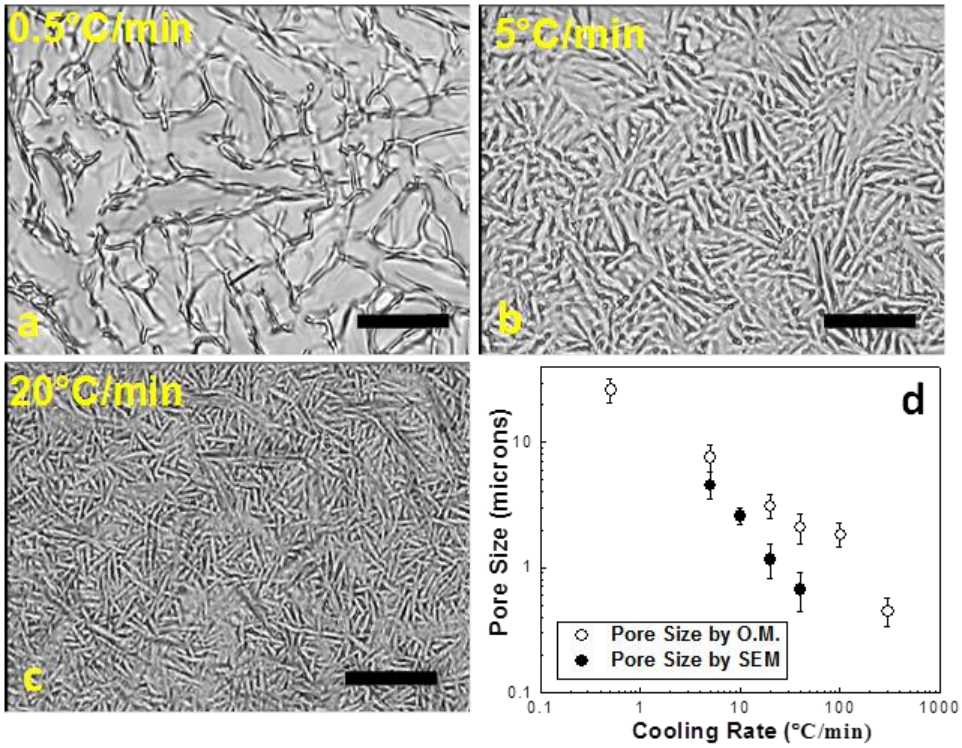

Figure 5.2: Cooling Rate Dependence on the size of structure. Optical micrographs of 5% amine grafted silica particles forming network structures at the domain boundaries of the H_1 phase at different cooling rates of (a) 0.5 °C/min (b) 5 °C/min and (c)20 °C/min. Scale Bar in the optical micrographs is 50 microns. As the cooling rate is increase the nucleation density of the H_1 phase also increase resulting in larger number of small sized domains. Figure (d) shows the plot of the pore size vs cooling rate obtained from optical micrographs and SEM images. (Taken from the Ph.D thesis of Kamendra P Sharma with permission)

This technique also allows the network mesh size to be varied from submicrometers to tens of micrometers by controlling the cooling rate.[10] On cooling below T_{HI}, H_1 domains nucleate and grow to impingement. Thus, by varying the nucleation density of H_1 domains, it is possible to vary the size of the domains and, therefore, the characteristic spacing of the particulate network. For example, fast cooling at 20 ^{o}C/min, results in particulate networks with smaller "strut" spacing as compared to cooling at 5 ^{o}C/min (Compare Figure 5.2 c and b). As the sample is cooled at even slower cooling rates of 0.5 ^{o}C/min, the strut spacing increases further (Figure 5.2 a). Optical micrographs of networks formed by cross-linking amine grafted silica particles reveal that the average mesh spacing can be varied from ~3.1 μm to ~26.4 μm on decreasing the cooling rate from 40 to 0.5 ^{o}C/min. After removal of surfactant, the SEM of various samples formed using different cooling rates show very good agreement of average mesh spacing that was obtained from optical micrographs with pore sizes obtained from SEM (Figure 5.2 d).

A significant advancement of this technique would be to extend this technique to produce hierarchically porous meso-macroporous materials using a convenient one-pot strategy, while still using mild synthetic conditions. We imagined that, it would be possible to generate hierarchically porous materials by starting with preformed micro- or mesoporous silica nanoparticles instead of silica nanoparticle and assembling these so as to generate macroporosity. The pores generated by the jamming of nanoparticles fall in the order of micropore region. The major advantage of this technique, over reported schemes, is its versatility; it allows independent control over (a) meso and macroporosity; (b) the organic and inorganic content of the hybrid; (c) spatial control of macroporosity and (d) chemical functionalization. In this chapter, all the above mentioned points have been demonstrated by assembling mesoporous silica nanoparticles. Different mesopore sized particles have been prepared and assembled by using dynamic templating of hexagonal mesophase domain of $C_{12}E_9$ surfactant. Macropore has been easily tuned by varying the cooling rate as described earlier. So size of mesopore and macropore could be easily tuned depending on need. A catalyst has also embedded inside hierarchical self standing monolith and its catalytic activity has been discussed in the last part of this chapter.

5.2 Experimental section:

5.2.1 Materials:

Tetraethyl orthosilicate (TEOS) and nonionic surfactant, nonaethylene glycol monododecyl ether ($C_{12}E_9$) sodium cyanoborohydride, 3-[2-(2-aminoethylamino)ethylamino]propyltrimethoxysilane, Poly(ethylene glycol) diglycidyl ether**,** orange II, disodium banthophenanthroline sulfonate and copper iodide were used as received from Sigma Aldrich. Glutaraldehyde was purchased from Merck, India. All other chemicals were used as obtained from Sigma Aldrich. All the other solvents were purchased from Merck, India. 3-Azidopropyltriethoxysilane (AzPTES), sodium dithiocarbamate were prepared as reported before.

5.2.2 Synthesis and Characterization:

5.2.2.1 Synthesis of mesoporous silica nanoparticles small pore (MSN-S):

Mesoporous Silica Nanoparticles (MSN) was prepared by following reported procedure with slight modifications.[13] Cetyltrimethylammonium bromide (CTAB, 1.00 g, 2.74×10^{-3} mol) was dissolved in 480 mL of millipore water. NaOH (aq) (2.00 M, 3.50 mL) was then added to CTAB solution, followed by adjusting the solution temperature to 80 °C. Tetraethyl orthosilicate (5.0 mL, 21.9 mmol) were then added drop wise and the mixture was stirred vigorously at 80 °C for 2 h. The resulting white precipitate was isolated by filtration, washed with abundant methanol, and dried under vacuum at 100 °C for 12 h. Yield: 1.8 g

5.2.2.2 Synthesis of mesoporous silica nanoparticles large pore (MSN-L):

The large pore sized mesoporous silica nanoparticles were prepared by following the reported procedures with slight modification.[14] Cetyltrimethylammonium bromide (CTAB, 1.0 g, 2.7 mmol) was dissolved in a solution of 480 mL millipore water and NaOH (aq) (2M, 3.5 mL), mesitylene (7.0 mL, 50.30 mmol) were then added to the solution. The mixture was stirred vigorously at 80 °C for 2 hrs. Tetraethyl orthosilicate (5.0 mL, 22.56 mmol) was then added dropwise. The reaction mixture was stirred vigorously at 80 °C for another 2 h. The resulting white precipitate was isolated by filtration, washed with abundant methanol, and dried under vacuum at 100 °C for 12 hrs. Yield: 1.95g

5.2.2.3 Synthesis of MSN-L-NH_2 and MSN-S-NH_2 by grafting of 3-[2-(2-aminoethylamino)ethylamino]propyltrimethoxysilane onto MSN-L and MSN-S

The grafting of organoamine was performed according to procedure reported before. [15] In a typical reaction, 500 mg of MSN particle (MSN-S or MSN-L) was added to 50 mL dry toluene and the reaction mixture was sonicated until it formed a clear dispersion. To this dispersion was added 3-[2-(2-aminoethylamino)ethylamino] propyltrimethoxysilane (0.200 mL; 0.75 mmol) and the resultant reaction mixture was heated at 85 ^{o}C for 16 hrs. After completion of the reaction, the resultant amine grafted MSN particles were washed several times with ethanol to remove the unreacted 3-[2-(2-aminoethylamino)ethylamino] propyltrimethoxysilane. Finally, the CTAB template was removed from these amine grafted MSN particles by treating the amine grafted MSN with 5 ml conc. HCl in 120 mL EtOH under reflux. After 2 hrs, the reaction mixture was centrifuged at 8000 rpm for 20 mins. The resultant solid powder was washed an additional three times with ethanol to afford amine grafted MSN particles MSN-L-NH_2 and MSN-S-NH_2. These particles were stored as dispersion in ethanol for further usage.

5.2.2.3.1 TEM analysis of the particles:

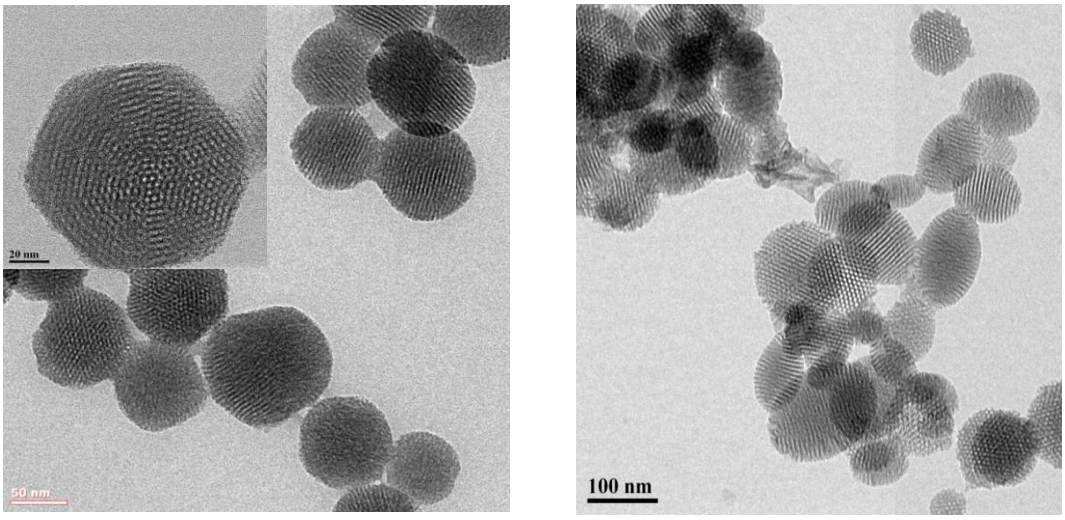

Figure 5.3: (A) HRTEM of MSN-S-NH_2 (B) HRTEM of MSN-L-NH_2

Transmission electron microscopy (TEM) images of MSN-L-NH_2 and MSN-S-NH_2 are displayed in Figure 5.3. TEM showed formation of well-ordered two-

dimensional hexagonal mesoporous particles with a spherical morphology. The size of these particles was calculated by using TEM. TEM of the MSN-S-NH_2 and MSN-L-NH_2 particles clearly indicate the mesoporous structure and particle sizes of ~100 nm and ~150 nm.

5.2.2.3.2 Nitrogen adsorption-desorption studies

Nitrogen adsorption-desorption isotherm of these particles exhibit the characteristic type IV isotherm with slight increase in adsorption at P/P_0 0.2-0.4 due to slight capillary condensation of the nitrogen in the mesopores (Figure 5.4). The pore size was determined applying N_2 adsorption isotherm. The nitrogen surface sorption measurements exhibited a type IV isotherm with a BET surface area of 836 m^2/g and 842 m^2/g (Table 5.1). The BJH pore-size distribution (PSD) analysis shows very narrow PSD values in the range of 2.5 nm and 3.7 nm for MSN-S-NH_2 and MSN-L-NH_2 respectively.

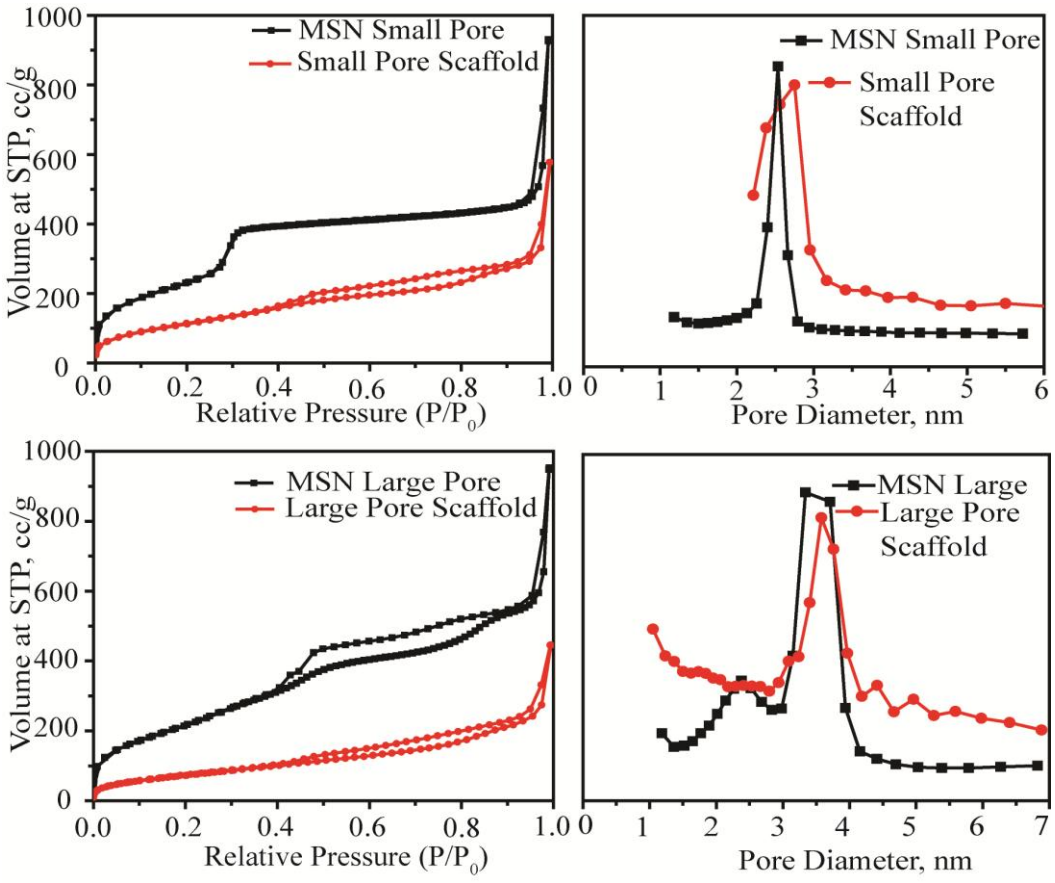

Figure 5.4: (A) N_2 absorption isotherm of MSN-S-NH_2 and small pore scaffold. (B) Pore size distribution of MSN-S-NH_2 and small pore scaffold. (C) N_2 absorption isotherm of MSN-L-NH_2 and large pore scaffold. (D) Pore size distribution of MSN-L-NH_2 and large pore scaffold.

Sample Name	M_{BET} (m^2/g)	Pore Diameter (nm)	Total Pore Volume (cm^3/g)
MSN-S-NH_2	836	2.5	1.44
Small Pore Scaffold	407	2.3	0.89
MSN-L-NH_2	842	3.7	1.47
Large Pore Scaffold	251	3.5	0.69

Table 5.1: Properties of MSN particles and scaffolds from BET measurements

5.2.2.4 Methodology for assembly of nanoparticles for making a self-standing scaffold:

5.2.2.4.1 Using glutaraldehyde/$NaCNBH_3$ for cross-linking:

Amine grafted mesoporous nanoparticles MSN-L-NH_2 and MSN-S-NH_2 were assembled into self-standing scaffold by using the dynamic templating procedure.[10,12] Typically, 165 mg of a dispersion of **MSN-S-NH_2** nanoparticles (10 wt%) was added to surfactant $C_{12}E_9$ (135 mg) and homogenized in a water bath at 50 ºC such that the surfactant to water ratio was 1:1. To this, glutaraldehyde (10 mg, 25 wt% solution) was added and the sample was then cooled to room temperature in a feedback controlled convective oven. The particle concentration in the overall composite was ~ 9 wt %. The sample was then allowed to crosslink on standing at room temperature for a week. 0.1 M $NaCNBH_3$ was then added to the gel to reduce the imine groups formed upon crosslinking of amine and glutaraldehyde. Finally, the scaffold was washed repeatedly with ethanol and water (6-7 times) to remove the surfactant and afford the free-standing macroporous material. The silica scaffold was then dried in a vacuum oven at 120 ºC.

5.2.2.4.2 Using poly(ethylene glycol) diglycidyl ether as the cross-linker:

To 165 mg of dispersion of MSN-S-NH_2 nanoparticles 10% (by weight) was added to surfactant $C_{12}E_9$ (135 mg) and homogenized in a water bath at 50 ºC such that the surfactant to water ratio was 1:1. To this poly(ethylene glycol) diglycidyl ether (10 mg) was added and the sample was then cooled to room temperature in a feedback controlled convective oven. The particle concentration in the overall

composite was ~ 9 wt %. The sample was then allowed to crosslink on standing at room temperature for 12 hrs. Finally, the scaffold was washed repeatedly with ethanol and water (6-7 times) to remove the surfactant and afford free-standing macroporous material. The silica scaffold was then dried in a vacuum oven at 120 ºC.

5.2.2.5 One-pot synthesis of hierarchical self-standing scaffold:

5.2.2.5.1 Using glutaraldehyde/$NaCNBH_3$ for cross-linking:

To an aqueous solution of CTAB (166 mg, 0.00045 mol, 80 mL) and NaOH (2M, 0.5833mL), tetraethyl orthosilicate (0.75 mL, 0.0036 mol) was added drop wise and the mixture was stirred vigorously at 80 °C. After 30 mins, 3-[2-(2-aminoethylamino)ethylamino]propyltrimethoxysilane (0.1077 mL, 0.0004 mol) was added to the reaction mixture and stirred for 1.5 hrs further for amine grafting. After completion of reaction, 20 mg of particles was taken out and mixed with 90 mg of $C_{12}E_9$ and 90 mg of H_2O. The mixture was heated to 55 ^oC and to this glutaraldehyde was added and cooled to room temperature. The sample was then allowed to crosslink on standing at room temperature for a week. 0.1 M $NaCNBH_3$ was then added to the gel to reduce the imine groups formed upon crosslinking of amine and glutaraldehyde. Finally, the scaffold was washed repeatedly with ethanol and water (6-7 times) to remove the surfactant and afford the free-standing macroporous material.

5.2.2.5.2 Using poly(ethylene glycol) diglycidyl ether as the cross-linker:

To an aqueous solution of CTAB (166 mg, 0.00045 mol, 80 mL) and NaOH (2M, 0.5833 mL), tetraethyl orthosilicate (0.75mL, 0.0036 mol) was added drop wise and the mixture was stirred vigorously at 80 °C. After 30 mins, 3-[2-(2-aminoethylamino)ethylamino]propyltrimethoxysilane (0.1077 mL, 0.0004 mol) was added to the reaction mixture and stirred for 1.5 hrs more for amine grafting. After completion of reaction, 20 mg of particles was taken out and mixed with 90 mg of $C_{12}E_9$ and 90 mg of H_2O. The mixture was heated to 55 ^oC and to this poly(ethylene glycol) diglycidyl ether was added and cooled to room temperature. The sample was then allowed to crosslinked on standing at room temperature for 12 hrs. Finally, the scaffold was washed repeatedly with ethanol and water (6-7 times) to remove the surfactant and afford the free-standing macroporous material. The silica scaffold was then dried in a vacuum oven at 120 ºC.

5.2.2.6 Temperature gradient experiments:

To obtain a stable temperature gradient across a glass slide, we held a glass slide over a beaker containing water that was maintained at 90 ^{o}C (Scheme 5.1). One end of the slide was maintained in dry ice. We observed that the arrangement resulted in a temperature gradient from 60 ^{o}C to -10 ^{o}C over a ~8 cm length of the slide. On the slide, we deposited a uniform thin film of the MSN containing $C_{12}E_9/H_2O$ sample at 60 ^{o}C using a micropipette.

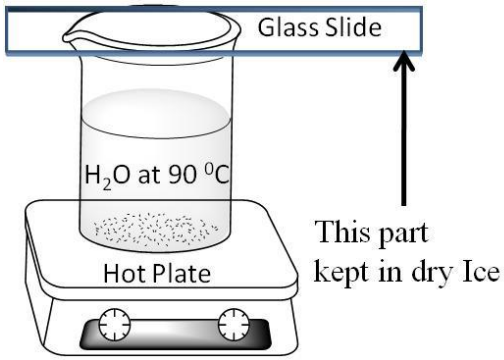

Scheme 5.1: The above schematic represents control of macroporosity within a single sample, simply by imposing a spatial variation in cooling rates.

5.2.2.7 Functionlization of scaffold with fluorescent streptavidin-phycoerythrin:

The scaffold (~10 mg) was added to a 1 mL solution of biotin-NHS ester (3 mg) in pH 7.4 PBS buffer and incubated overnight at room temperature. After completion of the reaction, this suspension was washed with buffer solution (3 times) followed by washing with Millipore water (3 times). The biotin labelled scaffold was then resuspended in phycoerythrin-streptavidin (1 mL, 20 μg) conjugate in PBS buffer and the suspension was incubated at 4 °C for 2 hrs. The scaffold was then washed extensively with PBS buffer multiple times to remove the unreacted phycoerythrin-streptavidin conjugate. Control samples using scaffold which was not conjugated with biotin but was incubated with phycoerythrin-streptavidin was also synthesized.

5.2.2.8 Synthesis of Fe-Cat embedded hierarchical self-standing scaffold:

5.2.2.8.1 Synthesis of MSN particles (N_3-MSN-S-NH_2) with organoazide and organoammine grafted in the inner and outer surface respectively:

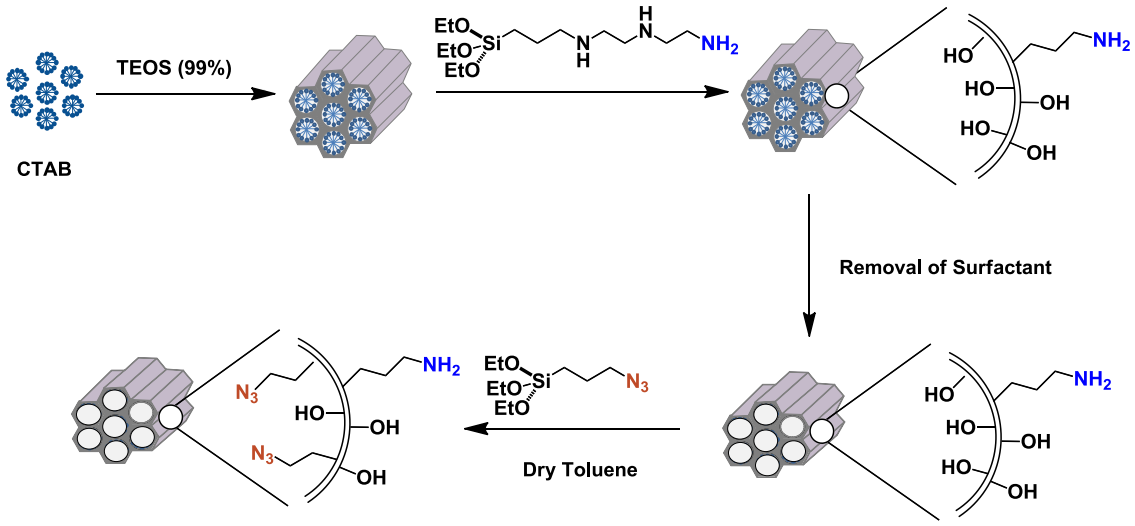

Scheme 5.2: The above schematic represents the formation of **N_3-MSN-S-NH_2** particles with organoazide and organoammine grafted in the inner and outer surface respectively.

MSN particles (N_3-MSN-S-NH_2) with organoazide grafted in the inner surface and organoammine grafted in outer surface was synthesized by grafting organoazides onto MSN-S-NH_2 mesoporous nanoparticles (Scheme 5.2).[16] In short, MSN-S-NH_2 nanoparticle (500 mg) was dispersed in 50 mL dry toluene. In this reaction mixture azido-propyl trimethoxy silane (0.150 mL, 0.70 mmol) was added and refluxed at 85^{o}C for 16 hrs. After the completion of reaction, the reaction mixture was centrifuged and the resultant solid powder was washed with an additional three times with ethanol to afford organoazide N_3-MSN-S-NH_2. The sample was stored in EtOH for further usage. Yield: 460 mg.

5.2.2.8.2 Synthesis of alkyne tagged Fe-Cat catalyst:

The alkyne tagged Fe-Cat was synthesized by procedure reported elsewhere. [17]

5.2.2.8.3 Immobilization of Fe-Cat catalyst on N_3-MSN-S-NH_2 to afford Fe-cat-MSN-S-NH_2:

Fe-Cat catalyst was immobilized on N_3-MSN-S-NH_2 using "Click Chemistry" as has been reported before by our group (Scheme 5.3).[18] For CuAAC, N_3-MSN-S-NH_2 nanoparticles were incubated with 2 equivalents of the alkyne substituted Fe-Cat in a DMSO–H_2O solvent mixture (2:8) containing CuI (2.0 equivalents), disodium bathophenanthrolene sulfonate (2.0 equivalents), sodium ascorbate (4.0 equivalents). In a typical reaction, N_3-MSN-S-NH_2 (10 mg) were incubated with alkyne substituted Fe-Cat (4 mg, 0.04 mmol, 2 eq.) in a DMSO/water mixture (1.6 mL H_2O + 0.4 ml DMSO) containing sodium ascorbate (0.016 g, 0.08 mmol, 4 eq.) and copper iodide (0.008 g, 0.0.04 mmol, 2 eq.) and disodium sulfonated bathophenanthroline (0.02 g, 0.04 mmol, 2 eq. The reaction mixture was subjected to three freeze–pump–thaw cycles for rigorous exclusion of dioxygen. The CuAAC was allowed to proceed for 24 hrs with stirring. After the completion of reaction, the reaction mixture was centrifuged and the solid residue was first washed with water twice and then sequentially washed with 0.1 M N,N-diethyldithiocarbamate sodium in PBS buffer (100 mM, pH 7.5), and acetone twice respectively. The last three washings were repeated thrice. Finally, the orange colored solid powder obtained (Fe-Cat-MSN-S-NH_2) was dispersed in ethanol for further usage. Yield: 8mg

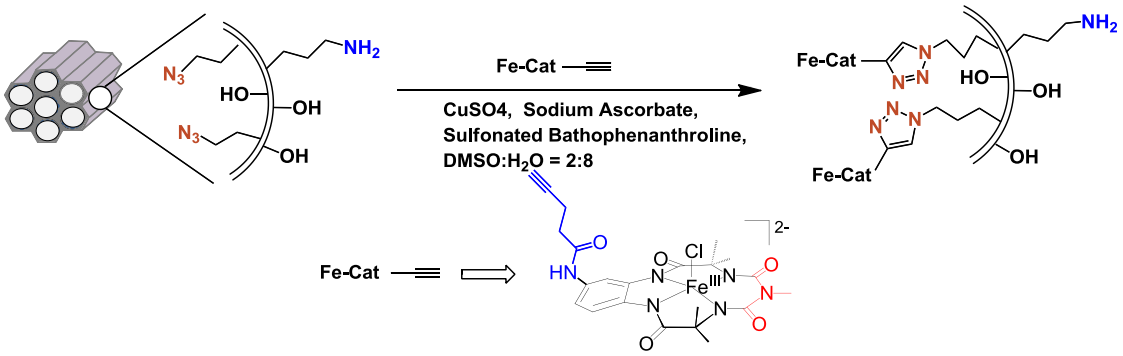

Scheme 5.3: The above schematic represents immobilization of Fe-cat on N_3-MSN-S-NH_2 particles with organoazide and organoammine grafted in the inner and outer surface respectively

5.2.2.8.3.1 Powder X-ray diffraction:

Powder XRD patterns of the obtained mesoporous materials are shown in Figure 5.5. Powder XRD pattern of MSN-S-NH_2 shows characteristic high intensity 100 peak at 2θ = ~2.5º. The other significant peaks corresponding to 110 and 200 diffractions were also observed indicating that well-ordered two-dimensional hexagonal mesoporous channels were formed and remained intact under functionalization environment. N_3-MSN-S-NH_2 particles were also characterized by p-XRD patterns. p-XRD patterns showed one intense (100) diffraction peak near 2θ ~ 2.5° showing that the mesoporosity of the material does not change after azide grafting reaction.

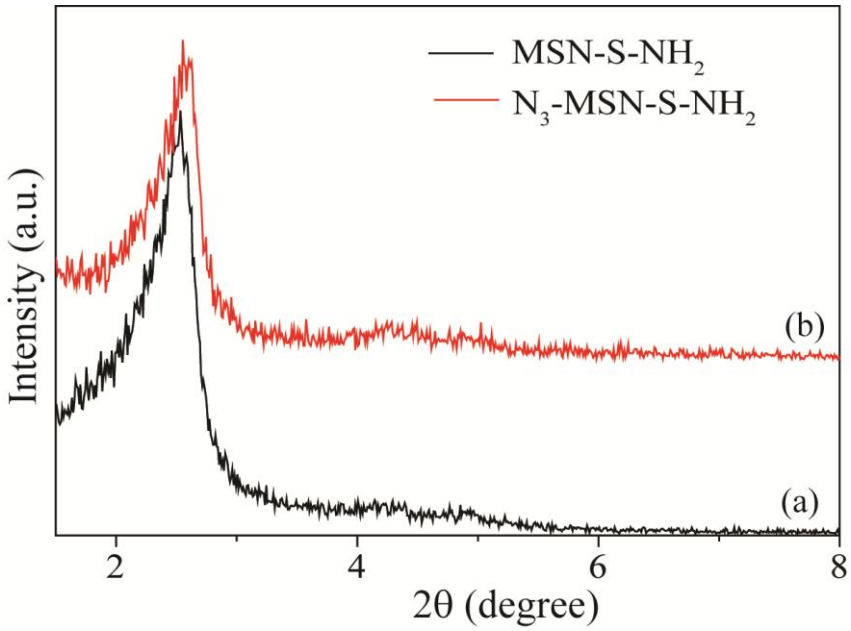

Figure 5.5: Powder XRD patterns of (a) MSN-S-NH_2 (b) N_3-MSN-S-NH_2

5.2.2.8.3.2 Transmission electron microscopy:

Transmission electron microscopy (TEM) images of N_3-MSN-S-NH_2 and Fe-Cat-MSN-S-NH_2 are displayed in Fig. 5.6 A and B respectively. TEM showed the retention of well-ordered two-dimensional hexagonal mesoporous particles with a spherical morphology after click reaction. The size of these particles was calculated by using TEM and remained unchanged after the click reaction also. TEM of the N_3-MSN-S-NH_2 and Fe-Cat-MSN-S-NH_2 particles clearly indicate the mesoporosity structure and particle sizes of ~100 nm.

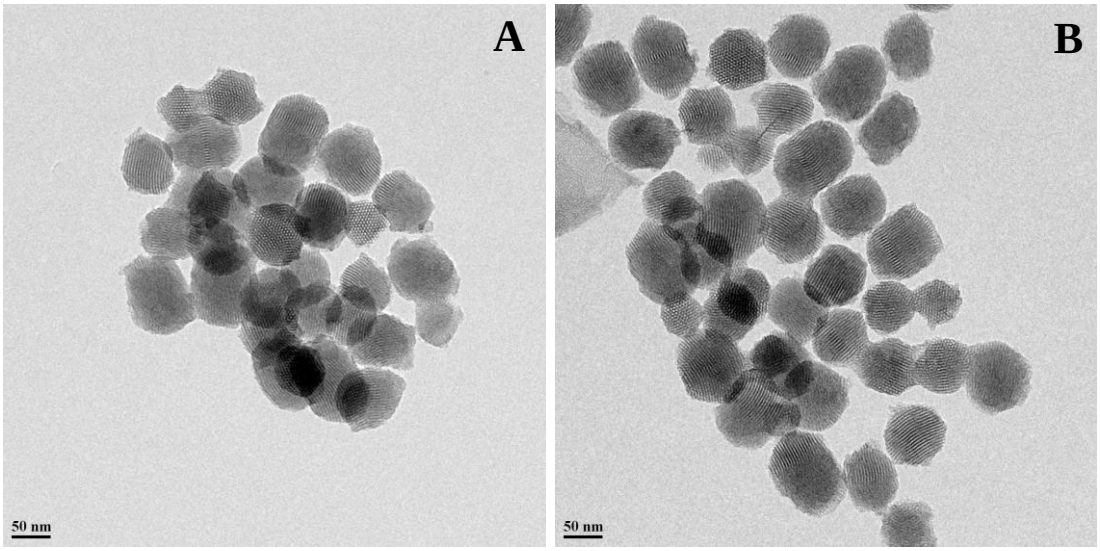

Figure 5.6 (A) TEM image of N_3-MSN-S-NH_2 particles (B) TEM image of Fe-Cat-MSN-S-NH_2

5.2.2.8.3.3 FT-IR spectroscopy:

The FT-IR spectra of various materials are presented in the Figure 5.7. The spectra of the N_3-MSN-S-NH_2 display an absorbance at ~2100 cm^{-1}, which is the characteristic stretching vibration of an organic azide. The presence of this peak shows that the azidopropyl groups were successfully incorporated into N_3-MSN-S-NH_2 samples. The samples also showed absorbance peaks at 1230, 1080, 805 cm^{-1} respectively. These peaks are typical of Si-O-Si bands that are associated with the formation of the silica networks. Weak peaks associated with Si-OH groups in the 940-960 cm^{-1} range were also observed for the functionalized mesoporous materials. The strong peak around 1658 cm^{-1} might be attributed to the bending vibration of H_2O. Thus, the FT-IR spectra indicate that the azido groups were efficiently incorporated in the matrix of the mesoporous silica nanoparticles by the one-pot co-condensation technique. IR spectrum of Fe-Cat-MSN-S-NH_2 shows about 50% decrease in the integrated intensity of $\nu_{as}(N_3)$ at 2100 cm^{-1} (Figure 5.7).

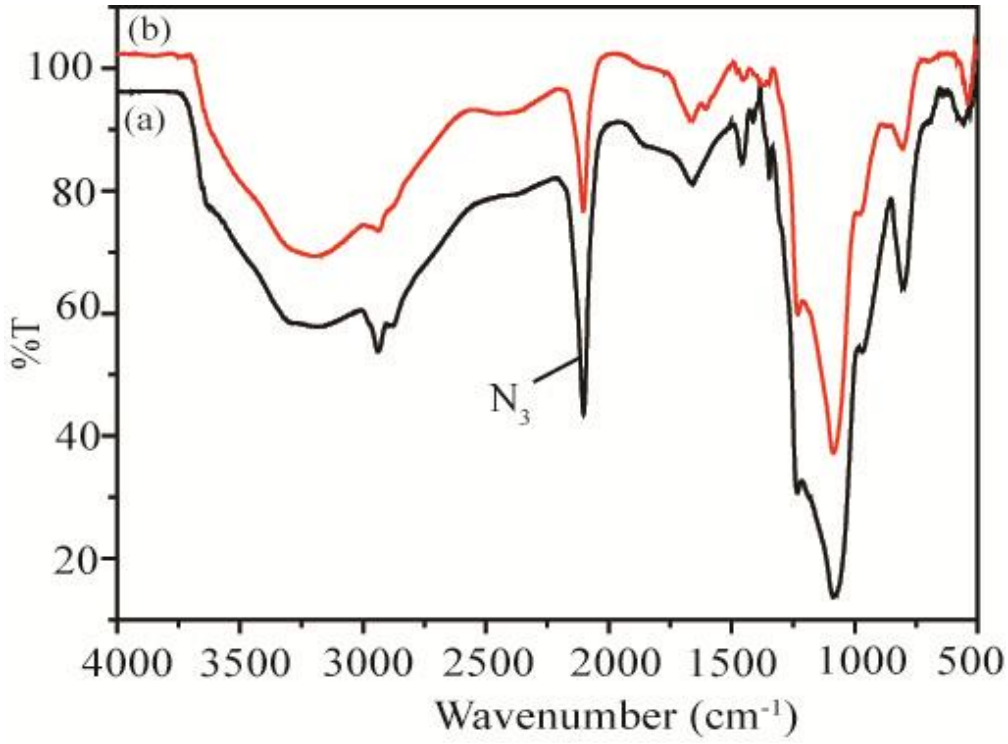

Figure 5.7: FT-IR spectra of (a) N_3-MSN-S-NH_2 and (b) Fe-Cat-MSN-S-NH_2

From semi quantitative IR,[18] it was established that 50% of the available azides have been converted to the corresponding triazoles. This corresponds to 0.4 mmol of Fe-Cat /g of silica material. The percentage of catalyst immobilized was also calculated from ICP analysis and was determined to be 0.357 mmol of Fe-Cat /g of silica material.

5.2.2.8.3.4 Electron paramagnetic resonance spectroscopy:

The EPR spectrum of Fe-Cat-MSN-S-NH2 is shown in Figure 5.8. The solid Fe-Cat-MSN-S-NH_2 sample was taken in a quartz tube and the spectrum was recorded at 94 K. The resonance peak at around 3390 G corresponds to 'g' value of 1.96 and the other resonance peak at around 1570 G corresponds to 'g' value of 4.2 this is typical of such Fe(III) complexes having intermediate spin S=3/2.

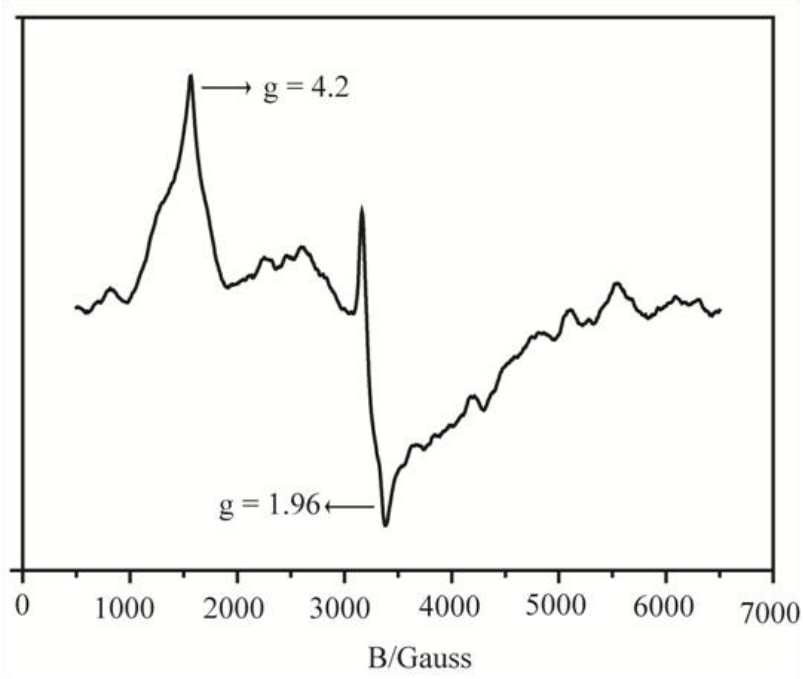

Figure 5.8: X-band EPR spectrum of solid Fe-Cat-MSN-S-NH_2 at 109K.

5.2.2.8.4 Synthesis of Fe-Cat embedded self-standing monolith type scaffold:

A mixture of Fe-Cat-MSN-S-NH_2 (4mg) and N_3-MSN-S-NH_2 (20mg) was added to surfactant $C_{12}E_9$/water mixture (1:1; 108 mg surfactant) at 50 °C such that the amount of nanoparticles was 10 % by weight. These particles were assembled into macroporous networks in $C_{12}E_9$/water matrices, by cooling from 50 °C to below T_{HI}, and were cross-linked with poly(ethylene glycol) diglycidyl ether as described above. Subsequent to cross-linking, the surfactant was readily removed by washing with water, to afford catalyst embedded free standing scaffold. The amount of Fe-cat embedded in the monolith was estimated to be 0.027 mmol/g of monolith.

5.2.2.8.5 Degradation of Orange II by Fe-Cat embedded scaffold:

To a solution of Orange II (2 ml, 10^{-5} M) was added Fe-cat embedded scaffold. H_2O_2 (20 μL, 10^{-3} M) was added to start the reaction (Scheme 5.4). 200 μL aliquot was taken out every one minute interval to measure the UV. All kinetic measurements were performed at 298 K. After completion of reaction (6 min), the scaffold was thoroughly washed with water and further cycles of the above reaction were carried out.

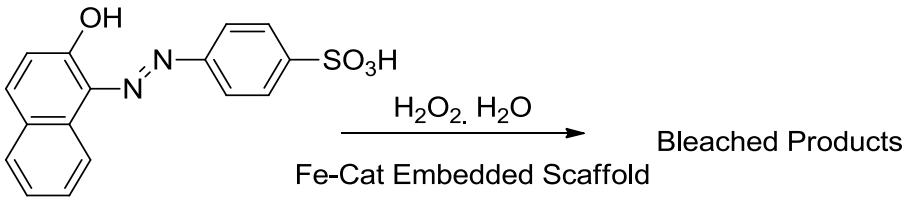

Scheme 5.4: Degradation of orange II to bleached products

5.3 Results and Discussion:

Our strategy to synthesize free standing monolith involves three steps (Scheme 5.5). The first step in this endeavour was the synthesis of amine grafted mesoporous silica shell nanoparticles. In the second step, the particles are assembled using surfactant $C_{12}E_9$ mesophase followed by crosslinking of amine grafted particles using organic crosslinker. Finally surfactant was removed by washing with ethanol water mixture to generate free standing hieratical monolith.

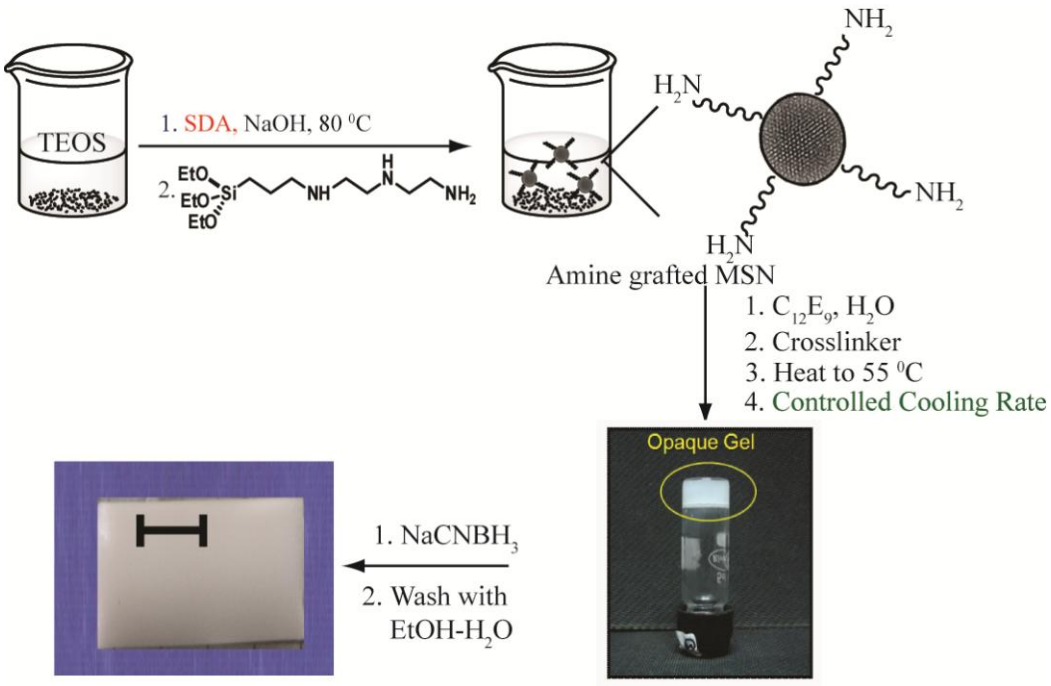

Scheme 5.5: Schematic illustration of formation of self standing monolith. Scale bar indicates 1 cm.

Hierarchical silica scaffolds were prepared using two mesoporous silica nanoparticles (small pore and large pore MSNs). The size of the mesopores depends on structure directing agent (SDA). If CTAB is only used as a SDA for preparation of mesoporous silica nanoparticles, small pore size particles were ascertained. The pore size of the particles could be enlarged by using mesitylene along with CTAB. So pore size could be varied by SDA addition.

Organoamine functionalized mesoporous silica nanoparticles (MSN) were synthesized by co-condensation of TEOS and 3-[2-(2-aminoethylamino)ethylamino]propyl triethoxysilane, as described earlier.[14] The presence of the triamine groups on the particle surface enhances particle dispersibility, as well as, allows the possibility of crosslinking the particles. After synthesis of the organoamine coated MSN particles, non-ionic surfactant, $C_{12}E_9$, and glutaraldehyde were added into the reaction mixture at 50 ^{o}C, such that the $C_{12}E_9$: water ratio was 1:1. At 50 ^{o}C, the $C_{12}E_9$/water matrix is a viscous liquid that transforms to a hexagonal (H_1) mesophase gel, on cooling below the isotropic-hexagonal transition temperature ($T_{HI} \approx 44$ ^{o}C). Below T_{HI}, H_1 domains nucleate and grow to impingement. The MSN particles (typical size $\approx$ 100 nm) are excluded from the growing H_1 domains and jam at the domain boundaries to form a particulate network. Thus, segregation of mesoporous silica particles to the H_1 domain boundaries results in the optical contrast observed under crossed and parallel polarisers. In contrast, for an H_1 phase not containing MSN particles, domain boundaries are not visible between parallel polarisers. Thus, the optical contrast observed in Figure 5.9 is ascribed to the segregation of silica particles to the H_1 domain boundaries.

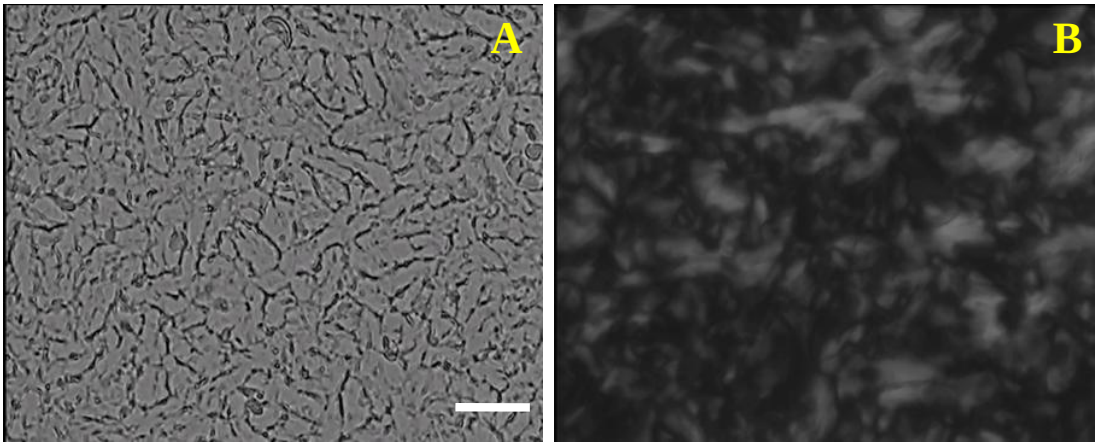

Figure 5.9: Optical microscopy of amine grated silica particles in H_1 phase at room temperature (sample thickness $\approx$ 10 μm). The sample was cooled from isotropic phase at 50°C to room temperature at 5°C/min. (a) between crossed polarisers; we observe birefringent H1 domains grown to impingement. (b) The same sample as (a), viewed between parallel polarisers shows that the boundaries of the H_1 domains are optically dense due to aggregation of silica particles. The scale indicates 20 μm.

To stabilize the particulate network against dispersion after H_1 template removal, the triamine grafted mesoporous silica particles were crosslinked with glutaraldehyde upon network formation. Glutaraldehyde crosslinks this particle network through the surface amine groups over a period of several hours, and the resultant imine bonds are reduced using $NaCNBH_3$. Alternatively, poly(ethylene glycol) diglycidyl ether was also used to crosslink the surface amine groups of the nanoparticles. Subsequent to crosslinking, the surfactant could be readily removed by washing with water, to yield a free standing particulate macroporous solid (Scheme 5.5). Scanning electron microscopy reveals a network structure (Figure 5.10 A) comprised of a dense mesh of strands, with strand thickness varying from about 100 nm to a micron as seen at higher magnification. While mm to cm size samples of the macroporous materials were readily prepared (Scheme 5.5), these materials are fragile. Thus, porosity in such materials is observed at a hierarchy of length scales ranging from the mesoporosity of the particles, ~O(2-4 nm); to the inter-particle pore spaces, ~O(10 nm), and; to the macroporous network mesh size ~O(1000 nm).

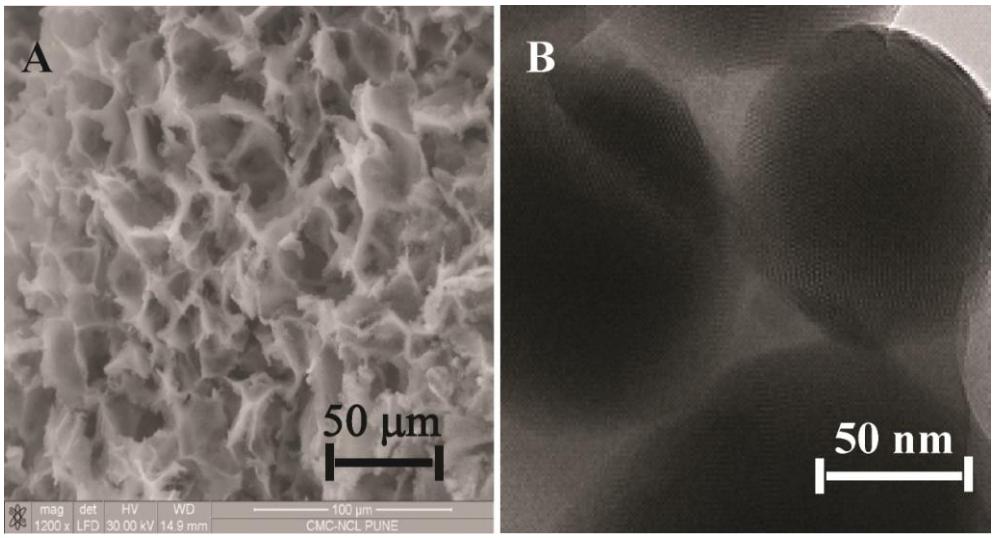

Figure 5.10: (A) The SEM of 10% Triamine Grafted silica 3-D scaffold prepared by crosslinking with glutaraldehyde in H_1 phase and subsequent washing with $NaCNBH_3$. (B) HRTEM of MSN-Triamine particles after formation of self standing scaffold in the H_1 phase followed by embedding in the epoxy and microtoming to view the sample under HRTEM.

Furthermore, a single pot synthesis of the scaffold was also accomplished. Here the triamime was grafted during the preparation of mesoporous silica particles. The ratio of TEOS and triamine was kept as 25:1 since the usage of higher amounts of organosilica precursor may lead to functionalized materials with reduced long range order. The reaction mixture was heated to 80 ^{o}C for hours. Then the generated mesoporous silica particles were dispersed in $C_{12}E_9$ surfactant. On cooling below T_{HI} (at 5 ^{o}C/min), the particles are expelled by growing H_1 domains as previous described. The optical micrograph under parallel and cross polarisers (Figure 5.11 (a) and (b)) show the phase separated mesoporous silica particles forming a network at the boundaries of the birefringent domains. In both cases, particle assembly follows the route that we described in previous reports. The silica nanoparticles were now crosslinked using glutaraldehyde and $NaCNBH_3$. A self standing scaffold has been generated after removing the surfactant, which was characterized by SEM. (Fig 5.11 (c)).

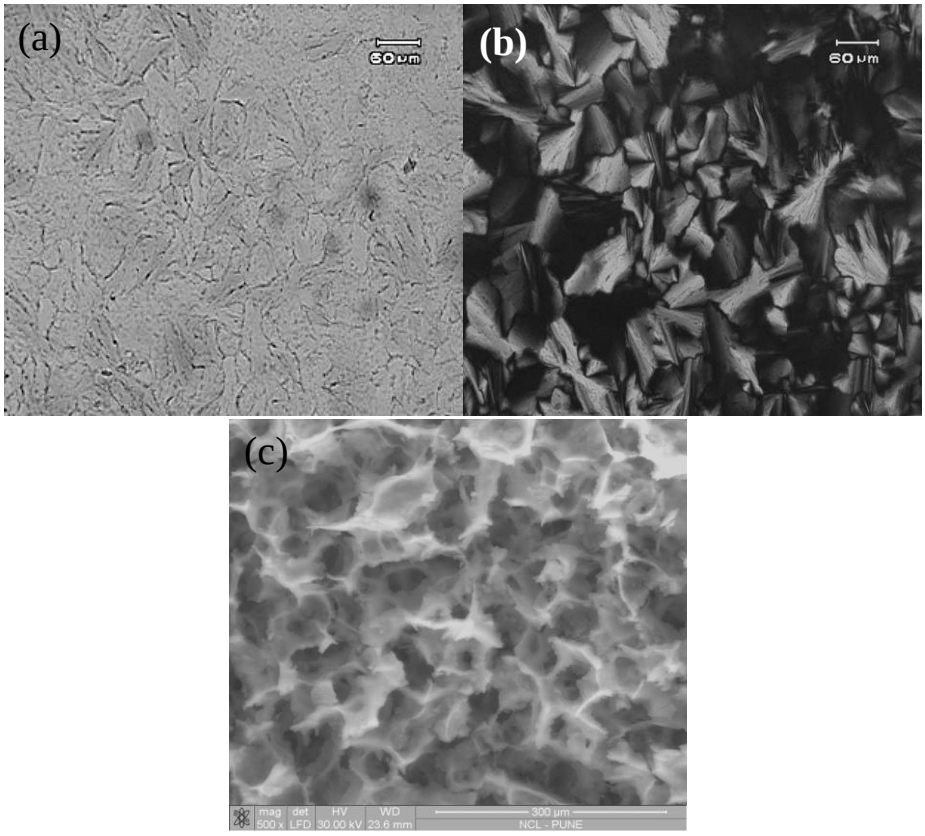

Figure 5.11: Optical micrographs and SEM images of Scaffold obtained by one pot synthesis. (a) under parallel polarisers (b) under crossed polarisers (c) SEM of the scaffold obtained by one pot synthesis.

5.3.1 Tuning macroporosity and mesoporosity:

Our scheme allows us to combine the advantages of dynamic templating with the highly developed chemistry of MSN synthesis. Specifically, it is possible to independently tune the length scale that characterizes the porosity at each structural hierarchy. The preparation of scaffolds documented here allows independent tuning of the particle level mesoporosity and the network level macroporosity is possible. The mesh size of the macroporous particulate network is governed by the domain size of the H_1 domains, since the network forms by templating the domain structure. On cooling below T_{HI}, H_1 domains nucleate and grow to impingement. Thus, by varying the nucleation density of H_1 domains, it is possible to vary the size of the domains, and therefore, the characteristic spacing of the particulate network. Previously it has been also demonstrated from our group that it is possible to systematically control the H_1 domain size by varying the cooling rate of the dispersion. Fast cooling, for example at 20 ^{o}C/min results in particulate networks with smaller "strut" spacing as compared to cooling at 5 ^{o}C/min. The optical micrographs of particulate dispersion at different cooling rate are documented inn Figure 5.12.

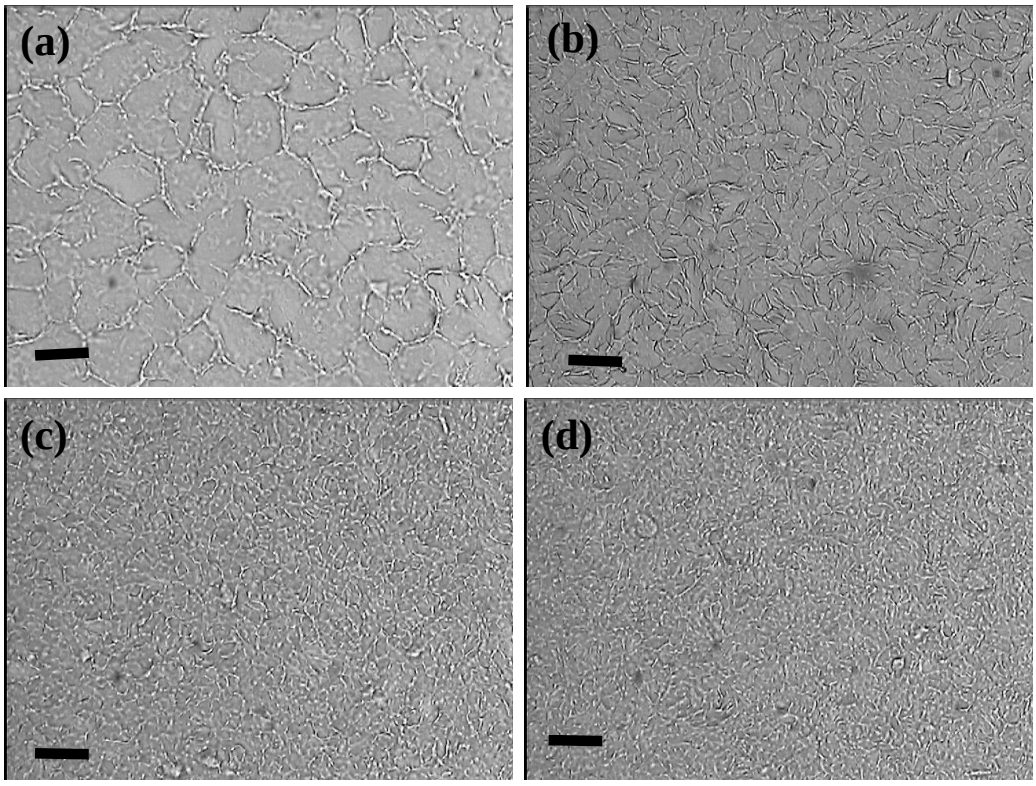

Figure 5.12: Temperature dependent optical micrograph. (a) 0.5 ^{o}C per minute (b) 5 ^{o}C per minute (c) 10 ^{o}C per minute (d) 20 ^{o}C per minute. The scale bar corresponds to 50 microns.

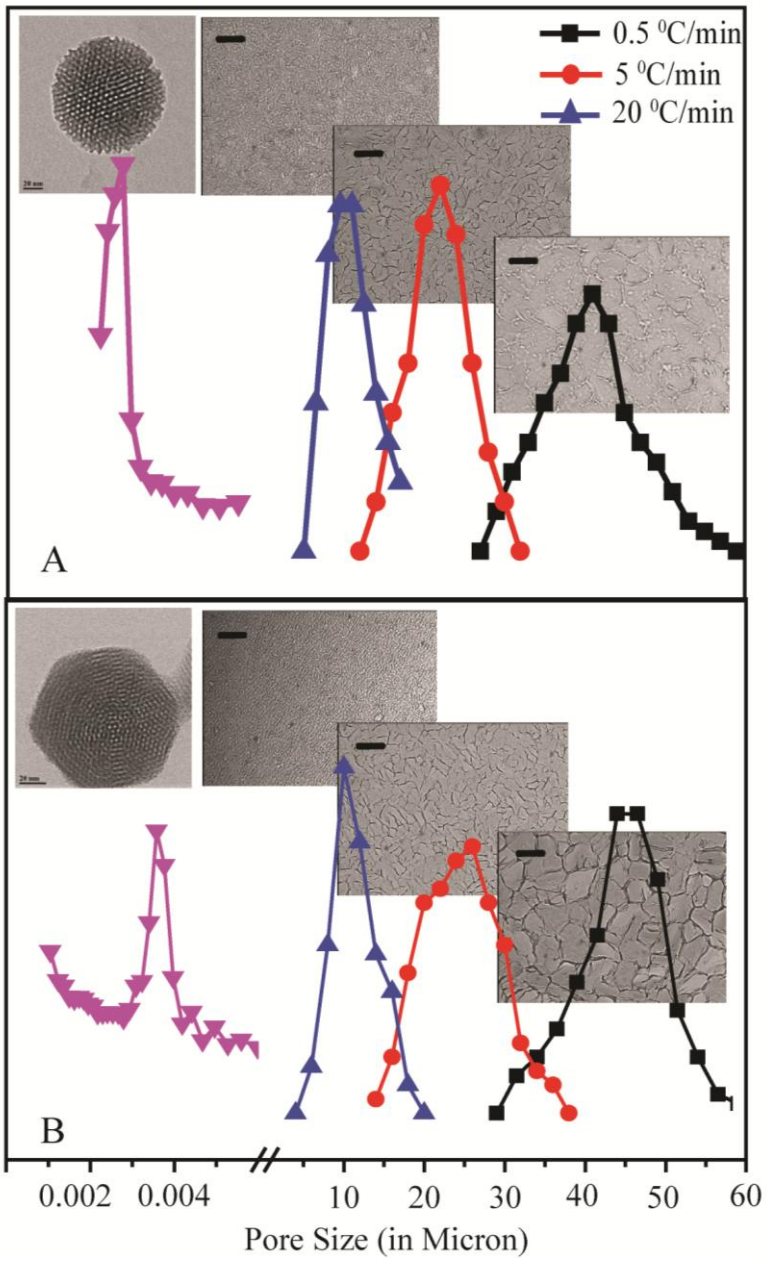

Figure 5.13: Pore size distributions for six scaffolds, demonstrating independent control over meso- and macro-porosity. The scaffolds in the top pane were assembled from MSN-S-NH_2 (top) at cooling rates as indicated. Mesoporosity in the MSN-S-NH_2 scaffold, from BET analysis of nitrogen adsorption data is represented by the pore size distribution shown on the left, and (on a different scale) the macropore size distribution for scaffolds for cooling at 20, 5 and 0.5 ^{o}C/min (left to right) is obtained from analysis of several optical micrographs. The scale bars represent 50 microns. Insets represent TEM of an individual MSN-S-NH_2 particle and optical micrographs at cooling rates of 20, 5 and 0.5 ^{o}C/min (left to right). The bottom pane shows corresponding data for the MSN-L-NH_2 particle scaffolds.

Dispersions of MSN-S-NH_2 and MSN-L-NH_2 were assembled into macroporous networks in $C_{12}E_9$/water matrices, by cooling from 50 ^oC to below T_{HI}, and were crosslinked with glutaraldehyde, as described above. Increasing the cooling rate from 0.5 ^oC/min to 5 ^oC/min to 20 ^oC/min increases the nucleation rate for the formation of the H_1 phase and results in smaller domain sizes at impingement. Optical micrographs for samples cooled at rates of 0.5, 5, 10 and 20 ^oC/min show dark regions at the domain boundaries due to optical contrast from the segregated particles (Figure 5.13). A systematic decrease in the average domain size from ~44.7 to ~25.3 to ~9.8 microns, and a decrease in the breadth of the size distribution, with increase in cooling rate from 0.5, 5 and 20 ^oC/min respectively have been observed (Figure 5.13). The domain spacings were obtained by averaging over at least 150 domains from optical micrographs taken at more than 10 separate locations. The average domain size and breadth of the distribution are, at best, weakly influenced by whether MSN-S-NH_2 or MSN-L-NH_2 particles are dispersed, and are predominantly influenced by only the cooling rate (compare Figure 5.13 top and bottom).

Therefore, this technique allows us to prepare designer scaffolds, with independent control over mesoporosity (through choice of the SDA, with mesopore size varying from about 1.5 nm to 4 nm) and over the macroporosity (from about 0.5 to 50 microns, through choice of cooling rate).

5.3.2 Tune macroporosity spatially:

A significant advantage of the dynamic templating technique is the ease with which we can controllably tune the macroporosity within a single sample, simply by imposing a spatial variation in cooling rates. To illustrate this, we cooled the high temperature micellar dispersion of MSN-S-NH_2 particles onto a glass slide across the length of which a temperature gradient was maintained. The measured temperature profile across the slide results in a variation in cooling rate from the isotropic phase. The consequence of the cooling rate variation can be visualized under the optical microscope (Figure 5.14). The average spacing that characterizes the particulate network varies from 23±2.4 microns, for a location where the slide temperature was maintained as 40 ^oC, to 15.1±1.6 and 2±0.5 microns for slide temperatures of 24 ^oC, and -10 ^oC respectively (Figure 5.15). We anticipate that the ability to engineer such

spatial variations in the pore size might be important for size-based separation applications.

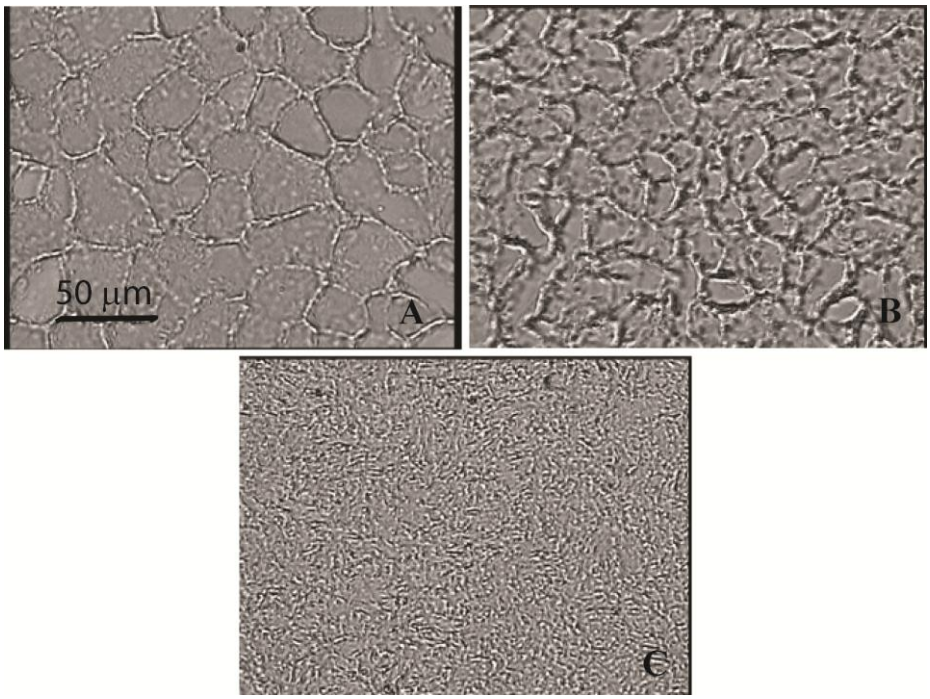

Figure 5.14: Optical micrographs were taken at different positions (2 cm, 4 cm, 6 cm) across the glass slide of length ≈ 7 cm. These micrographs indicate the variation in scaffold spacing (right axis) across the slide.

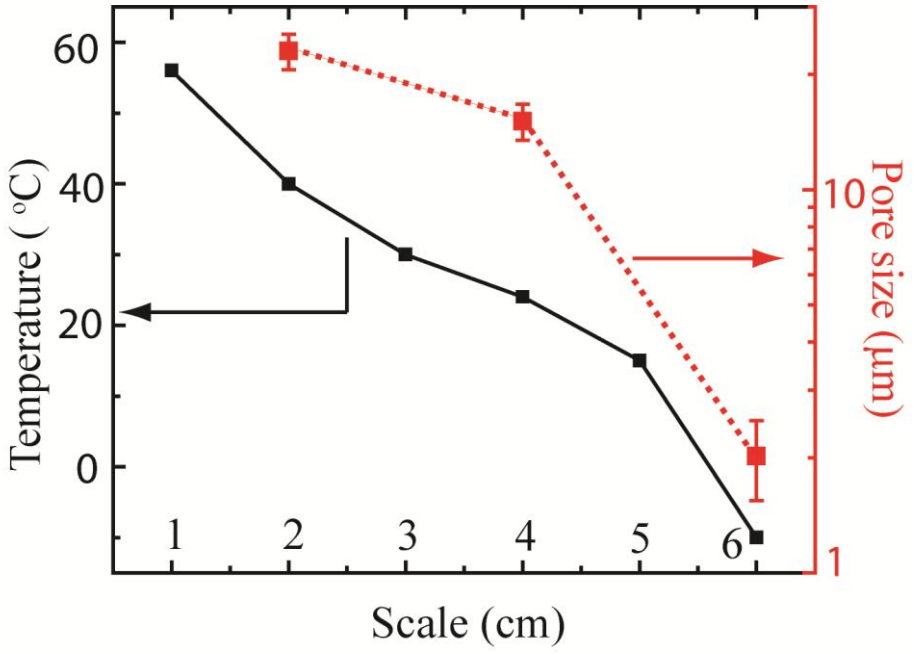

Figure 5.15: Temperature gradient (left axis) measured along the length (≈ 7 cm, x-axis) of a heated slide, one end of which is cooled using dry ice. An MSN-S scaffold in the form of a thin continuous film is formed by depositing out of a $C_{12}E_9/H_2O$ dispersion.

5.3.3 Stability of scaffold:

The stability of the scaffold upon heating was also examined. To study that, the scaffold has been subjected to calcinations in N_2 atmosphere at 600 ^oC. It has been observed from SEM that after calcinations the morphology of the scaffold did not change. SEM of burnt scaffold is presented in Figure 5.16 A. To study the organic content of the scaffold, TGA analysis was performed. The TGA analysis reveals that 18% wt has reduced after calcinations. TGA analysis was documented in Figure 5.16 B.

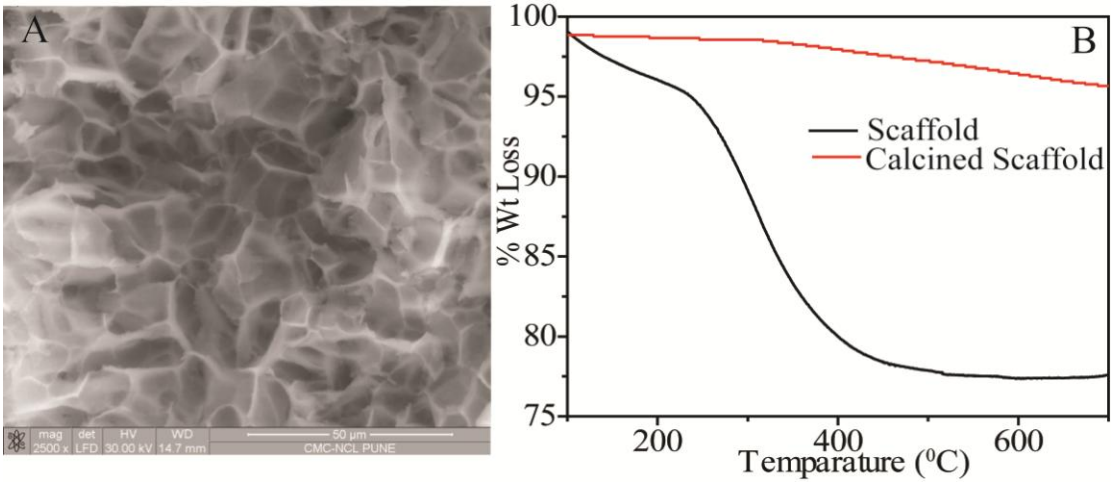

Figure 5.16: (A) SEM of burnt scaffold. (B) TGA analysis of scaffold and burnt scaffold.

5.3.4 Chemical functionalization of scaffold:

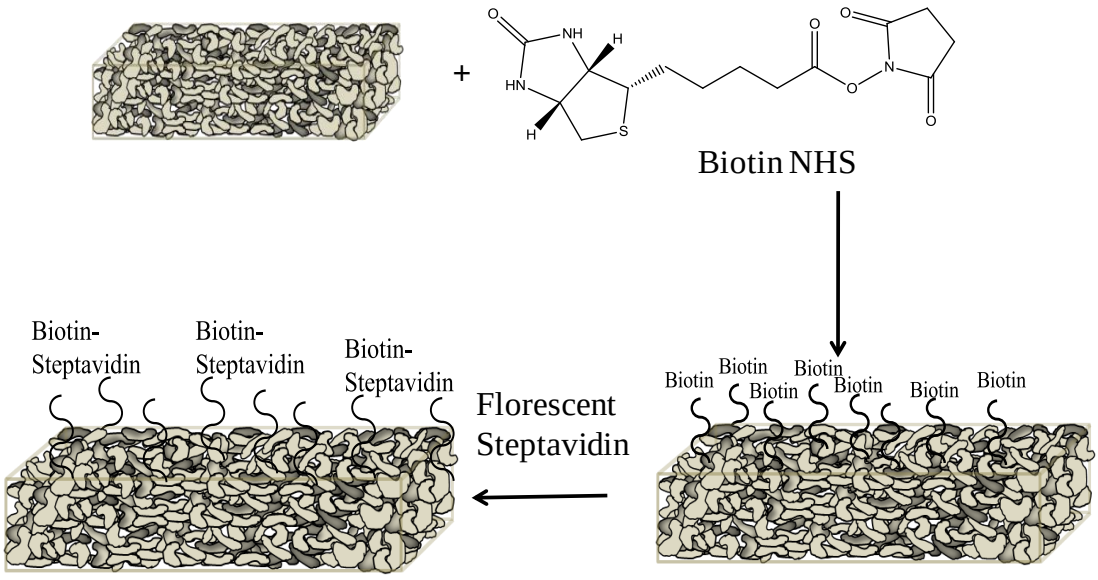

Scheme 5.6: Schematic illustration for biotinlylation of macroporous scaffold

We also wanted to investigate if the scaffold can be further functionalized with organic groups. Since the scaffold is made with amine grafted mesoporous silica it was expected the surface amine group will intact with the organic molecules. To demonstrate the possibility of chemical modification, the amine groups were further reacted with a biotin-NHS (Scheme 5.6). The presence of the biotin on the scaffold was then probed using fluorescently labelled streptavidin, a tetrameric protein, which has a very high binding affinity for biotin. The biotin modified macroporous scaffold upon incubation with streptavidin-phycoerythrin turned fluorescent and could be imaged using confocal microscopy (Figure 5.17). Control samples of scaffolds not treated with biotin-NHS did not show significant fluorescence. Thus, these macroporous materials allow diffusion of reactants through them and allow on-demand surface functionalization through the amine groups.

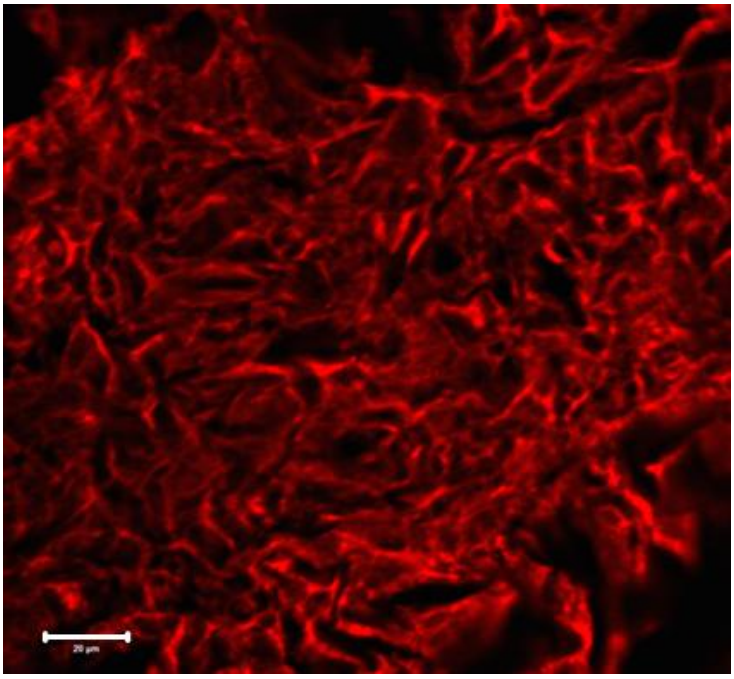

Figure 5.17: Laser scanning confocal micrograph (514 nm filter) showing 3D image of self-standing silica scaffold. The scaffold is functionalized with biotin, and the biotin functionalized network is incubated with fluorescent streptavidin-phycoerythrin and imaged using confocal. The scale indicates 20 μm.

5.3.5 Catalytic activity of the scaffold:

Finally, we also demonstrate the synthesis of functional catalytically active hierarchical monolith-type scaffolds.[19] Our methodology to prepare hierarchical monolith allow us to use catalyst embedded mesoporous silica particles instead of only mesoporous silica particles (Scheme 5.7). For this a model catalyst Fe-Cat, which is developed in our group, was chosen to embedded inside the mesoporous silica nanoparticles. Fe-Cat is a Fe-based catalyst that activates hydrogen peroxide and can degrade environmentally pollutant dyes like orange II. Fe-cat was anchored inside the mesopore applying "Click Chemistry". Initially, MSN particles (N_3-MSN-S-NH_2) was synthesized with organoazide and organoammine grafted in the inner and outer surface respectively. The azido propyl labelled MSN's (N_3-MSN-S-NH_2) were subjected to Cu(I) catalyzed azide-alkyne cycloaddition reaction(CuAAC) with Fe-Cat complex using CuI/sulfonated bathophenanthroline in DMF and H_2O mixture at a ratio of 80:20 for 24 h. After the reaction, an extensive washing protocol was followed to remove the Cu(I), ascorbate and any unreacted starting materials. One of the key steps in the washing was the usage of dithiocarbamate to remove the Cu(I), as discussed earlier in chapter 2. Efficient removal of copper during the washing protocol has been observed from the absence of copper in ICP analysis. The extent of the reaction was estimated using FT-IR spectroscopy, by monitoring the decrease in the integrated intensity of the $\upsilon_{as}(N_3)$ at 2100 cm^{-1}.

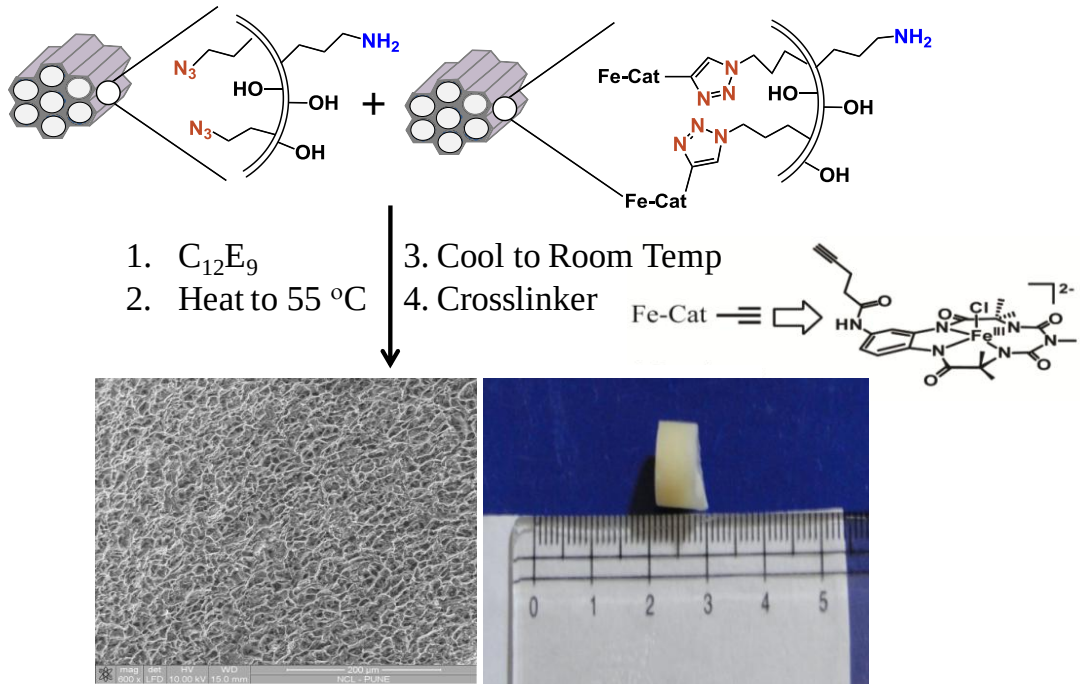

Scheme 5.7: The above schematic represents the synthesis of Fe-cat embedded self-standing monolith type scaffold. The SEM and optical picture of the resultant scaffold is also shown below.

Dispersions of catalyst embedded mesooporous silica particles were assembled into macroporous scaffolds in $C_{12}E_9$/water matrices, by cooling from 50°C to below T_{HI}, and were crosslinked with glutaraldehyde, as described before. Optical micrographs and SEM of catalyst embedded scaffold is presented in Figure 5.18. The optical micrographs show well defined network formation in hexagonal mesophase. After removal of surfactant SEM of the scaffold was taken, which was porous in nature and same as before Figure 5.18 C.

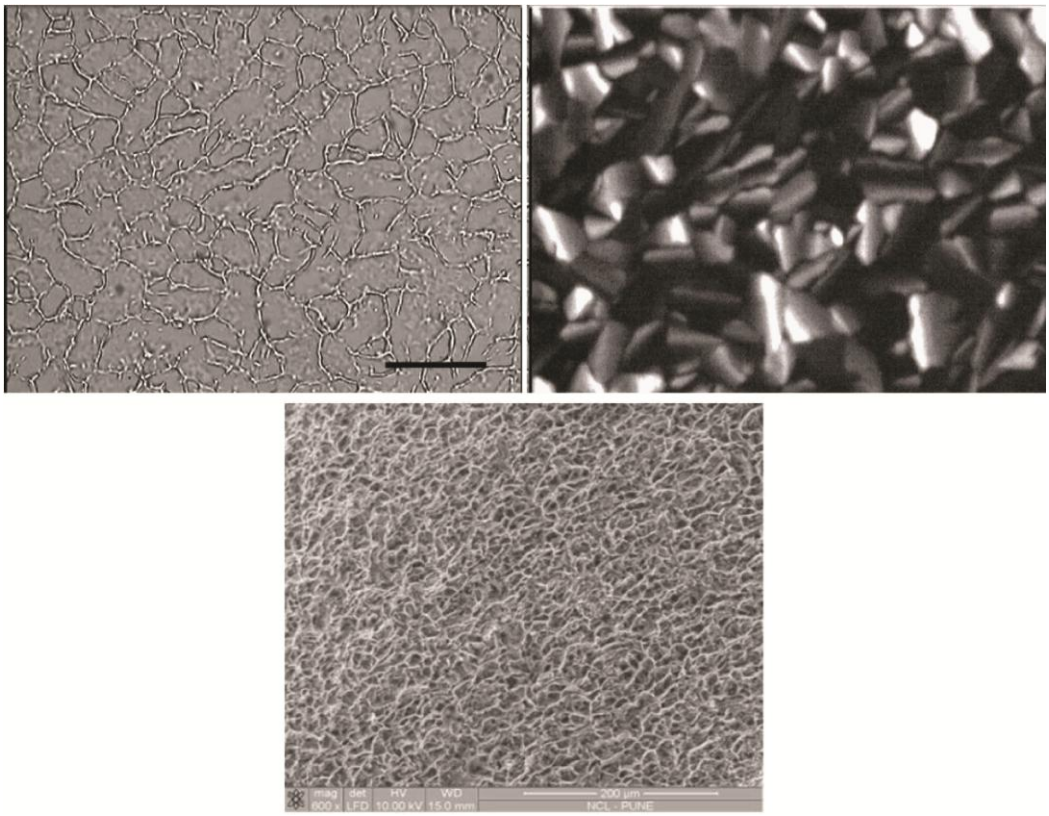

Figure 5.18: Optical micrographs and SEM of catalyst embedded scaffold (a) Corresponding optical micrograph under parallel polarisers showing the phase separated mesoporous silica particles forming a network at the boundaries of the birefringent domains. The scale bar represents 50 microns. (b) Corresponding crossed optical microscope image (showing birefringence due to different domains of the H_1 phase. (c) SEM of the Fe-Cat embedded scaffold.

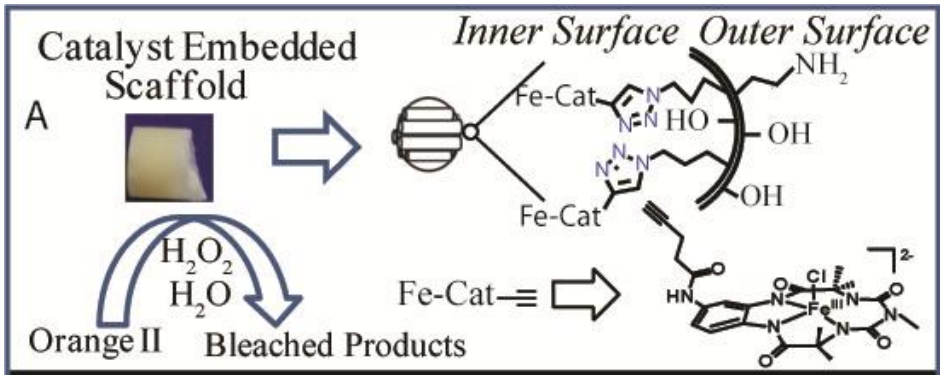

Scheme 5.8: Synthesis of Fe-Cat embedded scaffold

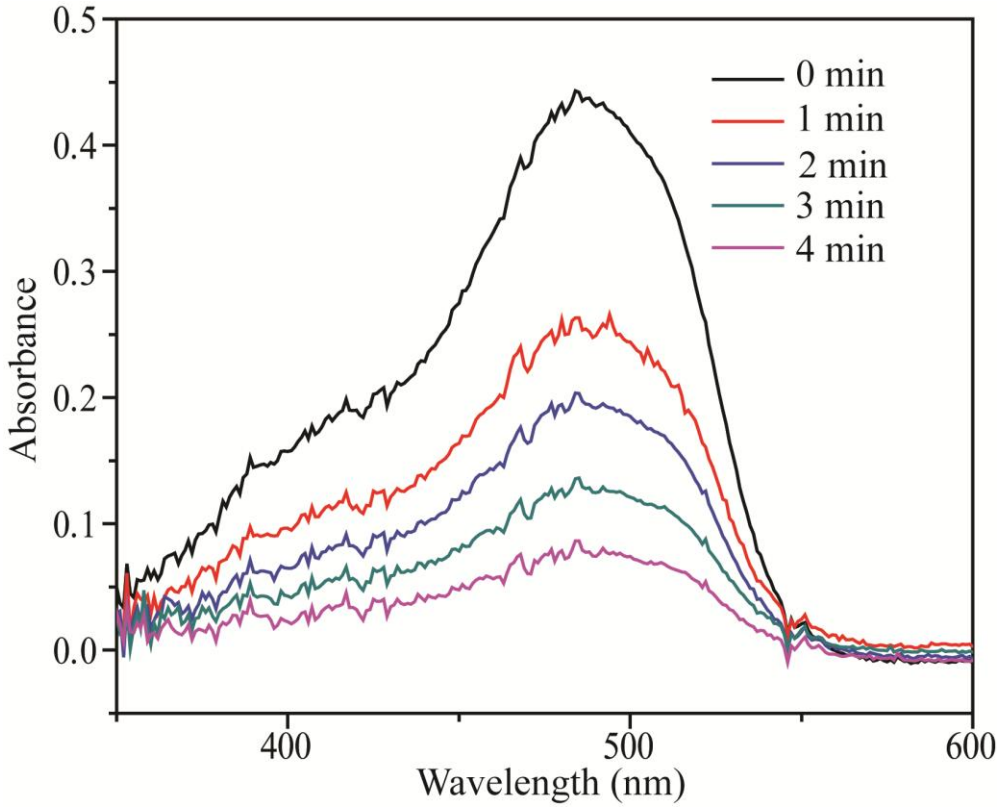

Figure 5.19: Spectral changes that accompany the catalytic oxidation of Orange II by H_2O_2 in the presence of Fe-Cat embedded scaffold.

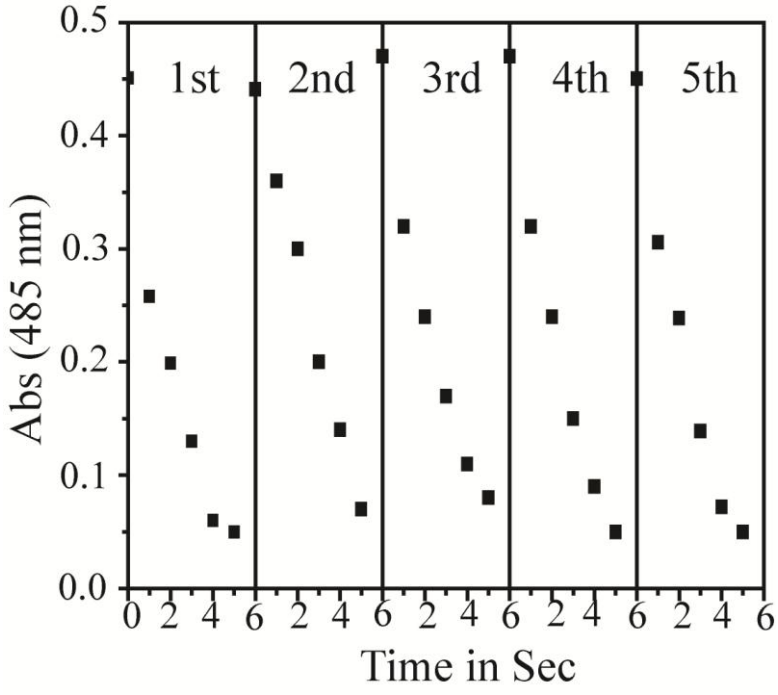

Figure 5.20: Catalytic activity of Fe-Cat embedded Scaffold for degradation of Orange II dye over 5 cycles. Abs at 485 nm (y-axis) represents the λ_{max} of Orange II.

After formation of the scaffold the catalytic activity of oxidation of orange II dye (Scheme 5.8) was checked.[20] The dye has an intense absorption band with a maximum at 485 nm in water. Hydrogen peroxide itself oxidizes Orange II very slowly. Fe-Cat activators increase the rate immensely. The spectral changes observed during 1a-catalyzed oxidation of Orange II are presented in Figure 5.19. Due to oxidation of orange II there is a gradual decrease in the intensity at 485 nm. The collapse of the chromophore is due to the loss of conjugation in the dye leading to colourless oxidation products. Control reaction with scaffolds containing no embedded Fe-Cat did not show any removal of colour under identical conditions. We also examined its activity for further cycles of the same orange II oxidation. It has been seen that the scaffold can effectively degrade the model waste water dye Orange II in presence of H_2O_2 and its activity is unchanged for at least 5 cycles (Figure 5.20).[21]

5.4 Conclusion:

The synthesis of hierarchically porous monolith scaffolds using mesoporous silica particles is demonstrated and this methodology can be readily extended to meso-macroporous materials from other mesoporous materials. The mesoporosity and macroporosity in a sample could be easily tuned by this methodology. Also spatial variation of the macropore in a single sample has been demonstrated in this chapter which is very eye catching for size selective separation. We believe that such hierarchically porous materials might have relevance for several applications, including, for example, as scaffolds for cell growth. Here, we anticipate that encapsulation and controlled release of nutrients and growth factors in the mesopores would offer advantages over conventional scaffolds. A future direction of this study could include a programme to chemically anchor catalysts within the MSN mesopores, to test the possibility that packings of such scaffolds in microreactor channels will enable efficient mixing at low pressure drops with simultaneous catalytic chemical conversions.

5.5 References:

1. Yuan, Z.-Y.; Su, B.-L., Insights into hierarchically meso-macroporous structured materials. *Journal of Materials Chemistry*, **2006,** 16, (7), 663-677.

2. Nakanishi, K.; Kobayashi, Y.; Amatani, T.; Hirao, K.; Kodaira, T., Spontaneous Formation of Hierarchical Macro-Mesoporous Ethane-Silica Monolith. *Chemistry of Materials*, **2004,** 16, (19), 3652-3658.

3. Innocenzi, P.; Malfatti, L.; Soler-Illia, G. J. A. A., Hierarchical Mesoporous Films: From Self-Assembly to Porosity with Different Length Scales. *Chemistry of Materials*, **2011,** 23, (10), 2501-2509.

4. Yang, X.-Y.; Leonard, A.; Lemaire, A.; Tian, G.; Su, B.-L., Self-formation phenomenon to hierarchically structured porous materials: design, synthesis, formation mechanism and applications. *Chemical Communications*, **2011,** 47, (10), 2763-2786.

5. Dhainaut, J.; Dacquin, J.-P.; Lee, A. F.; Wilson, K., Hierarchical macroporous-mesoporous SBA-15 sulfonic acid catalysts for biodiesel synthesis. *Green Chemistry*, **2010,** 12, (2), 296-303.

6. Zhao, X. S., Novel porous materials for emerging applications. *Journal of Materials Chemistry*, **2006,** 16, (7), 623-625.

7. Davis, M. E., Ordered porous materials for emerging applications. *Nature*, **2002,** 417, (6891), 813-821.

8. Stein, A., Advances in Microporous and Mesoporous Solids-Highlights of Recent Progress. *Advanced Materials*, **2003,** 15, (10), 763-775.

9. Léonard, A.; Vantomme, A.; Bouvy, C.; Moniotte, N.; Mariaulle, P.; Su, B.-L., Highly Ordered Mesoporous and Hierarchically Nanostructured Meso-macroporous Materials for Nanotechnology, Biotechnology, Information Technology and Medical Applications. *Nanopages*, **2006,** 1, (1), 1-44.

10. Sharma, K. P.; Ganai, A. K.; Gupta, S. S.; Kumaraswamy, G., Self-Standing Three-Dimensional Networks of Nanoparticles With Controllable Morphology by Dynamic Templating of Surfactant Hexagonal Domains. *Chemistry of Materials*, **2011,** 23, (6), 1448-1455.

11. Sharma, K. P.; Aswal, V. K.; Kumaraswamy, G., Adsorption of Nonionic Surfactant on Silica Nanoparticles: Structure and Resultant Interparticle Interactions. *The Journal of Physical Chemistry B*, **2010,** 114, (34), 10986-10994.

12. Sharma, K. P.; Kumaraswamy, G.; Ly, I.; Mondain-Monval, O., Self-Assembly of Silica Particles in a Nonionic Surfactant Hexagonal Mesophase. *The Journal of Physical Chemistry B*, **2009,** 113, (11), 3423-3430.

13. Mortera, R.; Vivero-Escoto, J.; Slowing, I. I.; Garrone, E.; Onida, B.; Lin, V. S. Y., Cell-induced intracellular controlled release of membrane impermeable cysteine from a mesoporous silica nanoparticle-based drug delivery system. *Chemical Communications*, **2009**, (22), 3219-3221.

14. Slowing, I. I.; Trewyn, B. G.; Lin, V. S. Y., Mesoporous Silica Nanoparticles for Intracellular Delivery of Membrane-Impermeable Proteins. *Journal of the American Chemical Society*, **2007,** 129, (28), 8845-8849.

15. Huang, Y.; Xu, S.; Lin, V. S. Y., Bifunctionalized Mesoporous Materials with Site-Separated Brønsted Acids and Bases: Catalyst for a Two-Step Reaction Sequence. *Angewandte Chemie International Edition*, **2011,** 50, (3), 661-664.

16. de Juan, F.; Ruiz-Hitzky, E., Selective Functionalization of Mesoporous Silica. *Advanced Materials*, **2000,** 12, (6), 430-432.

17. Malvi, B.; Panda, C.; Dhar, B. B.; Gupta, S. S., One pot glucose detection by [FeIII(biuret-amide)] immobilized on mesoporous silica nanoparticles: an efficient HRP mimic. *Chemical Communications*, **2012,** 48, (43), 5289-5291.

18. Ganai, A. K.; Bhardwaj, R.; Hotha, S.; Gupta, S. S.; Prasad, B. L. V., 'Clicking' molecular hooks on silica nanoparticles to immobilize catalytically important metal complexes: the case of gold catalyst immobilization. *New Journal of Chemistry*, **2010,** 34, (11), 2662-2670.

19. Brun, N.; Babeau Garcia, A.; Deleuze, H.; Achard, M. F.; Sanchez, C.; Durand, F.; Oestreicher, V.; Backov, R., Enzyme-Based Hybrid Macroporous Foams as Highly Efficient Biocatalysts Obtained through Integrative Chemistry. *Chemistry of Materials*, **2010,** 22, (16), 4555-4562.

20. Chanda, A.; Ryabov, A. D.; Mondal, S.; Alexandrova, L.; Ghosh, A.; Hangun-Balkir, Y.; Horwitz, C. P.; Collins, T. J., Activity-Stability Parameterization of Homogeneous Green Oxidation Catalysts. *Chemistry-A European Journal*, **2006,** 12, (36), 9336-9345.

21. Chahbane, N.; Popescu, D.-L.; Mitchell, D. A.; Chanda, A.; Lenoir, D.; Ryabov, A. D.; Schramm, K.-W.; Collins, T. J., Fe(III)-TAML-catalyzed green oxidative degradation of the azo dye Orange II by H_2O_2 and organic peroxides: products, toxicity, kinetics, and mechanisms. *Green Chemistry*, **2007,** 9, (1), 49-57.

Chapter 6

Conclusions and Future work

This chapter summarizes salient features of the work embodied in this thesis. In addition, scope for future work relevant to the present study is discussed.

6.1 Conclusion:

The objectives of this thesis work as explained in chapter 1 were the synthesis and functional methodologies of silica and mesoporous silica nanaoparticles. In addition, effective methodologies to assembling nanoparticles to form hierarchical monolithic structure also envisaged. Herein, a summary of the thesis work and scope of future work are presented.

The salient features of the results are as follows:

(A) A functional group was created using "*Click Chemistry"* on the surface of silica so that it can bind Au(III) ions. The resulting composite material has shown catalytic activity in Hashmi's phenol synthesis – a reaction in which Au(III) activates a terminal alkynes to isomerise o-alkynylfurans to phenols. This process can be easily generalized for other molecular/metal based catalysts.

(B) Development of composite material by which it is possible to carry out two tandem reactions was also considered next. To achieve the aim, glucosidase enzyme was immobilized on Au core and mesoporous silica shell type architecture. The novelty of the design ensured that a two step consecutive reactions, where surface bound enzyme catalyses the 1^{st} reaction and the metal nanoparticles bring out the 2^{nd} reaction on the product released from the 1^{st} reaction, could be easily carried out.

(C) A great control and tenability of the hydrophobicity and hydrophilicity of the inner and outer surface of the mesoporous silica nanoparticles have been reported in the next chapter. Hydrophilic PEG group was grafted outside the surface of mesoporous silica nanoparticles, whereas the inner surface was functionalized with methyl groups.

(D) As a step forward in our endeavour to mimic the 'living' system, the mesoporous silica nanoparticles were assembled using dynamic templating of liquid crystalline mesophases. It was possible to tune over nanoparticle mesoporosity and scaffold macroporosity controllably. Using this technique, it has been shown that macroporosity in a single sample can be tuned spatially. These scaffolds can also functional. This monolith type architecture can be also used for continuous flow reactor.

6.2 Scope of future work:

The development of novel grafting methodologies for silica and mesoporus silica for catalytic application was the focus of this thesis work. It needs to be noted that the findings do indicate good potential for future applications. Some of them are listed in the next page.

(A) Immobilization of molecular catalysts:

A huge class of molecular catalysts can be grafted on silica surface using "click chemistry" as described in chapter 2. Also it is possible to generate magnetically separable materials. Silica coated core shell Fe_2O_3 particles could be synthesized by reported procedure and functionalized with azido group will not be difficult.[1] Later the alkyne terminated molecular catalyst could be grafted on the surface as shown in chapter 2. These kind of material could be easily separated from the reaction mixture by magnetic separation.

(B) Nanoparticle embedded scaffold for catalytic applications:

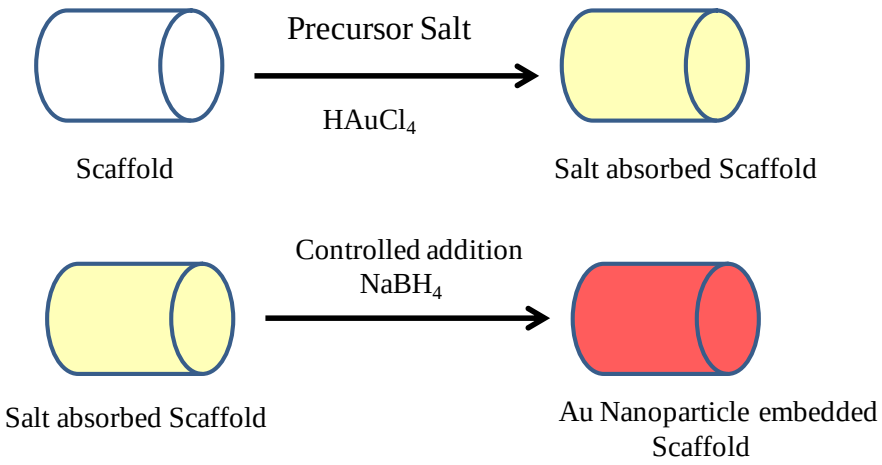

Scheme 6.1: The above schematic represents the formation of Au nanoparticles embedded scaffold

The hierarchical monolithic scaffold made of meso-porous silica can be used to embed different nanoparticles.[2] For example, the scaffold can be treated with precursor salt of Au nanoparticles, i.e. $HAuCl_4$. So the salt solution will go to the meso pore region of the porous scaffold. Later, Au nanoparticle embedded scaffold can be generated upon reduction of the salt solution. While making this kind of scaffold inside the glass channel, can perform catalytic reaction in continuous flow manner. Efforts are also ongoing in our laboratory, to chemically anchor catalysts

within the MSN mesopores, to test the possibility that packings of such scaffolds in microreactor channels will enable efficient mixing at low pressure drops with simultaneous catalytic chemical conversions.

(C) Tissue engineering materials:

In the past few years of research it is known that silica mesoporous materials can play a double role: bioactivity and release systems for biologically active species. In the near future it could be possible to amalgamate both aspects and able to generate bio-material. [3, 4] The dimensions of the natural cells lie on the order of hundreds of μm. Thus it is appreciable to generate a material which can preserve the mesoporosity of these silica materials while providing interconnected macroporosity, at least within the 20 to 400 μm range, which is the minimum to allow cells to attach and develop. The preparation of hierarchical scaffolds has been discussed in Chapter 5. The macroporosity of the scaffold can be used for cell generation and vascularisation, while the mesoporosity can be used to load drugs or biologically active molecules and then released. As a consequence of this, it would be possible to produce three dimensional hierarchical scaffolds with interconnected porosity, so cells could proliferate and form tissue in a similar way to the process in human tissues. In this way, the designed materials could help the human body to improve its regenerative capabilities, not only recovering the structure of the damaged tissue, but also its function.

6.3 References:

1. Lu, A.-H.; Salabas, E. L.; Schüth, F., Magnetic Nanoparticles: Synthesis, Protection, Functionalization, and Application. *Angewandte Chemie International Edition,* **2007,** 46, (8), 1222-1244.

2. Du, X.; He, J., Amino-functionalized silica nanoparticles with center-radially hierarchical mesopores as ideal catalyst carriers. *Nanoscale,* **2012,** 4, (3), 852-859.

3. Manzano, M.; Vallet-Regi, M., New developments in ordered mesoporous materials for drug delivery. *Journal of Materials Chemistry,* **2010,** 20, (27), 5593-5604.

4. Vallet-Regí, M.; Balas, F.; Arcos, D., Mesoporous Materials for Drug Delivery. *Angewandte Chemie International Edition,* **2007,** 46, (40), 7548-7558.

Appendix-1: Instrumental details

Confocal microscope:

An LSM 710 Carl Zeiss Laser Scanning Confocal Microscope (LSCM) was used to image the fluorescent samples. He-Ne laser (543 nm) and Argon-ion laser (488 nm and 514 nm) was used for our experiments.

FTIR spectrophotometer:

FT-IR spectra were recorded on Perkin Elmer FT-IR spectrum GX instrument by making KBr pellets in diffuse reflectance mode, operating at a resolution of 4 cm^{-1}. Pellets were prepared by mixing 3 mg of sample with 97 mg of KBr.

High resolution transmission electron microscope:

HR-TEM images were taken on a FEI Technai F30 operating at 300 kV. The samples were prepared by dispersing a 0.1 mg/mL of nanoparticles by sonication, and drop casting the resulting suspension on a carbon coated copper grid of 400 mesh and allowed to dry in air. The TEM of scaffold samples was prepared by embedding the scaffold in the epoxy resin and microtome to view the sample under HRTEM.

Inductive coupled plasma instrument:

ICP experiments were performed on a Thermo IRIS Intrepid spectrum apparatus. The typical procedure used is as follows: The calculated amount of sample was dried in vacuo overnight was taken into a beaker and heated with aqua-regia for 20 mins. It was then filtered and diluted with aqua-regia into a 25 ml volumetric flask using. This stock solution was then diluted using milipore water and was analyzed by using the ICP instrument for quantitative determination of Au.

Optical Microscope:

Optical microscopy was performed using an Olympus-BX 50 equipped with a crossed polarizer setup and images were obtained using a Lookman CCTV camera. The samples were prepared by sandwiching dispersed samples between the glass slide and cover slip.

Thermogravimetric Analyser:

Thermo gravimetric analysis (TGA) of the silica nanoparticles were carried out using a TA Instrument SDT Q600 analyzer between 20 and 800 °C in air (flow 50 ml min^{-1}) at a heating rate of 10 °C min^{-1}. All samples were dried under vacuum at 60 °C overnight prior to TGA runs. The graft density of the grafted moitey on the silica

surface was determined by thermo gravimetric analysis (TGA) using following equation as described before.

Graft density (μmol/m^2) =

$$\frac{\frac{W_{GraftedSilica(150-700)}}{100-W_{GraftedSilica(150-700)}}\times 100 - W_{Silica(150-700)}}{M \times S \times 100}\times 10^6$$

Where $W_{150\text{-}700}$ is the weight loss between 150 and 700 °C corresponding to the decomposition of the grafted silica molecule corrected from the thermal degradation and M is the molecular weight of the grafted silane. *S* represents the specific surface area of the silica nanoparticle (measured as 110 m^2/g) while W_{Silica} represents the determined weight loss of silica before grafting.

Scanning Electron microscope:

Samples were imaged using a Quanta 200 3D scanning electron microscope (SEM). Samples were placed on carbon tape which was gummed on a sample holder.

Solid State NMR:

^{29}Si and ^{13}C Cross Polarization Magic Angle Spinning (CPMAS) NMR experiments were carried out on a Bruker AVANCE 300 wide bore spectrometer equipped with a superconducting magnet with a field of 7.1Tesla. The operating frequencies for ^{13}C and ^{29}Si were 300MHz, 75.4MHz and 59.6MHz respectively. The samples were packed into a 4mm zirconia rotor and loaded into a 4mm BL MAS probe and spun about the magic angle (54.74) at 10KHz using a standard ramp-CP pulse sequence was used for both the experiments. The RF-powers were 50kHz and 60kHz for the ^{29}Si and ^{13}C CPMAS experiments. The contact times were 6ms and 3ms for the ^{29}Si and the ^{13}C CPMAS experiments. All the chemical shifts were referenced to TMS. Typically 10,000 to 25,000 scans with a recycle delay of 3s were collected depending on the sensitivity of the sample.

Surface area measurement instrument:

Nitrogen adsorption and desorption studies were carried out using Quadrasorb *SI* instrument. Before the nitrogen adsorption measurement, the samples were degassed overnight under vacuum using FloVac Degasser at 300 °C (for silica) or at

100 °C (for modified silicas). Multi point BET surface area was obtained from adsorption isotherm from P/P_0 0.01-0.1. Pore size distributions were calculated from adsorption isotherm using the BJH method.

UV-visible spectrophotometery:

The catalytic reaction was monitored by UV-vis spectra on a Cary 300 Conc UV-Visible spectrophotometer operated at a resolution of 2 nm.

X-ray diffraction:

Powder X-ray diffraction of all the mesoporous samples was carried out in a PAN alytical X'pert Pro dual goniometer diffractometer. A proportional counter detector was used for low angle experiments and an X'celerator solid state detector was employed in the low angle experiments. The radiation used was Cu K_α (1.5418 Å) with a Ni filter and the data collection was carried out using a flat holder in Bragg–Brentano geometry (0.5 to 10°; 0.2° min^{-1}). Care was taken to avoid sample displacement effects.

Solid dried core-shell nanoparticle samples were coated on glass slides and characterized with powder X-ray diffraction (Xpert Pro, Panalytical, Cu K_α) in the 2θ range of 30-80 degree which was operated at 40 kV and 30 mA.

X-ray photoelectron spectroscopy

XPS measurements of the samples were deposited on sample holder and were carried out on a VG MicroTech ESCA 3000 instrument at a pressure of better than 10^{-9} Torr. The general scan and Si 2p, C 1s, N 1s, O 1s, Cl 2p and Au 4f core level spectra were recorded with unmonochromatized Mg-K_α radiation (photon energy ~ 1253.6 eV) at pass energy of 50 eV and electron take off angle (angle between electron emission direction and surface plane) of 60 ^{o}. The overall resolution of measurement is thus 1 eV for the XPS measurements. The core level spectra were background corrected using the Shirley algorithm. The core level binding energies (BE) were aligned with the silica binding energy of 103.4 eV.

Appendix-2: NMR details

^{1}H NMR (500 MHz, $CDCl_3$) and ^{13}C NMR (50 MHz, $CDCl_3$) of compound of **3-azidopropyltriethoxysilane**

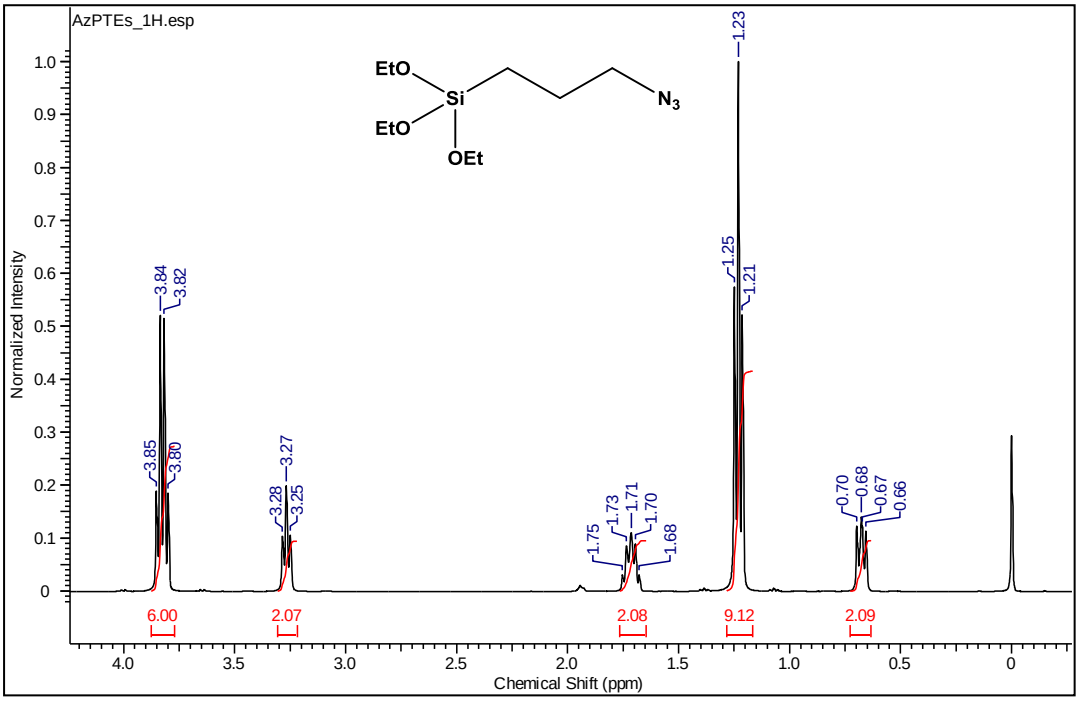

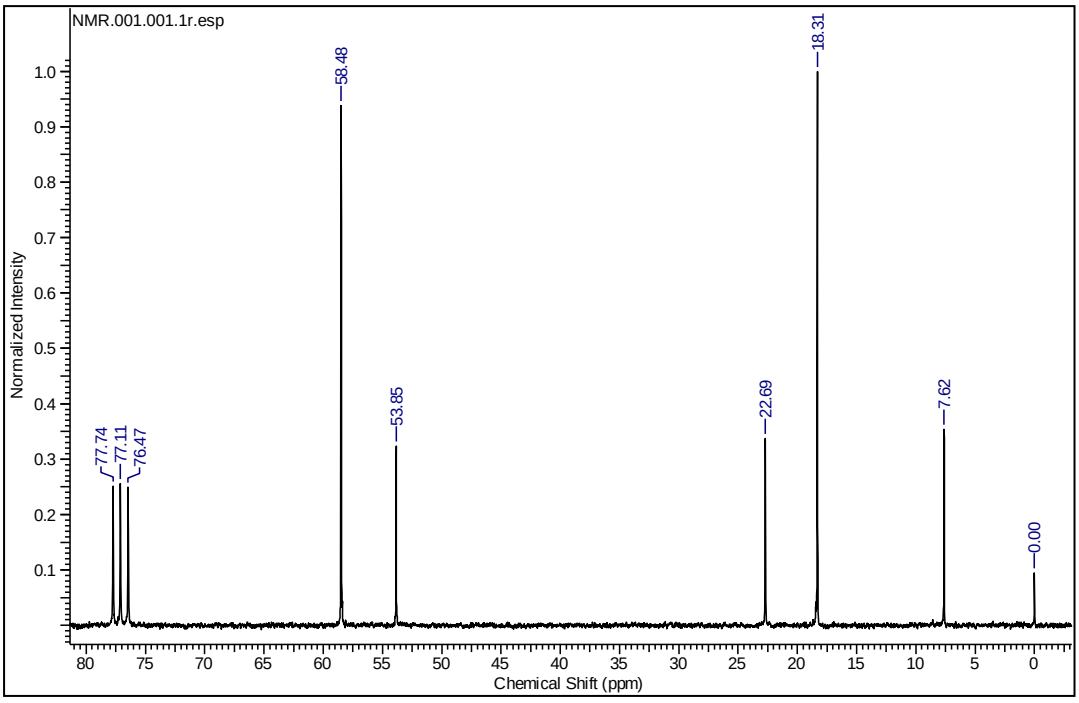

^{1}H NMR (200.13 MHz, $CDCl_3$) and ^{13}C NMR (50.32 MHz, $CDCl_3$) of compound of **prop-2-ynyl 3-(prop-2-ynyloxy)picolinate**

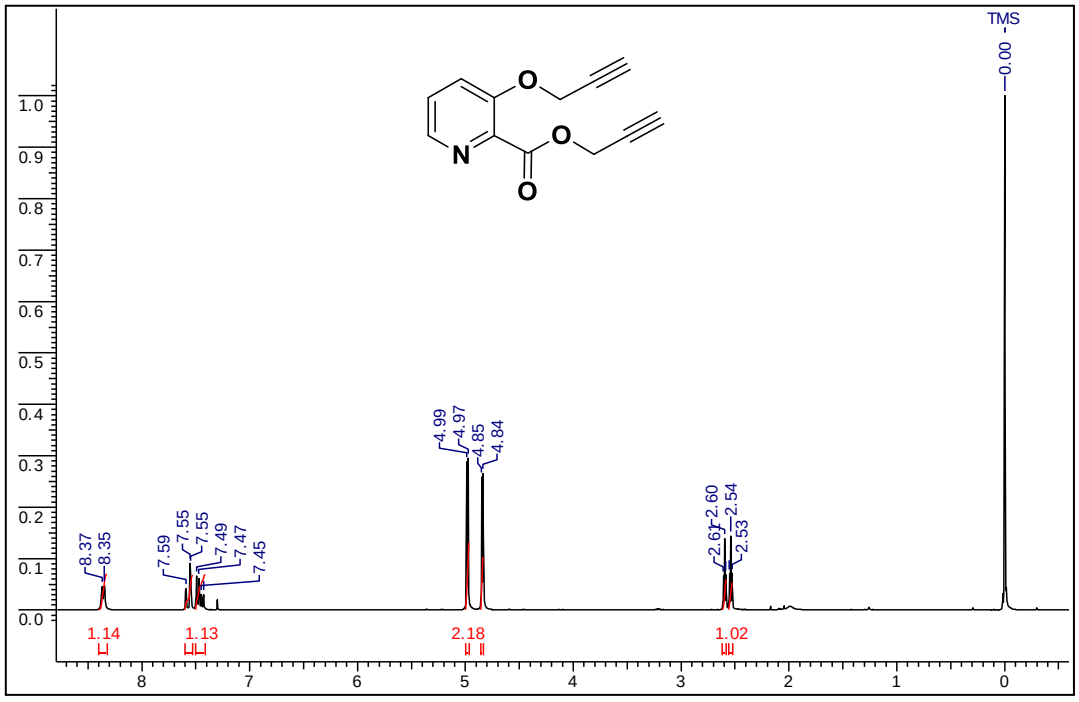

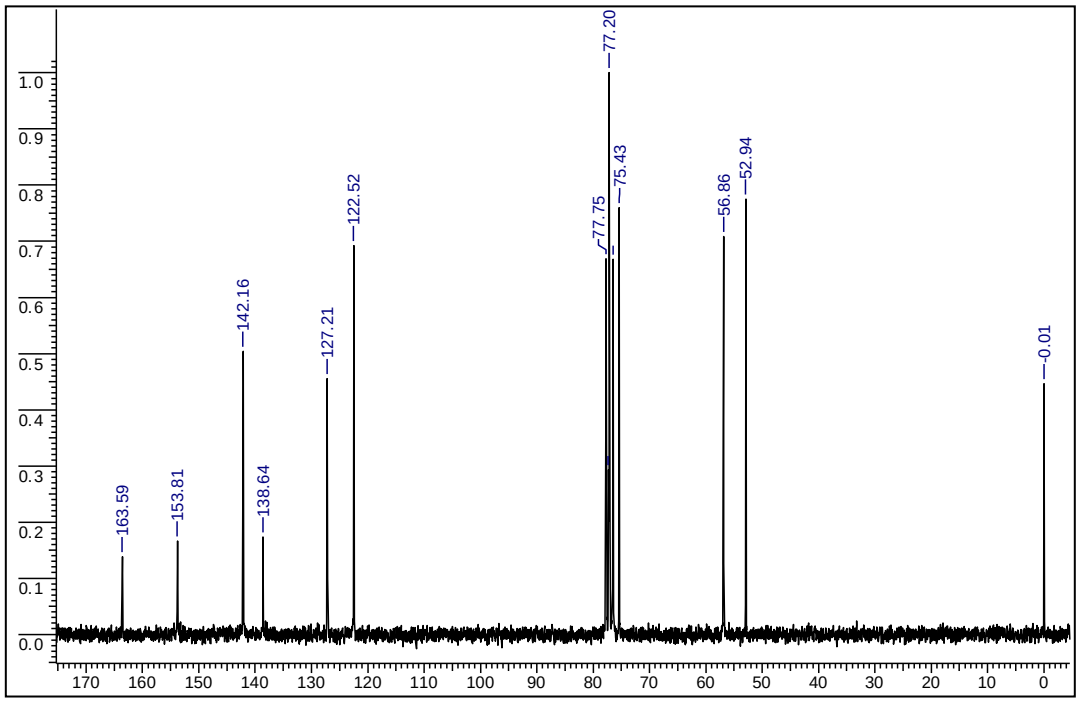

^{1}H NMR (200.13 MHz, $CDCl_3$) and ^{13}C NMR (50.32 MHz, $CDCl_3$) of compound **prop-2-ynyl 3-(prop-2-ynyloxy)picolinic acid**

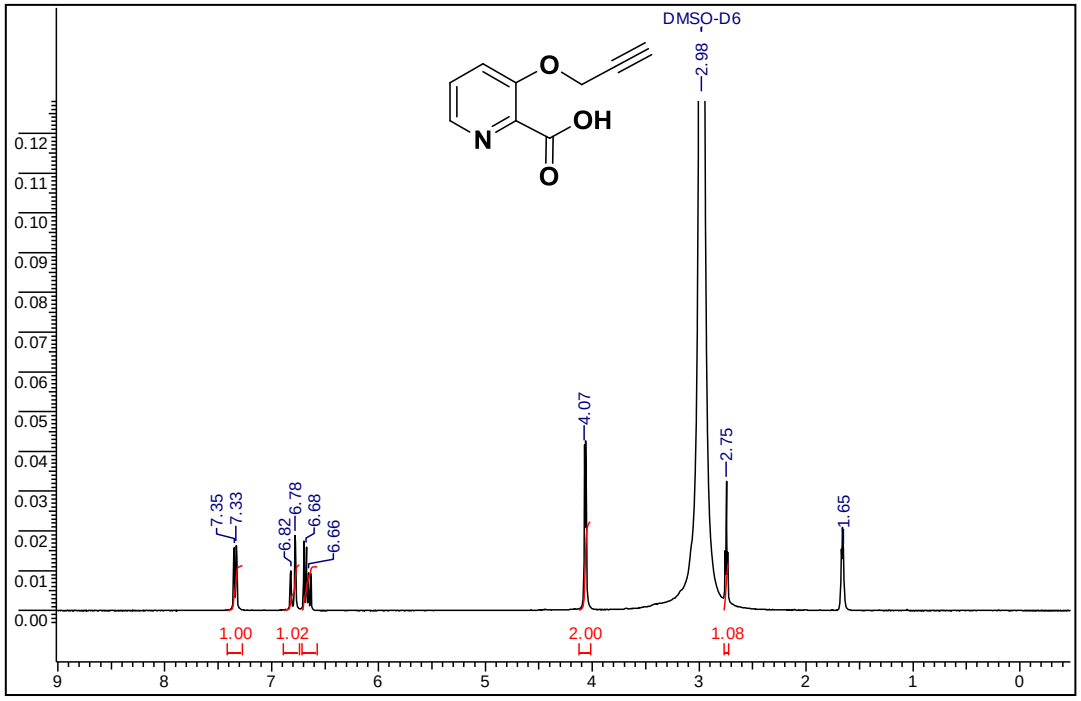

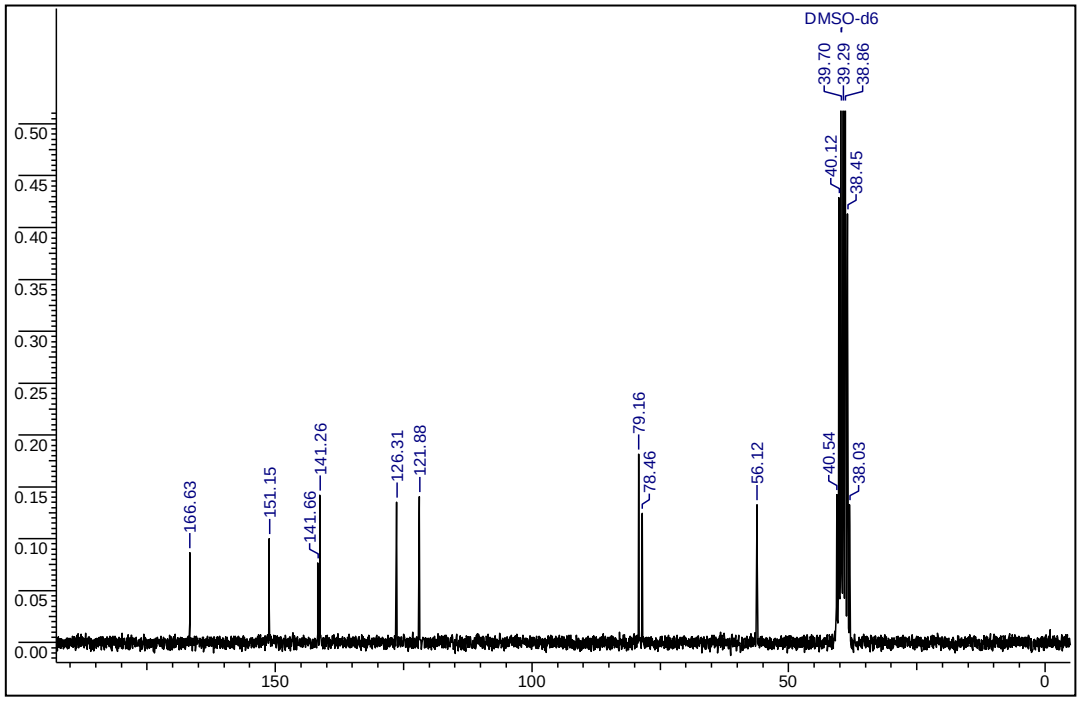

^{1}H NMR (500.13 MHz, $CDCl_3$) and ^{13}C NMR (125.76 MHz, $CDCl_3$) of compound **prop-2-ynyl 2-(prop-2-ynyloxy)benzoate**

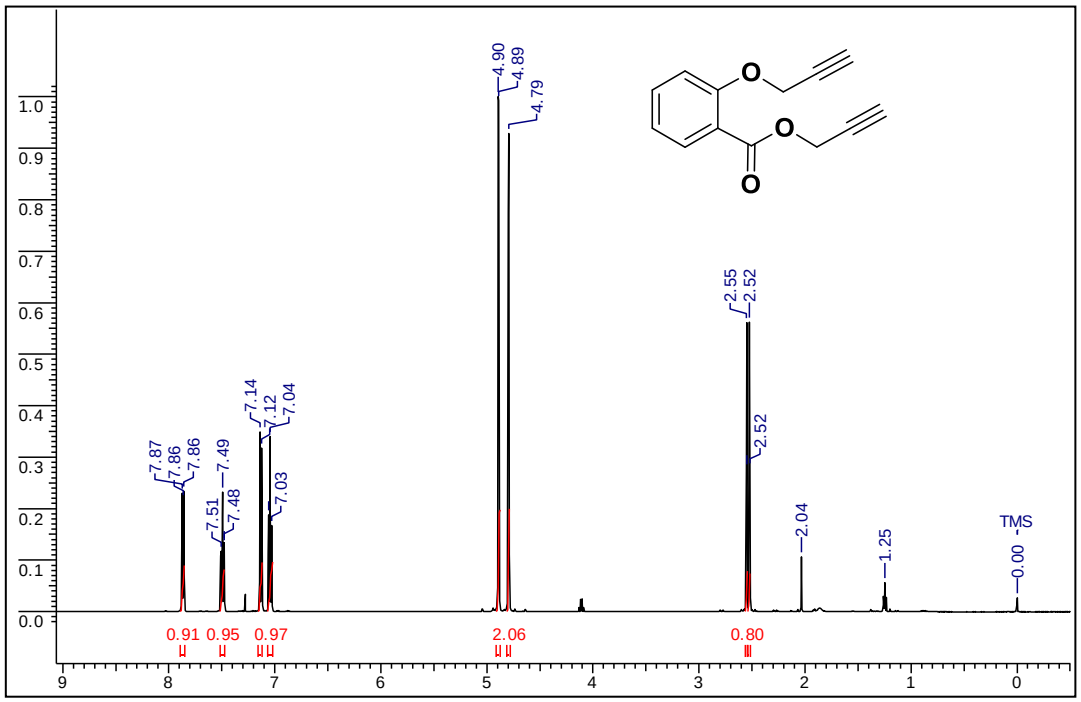

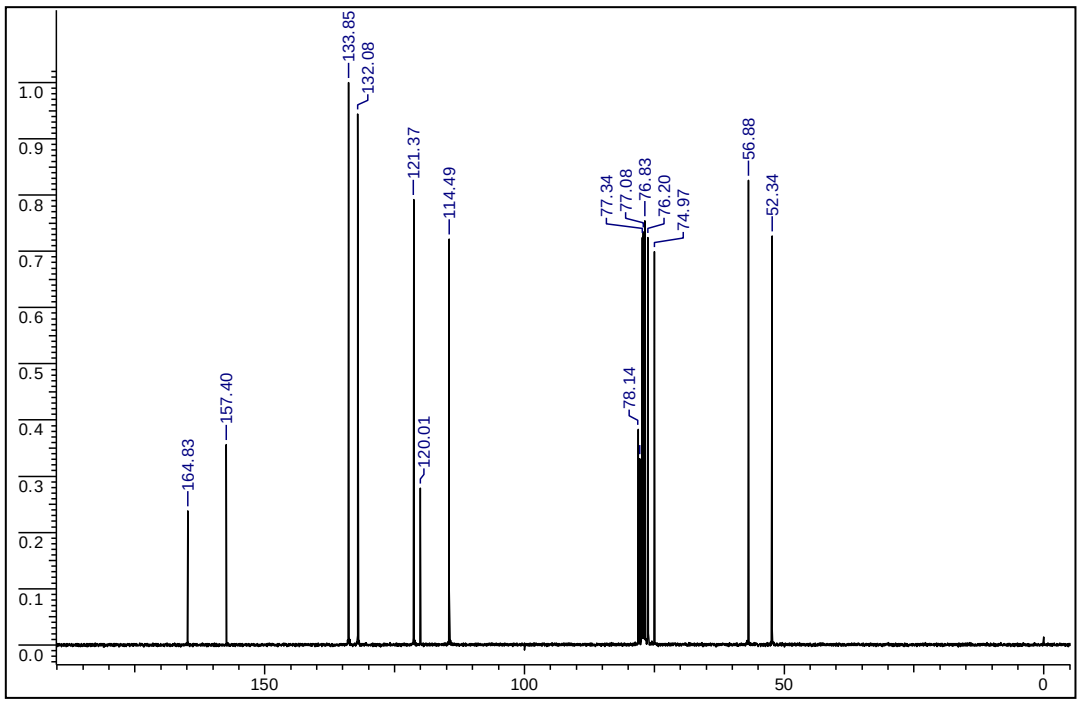

^{1}H NMR (200.13 MHz, $CDCl_3$) and ^{13}C NMR (50.32 MHz, $CDCl_3$) of compound **prop-2-ynyl 2-(prop-2-ynyloxy)benzoic acid**

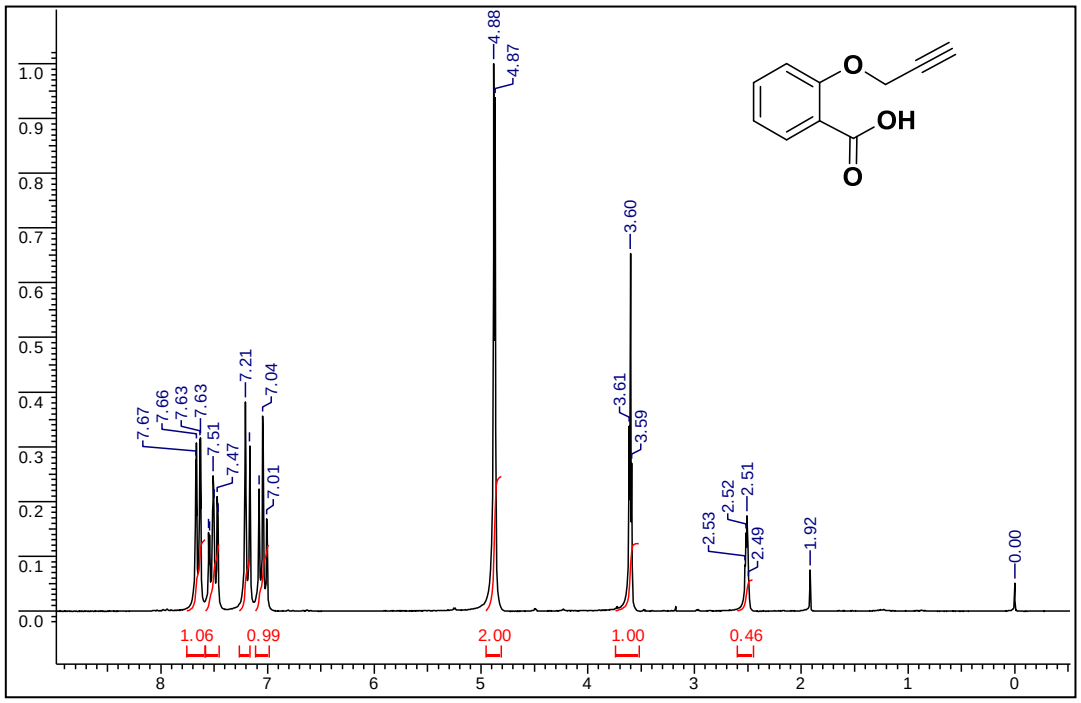

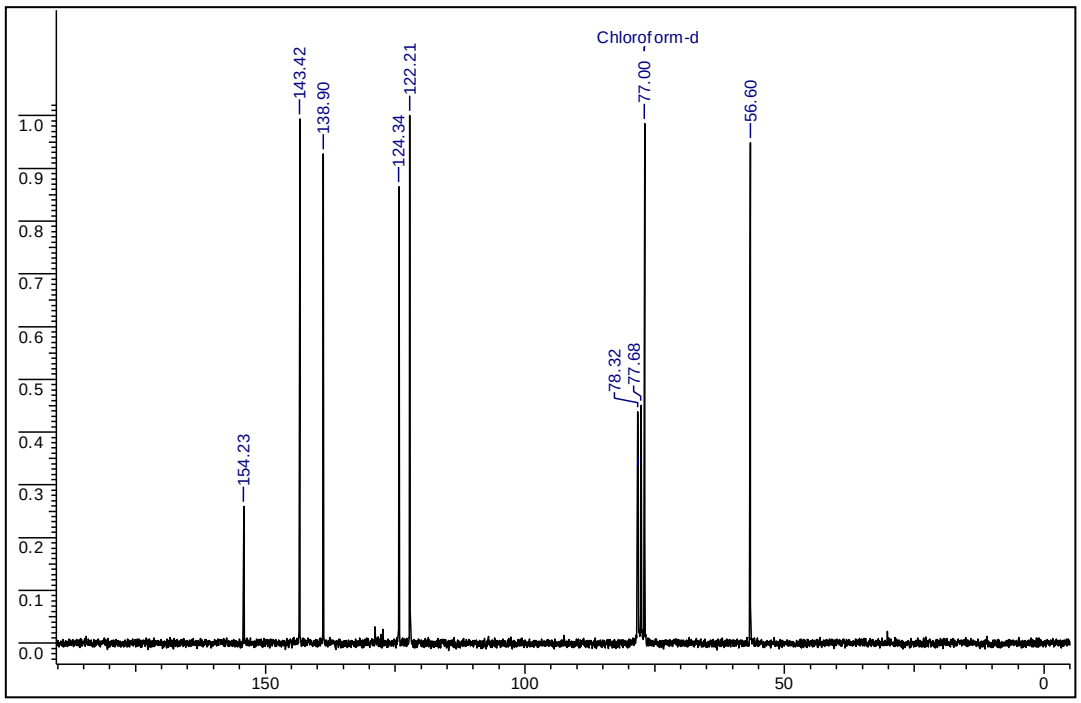

^{1}H NMR (400.13 MHz, $CDCl_3$) and ^{13}C NMR (50.32 MHz, $CDCl_3$) of compound **4-methyl-1, 3-dihydroisobenzofuran-5-ol**

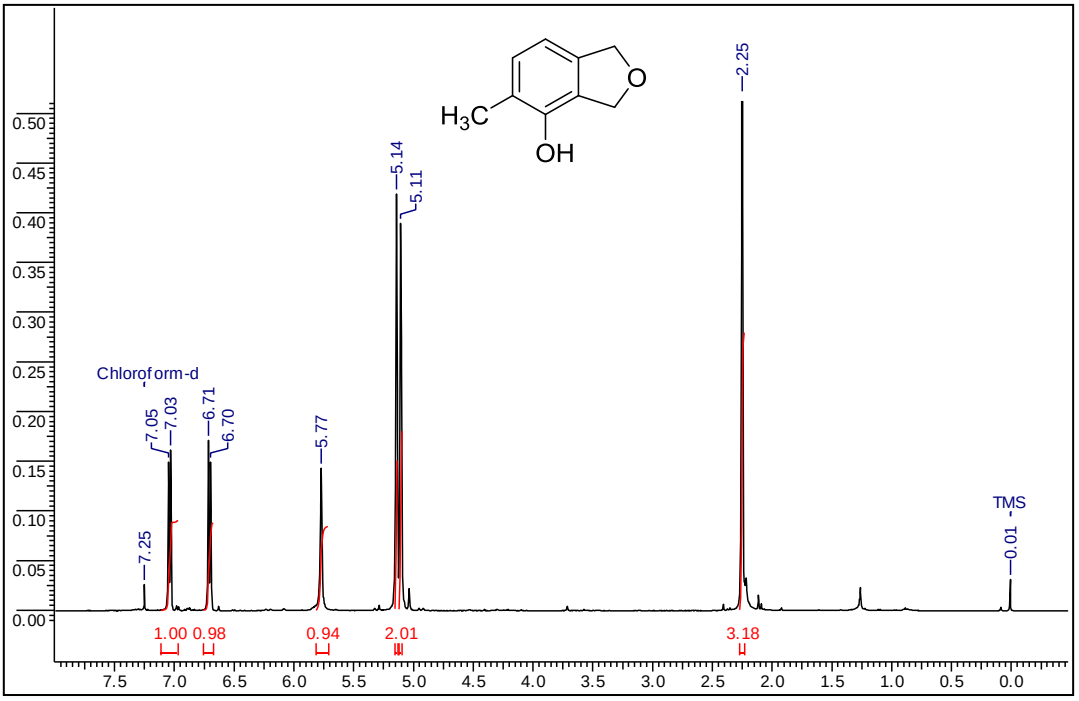

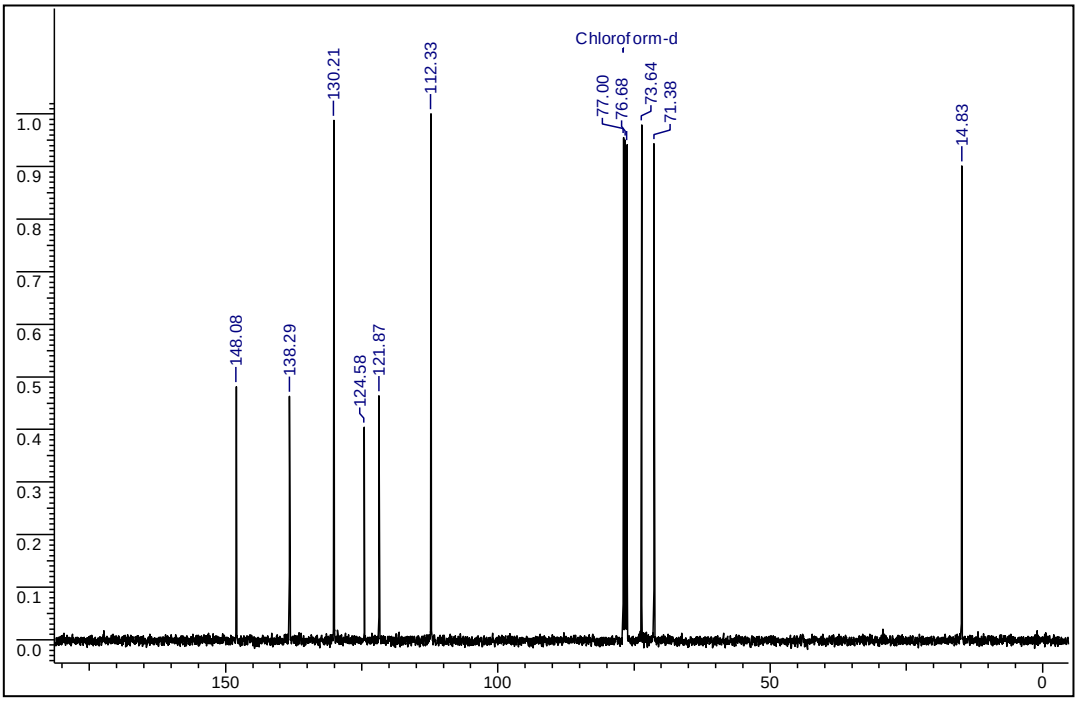

^{1}H NMR (200.13MHz, $CDCl_3$) and ^{13}C NMR (100.61MHz, $CDCl_3$) of compound **5-methyl-2-tosylisoindolin-4-ol**

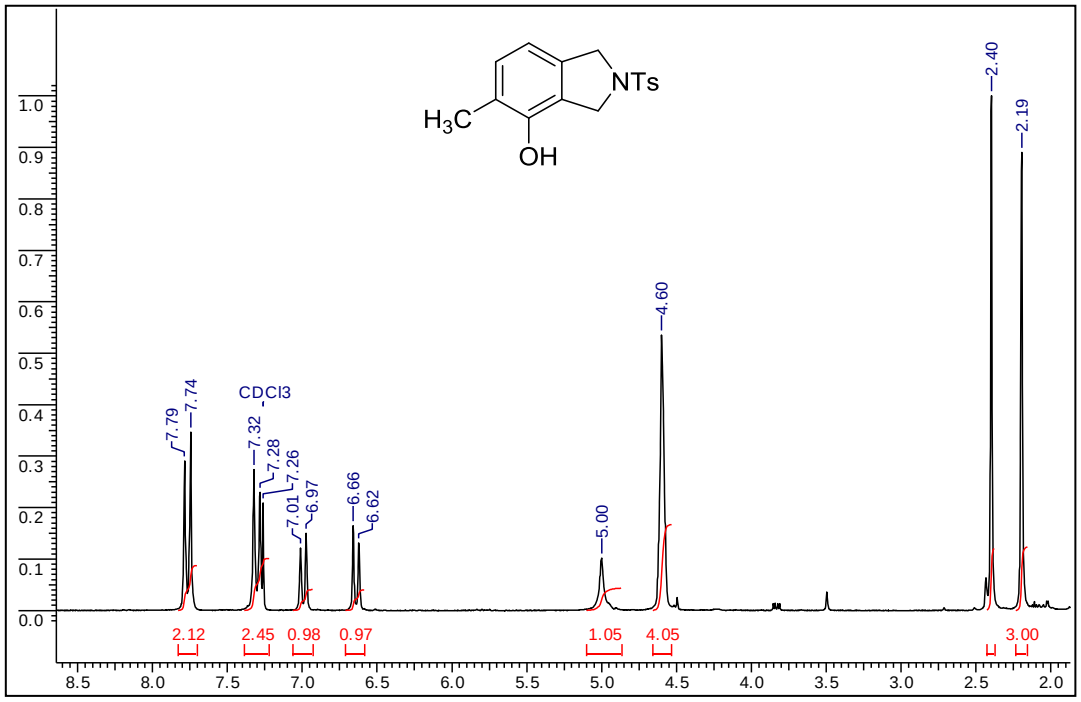

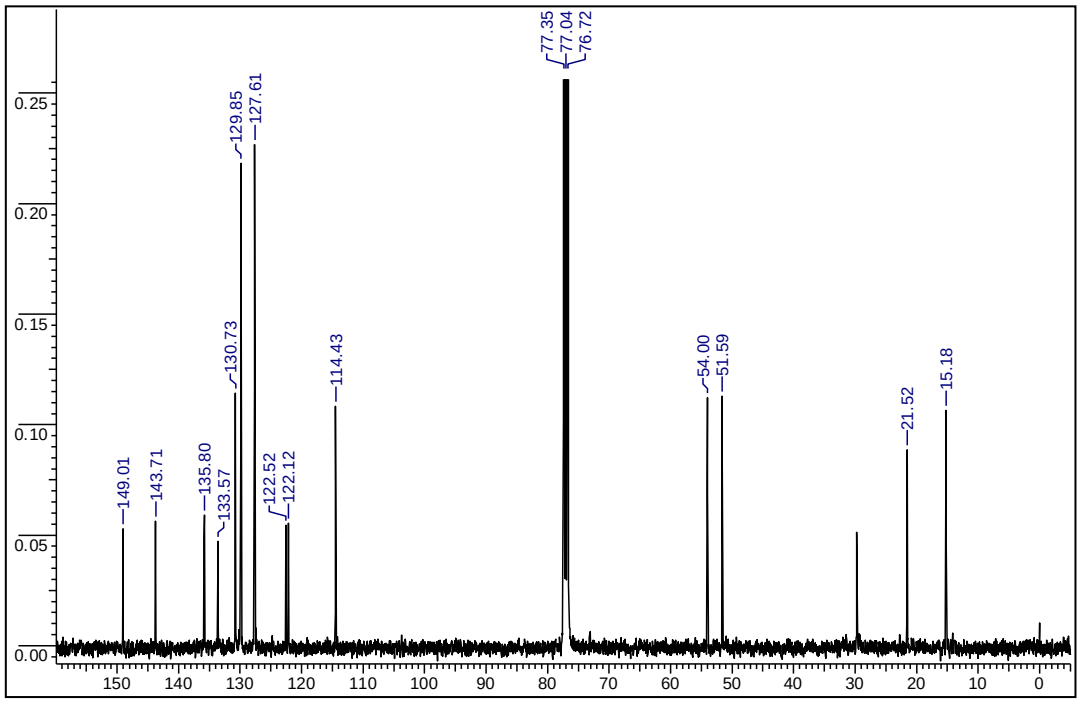

^{1}H NMR (400.13MHz, $CDCl_3$) and ^{13}C NMR (100.61MHz, $CDCl_3$) of compound **dihydroisobenzofuran-4-ol**

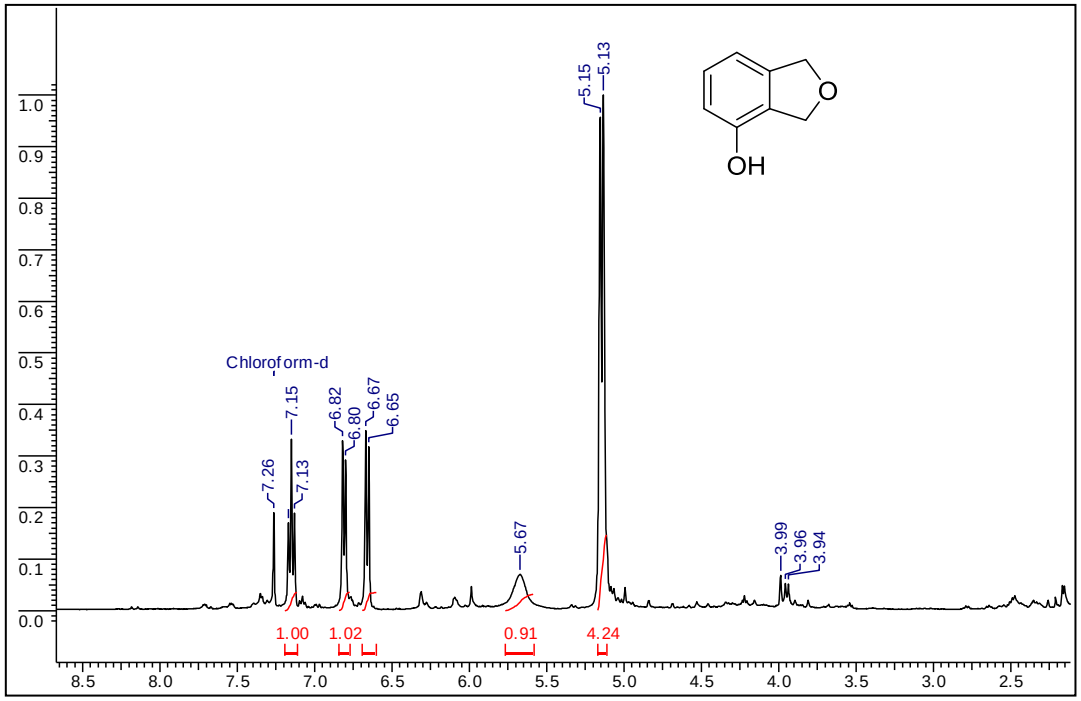

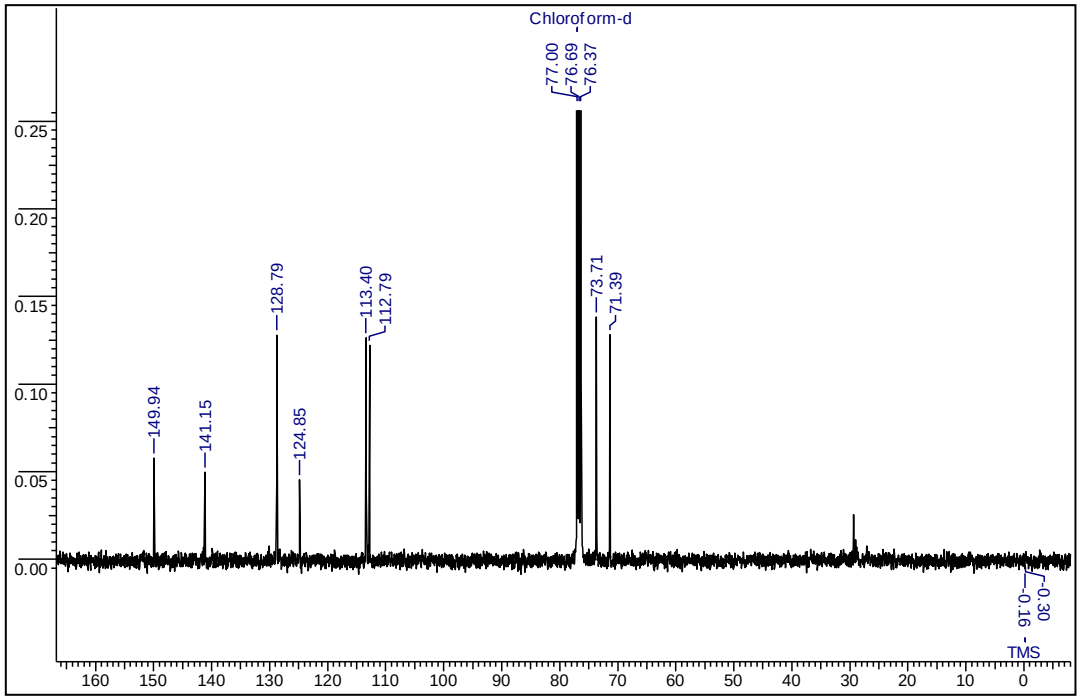

^{1}H NMR (200.13MHz, $CDCl_3$) and ^{13}C NMR (50.32MHz, $CDCl_3$) of compound **1,3-dihydroisobenzofuran-5-ol**

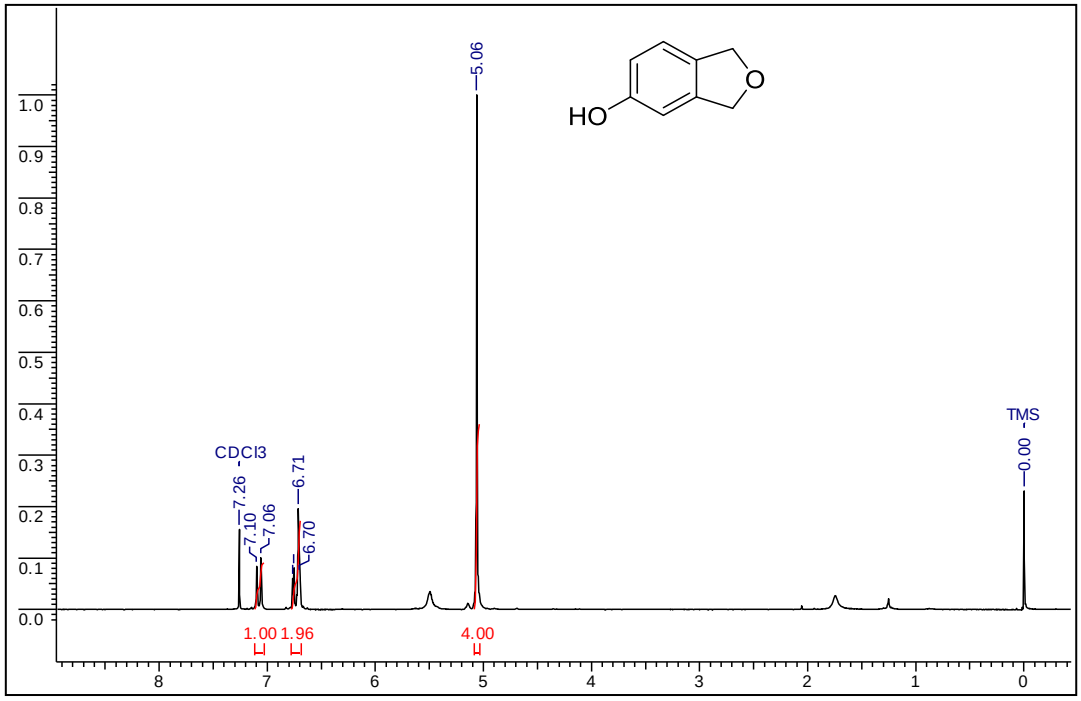

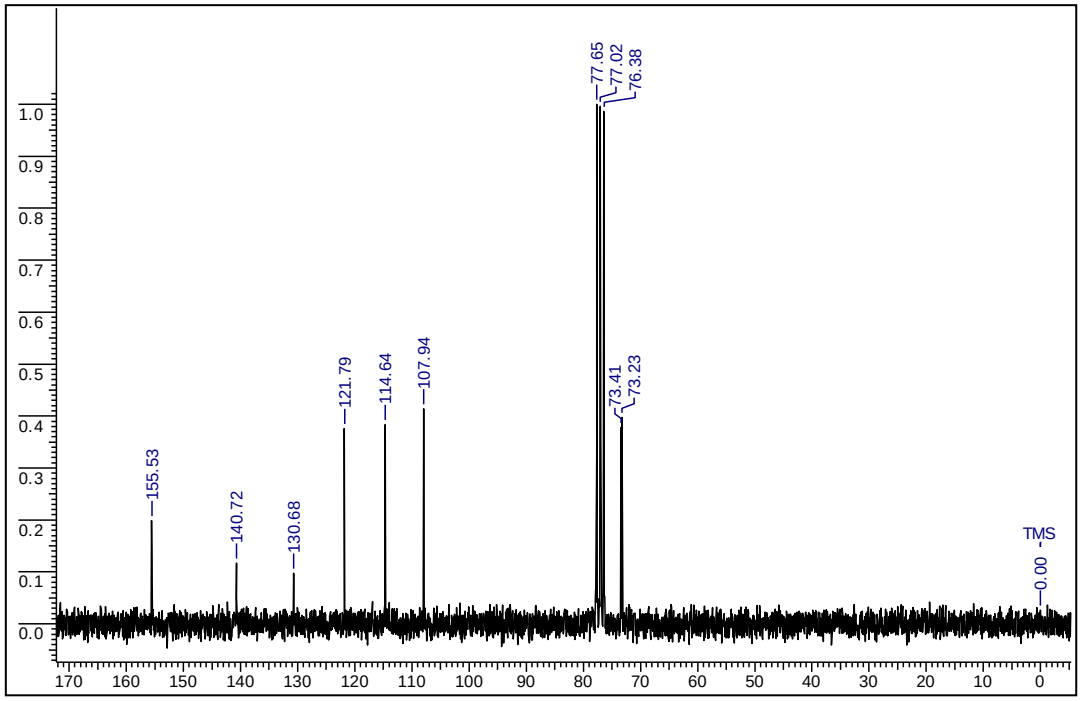

^{1}H NMR (200.13MHz, $CDCl_3$) and ^{13}C NMR (100.61MHz, $CDCl_3$) of compound **2-tosylisoindolin-4-ol**

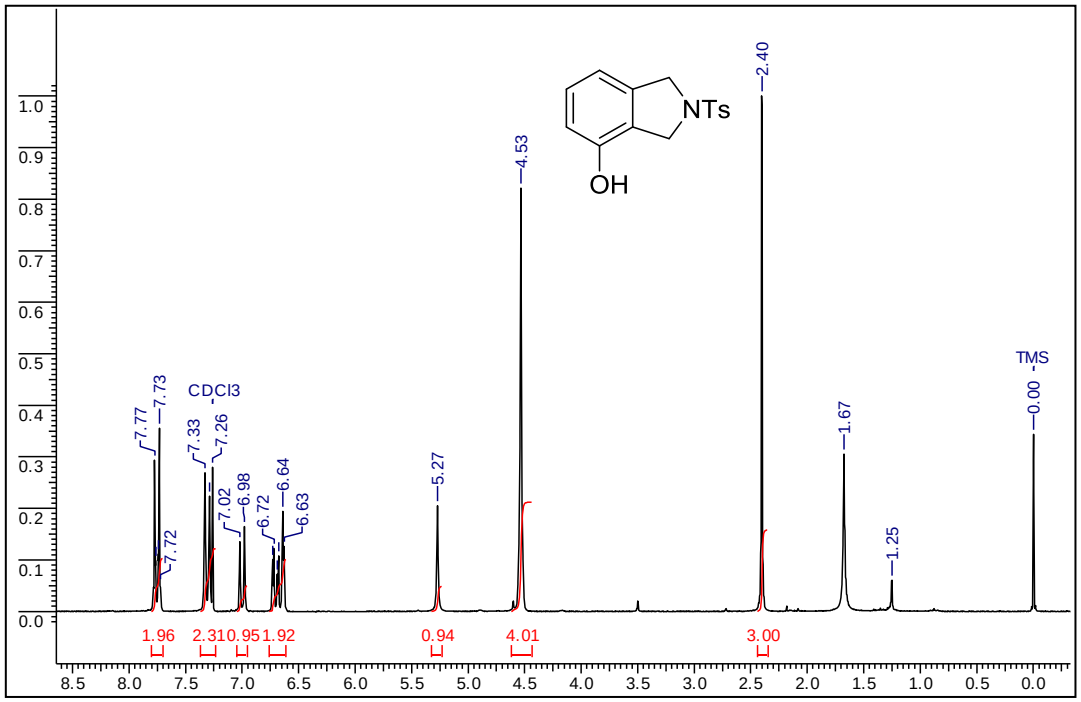

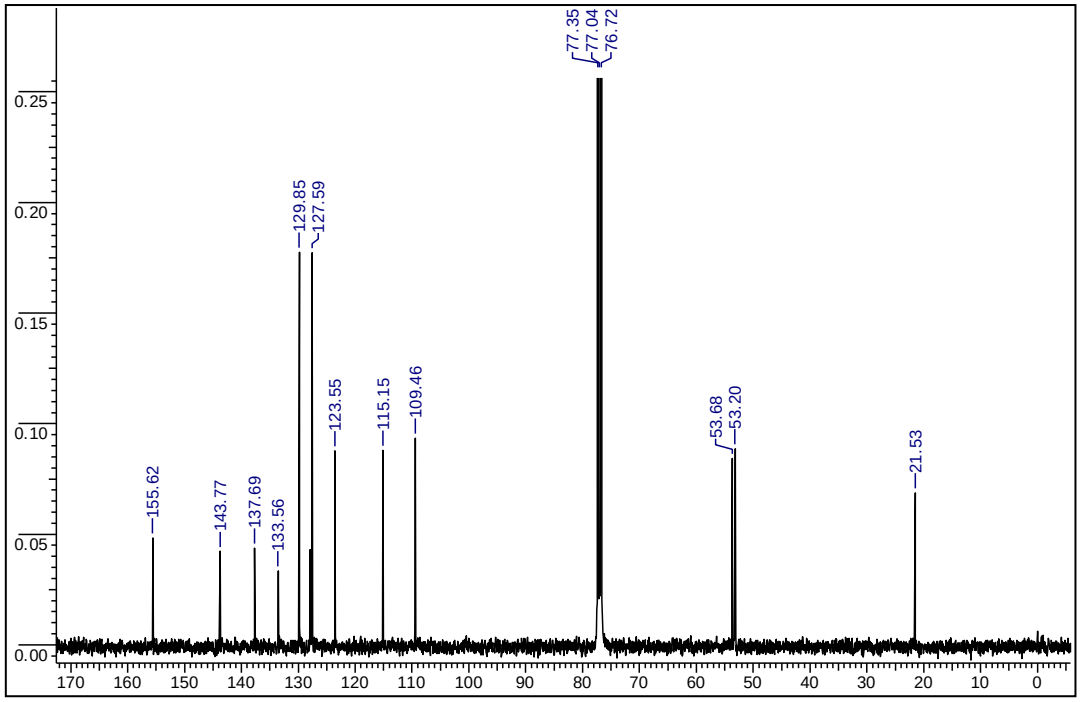

^{1}H NMR (200.13MHz, $CDCl_3$) and ^{13}C NMR (50.32MHz, $CDCl_3$) of compound **2-tosylisoindolin-5-ol**

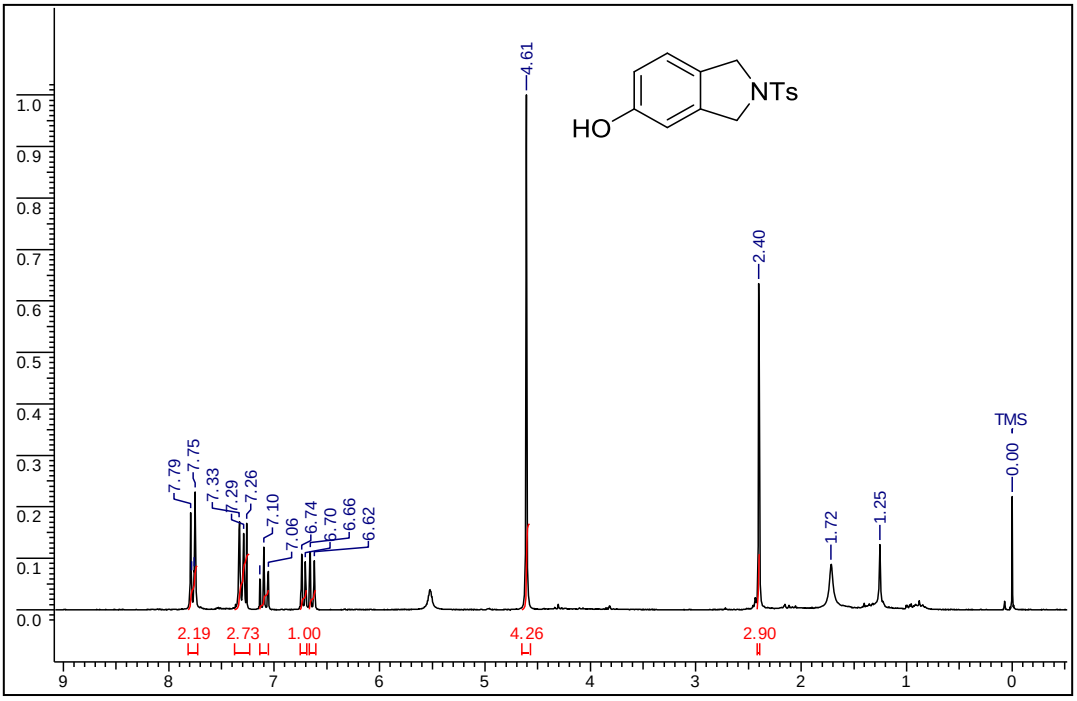

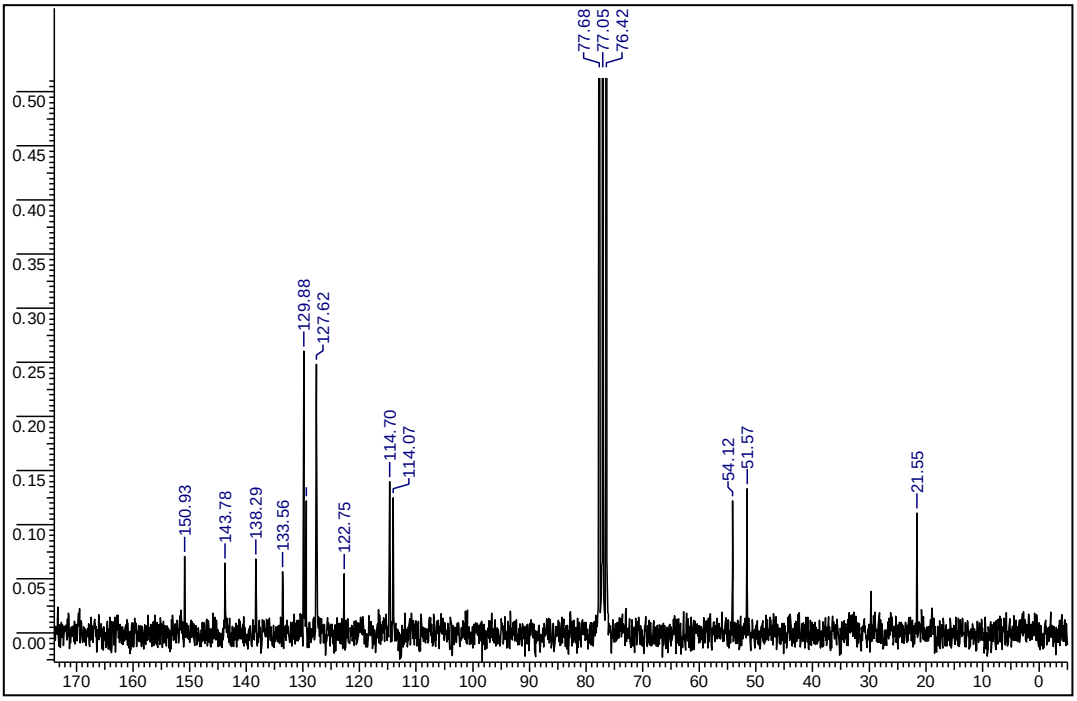

Appendix-3: List of Research Credentials, Awards and Conferences

List of Publications and Patents:

1. Development of a Bifunctional catalyst for Tandem Reactions
   Anal Kr. Ganai, Pravin Shinde, Basav Dhar, Sayam Sen Gupta, B. L. V. Prasad, *RSC Adv.*, **2013**,3, 2186-2191

2. Synthesis of functional hybrid silica scaffolds with controllable hierarchical porosity by dynamic templating
   Anal Kr. Ganai, Sushma Kumari, Kamendra P. Sharma, Chakadola Panda, Guruswamy Kumaraswamy, Sayam Sen Gupta, *Chem. Commun*., **2012**, 48, 5292-5294

3. Functionalization of SBA-15 Mesoporous Materials using "Thiol-Ene Click" Michael Addition Reaction
   Sushma Kumari, Bharmana Malvi, **Anal Kr. Ganai**, Vijayamohanan K. Pillai, and Sayam Sen Gupta, *J. Phys. Chem. C*, **2011**, 115 (36), 17774–17781

4. Self Standing Three Dimensional Networks of Nanoparticles, With Controllable Morphology by Dynamic Templating of Surfactant Hexagonal Domains
   Kamendra P. Sharma, **Anal Kr. Ganai**, Sayam Sen Gupta, and Guruswamy Kumaraswamy, *Chem. Mater.*, **2011**, 23 (6), 1448–1455 (Cover Page Article)

5. "Clicking" molecular hooks on silicananoparticles to immobilize catalytically important metal complexes: the case of gold catalyst immobilization
   Anal Kr. Ganai, Rima Bhardwaj, Srinivas Hotha, Sayam Sen Gupta and B. L. V. Prasad, *New J. Chem.*, **2010**, 34, 2662-2670.

6. Rod-like Particles in Non-ionic surfactant H_1 phases: End-to-End Assemblies from Interplay of Particle Geometry and Exclusion from H_1 Domains
   Kamendra P. Sharma, **Anal Kr. Ganai**, Debasis Sen, B. L. V. Prasad and Guruswamy Kumaraswamy (Manuscript under preparation)

7. Selective functionalization to change hydrophobicity and hydrophilicity in mesoporous silica
   Anal Kr. Ganai, Pravin Shinde, Sayam Sen Gupta, B. L. V. Prasad, (Manuscript under preparation)

8. Indian Provisional Patent filed on "Meso/macroporous hierarchical monolith scaffolds embedded with catalyst for oxidative remediation"
   Guruswamy Kumaraswamy, Sayam Sen Gupta, **Anal Kr. Ganai**, Kamendra P. Sharma, Sushma Kumari, Filing No: 0355/DEL/2012

9. Stereoregularity evolution of methyl acrylate and vinyl acetate copolymers by 2D NMR spectroscopy
   A. S. Brar, Ashok Kumar Goyal, **Anal Ganai**, Sunita Hooda, *Jour.of Mol Str.*, **2008**, 888, 257-265

Poster presentations in International Conferences and Symposia:

1. "One Pot Synthesis of Hybrid Silica Scaffolds with Controllable Hierarchical Porosity"- at International Conference on Nano Science and Technology (ICONSAT), Hyderabad, India (February 2012).

2. "Clicking" molecular hooks on silica nanoparticles to immobilize catalytically important metal complexes: the case of gold catalyst immobilization"- at National Review Meeting of Nanoscience and Nanotechnology (NSNT), New Delhi, India (February, 2011).

3. "Heterogenization of Au(III) and Au(0) By Different Techniques and Their Catalytic Application"- Abstract accepted at 6th International Conference on Gold Science Technology and its Application (Gold 2012) held in Tokyo, Japan on September, 2012.

Awards and Achievements:

- Joshi-Sivaram award for the Best Publication in Polymer Science and Organic Inorganic hybrid Materials with highest impact factor 2011.
- Awarded *Junior and Senior Research Fellowship* by Council of Scientific and Industrial Research (CSIR), India, for 5 years duration.
- Qualified GATE with AIR 83 in the year of 2007.